Solvates and salts of selected fenamates

by

JACKY SORREL BOUANGA BOUDIOMBO

Thesis submitted in fulfilment of the requirements for the degree

Master of Technology in Chemistry
in the Faculty of Applied Sciences
at the Cape Peninsula University of Technology

Supervisor: Professor Ayesha Jacobs

Cape Town

December 2015

▪ DECLARATION

I, Jacky Sorrel Bouanga Boudiombo, declare that the contents of this dissertation/thesis represent my own unaided work, and that the dissertation/thesis has not previously been submitted for academic examination towards any qualification. Furthermore, it represents my own opinions and not necessarily those of the Cape Peninsula University of Technology.

Signed **Date**

▪ ABSTRACT

Solvatomorphism of an active pharmaceutical ingredient (API) is one of the most studied areas in pharmaceutical science. Since APIs are exposed to solvents during many stages of their production, knowledge of the consequences from such exposure is essential. Salt formation has been known to improve some physicochemical properties of an API. Amongst these properties, API solubility is one of the most important characteristics as their use in the market is determined by this feature. Research presented here investigated the solvates and salts of mefenamic acid (MA) and tolfenamic acid (TFA); both representing fenamic acids belonging to a class of non-steroidal anti-inflammatory drugs (NSAIDs). Solvates were obtained by reactions of TFA and MA with the solvents 2-picoline, 3-picoline, 4-picoline, 3-bromopyridine and 3-chloropyridine. A solvate polymorph of MA and 2-picoline was isolated. The salts were obtained by using diethanolamine, ethylenediamine, 1-methylpiperazine, and triethylamine in combination with the fenamic acids. Morpholine formed a salt with TFA, but not with MA. Instead a zwitterionic form of MA was synthesised when the latter was mixed with morpholine.

The resulting compounds were characterised and their crystal structures analysed. It was found that the conformation of the acids in the solvate and the salt compounds differed. Moreover, within the solvates, the conformation of the fenamate backbone varied depending on the acid and the solvent used for crystallisation. Although similar solvents were utilized, the structural packing arrangements of TFA solvates were very different from the arrangements associated with MA. The thermal analyses of the salts/solvates were determined by using both thermogravimetry and differential scanning calorimetry.

The compounds were further investigated after manual grinding and the preparation of slurries. These preparation methods were successful for most compounds but not for **MA•2PIC** and **$(MA^-)(EDM^+)$**. Instead, the recrystallization, grinding and slurry investigations of **MA•2PIC** yielded a polymorph of this particular solvate. In the case of **$(MA^-)(EDM^+)$**, the PXRD results obtained from both the pulverised and slurry samples were completely different from one another and also from those determined for the starting materials.

Generally, the desolvation studies of the MA salts and solvates produced the same crystal form as occurred in the starting material. The exception was **$(MA^-)(TA^+)$** wherein desolvation produced a mixture of two polymorphs of MA.

▪ ACKNOWLEDGEMENTS

I wish to thank:

- **God, for His infinite love,**
- **Professor Ayesha Jacobs, for her patience in helping me to complete this work,**
- **My friends, for their cheerful presence and help,**
- **The Cape Peninsula University of Technology, for increasing my knowledge and**
- **Any person who contributed to the accomplishment of this thesis directly or indirectly, may God bless you.**

▪ DEDICATION

I dedicate this thesis to my family and friends

▪ TABLE OF CONTENTS

○ LIST OF FIGURES

CHAPTER 1: INTRODUCTION

CHAPTER 2: EXPERIMENTAL PROCEDURE

CHAPTER 3: SOLVATES OF MEFENAMIC AND TOLFENAMIC ACIDS

CHAPTER 5: ZWITTERIONIC FORM OF MEFENAMIC ACID

▪ LIST OF TABLES

CHAPTER 1: INTRODUCTION

CHAPTER 2: EXPERIMENTAL PROCEDURE

CHAPTER 3: SOLVATES OF MEFENAMIC AND TOLFENAMIC ACIDS

CHAPTER 4: SALTS OF MEFENAMIC AND TOLFENAMIC ACIDS

CHAPTER 5: ZWITTERIONIC FORM OF MEFENAMIC ACID

▪ GLOSSARY

Terms/Acronyms/Abbreviations	Definition/Explanation
API	**Active pharmaceutical ingredient**
CSD	**Cambridge Structural Database**
HSM	**Hot stage microscopy**
DSC	**Differential Scanning Calorimetry**
TGA	**Thermogravimetry analysis**
PXRD	**Powder X-Ray Diffraction**
dslv	**desolvation**
MA	**Mefenamic acid**
TFA	**Tolfenamic acid**
2PIC	**2-Picoline**
3PIC	**3-Picoline**
4PIC	**4-Picoline**
3ClPYR	**3-Chloropyridine**
3BrPYR	**3-Bromopyridine**
DOHA	**Diethanolamine**
EDM	**Ethylenediamine**
MP	**1-methylpiperazine**
MOP	**Morpholine**
TA	**Triethylamine**
a, b, c	**Unit cell axes**
α	**Angle between b and c unit cell axes**
β	**Angle between a and c unit cell axes**
γ	**Angle between a and b unit cell axes**
V	**Unit cell volume**
Z	**Number of formula units per cell**
T_{on}	**Onset temperature**
D_{calc}	**Calculated density**
GOOF	**Goodness of fit**
R	**Universal gas constant**
E_a	**Activation energy**
h	**Hour**
mth	**Month**
T	**Temperature**
kJ mol^{-1}	**Kilojoules per mole**
β	**Heating rate**
bp	**Boiling point**
Exp	**Experimental**
Theo	**Theoretical**

Atoms colours

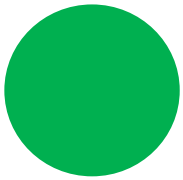

Bromine

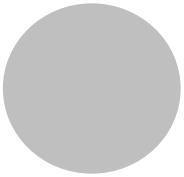

Carbon

Chlorine

Hydrogen

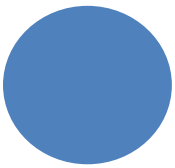

Nitrogen

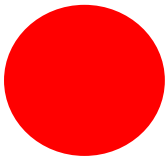

Oxygen

CHAPTER 1

INTRODUCTION

1.1 Supramolecular chemistry

1.1.1 Brief overview

Chemistry as an authentic science is diverse and multifaceted. Traditionally, organic and inorganic chemistry focus on the use of covalent bonds for the formation of molecules. Conversely, supramolecular chemistry is an extension of molecular chemistry wherein the formation of supramolecules results from non-covalent interactions (Barbour et al. 2012) (Figure 1.1). Lehn (2007) defined supramolecular chemistry as the chemistry based on composite units resulting from the interaction of two or more chemical species by means of non-covalent intermolecular forces. Moreover, Steed et al. (2007) described supramolecular chemistry as the study of compounds formed from molecules or ions bonded with one another through electrostatics, dispersion, hydrogen bonding interactions or solvophobic effects (Wang et al. 2013). Similarly, Moulton & Zaworotko (2001) indicated that the rational design of supramolecules relies on the potential of molecules to self-assemble by exploiting diverse forces. These latter forces may be hydrogen bonding, coordinate covalent bonds or aromatic π-stacking, charge transfer and electrostatic interactions (Bhattacharya & Saha, 2011; Wang et al. 2013).

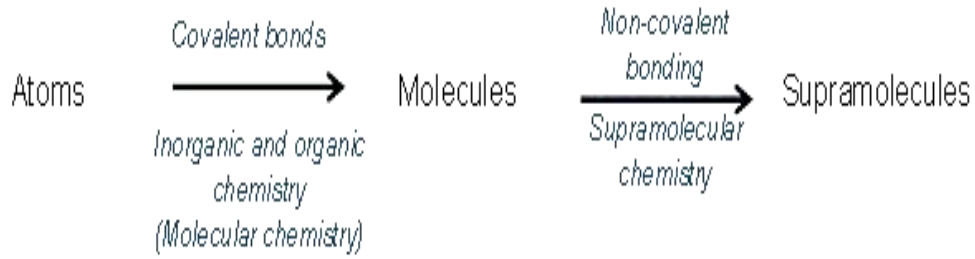

Figure 1-1: Molecular chemistry and supramolecular chemistry (adapted from Lehn, 2007).

1.1.2 Supramolecular synthons

Supramolecular synthons are referred to as the basic tools of supramolecular chemistry (Moulton et al. 2001). They are considered to be the principal building blocks for new compounds. Desiraju (1995) cited by Wang et al. (2013:10079) characterised supramolecular synthons as “structural units within supermolecules, which can be formed

and/or assembled by known or conceivable synthetic co-operation". These synthetic co-operations involve intermolecular interactions, which are predominantly hydrogen bonds because of their directionality, occurrence and strength (Nangia & Desiraju, 1998; Moulton & Zaworotko, 2001; Bhattacharya & Saha, 2011; Wang et al. 2013). Synthons enabled the creation of molecules with special properties and also pioneered other fields of study such as crystal engineering. Figure 1.2 illustrates the chemical structures of various supramolecular synthons.

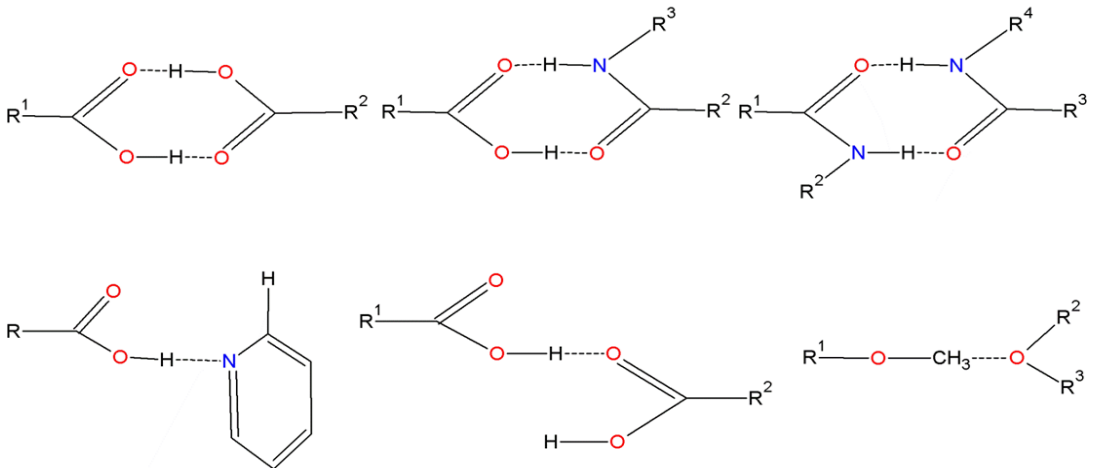

Figure 1-2: Chemical structural representation of some supramolecular Synthons (R is any organic or inorganic group) (adapted from Desiraju, 2011).

1.1.3 Host and guest compounds

During the formation of supramolecules, compounds meld as guest and host complexes or supramolecules. A host is defined by Steed & Atwood, (2009) as a large molecule or aggregate having a significant central hole and cavity. It is known as a "molecule containing convergent binding sites" (Steed & Atwood, 2000:3). On the other hand, any molecule or complex containing "divergent binding sites" is termed a guest (Steed et al. 2007; Steed & Atwood, 2000:3). A binding site on a host or guest is any segment of correct size, geometry and chemical nature that would interact or bind with the sites of the other species (Steed *et.al*. 2007:2). An example of a host-guest complex is an enzyme (host) and its substrate (guest).

Host-guest complexes are divided into two distinct classes and their differences are illustrated in Figure 1.3. The two classes are:

- Cavitands: the host has intramolecular cavities and the host-guest aggregate is termed a cavitate.
- Clathrands: the host has extramolecular cavities and the host-guest aggregate is termed a clathrate.

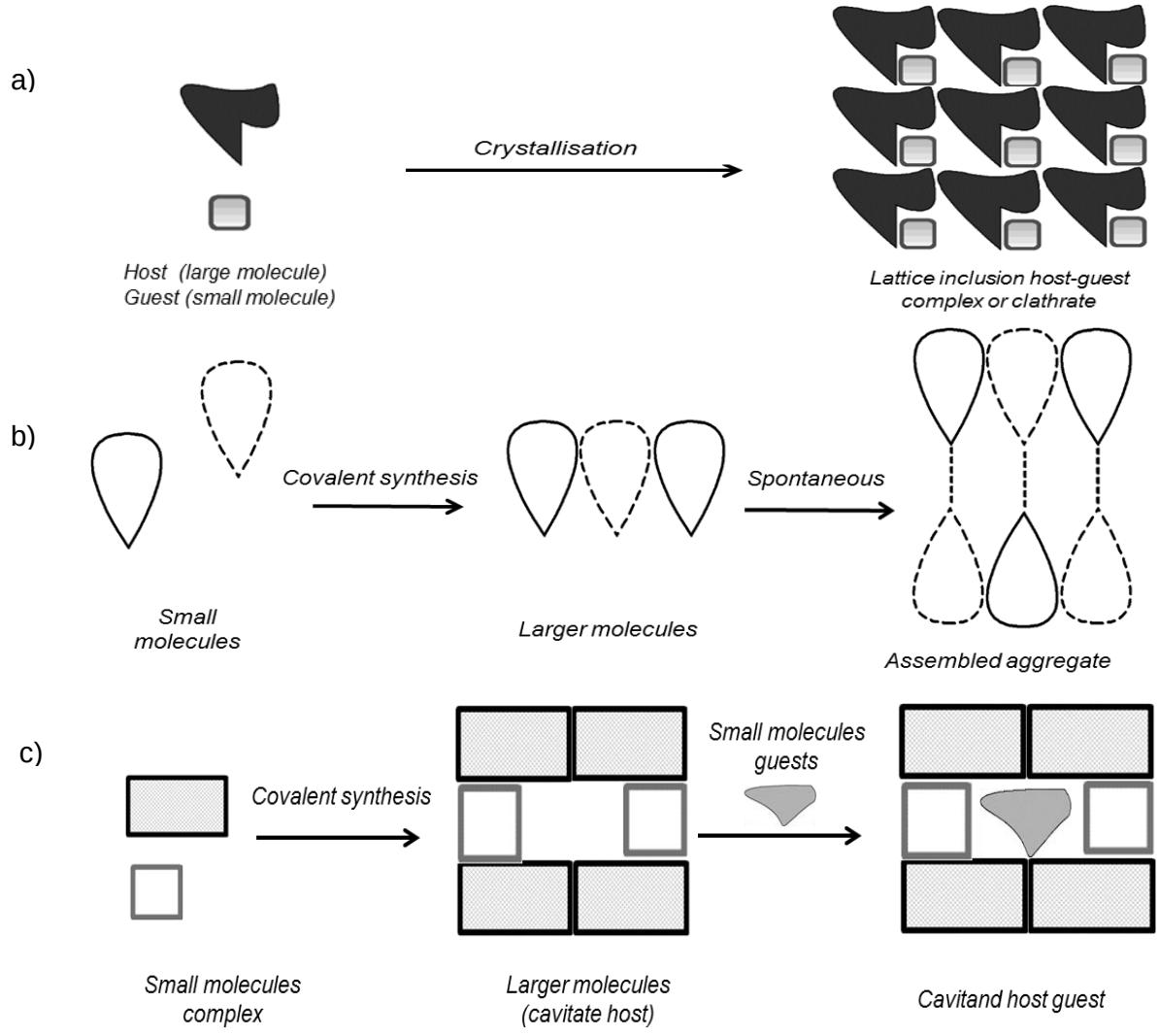

Figure 1-3: Differences amongst cavitate and clathrate complexes: a) Conversion of a clathrand into a clathrate through inclusion of the guest in the cavities of a host b) Self-assembly of a supramolecular aggregate and c) synthesis and conversion of a cavitate from a cavitand by the inclusion of a particular guest in the host cavity (adapted from Steed et al 2007:2).

1.2 Crystalline structures and their properties

Solids are divided into two different groups viz. amorphous and crystalline. Amorphous compounds are defined as solids with no definite regular internal structure (Snyder, 1966; Miller, 1972; Bauer et al. 2007; Brown et al. 2008). Barbour et al. (2012) described amorphous compounds as materials with too poor periodicity of their constituents to be considered crystalline. Crystalline solids are compounds with a defined arrangement of their components (Bassett et al. 1966; Snyder, 1966; Miller, 1972; Bauer et al. 2007; Bhattacharya & Saha, 2011; Barbour et al. 2012). They are categorised according to the types of forces, atoms and bonding involved in the formation of their structures. Generally, crystalline solids are divided into: covalent networks, ionic compounds, metallic compounds and molecular compounds (Drago, 1974: 202-205). These solids are identified by the type of intermolecular interactions in the crystal lattice which influence various properties such as melting point and conductivity.

1.2.1 Unit cells: basis of crystalline compounds

Unit cells are used to describe the shape of an internally repeating unit within crystalline compounds (Windle, 1977; Smith, 1982). Atkins (2000) presented the crystal lattice as species characterised by a space lattice formed by points representing the locations of molecules. In this case a unit cell is considered to be an imaginary parallelepiped containing one unit of a translationally repeating pattern of the lattice (Petrucci & Harwood, 1997: 419-457). It is the smallest repetitive arrangement of atoms occurring in a crystalline solid (Bassett et al. 1966; Miller, 1972; Brescia, 1975; Butler & Harrod, 1989; Chang, 2006: 376-395).

Unit cells define the entire crystal structure where the atoms are positioned at each end of the parallelepiped. They are mathematically described by the use of cell edges (a, b, c) and angles (α, β, γ) (Hammond, 2001). The angle between a and b unit cell axes is denoted α, the angle β is between a and c while the angle between b and c is denoted γ (Bassett et al. 1966; Butler & Harrod, 1989; Hammond, 2001). These different symbols describe the unit cell and lead to the seven crystal systems: hexagonal, triclinic, trigonal, tetragonal, monoclinic, cubic and orthorhombic (Butler & Harrod, 1989). Table 1.1 shows the different values of cell edges with the angles belonging to the primitive lattices combined with the

other seven important lattice structures called the fourteen Bravais lattices (Hammond, 2001).

Table 1-1: The fourteen Bravais lattices characteristics and parameters (adapted from Butler Harrod, 1989).

Crystal systems	Number of Bravais Lattices	Parameters	Possible type of unit cell
Hexagonal	1	a= b = c, α = β =90° γ = 120°	Primitive
Triclinic	1	a ≠ b ≠ c, α ≠ β ≠ γ	Primitive
Trigonal	1	a= b = c, α = β =γ <120 ≠ 90°	Primitive
Tetragonal	2	a= b ≠ c, α = β =γ = 90°	Primitive, body-centred
Monoclinic	2	a≠ b ≠ c, α = β =γ = 90°	Primitive, base- centred
Cubic	3	a= b = c, α = β =γ = 90°	Primitive, body-centred, face-centred
Orthorhombic	4	a≠ b ≠ c, α = β =γ = 90°	Primitive, body-centred, base-centred, face-centred

Depending on the arrangement of atoms in the crystal lattice, crystalline compounds show two behaviours: anisotropic and isotropic. Anisotropic crystalline materials present atoms spaced differently when viewed in any or all of the directions x, y and z. Conversely isotropic crystals have atoms with identical spacing and arrangement in all of the three planes (Butler & Harrod, 1989). Sodium chloride is an example of an isotropic crystal whereas quartz represents an example of anisotropic behaviour.

1.2.2 Types of crystalline solids

1.2.2.1 Ionic solids

Ionic compounds such as sodium hydroxide are formed from non-metal and metal atoms which are held together by the interaction of their charges (Dickson, 1975: 107 – 111). Drago (1974: 202-205) described ionic compounds as structures wherein cations and anions occupy the lattice sites and their opposite charges are used to bind them by means of electrostatic forces.

Ionic compounds usually exist as solid forms with hard and brittle characteristics (Miller, 1972; Bauer et al. 2007). Their melting point usually occurs between 300-1000 °C. These crystalline compounds are not malleable and tend to be non-volatile at room temperature (Clugston et al. 2002). The strong attraction between the ions and the polar heads of water molecules allows them to dissolve in water. Also, ionic solids conduct electricity in solution but do not when in the solid form (Miller, 1972; Clugston et al. 2002: 82-109; Bauer et al. 2007).

1.2.2.2 Molecular solids

Two non-metals held together by sharing of electrons or covalent bonding form the basis of a molecular compound (Pimentel & Spratley, 1971; Dickson, 1975: 107 – 111; Bloomfield & Stephens, 1996). When the molecular complexity of a substance increases, these compounds tend to be found in their solid forms at room temperature (Kotz et al. 2009).
Molecules in molecular solids are held together by weak intermolecular forces and therefore require less energy to disintegrate when compared with ionic compounds (Miller, 1972). Molecular solids are generally not good conductors of electricity (Clugston et al. 2002; Bauer et al. 2007; Brown et al. 2008).

1.2.2.3 Network covalent solids

Covalent network compounds are comprised of non-metals bonded by the sharing of electrons (Miller, 1972; Dickson, 1975: 107 – 111; Bloomfield & Stephens, 1996). Instead of having molecular bonding by means of weak interactions as occurs in molecular solids, the

atoms in these compounds form a regular extended network brought about by covalent bonding. Examples include diamond and graphite (Petrucci & Harwood, 1997: 419-457). As the entire crystal structure is a result of strong bonds, these compounds require much energy to decompose. Hence the boiling and melting points are unusually elevated (Miller, 1972; Petrucci & Harwood, 1997: 419-457; Bauer et al. 2007).

Covalent network compounds are characteristically insoluble. This is attributable to the difficulty associated with dissolving these large molecules (Clugston et al. 2002). Electrons in these compounds are delocalised and move freely in the different layers formed by the non-metals. Therefore, these compounds are known to conduct electricity in the direction of the electrons. Graphite is an example and is often used as an electrode in batteries (Pimentel & Spratley, 1971; Bauer et al. 2007).

1.2.2.4 Metallic solids

Metallic solids are characterized by metals bonded together by the use of metallic bonds. An example would be zinc coating or brass alloy. In metallic solids, electrons have the tendency not to remain between atoms but instead they travel throughout the solid (Bassett et al. 1966; Miller, 1972). This leads to the delocalization of electrons, and positive metal nuclei float around in an ocean of negative electrons termed an electron sea. Consequently, the positive ions remain immersed in the sea and occupy the lattice positions of the solid.

Due to the strong attractive forces between the metals, these solids have high melting and boiling points. These forces also give rise to very dense solids associated with a low volatility (Miller, 1972; Clugston et al. 2002: 82-109). The cations in the sea of electrons are able to slide within the solid and do not disrupt the strong bonds within the crystal. The result is that unlike covalent bonds, metallic solids are not stiff or brittle but are rather soft, malleable and ductile. They have the ability to conduct electricity because of the delocalization of the electrons (Clugston et al. 2002).

1.2.3 Intermolecular interactions

Intermolecular interactions are interactive forces found between molecules, whereas intramolecular interactions involve connections between atoms within a molecule (Bauer et al. 2007; Chang, 2006: 376-395). The state of matter is determined by the strength of these

interactions. For example, weak intermolecular forces between molecules would allow the matter to occur in a gaseous state but as the interactions increase in strength the resultant compounds can condense to form liquids or solids (Kotz et al. 2009). In supramolecular chemistry, the use of intermolecular interactions is associated with the formation of new compounds caused by the bonding of molecules using supramolecular synthons.

1.2.3.1 Ion-ion interactions

Ion-ion interactions (energy: 200-300 kJ mol^{-1}) refer to the forces existing between two ions in ionic crystals (Kotz et al, 2009; Clugston et al. 2002). The strength of an ionic bond is comparable to that of a covalent bond. Thus a large amount of energy is necessary for the breaking of the bonds between atoms. Figure 1.4 illustrates one type of ionic interaction observed in tetrabutylammonium chloride.

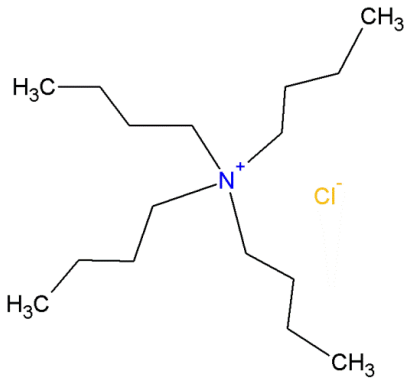

Figure 1-4: Tetrabutylammonium chloride ion-ion interaction (adapted from Steed & Atwood, 2000).

1.2.3.2 Van der Waals interactions

Van der Waals interactions (energy: < 5 kJ mol^{-1} depending on the surface area) are general forces that occur among neutral atoms or molecules. Also called London forces, they are responsible for the bonding which is found in the solid state of rare gases, organic molecules and non-charged carbon layers (Kotz et al, 2009). According to Steed and Atwood, 2009, these forces represent the weak electrostatic attraction that occurs when a polarised

electron cloud is close to a nucleus. Van der Waals interactions vary with the size of the molecule and are inversely proportional to the sixth power of the distance.

These interactions are balanced by repulsive forces and tend to give shape to molecules, thus making them useful for shaping crystals. Van der Waals forces are moderately weak, dispersive and isotropic thereby leading to low melting and boiling points (Eerdenbrugh & Taylor, 2011). Steed and Atwood (2009) showed the importance of these forces in chemistry as they are utilised to include small molecules within the crystal lattice of particular compounds or hosts.

1.2.3.3 Dipole-dipole interactions

Dipole-dipole interactions (Energy: 5-50 kJ mol^{-1}) are exhibited by contact between polar molecules (Kotz et al. 2009). As a consequence, the resulting modified species attract each other through the charge interaction. The attraction can also result from the interaction of "dipoles located on adjacent molecules or the opposing alignment of one dipole with the other" (Steed & Atwood, 2000:22). Figure 1.5 shows an example of this type of interaction where the acetone dipole moment is illustrated.

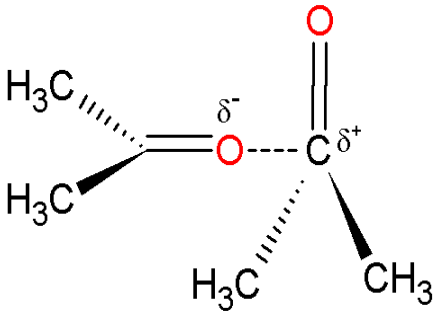

Figure 1-5: Acetone dipole-dipole moment (adapted from Steed et al. 2007).

1.2.3.4 Ion-dipole interactions

When ions bond with polar molecules, forces of attraction are generated between them and this leads to an ion-dipole interaction (energy: 50-200 kJ mol^{-1}) (Clugston et al. 2002). It can also result from ions dissolved in water (common polar compound) or any polar solvent. These ions would tend to be surrounded with the solvent molecules (Figure 1.6) and are

thus stabilized (Kotz et al, 2009). However, this type of bonding can also be observed in solids as well as in liquids e.g. cation-binding hosts and metal complexes illustrated in Figure 1.6.).

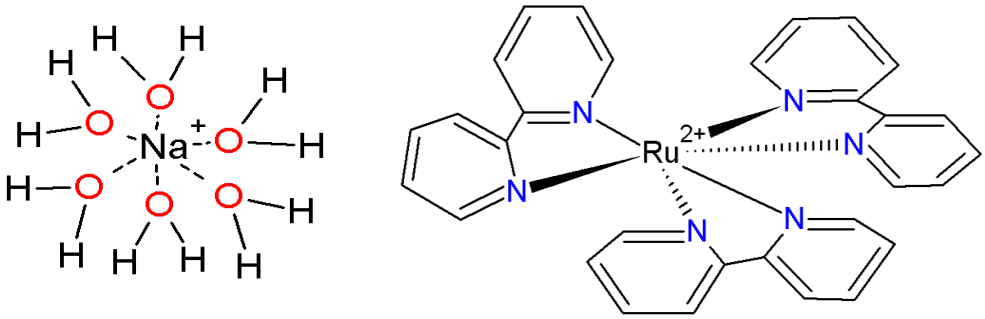

Figure 1-6: Ion-dipole interaction for cation-binding hosts, solvation and metal complexes (adapted from; Steed et al. 2007; Steed & Atwood, 2009).

1.2.3.5 Cation-π interactions

Benzene is an aromatic compound characterised by an electron-rich π-system. Six local $C^{\delta-}$-$H^{\delta+}$ bonds around the aromatic group are usually created by sp^2 carbons. When these bonds are added, an overall charge distribution is formed resulting from the build-up of negative and positive charges in the centre and edges of the benzene aromatic ring (Lindoy and Atkinson, 2000; Atwood & Steed, 2004). Therefore, any cation with a positive charge would be attracted to the negative electrostatic charge on the face/outside of the benzene ring (Lindoy and Atkinson, 2000; Steed & Atwood, 2009). This gives rise to an interaction between a cation and an electron rich π-system or a cation-π interaction (energy: 5-80 kJ mol^{-1}). Figure 1.7 represents cation-π interactions with the use of benzene as an electron rich π-system.

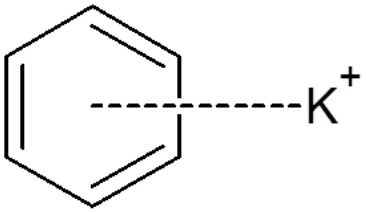

Figure 1-7: Interaction of potassium with a benzene ring (adapted from Dougherty, 2007).

1.2.3.6 The π-π interactions

The π-π interactions (energy: 0-50 kJ mol^{-1}) refer to interactions occurring between aromatic rings. They commonly arise when one aromatic ring has a relatively high electron density when compared to another (Steed & Atwood, 2009). Two general groups of π-π interactions are usually observed: face to face and edge to edge interactions. Edge to edge interactions occur when a weak hydrogen bond is formed between the slightly electron deficient hydrogen atom and the electron-rich π-cloud of aromatic compounds. A face to face interaction is observed when two faces of aromatic compounds interact with one another (Atwood & Steed, 2004; Steed & Atwood, 2009). An example of face to face interactions is shown in Figure 1.8.

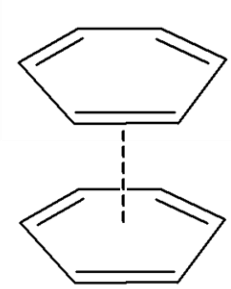

Figure 1-8: Examples of face to face π-π interactions (adapted from Steed et al. 2007).

1.2.3.7 Hydrogen bonding (4-120 kJ mol^{-1})

Hydrogen bonding is an unusual type of dipole-dipole interaction whereby the hydrogen is one of the atoms belonging to one of the interacting species (Petrucci & Harwood, 1997: 419-457; Clugston et al. 2002; Chang & Goldsby, 2014; Chang, 2006, Dhotel et al. 2013). Usually, it is characterised by an electrostatic interaction existing between hydrogen and an electronegative atom located on a different compound (see Figure 1.9) (Brescia, 1975; Clugston et al. 2002; Bauer et al. 2007; Kotz et al, 2009). Normally, the large difference in electronegativity creates a partially positive charge on the hydrogen atom when bonded to a highly electronegative species. Consequently, when an element with partial negative charge

is in the vicinity of this charge, an attractive force is created and the hydrogen bonds to that atom (Bloomfield & Stephens, 1996).

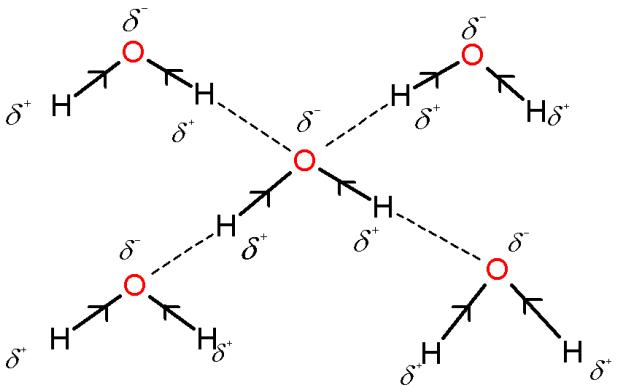

Figure 1-9: Illustration of the formation of hydrogen bonding in water.

For the interaction to occur there must be two different components; a donating and an accepting species. The typical functional groups forming hydrogen-donating assemblies are: O-H, N-H, C-H, Br-H and Cl-H (Atkins et al. 2000; Kotz et al. 2009). Alternatively, acceptor groups such as N, O, Cl, Br, P, S or aromatic-π systems have the ability to attract the hydrogen atom. An example of hydrogen bonding observed during the progress of the research reported on here can be observed in Figure 1.10 and its description is presented in Chapter 3.

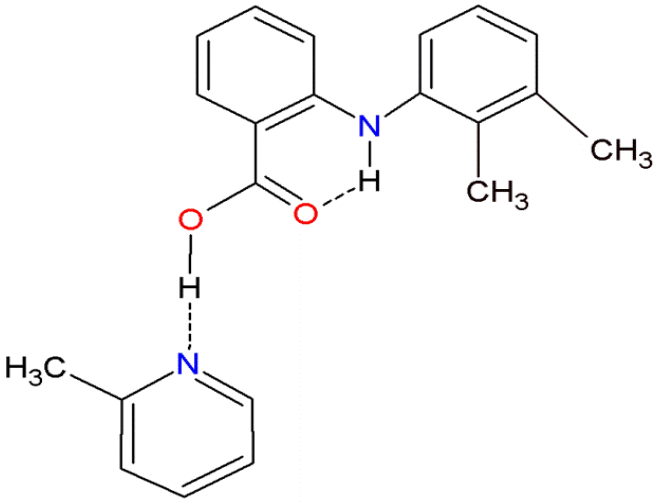

Figure 1-10: Hydrogen bonding observed in mefenamic acid with 2-picoline solvate.

Hydrogen bonding can be represented as D-H•••A, where D-H represents the donor group and A the acceptor (Desiraju et al. 2011). The distance D•••A and the angle between donor and acceptor may be used for the identification of the type of atoms bonded to the hydrogen. According to Steed and Atwood (2009: 28-31) “hydrogen bonding is characterised by a multitude of strengths, lengths and geometries” depending on the atoms to which the hydrogen is attached (see Table 1.2). Weak hydrogen bonds such as C-H•••O are important in stabilising the structure of lattices. The following summary represents the strength and energy required to break a hydrogen bond, depending on the attached atom.

Table 1-2: The properties of hydrogen bonds (adapted from Desiraju et al. 2011).

Strength	Examples	D•••A/Å	H•••A/Å	D-H•••A/°
Weak	C-H•••O	3.0-4.0	2.0-3.0	110-180
Strong	O-H•••O-H	2.6-3.0	1.6-2.2	145-180
	O-H•••N-H	2.6-3.0	1.7-2.3	140-180
	N-H•••O=C	2.8-3.0	1.8-2.3	150-180
	N-H•••O-H	2.7-3.1	1.9-2.3	150-180
	N-H•••N-H	2.8-3.1	2.0-2.5	135-180
Very strong	$[F\text{-}H\text{-}F]^-$	2.2-2.5	1.2-1.5	175-180

Hydrogen bonding is one of the most important tools for a crystallographer to build new compounds due to its affinity (strength), directionality, hydrophobicity and reversibility (Braga & Grepioni, 2000; Braga & Grepioni, 2005; Eerdenbrugh & Taylor, 2011; Lemmerer et al. 2011; Dey et al. 2012; Cunha et al. 2013; Dhotel et al. 2013; Wasio et al. 2015). According to Bhattacharya & Saha (2011) supramolecular chemistry is heavily dependent on non-covalent interactions originating from hydrogen bonding and van der Waals forces. Similarly, Braga and Grepioni (2000: 602-603) showed that the directionality of a hydrogen bond is essential for the “reproducibility and construction of new solids passing from one supermolecule to another”. Moulton & Zawarotko (2001) supported the idea of Desiraju

(1995) that hydrogen bonding is a key element in crystal design due to its strength and directionality. These statements indicate the importance of hydrogen bonding in supramolecular chemistry with regard to the design of novel useful compounds.

Recently halogen bonding has been the subject of several analyses as it has characteristics similar to hydrogen bonding (Desiraju 2011; Ji et al. 2011; Amombo Noa et al. 2015). It is described as an alternative to hydrogen bonding and metal ion coordination (Ji et al. 2011). This non-covalent contact results from the electrostatic interaction between a polarized halogen and any negatively polarised species situated close to the halogen (Desiraju et al. 2011).

1.3 Crystal engineering

As a subdivision of supramolecular chemistry, crystal engineering is described as a modern and important implement for the synthesis of non-covalent compounds (Desiraju & Gavezzotti, 1989; Desiraju, 2013; Jacobs & Amombo Noa, 2015). As Khan et al. (2010) stated, the fundamental behaviour of crystalline materials originates from both the structural arrangements within the solid and the diverse interactions amongst molecules. This allows scientists to comprehend the relationship between structure, characteristics and functions of materials to be analysed. Additionally, crystal engineering regroups the understanding of intermolecular interactions and their applications in the formation of improved and sophisticated superstructures with the desired chemical and physical characteristics (Seddon and Zaworotko, 1999; Braga et al. 2005; Steed et al. 2007; Desiraju, 2013).

Crystallography is a branch of physics that is particularly focused on the investigation of atomic and molecular structures. The discovery of X-rays circa in1895 and the effects of X-ray diffraction circa 1912 by Max Laue, Walter Friedrich and Paul Knipping stimulated the growth of this field (Kovalchuk, 2011). Its launch was propelled by William Lawrence Bragg and William Henry Bragg in 1912 when they discovered how the observed diffraction pattern could be used to determine the positions of atoms in a crystal. That discovery helped in the description of the crystal lattice of some minerals like diamond in 1913.

Today crystals are used for many different purposes which include their applications in different areas such as drug design and organic electronics (Saha et al. 2015). This allows for the design of solvates, co-crystals, salts and polymorphs (Figure 1.11).

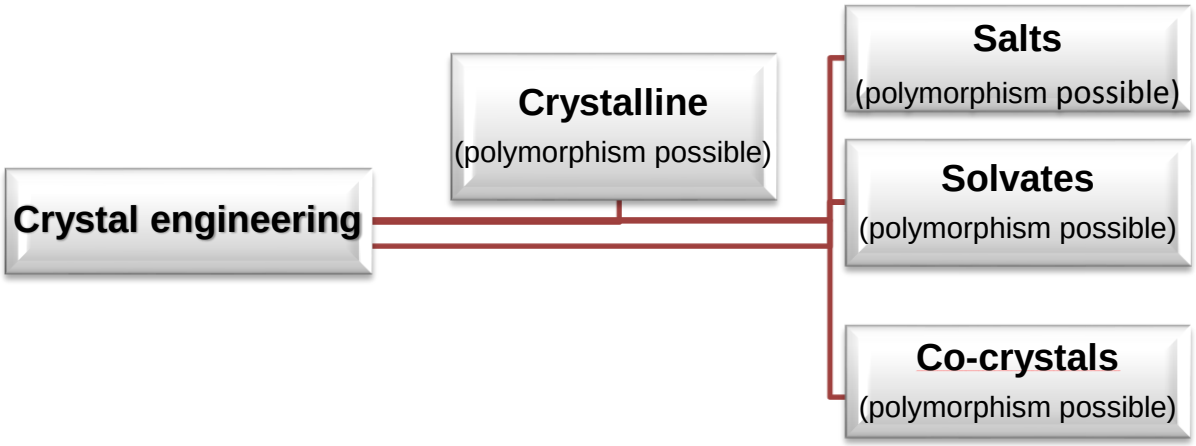

Figure 1-11: The formation of new compounds with improved physicochemical properties through the use of crystal engineering (adapted from Kovalchuk, 2011).

1.3.1 Polymorphism

"Polymorphism" is derived from two Greek words viz. "poly" which refers to multiple and "morfé" which refers to shape (Kratochvíl, 2011: 129–140; Barbour et al. 2012). In general, polymorphism is defined as the existence of many forms of a particular compound (Morissette et al. 2004; Kato et al. 2006; Lee et al. 2006; Nauha et al. 2009; Bhattacharya & Saha, 2013; Wei et al. 2013). Furthermore, Lee et al. (2011:260) stated that in their solid forms, "molecules may adopt more than one packing arrangement and/or conformation in the crystal lattice". Chemical compounds have a tendency to rearrange themselves when conditions surrounding them are altered. At times, the same crystalline structure arises, but it is apparent that structures with different structural arrangements can on occasion also be formed. Such is the case with polymorphism. Figure 1.12 illustrates the general structural arrangement of two different polymorphs. Alterations in certain experimental conditions such as temperature, or the solvents used to induce crystallisation can cause a rearrangement of the molecules.

Figure 1-12: The general structural arrangement of two different polymorphs (adapted from Braga & Grepioni, 2005).

It is generally recognised that there are two classes of polymorphism viz. packing and conformational. Conformational polymorphs group molecules with more than one conformation within the solid state. An example is the solvate of MA with 2-picoline, as will be discussed in Chapter 3 (Figure 1.13) where form II showed a conformation and packing arrangement different from the ones observed in form I. Packing in polymorphs consist of diverse arrangements of conformationally rigid molecules (Lee et al. 2011). Examples include the antidepressant venlafaxine hydrochloride (Effexor), the antipsychotic olanzapine (Zyprexa) and the antibacterial sulfonamide sulphapyridine (Lee et al. 2011; Kratochvil, 2011: 129–140).

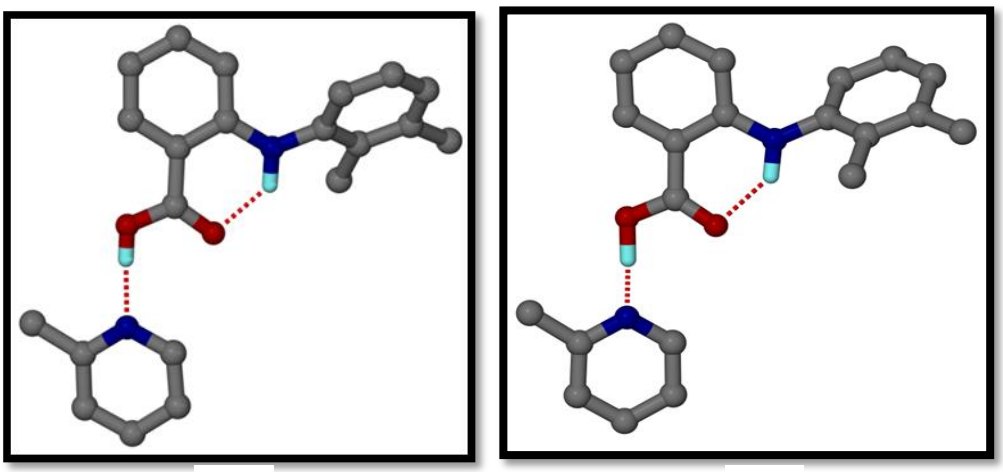

Figure 1-13: Polymorphism observed in solvate of mefenamic acid with 2-picoline; Form I (a) and Form II (b)

Bhattacharya & Saha (2013) reported that the form of every polymorph can be regarded as a unique compound with specific physical and chemical characteristics. This is primarily due to a difference in internal structure which causes variable performance and properties in a specific compound (Fantin et al. 2003; Lee et al. 2006; Kratochvil, 2011: 129–140). As Kratochvil (2011:138) stated “the progress in the theory of chemical bonds, prediction of crystal structures and the development of supramolecular chemistry enable better understanding of polymorphism”.

1.3.2 Solvates

Solvates are one of the simplest forms of inclusion compounds observed by scientists. They are formed from one or more solvent molecules incorporated in a specific stoichiometry within a crystal lattice (Aitipamula et al. 2011; Kratochvíl, 2011: 129–140; Aitipamula et al. 2012; Vangala et al. 2013; Wei et al. 2013). Solvates are also referred to as host-guest complexes where the solvent molecules are included in the voids created by the packing of another compound (Desiraju, 2011; Barbour et al. 2012).

The precise process of solvent inclusion is not understood. Bacchi et al. (2008) showed that the ability of a guest to be included in the porous framework of a host is usually dependent on the size and shape of the guest. Thus, solvent inclusion is reliant on the molecular solid state organization of the guest and its structure. Furthermore, the formation of solvates is also based on the incorporation of the solvent into the host framework to fill the voids and therefore generate close packing (Figure 1.14) (Barbour et al. 2012). In the latter case, a number of factors must be taken into consideration. These include the temperature of crystallization and the type of solvent used for a specific host. For instance, an organic base such as 2-picoline could be used as a solvent for inclusion into the molecule of an acid host (fenamate) (Wei et al. 2013). The interaction between the acid and the base enables the inclusion of the solvent in the crystal lattice (Desiraju et al. 2011). Additionally, solvates could be formed due to an increase in the packing efficiency without any specific host-guest interactions for the purpose of lattice stabilization. This uncontrollable process can cause problems in the reproduction of compounds due to the simultaneous formation of variable phases (Bhattacharya & Saha, 2013).

Solvatomorphism is the process of the inclusion of a solvent in a crystal lattice of any compound (Barbour et al. 2012). Most pharmaceutical chemists prefer the use of pseudo-polymorphism (false polymorphs) which Barbour et al. (2012) cautioned against. This author

pointed out that as solvates are inclusion compounds or crystals, it is not advisable to name them false polymorphs or pseudo-polymorphs.

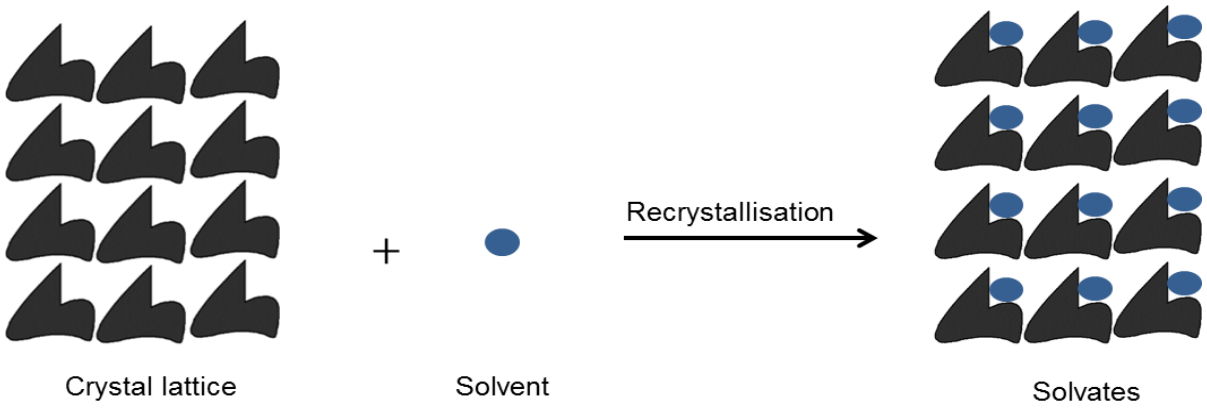

Figure 1-14: Formation of a solvate from any crystalline compound mixed with solvent (adapted from Braga & Grepioni, 2005).

The inclusion of organic molecules into compounds is important in the production of food or pharmaceutical products as many complexes are usually exposed to organic solvents during production and processing (Aitipamula et al. 2011; Wei et al. 2013). Hence, during the production of drug or food material, the solvent could be included in the new composites (Aitipamula et al. 2011; Aitipamula et al. 2012; Byard et al. 2012; Chadha et al. 2012) Vangala et al. 2013; Wei et al. 2013). It is possible that the included solvent could alter certain properties of the drug or food material which may be undesirable. Properties which are altered could include physical properties such as solubility, density, dissolution rate as well as bioavailability (Vishweshwar et al. 2006; Chavez & Rousseau, 2010; Aitipamula et al. 2012; Douillet et al. 2011; Vangala et al. 2013; Wei et al. 2013). An example of this is the difference observed in the aqueous solubility of the anhydrous and trihydrated forms of ampicillin as reported by Wei and co-workers in 2013. It was observed that the concentration of the anhydrous form in blood serum was far higher than that observed for the trihydrated form (Wei et al. 2013). This could then impact on the different stages of processing during manufacturing and on the safety, quality and performance of the final product (Byard et al. 2012).

Desolvation studies were carried out by many scientists since the outcome of this experiment can lead to the formation of a polymorph of the starting material (Aitipamula et al. 2011; Byard et al. 2012). Each polymorphic form of an active pharmaceutical ingredient (API) has specific characteristics. Therefore, knowledge of the composition of the resulting

product of a desolvation study is important to prevent unwanted side effect of drugs (Suitchmezian et al. 2006).

1.3.3 Salts

Salts are defined as ionic substances arising from the transfer of a proton between two compounds (Jampilek & Dohnal, 2012). An ionic form of an API is usually the preferred solid state product of a drug material since most medicines on the market are distributed in the form of a salt (Serajuddin, 2007; Stahl & Wermuth, 2008; Jampilek & Dohnal, 2012). For any proton transfer (H^+) to occur a base B and an acid A-H are required. The reaction taking place could be expressed as follows:

$A\text{-}H + B \rightarrow (A^-)\ (B^+\text{-}\ H)$

In this case, the base acts as the guest and the acid as the host. In the diagram below, the example given is a salt formed during the course of this study (chapter 4) (Figure 1.15).

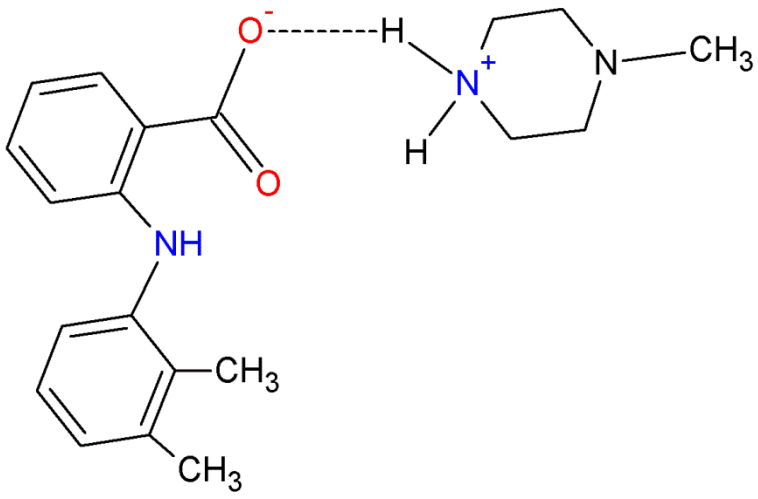

Figure 1-15: Salt formed from mefenamic acid with 1-methylpiperazine interacting through hydrogen bonding.

The formation of a salt depends on the differences of the pK_a values between the base and the acid. For a ΔpK_a above 2.7, proton transfer would occur, but if the ΔpK_a is less than 2.7, the resulting neutral crystal is referred to as a co-crystal (Sekhon, 2009). To validate the pK_a rule, Cruz Cabeza (2012) carried out a study on several acid-base crystalline complexes. A

linear relationship was then established whereby the ΔpK_a and salt formation of the different complexes was found to be in the range of -1 and 4. Conversely, other studies showed that a salt is expected to be produced when the ΔpK_a is greater than 2- 3 which also agreed with the findings of Seckon, (2009) (Bastin et al. 2000; Stahl & Wermuth, 2008). Bastin et al. (2000) found that a minimum difference of 3 units between the pK_a values of the two starting materials should be present in order to form a stable salt. The stability of the salt is essential. Should an unstable salt occur, there could be an undesirable reversion to the original structure. Serajuddin, (2007) showed that when salts of compounds are formed, the stability is superior to that of the starting material. This stability is dependent on the interrelationships of several factors, including intrinsic solubility, pH, K_{sp} (solubility product) and pH_{max} (pH of maximum solubility).

According to Douillet et al. (2012) salt formation offers the simplest and most cost effective technique to alter the solubility and bioavailability of compounds. Moreover, salts rather than a free acid or base are selected as these improve both crystallinity and various physical properties of a pharmaceutical compound (Serajuddin, 2007; Sekhon, 2009; Cruz-Cabeza, 2012; Elder et al. 2013). In 2010, Elder et al. reported mesylate salts to be the most soluble of the amine drugs. These authors showed by means of analyses of salts that the solubility of delveridine mesylate increased over 2000 fold when compared to the free base form. In the production of pharmaceutical drugs, salts improve both the purity and isolation of an API. Furthermore, some of the side effects such as toxicity and irritancy of a drug were reduced in the process (Serajudin et al. 2007).

1.3.4 Selected studies on polymorphs, solvates and salts

Numerous studies have been done which focused on various characteristics associated with polymorphism, salts and solvatomorphism of selected compounds. Some of these are summarised in Table 1-3.

Table 1-3: Examples of various reported polymorphs, solvates and salts.

Authors	Year	Findings
Suitchmezian et al.	2006	• Solvates of triamcinolone diacetate.
Nauha et al.	2009	• Two different polymorphs were found where form I was discovered to be thermodynamically more stable than form II although their melting points were similar. • In addition, fourteen solvates of thiophanate-methyl were also reported.
Aitipamula et al.	2011	• Six solvates of sulfamerazine were characterised by means of thermochemical and desolvation studies.
Douillet et al.	2011	• Reported a solvate and exposed the risks of desolvation during the washing process. • They also found that the kinetics study allowed the understanding of the key parameters needed to design a robust process.
Aitipamula et al.	2012	• Characterised a monohydrate and five solvates of 2-chloro-4-nitrobenzoic acid.
Jacobs et al.	2013	• Kinetics of decomposition of (+)-deoxycholic acid salts were reported along with the correlation of some of these salts with their structural and thermal results.
Vangala et al.	2013	• Desolvation studies revealed that the removal of the pyridine and picoline solvents produced a thermodynamically stable nitrofurantoin compound in its β-form.
Wei et al.	2013	• Pseudopolymorphism transition points at various temperatures of meropenem in methanol-water mixture.
Jacobs et al.	2014	• Salt structures and thermal stability were obtained from a scissor-shaped racemic host with some amine solvents. • They found that the host formed constant hydrogen bonded rings involving the associations of two dicarboxylate anions and cations.

1.4 Fenamates: mefenamic acid and tolfenamic acid

Mefenamic, tolfenamic, flufenamic, niflunemic and meclofenamic acid are substances which belong to a group of antibiotics called fenamates. The latter are anti-inflammatory drugs (NSAIDs) (Nawaz et al. 2007; Surov & Surov, 2008; Fábián et al. 2011; López-Mejías et al., 2012; SeethaLekshmi & Guru Row, 2012; Surov et al. 2015). As derivatives of *N*-aryl-anthranilic acid, fenamates contain two important functional groups viz. the carboxylic acid and the amine groups (Figure 1.16) (Fábián et al. 2011; López-Mejías et al., 2012).

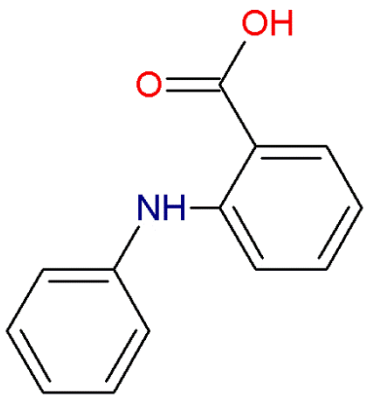

Figure 1-16: Schematic diagram of a fenamic acid (adapted from Wittering et al. 2015).

These substances have both basic and acidic properties. Hence they are able to donate and accept protons. Intermolecular dimerization of carboxylic acid groups presents a robust homomeric synthon. The carboxylic acid group has been used to assemble and order molecules (Fábián et al. 2011; Bacchi et al. 2014; Wasio et al. 2015). In addition, Ohlan et al. (2013) indicated that the ability of carboxylic acid groups to form directional and robust synthons with other compounds makes these the focus of many studies. Similarly, Fábián et al. (2011:3522) reported that "carboxylic acids form strong hydrogen bonds with nitrogen atoms in heteroaromatic rings" and this property favours their use in the formation of numerous supramolecular heterosythons.

According to Pentikainen *et al.* (1981) fenamates have been claimed to exert an inhibitory action on prostaglandin inhibitors (Krishna Murthy et al. 1982; Dhanaraj & Vijayan, 1983). Fenamates can be used for the treatment of other diseases and this is dependent on the nature of the substituents attached to the parent group,

1.4.1 The chemical structure of mefenamic and tolfenamic acids

Mefenamic acid (MA) is the most commonly used fenamate. The structure of this acid is comprised of two methyl groups attached to the parent compound (Figure 1.17). Tolfenamic acid (TFA) is similar in structure to MA but a chlorine atom replaces one of the two methyl groups, at the *meta*-position (Figure1.17).

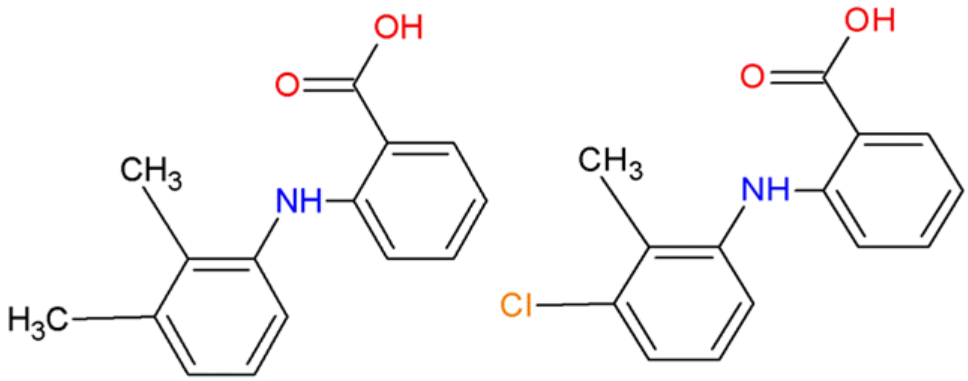

Figure 1-17: Schematic diagrams of mefenamic and tolfenamic acids (adapted from Fábián et al. 2011).

1.4.2 The clinical uses/properties of mefenamic and tolfenamic acids

Mefenamic acid is one of the non-steroidal anti-inflammatory drugs (NSAIDs) which are used to treat inflammatory diseases (Fang et al. 2004; Kato et al. 2006; Lee et al. 2006; Nawaz et al. 2007; SeethaLekshmi & Guru Row, 2012; Serap & Cihan, 2012). Mefenamic acid acts by inhibiting cyclooxygenase (COX). The latter enzyme limits the conversion of arachidonic acid to prostaglandins (Tantishaiyakul et al. 2002; Nawaz et al. 2007; SeethaLekshmi & Guru Row, 2012). Prostanoids (which consist of prostaglandins) are a group of complex fatty acids in the cellular system of human beings or animals derived from arachinoids (Ricciotti & FitzGerald, 2011). According to Moilanen, (1989:342) “prostanoids act as mediators in acute inflammation” and they are “involved in the pathogenesis of rheumathoid arthritis”. High concentrations of prostaglandins were observed to be present in synovial fluid extracted from patients who were diagnosed with rheumathoid arthritis. The use of MA which prevents the synthesis of these compounds assists in the healing process of patients suffering from this condition.

Other studies indicated that prolonged consumption of MA by patients with rheumathoid arthritis reduced the risk of their succumbing to Alzheimers disease. Joo et al. (2006) studied the effects of MA on patients suffering from Alzheimer disease. It was found that MA decreased the neurotoxicity of various peptides in neuronal cells. This suggested that MA has potential for the therapy of patients suffering from Alzheimers disease (El-Sisi, 2011).

Research done elsewhere showed that MA could be used for the reduction of menorraghia during menstrual periods in women between the ages of 30-40 years (Bonnar & Sheppard, 1996).

Tolfenamic acid has properties and a mode of action similar to those of MA as it is also an NSAID. Tolfenamic acid inhibits Cox-2 (Eslin et al. 2013; Gaglioti et al. 2014). In addition, it was reported that TFA can be clinically used for the treatment of dysmenorrhea, migraine and rheumatic diseases (Pentikaien et al. 1981). Cafaggi et al. (2008) stated that TFA can be used to treat inflammatory diseases and pain caused by rheumatic and non-rheumatic diseases.

The analgesic and antipyretic properties of TFA are the reasons for its extensive use in both human and veterinary medicine (Gaglioti et al, 2014). Research has also been done to investigate its role in the treatment of Alzheimer's disease and the impact that it could have on the conductivity of ionic channels to the brain (Subaiea, 2013; Subaiea et al. 2013; Adwan et al. 2014; Adwan et al. 2015). According to Cafaggi et al. (2008), new studies have been reported wherein TFA was used to treat pancreatic, lung, ovarian and prostate cancers (Cafaggi et al. 2008; Eslin et al. 2013)

1.4.3 Selected reported studies of mefenamic and tolfenamic acids

Over the years, fenamates have been investigated for their structural characteristics as co-crystals, solvates and salts. Their clinical characteristics were also investigated. Some of these studies are summarised in Table 1-4.

Table 1-4: Examples of studies done on mefenamic and tolfenamic acids.

Authors	Year	Findings
Keinänen et al.	1978	• The antipyretic activity of mefenamic acid, tolfenamic acid and flufenamic acid were studied. • After comparison of the free drugs, tolfenamic acid was found to be the most potent antipyretic agent.
Moilanen	1989	• The effect of tolfenamic acids and other compounds on the production of prostanoids. • Differences in prostanoid production between healthy and rheumatic synovial cells were diminished considerably by the use of those analgesics.
Pop et al.	2002	• Two inclusion compound models were found when β-cyclodextrin was mixed with mefenamic acid using a high-resolution synchrotron powder-diffraction method combined with molecular mechanics
Tantishaiyakul et al.	2002	• Synthesized mefenamic acid-guiacol ester was reported and was found to have the properties of a prodrug, due to the hydrolysis studies that were done.
Fang et al.	2004	• The characteristics of the physiochemical properties of mefenamic acid with alkanolamines (propanolamine, diethanolamine and triethanolamine) were reported. • They found that some hydrophilic and hydrophobic regions existed which caused those complexes to be more soluble compared to the parent compound.
López-Mejías et al.	2009	• Pentamorph of tolfenamic acid
SeethaLekshmi & Guru Row	2012	• Investigated a new polymorph of mefenamic acid during a co-crystallisation attempt. • Solvate of mefenamic acid with dimethylacetamide was reported.
Surov et al. and Wittering et al.	2015	• Reported co-crystals of tolfenamic acid and mefenamic acid with 4,4-bipyridine • Structural similarities between the co-crystals of the two acids were observed

1.5 Objectives of the study

Research into solvates obtained from active pharmaceutical ingredients is increasing. According to Aitipamula et al. (2012) solvates have been extensively studied during the recent past because the inclusion of a solvent in a crystal lattice could alter important physiochemical characteristics of drugs. This would include: improvements in chemical stability which could enhance the benefits of the resulting drug. However, the salts of APIs are the form most commonly selected for commercial use since the solubility of the product is much improved when in the form of a salt. Therefore, the objectives of this study were to:

- Prepare solvates and salts of selected fenamic acids,
- Characterise these new crystalline compounds by using thermal analysis,
- Elucidate structures using single crystal X-Ray diffraction,
- Develop different methods for solvate/salt preparation,
- Study the kinetic behaviour of the resultant solvates/salts,
- Study the desolvation process of the solvates/salts and
- Study the physical changes of the solvates/salt through hot stage microscopy.

Bibliography

- Adwan, L., Subaiea, G.M., Basha, R. & Zawia, N.H. 2015. Tolfenamic acid reduces tau and CDK5 levels: implications for dementia and tauopathies. *Journal of Neurochemistry*, 133(2):266–272.
- Adwan, L., Subaiea, G.M. & Zawia, N.H. 2014. Tolfenamic acid downregulates BACE1 and protects against lead-induced upregulation of Alzheimer's disease related biomarkers. *Neuropharmacology*, 79:596–602.
- Aitipamula, S., Chow, P.S. & Tan, R.B.H. 2011. The solvates of sulfamerazine: structural, thermochemical, and desolvation studies. *CrystEngComm*, 14(2):691–699.
- Amombo Noa, F.M., Bourne, S.A. & Nassimbeni, L.R. 2015. Halogen bonding in host–guest compounds: structures and kinetics of enclathration and desolvation. *Crystal Growth & Design*, 15(7):3271–3279.
- Atkins, P. W. 2000. *The elements of physical chemistry*. Oxford: Oxford University Press.
- Atwood, J.L. & Steed, J.W. 2004. *Encyclopedia of supramolecular chemistry*. New York, CRC Press.
- Bacchi, A., Cantoni, G., Crocco, D., Granelli, M., Pagano, P. & Pelagatti, P. 2014. Hydrogen-bond networks in polymorphs and solvates of metallorganic complexes containing ruthenium and aminoamide ligands. *CrystEngComm*, 16(6):1001–1009.
- Bacchi, A., Carcelli, M., Chiodo, T. & Mezzadri, F. 2008. Effects of 'changing the wheels' on the inclusion properties in metal–organic diols. *CrystEngComm*, 10(12):1916–1927.
- Barbour, L.J., Das, D., Jacobs, T., Lloyd, G.O. & Smith, V.J. 2012. Concepts and nomenclature in chemical crystallography. *Supramolecular chemistry*. John Wiley & Sons, Ltd. http://onlinelibrary.wiley.com/doi/10.1002/9780470661345.smc108/abstract 28 September 2015.
- Bassett, L.G., Bunce, S.C., Carter, A.E., Clark, H.M. & Hollinger, H.B. 1966. *Principles of chemistry*. New Jersey: Prenctice-Hall: 147-177.
- Bastin, R.J., Bowker, M.J. & Slater, B.J. 2000. Salt selection and optimisation procedures for pharmaceutical new chemical entities. *Organic Process Research & Development*, 4(5):427–435.
- Bauer, R.C., Birk, J.P. & Marks, P.S. 2007. *A conceptual introduction to chemistry*. McGraw-Hill Higher Education: 362-399.

- Bhattacharya, S. & Saha, B.K. 2011. Guest-induced isomerization of net and polymorphism in trimesic acid–arylamine complexes. *Crystal Growth & Design*, 11(6):2194–2204.
- Bhattacharya, S. & Saha, B.K. 2013. Polymorphism through Desolvation of the Solvates of a van der Waals Host. *Crystal Growth & Design*, 13(2): 1528-7483
- Bloomfield, M.M. & Stephens, L.J. 1996. *Chemistry and the living organism, chemlab experiments*. 6th ed. New York.
- Bonnar, J. & Sheppard, B.L. 1996. Treatment of menorrhagia during menstruation: randomised controlled trial of ethamsylate, mefenamic acid, and tranexamic acid. *British Medical Journal*, 313(7057):579–582.
- Braga, D., Brammer, L. & Champness, N.R. 2005. New trends in crystal engineering. *CrystEngComm*, 7(1):1–19.
- Braga, D. & Grepioni, F. 2000. Intermolecular interactions in. inorganic crystal engineering. *Accounts of Chemical Research*, 33(9):601–608.
- Braga, D. & Grepioni, F. 2005. Making crystals from crystals: a green route to crystal engineering and polymorphism. *Chemical Communications*, 29:3635–3645.
- Brescia, F. 1975. *Fundamentals of chemistry: laboratory studies,* 3rd ed. New York; London: Academic Press.
- Brown, T.E., LeMay, H.E.H., Bursten, B.E., Murphy, C. & Woodward, P. 2008. *Chemistry: the central science*. 11th ed. Upper Saddle River, NJ: Prentice Hall: 439-469.
- Butler, I.S. & Harrod, J.F. 1989*. Inorganic chemistry: principles and applications*. Redwood City, Calif: Benjamin-Cummings Pub Co.
- Byard, S., Abraham, A., T Boulton, P.J., Harris, R.K. & Hodgkinson, P. 2012. A multi-technique approach to the study of structural stability and desolvation of two unusual channel hydrate solvates of finasteride.
  Journal of Pharmaceutical Sciences, 101(1):176–186.
- Cafaggi, S., Russo, E., Caviglioli, G., Parodi, B., Stefani, R., Sillo, G., Leardi, R. & Bignardi, G. 2008. Poloxamer 407 as a solubilising agent for tolfenamic acid and as a base for a gel formulation.
  European Journal of Pharmaceutical Sciences, 35(1-2):19–29.
- Chadha, R., Kuhad, A., Arora, P. & Kishor, S. 2012. Characterisation and evaluation of pharmaceutical solvates of Atorvastatin calcium by thermoanalytical and spectroscopic studies. *Chemistry Central Journal*, 6(1): 114.
- Chang, R. 2006. *General chemistry - essential concepts* 4th.ed. Boston: McGraw-Hill:

- Chavez, K.J. & Rousseau, R.W. 2010. Solubility and pseudopolymorphic transitions in mixed solvents: sodium naproxen in methanol−water and ethanol−water solutions. *Crystal Growth & Design*, 10(8):3802–3807.
- Clugston, M.J., Flemming, R. & Vogt, D. 2002. *Chemistry: an introduction for Southern African students*. Oxford: Oxford University Press.
- Cruz-Cabeza, A.J. 2012. Acid–base crystalline complexes and the pKa rule. *CrystEngComm*, 14(20):6362–6365.
- Cunha, A.C., Ferreira, V.F., Jordão, A.K., Souza, M.C.B.V. de, Wardell, S.M.S.V., Wardell, J.L., Amelia Tan, P., Bettens, R.P.A., Kumar Seth, S. & Tiekink, E.R.T. 2013. Aryl -substituents moderate the nature of hydrogen bonds, N–H···N versus N–H···O, leading to supramolecular chains in the crystal structures of *N* -arylamino 1,2,3-triazole esters. *CrystEngComm*, 15(24):4917–4929.
- Desiraju, G.R. 2011. *Pharmaceutical salts and co-crystals: retrospect and prospects. Pharmaceutical salts and co-crystals.* **http://pubs.rsc.org/en/content/chapter/bk9781849731584-00001/978-1-84973-158-4** [1 March 2015].
- Desiraju, G.R. 2013. Crystal engineering: from molecule to crystal. *Journal of the American Chemical Society*, 135(27):9952–9967.
- Desiraju, G.R. 1995. Supramolecular synthons in crystal engineering—a new organic synthesis. *Angewandte Chemie* 34(21):2311–2327.
- Desiraju, G.R. & Gavezzotti, A. 1989. Crystal structures of polynuclear aromatic hydrocarbons. Classification, rationalization and prediction from molecular structure. *Acta Crystallographica Section B Structural Science*, 45(5):473–482.
- Desiraju, G.R., Vittal, J.J. & Ramanan, A. 2011. *Crystal engineering: a textbook*. Hackensack: World Scientific: IISc Press.
- Dey, S.K., Datta, B.K. & Das, G. 2012. Binding discrepancy of fluoride in quaternary ammonium and alkali salts by a tris(amide) receptor in solid and solution states. *CrystEngComm,* 14(16): 5305–5314.
- Dhanaraj, V. & Vijayan, M. 1983. A hydrated 1:1 complex between niflumic acid and ethanolamine, *Acta Crystallographica Section C*, 1398–1401.
- Dhotel, A., Chen, Z., Delbreilh, L., Youssef, B., Saiter, J.-M. & Tan, L. 2013. Molecular motions in functional self-assembled nanostructures. *International Journal of Molecular Sciences,* 14(2): 2303–2333.
- Dickson T.R.1975. *Introduction to chemistry*. Wiley, New York.
- Dougherty, D.A. 2007. Cation-π interactions involving aromatic amino acids. *The Journal of Nutrition*, 137(6):1504S–1508S.

- Douillet, J., Stevenson, N., Lee, M., Mallet, F., Ward, R., Aspin, P., Dennehy, D.R. & Camus, L. 2011. Development of a solvate as an active pharmaceutical ingredient: Developability, crystallisation and isolation challenges. *Journal of Crystal Growth*, 342(1):2–8.
- Drago R.S. 1974. *Principles of chemistry with practical perspectives*, Boston. Allyn & Bacon.
- Elder, D.P., Delaney, E., Teasdale, A., Eyley, S., Reif, V.D., Jacq, K., Facchine, K.L., Oestrich, R.S., Sandra, P. & David, F. 2010. The utility of sulfonate salts in drug development. *Journal of Pharmaceutical Sciences*, 99(7):2948–2961.
- Eerdenbrugh, B.V. & Taylor, L.S. 2011. An ab initio polymer selection methodology to prevent crystallization in amorphous solid dispersions by application of crystal engineering principles. *CrystEngComm*, 13(20): 6171–6178.
- Elder, D.P., Holm, R. & Diego, H.L. de. 2013. Use of pharmaceutical salts and co-crystals to address the issue of poor solubility. *International Journal of Pharmaceutics*, 453(1):88–100.
- El-Sisi, S. F. I. 2011. The possible protective effect of mefenamic acid, taurine, soy-phytoestrogen extract alone and in combination in experimental Alzheimer disease. *New York Science Journal*. 4(8): 89-101.
- Eslin, D., Lee, C., Sankpal, U.T., Maliakal, P., Sutphin, R.M., Abraham, L. & Basha, R. 2013. Anticancer activity of tolfenamic acid in medulloblastoma: a preclinical study. *Tumor Biology*, 34(5):2781–2789.
- Fábián, L., Hamill, N., Eccles, K.S., Moynihan, H.A., Maguire, A.R., McCausland, L. & Lawrence, S.E. 2011. Co-crystals of fenamic acids with nicotinamide. *Crystal Growth & Design*, 11(8):3522–3528.
- Fang, L., Numajiri, S., Kobayashi, D., Ueda, H., Nakayama, K., Miyamae, H. & Morimoto, Y. 2004. Physicochemical and crystallographic characterization of mefenamic acid complexes with alkanolamines. *Journal of Pharmaceutical Sciences*, 93(1):144–154.
- Fantin, G., Fogagnolo, M., Bortolini, O., Masciocchi, N., Galli, S. & Sironi, A. 2003. Polymorphism of dehydrocholic acid: crystal structure of the β-phase and guest-mediated solid phase conversion. *New Journal of Chemistry*, 27(12):1794–1800.
- Gaglioti, K., Chierotti, M.R., Grifasi, F., Gobetto, R., Griesser, U.J., Hasa, D. & Voinovich, D. 2014. Improvement of the water solubility of tolfenamic acid by new multiple-component crystals produced by mechanochemical methods. *CrystEngComm*, 16(35):8252.

- Hammond, C. 2001. *The basics of crystallography and diffraction*. 2nd ed. Oxford ; New York: Oxford University Press.
- Jacobs, A. & Amombo Noa, F.M. 2015. Co-crystals and co-crystal hydrates of vanillic acid. *CrystEngComm*, 17(1):98–106.
- Jacobs, A., Báthori, N.B., Nassimbeni, L.R. & Sebogisi, B.K. 2013. Salts of (+)-deoxycholic acid with amines: structure, thermal stability, kinetics of salt formation, decomposition and chiral resolution. *CrystEngComm*, 15(5):931–939.
- Jacobs, A., B. Báthori, N., Y., Kabwit, R. & Weber, E. 2014. Salts of the scissor-shaped racemic host 1, 1′-binaphthyl-2,2′-dicarboxylic acid with amines: structure and thermal stability. *CrystEngComm*, 16(12):2462–2469.
- Jampilek, J. & Dohnal, J. 2012. Investigation of carbohydrates and their derivatives as crystallization modifiers. In Chang, C.F. (ed). *Carbohydrates - comprehensive studies on glycobiology and glycotechnology*. http://www.intechopen.com/books/carbohydrates-comprehensive-studies-on-glycobiology-and-glycotechnology/investigation-of-carbohydrates-and-their-derivatives-as-crystallization-modifiers [21 February 2015].
- Ji, B., Wang, W., Deng, D. & Zhang, Y. 2011. Symmetrical bifurcated halogen bond: design and synthesis. *Crystal Growth & Design*, 11(8):3622–3628.
- Joo, Y., Kim, H.-S., Woo, R.-S., Park, C.H., Shin, K.-Y., Lee, J.-P., Chang, K.-A., Kim, S. & Suh, Y.-H. 2006. Mefenamic acid shows neuroprotective effects and improves cognitive impairment in in vitro and in vivo Alzheimer's disease models. *Molecular Pharmacology*, 69(1):76–84.
- Kato, F., Otsuka, M. & Matsuda, Y. 2006. Kinetic study of the transformation of mefenamic acid polymorphs in various solvents and under high humidity conditions. *International Journal of Pharmaceutics*, 321(1–2):18–26.
- Keinänen, S., Similä, S. & Kouvalainen, K. 1978. Oral antipyretic therapy: evaluation of the N-aryl-anthranilic acid derivatives mefenamic acid, tolfenamic acid and flufenamic acid. *European Journal of Clinical Pharmacology*, 13(5):331–344.
- Khan, M., Enkelmann, V. & Brunklaus, G. 2010. Crystal engineering of pharmaceutical co-crystals: application of methyl paraben as molecular hook. *Journal of the American Chemical Society*, 132(14):5254–5263.
- Kotz, J. C. 2009. *Chemistry and reactivity*. 7th ed. Australia: Thomson Brooks/Cole
- Kovalchuk, M.V. 2011. Crystallography as a methodology for scientific development in the 21st Century: A review. *Crystallography Reports*, 56(4):539–552.
- Kratochvíl, B. 2011. Solid forms of pharmaceutical molecules. In Šesták, J., Mareš, J.J. & Hubík, P. (eds). *Glassy, amorphous and nano-crystalline materials. Hot topics*

in thermal analysis and calorimetry. Springer Netherlands. **http://link.springer.com/chapter/10.1007/978-90-481-2882-2_8** [1 March 2015].

- Krishna Murthy, H.M., Bhat, T.N. & Vijayan, M. 1982. Structure of a new crystal form of 2-{[3-(trifluoromethyl) phenyl]amino}benzoic acid (flufenamic acid). *Acta Crystallographica Section B Structural Crystallography and Crystal Chemistry*, 38(1):315–317.
- Lee, A.Y., Erdemir, D. & Myerson, A.S. 2011. Crystal polymorphism in chemical process development. *Annual Review of Chemical and Biomolecular Engineering*, 2:259–280.
- Lee, E.H., Byrn, S.R. & Carvajal, M.T. 2006. Additive-induced metastable single crystal of mefenamic acid. *Pharmaceutical Research*, 23(10):2375–2380.
- Lehn, J.-M. 2007. From supramolecular chemistry towards constitutional dynamic chemistry and adaptive chemistry. *Chemical Society Reviews*, 36(2):151–160.
- Lemmerer, A., Bernstein, J. & Kahlenberg, V. 2011. Covalent assistance in supramolecular synthesis: in situ modification and masking of the hydrogen bonding functionality of the supramolecular reagent isoniazid in co-crystals. *CrystEngComm*, 13(19): 5692–5708.
- Lindoy, L.F., Atkinson, I.M., 2000. Self-assembly in Supramolecular Systems. Royal Society of Chemistry.
- López-Mejías, V., Kampf, J.W., Matzger, A.J., 2012. Nonamorphism in Flufenamic Acid and a New Record for a Polymorphic Compound with Solved Structures. J. Am. Chem. Soc. 134, 9872–9875.
- López-Mejías, V., Kampf, J.W. & Matzger, A.J. 2009. Polymer-induced heteronucleation of tolfenamic acid: structural investigation of a pentamorph. *Journal of the American Chemical Society*, 131(13):4554–4555.
- Miller, G.H. 1972. *Principles of college chemistry*. San Fransisco: Canfield Press.
- Moilanen, E. 1989. Effects of diclofenac, indomethacin, tolfenamic acid and hydrocortisone on prostanoid production in healthy and rheumatic synovial cells. *Agents and Actions*, 26(3-4):342–349.
- Morissette, S.L., Almarsson, Ö., Peterson, M.L., Remenar, J.F., Read, M.J., Lemmo, A.V., Ellis, S., Cima, M.J. & Gardner, C.R. 2004. High-throughput crystallization: polymorphs, salts, co-crystals and solvates of pharmaceutical solids. *Advanced Drug Delivery Reviews*, 56(3): 275–300.
- Moulton, B. & Zaworotko, M.J. 2001. From molecules to crystal engineering: supramolecular isomerism and polymorphism in network solids. *Chemical Reviews*, 101(6):1629–1658.

- Nangia, A. & Desiraju, G.R. 1998. Supramolecular synthons and pattern recognition. In Weber, P.D.E., Aoyama, Y., Caira, M.R., Desiraju, G. R., Glusker, J.P., Hamilton, A.D., Meléndez, R.E. & Nangia, A. (eds). *Design of organic solids*. *Topics in current chemistry.* Springer Berlin Heidelberg: 57–95. **http://link.springer.com/chapter/10.1007/3-540-69178-2_2** [2 March 2015].
- Nauha, E., Saxell, H., Nissinen, M., Kolehmainen, E., Schäfer, A. & Schlecker, R. 2009. Polymorphism and versatile solvate formation of thiophanate-methyl. *CrystEngComm*, 11(11): 2536–2547.
- Nawaz, H., Khawar Rauf, M., Ebihara, M. & Badshah, A. 2007. Methyl 2-(2,3-dimethyl-anilino)benzoate. *Acta Crystallographica Section E: Structure Reports Online*, 63(4):1658–1659.
- Ohlan, S., Nanda, S. & Pathak, D.P. 2013. Synthesis, characterization, in vitro hydrolysis and pharmacodynamic profiles of potential novel mutual prodrugs of N- (2,3-xylyl anthranilic acid). *Medicinal Chemistry Research*, 22(11):5120–5128.
- Pentikainen, P.J., Neuvonen, P.J. & Backman, C. 1981. Human pharmacokinetics of tolfenamic acid, a new anti-inflammatory agent. *European Journal of Clinical Pharmacology*, 19(5):359–365.
- Petrucci, R.H. & Harwood, W.S. 1997. *General chemistry: principles and modern applications*. 7th ed. New Jersey: Prentice Hall.
- Pimentel, G.C. & Spratley. 1971. *Understanding chemistry*. San Fransisco: Holden-Day.
- Pop, M.M., Goubitz, K., Borodi, G., Bogdan, M., De Ridder, D.J.A., Peschar, R. & Schenk, H. 2002. Crystal structure of the inclusion complex of beta-cyclodextrin with mefenamic acid from high-resolution synchrotron powder-diffraction data in combination with molecular-mechanics calculations. *Acta Crystallographica. Section B, Structural Science*, 58(6):1036–1043.
- Ricciotti, E. & FitzGerald, G.A. 2011. Prostaglandins and Inflammation. *Arteriosclerosis, thrombosis, and vascular biology*, 31(5): 986–1000.
- Saha, S., Rajput, L., Joseph, S., Mishra, M.K., Ganguly, S. & Desiraju, G.R. 2015. IR spectroscopy as a probe for C–HX hydrogen bonded supramolecular synthons. *CrystEngComm*, 17(6): 273–1290.
- SeethaLekshmi, S. & Guru Row, T.N. 2012. Conformational polymorphism in a non-steroidal anti-inflammatory drug, mefenamic acid. *Crystal Growth & Design*, 12(8):4283–4289.
- Seddon, K.R., Zaworotko, M., 1999. Crystal Engineering: The Design and Application of Functional Solids. Springer Science & Business Media.

- Sekhon B. S., 2009. Pharmaceutical co-crystals - a review. *ARS Pharmaceutica*: 50(3):99-117.
- Serajuddin, A.T.M. 2007. Salt formation to improve drug solubility. *Advanced Drug Delivery Reviews*, 59(7):603–616.
- Serap, C. & Cihan, Y. 2012. Optimum kinetic parameters of mefenamic acid crystallization by PBM. *Journal of Crystallization Process and Technology*, 2012. http://www.scirp.org/journal/PaperInformation.aspx?PaperID=21356 [28 September 2015].
- Smith, J.V. 1982. *Geometrical and structural crystallography*. New York: Wiley
- Snyder, M.K. 1966. *Chemistry: structure and reactions*. United States of America: Holt, Rinehart and Winston.
- Stahl, P.H. & Wermuth, C.G. 2008. *Handbook of pharmaceutical salts. Properties, selection, and use*. Weinheim: John Wiley & Sons.
- Steed, J.W. & Atwood, J.L. 2000. *Supramolecular chemistry*. Chichester: Wiley.
- Steed, J.W. & Atwood, J.L. 2009. Molecular guests in solution. *Supramolecular Chemistry*. John Wiley & Sons, Ltd: 307–384. http://onlinelibrary.wiley.com/doi/10.1002/9780470740880.ch6/summary [2 March 2015].
- Steed, J.W., Turner, D.R. & Wallace, K. 2007. *Core concepts in supramolecular chemistry and nanochemistry*. Chichester: John Wiley
- Subaiea, G.M. 2012. Brain penetration of tolfenamic acid and its ability to enhance the cognitive functions and to lower amyloid pathology in animal mouse models of Alzheimer's disease. Open Access Dissertations. Paper 9. University of Rhode Island,Kingston: **http://digitalcommons.uri.edu/oa_diss/9** [25 May 2015].
- Subaiea, G.M., Adwan, L.I., Ahmed, A.H., Stevens, K.E. & Zawia, N.H. 2013. Short-term treatment with tolfenamic acid improves cognitive functions in Alzheimer's disease mice. *Neurobiology of Aging*, 34(10):2421–2430.
- Suitchmezian, V., Jeß, I. & Näther, C. 2006. Crystal structures and properties of two new pseudopolymorphic modifications of the glucocorticoide triamcinolone diacetate. *Solid State Sciences*, 8(11):1373–1379.
- Surov, A.O., Simagina, A.A., Manin, N.G., Kuzmina, L.G., Churakov, A.V. & Perlovich, G.L. 2015. Fenamate co-crystals with 4,4′-bipyridine: structural and thermodynamic aspects. *Crystal Growth & Design*, 15(1):228–238.
- Surov, A.O. & Surov, O.V. 2008. Thermochemistry of fenamates vaporization. *Russian Journal of General Chemistry*, 78(8):1481–1487.

- Tantishaiyakul, V., Wiwattanawongsa, K., Pinsuwan, S., Kasiwong, S., Phadoongsombut, N., Kaewnopparat, S., Kaewnopparat, N. & Rojanasakul, Y. 2002. Characterization of mefenamic acid-guaiacol ester: stability and transport across Caco-2 cell monolayers. *Pharmaceutical Research*, 19(7):1013–1018.
- Vangala, V.R., Chow, P.S. & Tan, R.B.H. 2013. The solvates and salt of antibiotic agent, nitrofurantoin: structural, thermochemical and desolvation studies. *CrystEngComm*, 15(5):878–889.
- Vishweshwar, P., McMahon, J.A., Bis, J.A. & Zaworotko, M.J. 2006. Pharmaceutical co-crystals. *Journal of Pharmaceutical Sciences*, 95(3):499–516.
- Wang, J., Xiang, J., Wu, A. & Meng, X. 2013. Robust R22(8) hydrogen bonded dimer for crystal engineering of glycoluril derivatives. *CrystEngComm*, 15(46):10079-10085.
- Wasio, N.A., Quardokus, R.C., Brown, R.D., Forrest, R.P., Lent, C.S., Corcelli, S.A., Christie, J.A., Henderson, K.W. & Kandel, S.A. 2015. Cyclic hydrogen bonding in indole carboxylic acid clusters.
  The Journal of Physical Chemistry C, 119(36):21011–21017.
- Wei, Y., Zhang, X., Dang, L. & Wei, H. 2013. Solubility and pseudopolymorphic transitions in mixed solvent: Meropenem in methanol–water solution. *Fluid Phase Equilibria*, 349:25–30.
- Windle, A.H. 1977. *A first course in crystallography*. London: G. Bell.
- Wittering, K.E., Agnew, L.R., Klapwijk, A.R., Robertson, K., Cousen, A.J.P., Cruickshank, D.L. & Wilson, C.C. 2015. Crystallisation and physicochemical property characterisation of conformationally-locked co-crystals of fenamic acid derivatives. *CrystEngComm*, 17(19):3610–3618.

CHAPTER 2

EXPERIMENTAL PROCEDURE

2.1 Experimental design

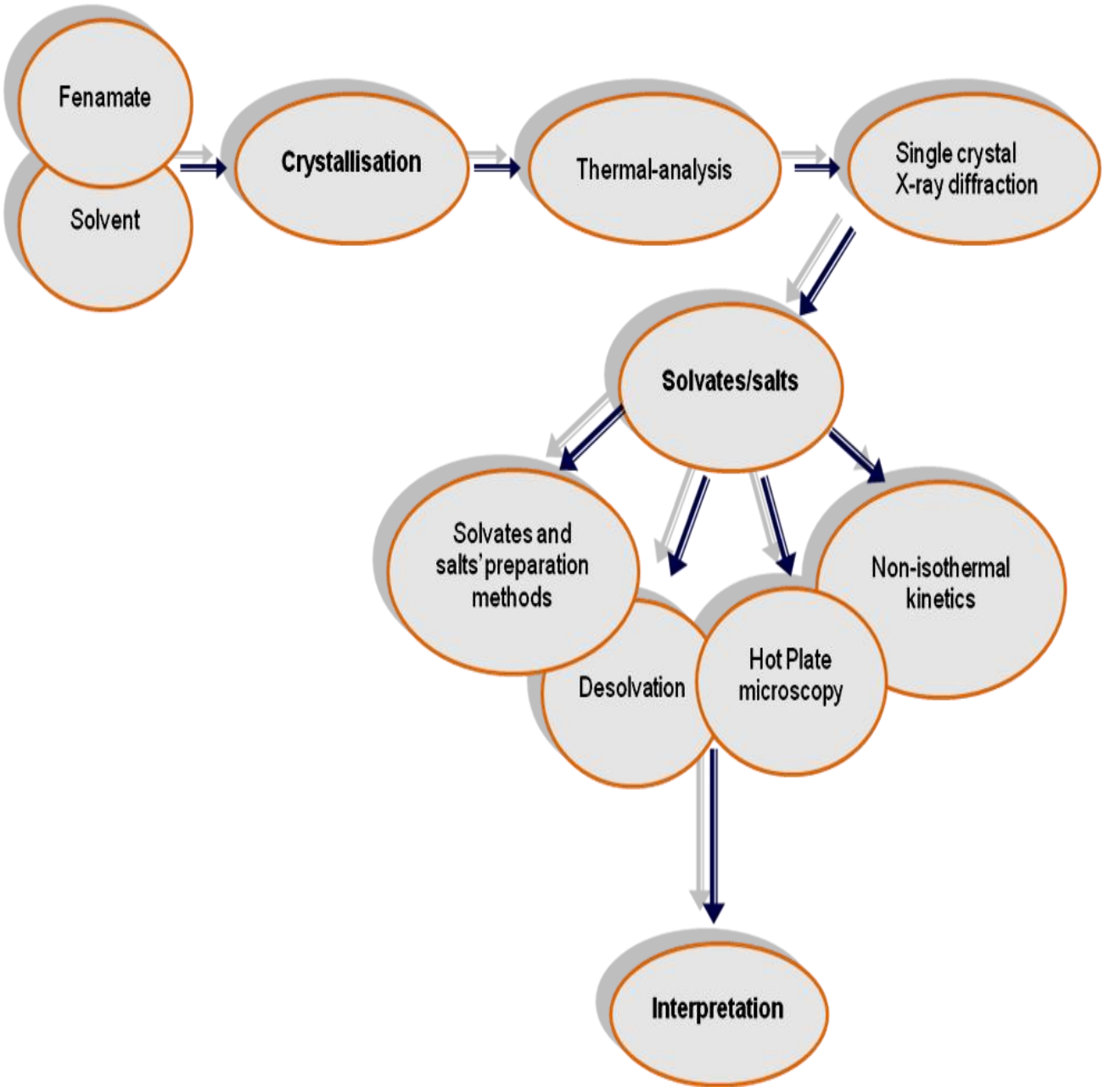

2.2 Introduction

Fenamates are pharmaceutical compounds used for the treatment of challenging diseases such as Alzheimer's, rheumatoid arthritis and painful musculoskeletal illnesses (Aboul-Fadl 2011; El-Sisi, 2011; SeethaLekshmi & Guru Row, 2012). However, the use of fenamates is limited because of the various side effects observed during their consumption (SeethaLekshmi & Guru Row, 2012; Surov et al. 2015). It is possible that the discovery of alternate forms of these compounds may lead to the improvement of certain of their physicochemical properties.

Solvates occur when a solvent is included in the crystal lattice of a host (Barbour et al. 2012). Salts are compounds resulting from the transfer of a proton between two species (Jampilek & Dohnal, 2012). A search conducted during this study of the Cambridge Structural Database (CSD version 5.36, Nov 2014) did not yield many structures of the solvated form and salts of fenamates. Thus it would be of interest to develop new compounds of these APIs.

Research presented here commenced with numerous attempts to crystallise two fenamates, mefenamic acid (MA) and tolfenamic acid (TFA) with selected solvents. The solvents had different functional groups; ketones, alcohols, amines, amides and pyridines. Solvates and salts were produced with amines, amides and pyridine derivatives. Certain solvents caused recrystallisation of the mother compound and these were subsequently used as co-solvents in further experiments.

Altogether 11 solvents resulted in 14 novel compounds from which five salts, eight solvates and a solvate polymorph were identified. In the case of MA, seven solvates were obtained when MA was combined with 2-picoline (2PIC), 3-picoline (3PIC), 4-picoline (4PIC), 3-chloropyridine (3ClPYR) and morpholine. Furthermore, three salts were formed when ethylenediamine, trimethylamine and 1-methylpiperazine were used. On the other hand, TFA formed three solvates by co-crystallisation with 2-picoline (2PIC), 3-picoline (3PIC) and 3-bromopyridine (3BrPYR) respectively. Additionally, two salts resulted from the use of the solvents diethanolamine and morpholine. An account follows in which the materials used together with the different methods implemented for the characterisation of the new compounds is described.

2.3 Materials used

2.3.1 Fenamate compounds

TFA and MA are compounds whose structural behaviour and characteristics were studied over the years by many scientists. The latter include Láznícek, (1986); Fang et al. (2004); Joo et al. (2006); Kato et al. (2006); Adwan et al.(2014); Surov et al. (2015) and Wittering et al. (2015). The principal difference between TFA and MA is the presence of a chlorine atom in TFA which replaces one of the two methyl groups in MA (Figure 2.1) situated on the non-acidic benzene ring. SeethaLekshmi & Guru Row (2012) reported that MA formed a solvate with *N, N*-dimethylformamide. Additionally, Fang et al. (2004) and Fonari et al. (2010) reported various salts of MA.

As it is able to form directional and robust synthons, carboxylic acid is one of the most commonly used functional groups in crystal engineering (Fabian, 2011; Ohlan et al. 2012; Bacchi et al. 2014). It was reported by Zhang et al. (2012) that carboxylic acids were used as pharmaceutical co-formers because of their ability to form hydrogen bonds with amides, amines, alcohols and many other chemical functional groups. Additionally, the fenamates studied in this project are composed of an amine functional group which is a strong hydrogen bond acceptor. Consequently, these substances can bond with other molecules by donating or accepting hydrogen bonds. Both the MA and TFA used in this study were purchased from Sigma Aldrich. Table 2.1 lists the physical properties of TFA and MA.

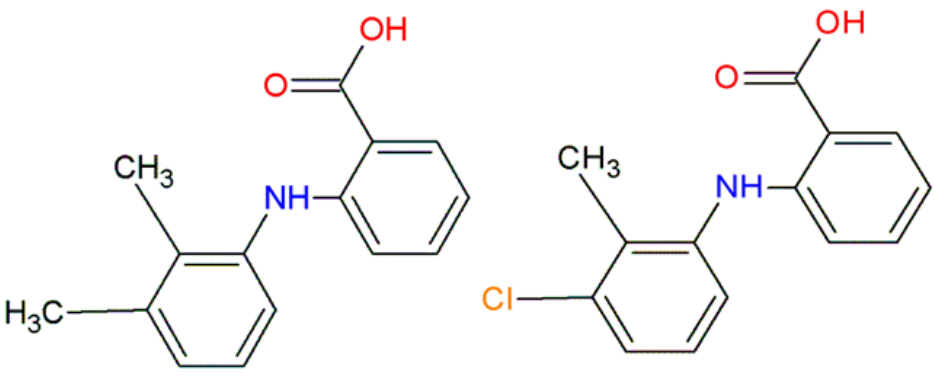

Figure 2-1: Structural representation of mefenamic acid (left) and tolfenamic acids (right): The donor and acceptor groups are shown in red and blue.

Table 2-1: Physical properties and pK_a values of tolfenamic acid and mefenamic acid.

Compound	Condensed formula	Formula weight (g mol^{-1})	Melting point (°C)	pKa
Mefenamic acid	$C_{15}H_{15}NO_2$*	241.3*	230-231*	4.2*
Tolfenamic acid	$C_{14}H_{12}ClNO_2$*	261.7*	207-208*	3.7**

*Budavari, 1989; **Calculated value.

2.3.2 Solvents

After conducting different trials, MA and TFA were found to co-crystallise with selected amines and pyridine solvents. The structural characteristics of the solvents varied from aromatic to linear to cyclic compounds. Table 2.2 shows the chemical structures and physical properties of the solvents used in this study. The purity of the solvents used was at least 99% and were all purchased from Sigma Aldrich. The solvents were used with no further purification.

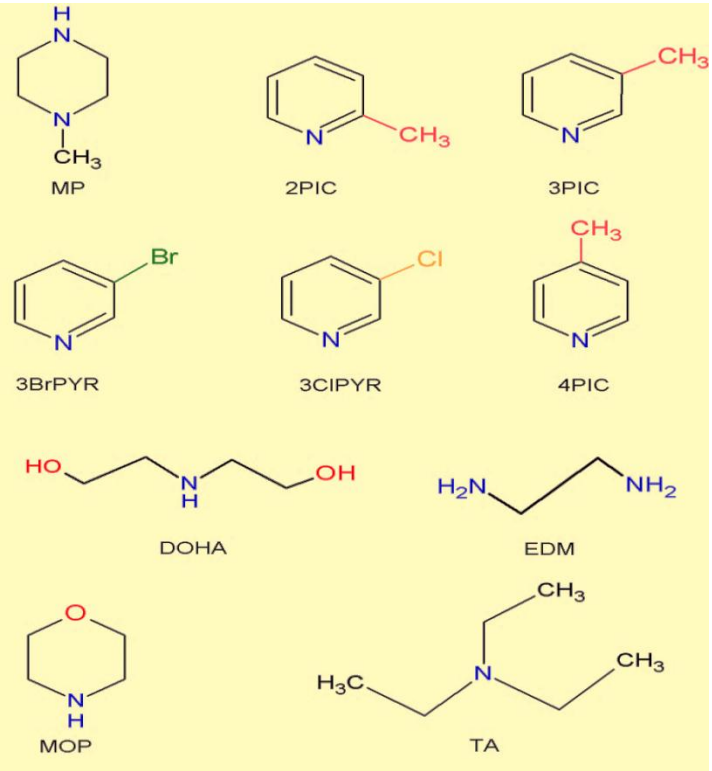

Figure 2-2: Chemical structures of solvents used.

Table 2-2: Physical properties and pKa values of the different solvents used (adapted from B

Solvent	Acronyms	Condensed formula	Formula weight (g mol^{-1})	Boiling Point (°C)	pKa
1-Methylpiperazine	MP	$C_5H_{12}N_2$	100.2	138	9.14*
2-Picoline	2PIC	C_6H_7N	93.1	129	5.97
3-Picoline	3PIC	C_6H_7N	93.1	144	5.68
3-Bromopyridine	3BrPYR	C_5H_4BrN	158	172	2.84
3-Chloropyridine	3ClPYR	C_5H_4ClN	113.6	148	2.84
4-Picoline	4PIC	C_6H_7N	93.1	145	6.02
Diethanolamine	DOHA	$C_4H_{11}O_2N$	105.1	271	8.88*
Ethylenediamine	EDM	$C_2H_6N_2$	60.1	117	10.71
Morpholine	MOP	C_4H_9NO	87.1	128	8.33
Triethylamine	TA	$C_6H_{15}N$	101.2	89	11.01

Retrieved from Weast, 1980; *retrieved from Khalili et al., 2009

2.4 Techniques

The following techniques were used during this study:

1- Crystallisation,
2- Thermal analysis (differential scanning calorimetry and thermogravimetric analysis),
3- Single crystal X-ray diffraction,
4- Powder X-ray Diffraction (PXRD),
5- Hot stage microscopy,
6- Solvates and salts' preparation methods,
7- Desolvation and
8- Non-isothermal kinetics.

2.4.1 Crystallization

Numerous methods are used to produce desired compounds; one of these is crystallisation. Crystallisation is the process whereby molecules rearrange themselves to form new structured crystalline lattices (Atwood & Steed, 2004; Stieger & Liebenberg, 2012; Lee et al. 2013; Samora & Cacialli, 2014). Crystallisation can be achieved by means of solvent or non-solvent based methods: addition of anti-solvent; cooling of solutions; adjusting pH; lyophilisation, sublimation, desolvation of solvate or recrystallisation of a melt (Stieger & Liebenberg, 2012). In the current research study, a slow evaporation method was used to form solvates or salts.

In a vial, approximately 30 mg of fenamate was transferred and approximately 2 ml of solvent was added to the solid. The mixture was stirred at a temperature of 60 °C to achieve complete dissolution of the acid. At times co-solvents were used when the solvent did not cause complete dissolution of the fenamate. The co-solvent was selected from those which induced recrystallization of MA or TFA. Crystals were visualised after days, weeks or months after evaporation of the solutions at ambient temperature.

2.4.2 Thermal analysis

Thermal analysis refers to a category of analytical chemistry techniques whereby physical and chemical changes of a sample are monitored as the sample temperature is either increased or decreased (Wunderlich, 1990; Charsley & Warrington, 1992; Brown, 1998; Brown, 2001; Haines, 2002; Brown & Gallagher, 2008). The methods used to analyse the crystals prepared during this study were differential scanning calorimetry (DSC) and thermogravimetric analysis (TGA). Table 2.3 provides the different parameters of the thermal analysis instrument used in the study.

2.4.2.1 Differential scanning calorimetry (DSC)

Differential scanning calorimetry (DSC) is a technique used to measure the difference in energy between an experimental sample and an inert reference sample as a function of time and temperature (Charsley & Warrington, 1992; Brown, 1998; Haines, 2002). Generally, the energy released or absorbed by the sample when heated or cooled is observed as

endothermic or exothermic peaks. Therefore, results of DSC analysis provide information on melting point, reaction energy and temperature as well as crystalline transition temperature (Charsley & Warrington, 1992; Haines, 2002; Brown & Gallagher, 2008; Steed, 2013). The instrument requires an empty standard aluminium pan as a reference, and a second pan for holding the sample. These are positioned in a furnace. Heat flow is measured by comparing the difference in temperature throughout both the test sample and the reference (Charsley & Warrington, 1992; Haines, 2002).

During the analysis, selected crystals were retrieved from the mother liquor and placed onto filter paper. The solid was then dried and crushed into a powder. Approximately 2-3 mg of the resulting powder was transferred into the aluminium pan and then placed into the furnace for analysis.

A Perkin Elmer 6 series instrument was used for the analysis of all crystals. The experiment was conducted over a temperature range of 303-573 K at a heating rate of 10 K/min. Nitrogen gas was used as a purge at a flow rate of 20 ml/min (see Table 2.3).

2.4.2.2 Thermogravimetric analysis (TGA)

Thermogravimetric analysis is a method used to measure the change in mass of a material as a function of increased temperature (Wunderlich, 1990; Charsley & Warrington, 1992; Brown, 1998; Haines, 2002; Brittain, 2012:Steed, 2013). The isothermal change can also be measured as a function of time in a known atmosphere. Generally, results yield a graph showing mass loss recorded in the sample versus temperature/time due to dehydration, decomposition or oxidation of a certain compound (Charsley & Warrington, 1992; Haines, 2002). Thus, the data retrieved from the TGA results are the temperature at which a change in mass occurs, the temperature at which a solvent is released from a crystal lattice and also information on the kinetics of desolvation of the compound undergoing analysis (Charsley & Warrington, 1992).

The sample was prepared in the same manner as for DSC analysis (refer 2.4.2.1). The results obtained from TGA confirmed the host: guest ratio of the compound.

Table 2-3: Thermal analysis parameters.

	DSC and TGA
Model	**Perkin-Elmer DSC 6 System instrument**
Purge gas	**Nitrogen gas @ 20 ml/min**
Temperature programme	**303 – 573 K @ 10 K/min**

2.4.3 Single crystal X-ray diffraction

Single crystal X-ray diffraction is one of the most definitive methods for elucidating the crystal structures of compounds (Clegg et al. 2001; Hammond, 2001; Karki et al. 2007; Kovalchuk, 2011; Brittain, 2012). In general, it determines the packing and conformation of molecules and the intermolecular interactions within a crystal.

Analysis of the crystals obtained during this study by single X-ray diffraction was carried out at the University of Cape Town. Suitable crystals were coated with paratone oil and mounted on a glass fibre and analysed for unit cell parameters. The crystal data were collected using a Bruker APEX II (2005, version 1.0-27) diffractometer or a Nonius Kappa CCD (1998) with a graphite-monochromated Mo Kα = 0.71073 Å at 173 K and an Oxford Cryostream 700.

The crystal structures were solved and analysed at the Cape Peninsula University of Technology with the aid of various computer software which is discussed further in section 2.4.4.

2.4.4 Computation

.Xseed (Barbour, 2003) was the graphical user interface used to analyse the data. This program utilises: SHELXS-97 (Sheldrick, & Schneider, 1997) to solve the structure to completion and SHELXL-97 (Sheldrick, & Schneider, 1997) which refined the structure. Additional computing programs were implemented to further interpret the final results. These were:

- Conquest, which was used to screen and obtain information from the Cambridge Structural Database regarding the compounds used as well as for comparative analyses of data obtained during this study (CSD, version 5.36, Nov 2014)

- LAZYPULVERIX, used to calculate the theoretical powder X-ray diffraction pattern from the single crystal X-ray diffraction data (Yvon et al. 1977);
- PovRay, which rendered graphics of the different structures (PovRay, Version 3, 1991-1999);
- DENZO-SMN which was used to reduce and scale the data obtained from the Nonius Kappa CCD (Otwinowski & Minor, 1997)
- SAINT which was used to reduce and measure the data obtained from the Bruker APEX II (Bruker, 2004);
- XPREP which was used to read both the raw data file and the parameter file obtained from the single crystal X-ray analysis and to prepare the input files for SHELXS. It was also used to determine the space group of a particular crystal (Version 5.1, 1997) and
- Mercury which generated information relating to the voids created by the solvents. A probe radius of 1.2 Å and an approximate grid spacing of 0.7 Å were used for the voids (Allen & Lipscomb, 2004).

2.4.5 Powder X-ray diffraction

Powder X-Ray diffraction (PXRD) is an analytical method utilized for the identification of a crystalline phase and it also provides information regarding unit cell dimensions (Karki et al. 2007; Peterson et al. 2011; Brittain, 2012; Dutrow, 2013). The PXRD can generate a fingerprint pattern for a particular crystalline structure thus making its use in qualitative analysis of importance (Steed, 2013). During this study, it was used to demonstrate that the crystalline form obtained after recrystallisation was different from that of the starting material. In addition, the calculated PXRD pattern was compared with the experimental PXRD pattern to determine whether the single crystal structure is representative of the bulk material. The PXRD was also used to ascertain whether other methods used to make solvates/salts produced the same crystal compound as that obtained from the slow evaporation process. Polymorphism studies were done by using PXRD after completion of the desolvation studies.

The powdered sample of the selected fenamate (40-50 mg) was transferred into a sample holder. This was tested with a Bruker D2 Phaser powder X-ray diffractometer with graphite-

monochromated Cu Kα radiation with a wavelength of 1.5418 Å. The sample was analysed at room temperature (RT) and a diffractogram was obtained under ambient conditions with a power setting of 40 kV and 20 mA. The resulting data yielded a graph of relative intensity versus two thetas. For each compound studied the experimental pattern was analysed and compared to the calculated pattern obtained from LAZYPULVERIX (Yvon et al. 1997).

2.4.6 Desolvation study

Desolvation is the process whereby a solvent is removed from the crystal lattice of a solvate (Suitchmezian et al. 2006). The study of desolvation is important to optimize drug production, reproduction and transportation methods. Pharmacists need to be aware of and implement procedures to enhance the use and storage of pharmaceutical drugs (Suitchmezian et al. 2006; Chadha et al. 2012; Vangala et al. 2013). This would include awareness of the temperature at which a given solvent would tend to escape from the structure in which it is incorporated. Such knowledge could contribute to the manufacture of the most stable form of an API under certain conditions (Aitipamula et al. 2011; Vangala et al. 2013).

The desolvation study was carried out in two different stages. Firstly, 100 mg of the solvate or salt used was subjected to a selected temperature for a period of 24 h and thereafter the PXRD analysis was completed. Secondly, identical masses of crystals were left in an open vessel at ambient temperature for a period of one month. Thereafter the final powder was also analysed by using PXRD. In both cases the PXRD patterns obtained were compared with those of the known polymorphs of the free acids to identify which form was present after desolvation.

2.4.7 Hot stage microscopy

Hot stage microscopy is a thermo-optometric method involving the use of the optical properties of a sample combined with thermoanalytical techniques (Vitez et al. 1998; Carlton, 2011; Stieger et al. 2012). Sample temperature is monitored against time or temperature and the resultant changes in the sample are observed by using a microscope (Boccaccini & Hamann, 1999; Carlton, 2011; Brittain, 2012; Brown, 2012; Steed, 2013). From the analyses, the characteristic state transformations such as desolvation, phase

transition, melting and decomposition of a given compound can be recorded (Vitez et al. 1998).

During the analysis of the solvate or salt, a small portion of the obtained crystal was retrieved from a vial. It was then placed on a platinum hot stage connected to a temperature controller where the maximum temperature attainable was 300 °C. Before commencing the experiment, a drop of silicon oil was placed on the crystal. The temperature set was between 303 – 573 K and the rate set at 10 K/min. Photographic images were taken at times when physical changes were observed from the crystals.

A MEIJI TECHNO EMZ-8TR transmitted light microscope fitted with a CANON DS126191 camera was used. The microscope was assembled with a platinum hot stage combined with a LINKAM TMS 94 temperature controller.

2.4.8 Alternative methods for the preparation of solvates/salts

Crystallization induced by slow evaporation of the fenamate and solvent mixture was generally used for the preparation of the solvates and salts. A disadvantage of this method is that it requires the use of substantial volumes of potential environmental pollutants. For this reason, it was decided to pursue other methods of preparation of the particular solvate or salts. The aim of this was to investigate alternative methodology to reproduce the particular salt or solvate obtained from the slow evaporation method.

2.4.8.1 Preparation of the solvate/salt by grinding

Mechanochemistry induces the reaction of compounds solely by the use of mechanical means (James et al. 2012; Delori et al. 2012; Bowmaker, 2013). Recently, research in this area has escalated as it is now recognised that mechanochemistry enhances quantitative reactions and the speed at which these reactions occur between a given solid and solvent (James et al. 2012).

The selected fenamate (40-60 mg) was added to a ball mill with a few drops of the solvent used to form the solvate or salt. The mixture was ground for 30-45 min by the use of a grinding machine and the resulting powder was analysed using PXRD. The PXRD pattern

obtained was compared with the theoretical PXRD pattern obtained from LAZYPULVERIX (Yvon et al. 1977).

2.4.8.2 The manufacture of a solvate/salt by preparing a slurry

A slurry of a material is created from the suspension of solid particles in a liquid or solvent (Takata et al. 2008). On a hot plate set at 60 °C, a mixture of the fenamate and an excess of a selected solvent were heated until dissolution occurred. The electrical supply to the hot plate was then terminated and the mixture was stirred in a vial until slurry formation occurred. The mixture was then transferred to a filter paper and left to dry. The powder residue was analysed by using PXRD and the resulting pattern was compared to the pattern derived from the single crystal analysis data.

2.4.9 Non-isothermal kinetics of solvates /salts

Crystals obtained from different solvates and salts were crushed and then analysed by using TGA operating at differing heating rates. The results were used to produce a graph with axes -log β versus T^{-1}.

After each experiment, the activation energy was calculated by using the slopes of the graphs where the slope = $(0.457E_a)/R$. This was obtained from the following equation:
$dC/dT = A / \beta f(C) e^{-Ea/RT}$

β is the heating rate,
C is the mass loss of the sample and
E_a is the activation energy.

This equation can be reduced to: $d \log \beta / d (1/T) = (0.457/ R) E_a$

Bibliography

- Aboul-Fadl T., Abdel-Aziz H.A., Kadi A., Bari A., Ahmad P., Al-Samani T. & Ng S.W. 2011 Microwave-assisted one-step synthesis of fenamic acid hydrazides from the corresponding acids. *Molecules*, 16: 3544-3551.
- Aitipamula, S., Chow, P.S. & Tan, R.B.H. 2011. The solvates of sulfamerazine: structural, thermochemical, and desolvation studies. *CrystEngComm*, 14(2):691–699.
- Allen, F.H. & Lipscomb, K.J. 2004. The Cambridge structural database. *Encyclopaedia of Supramolecular Chemistry*, 1:161-168.
- Atwood, J.L. & Steed, J.W. 2004. *Encyclopedia of supramolecular chemistry*. New York, CRC Press.
- Bacchi, A., Cantoni, G., Crocco, D., Granelli, M., Pagano, P. & Pelagatti, P. 2014. Hydrogen-bond networks in polymorphs and solvates of metallorganic complexes containing ruthenium and aminoamide ligands. *CrystEngComm*, 16(6):1001–1009.
- Barbour, L.J., Das, D., Jacobs, T., Lloyd, G.O. & Smith, V.J. 2012. Concepts and nomenclature in chemical crystallography. *Supramolecular chemistry*. John Wiley & Sons, Ltd. **http://onlinelibrary.wiley.com/doi/10.1002/9780470661345.smc108/abstract** [28 June 2015].
- Barbour, L.J. 2003. X-Seed: Graphical interface for SHELX program. *Journal of Supramolecular Chemistry,* 1:189-191.
- Boccaccini, A.R. & Hamann, B. 1999. Review In situ high-temperature optical microscopy. *Journal of Materials Science*, 34(22):5419–5436.
- Bowmaker, G. 2013. Solvent-assisted mechanochemistry. *Chemical Communications*, 49(4):334–348.
- Brown, M.E. & Gallagher, P.K. 2008. *Handbook of thermal analysis and calorimetry: recent advances, techniques and applications*. Ohio: Elsevier Science.
- Budavari, S. 1989. The Merck index: an encyclopedia of chemicals, drugs, and biologicals. Rahway, N.J.: Merck.
- Charsley, E.L. & Warrington, S.B. 1992. *Thermal analysis: techniques and applications*. Michigan: Royal Society of Chemistry.
- Clegg, W., Blake, A.J., Gould, R.O. & Main, P. 2001. *Crystal structure analysis: principles and practice*. Chester: International Union of Crystallography; Oxford University Press.
- COLLECT data collection software. 1998. Nonius, Delft, the Netherlands.

- El-Sisi, S. F. I. 2011. The possible protective effect of mefenamic acid, taurine, soy-phytoestrogen extract alone and in combination in experimental Alzheimer disease. *New York Science Journal,* 4 (8):89-101.
- Fábián L., Hamill N., Eccles K. S., Moynihan H. A. & Maguire A. R. 2011 Co-crystals of fenamic acids with nicotinamide. *Journal of the American Chemical Society*, 11:3522–3528.
- Fang, L., Numajiri, S., Kobayashi, D., Ueda, H., Nakayama, K., Miyamae, H. & Morimoto, Y. 2004. Physicochemical and crystallographic characterization of mefenamic acid complexes with alkanolamines. *Journal of Pharmaceutical Sciences*, 93(1):144-154.
- Fonari, M.S., Ganin, E.V., Vologzhanina, A.V., Antipin, M.Y. & Kravtsov, V.C. 2010. Persistent CH···π interactions in mefenamic acid complexes with cyclic and acyclic amines. *Crystal Growth & Design*, 10(8):3647–3656.
- Haines, P.J. 2002. *Principles of thermal analysis and calorimetry*. Cambridge: Royal Society of Chemistry.
- Hammond, C. 2001. *The basics of crystallography and diffraction*. 2nd ed. Oxford ; New York: Oxford University Press.
- James, S.L., Adams, C.J., Bolm, C., Braga, D., Collier, P., Friščić, T., Grepioni, F., Harris, K.D.M., Hyett, G., Jones, W., Krebs, A., Mack, J., Maini, L., Orpen, A.G., Parkin, I.P., Shearouse, W.C., Steed, J.W. & Waddell, D.C. 2012. Mechanochemistry: opportunities for new and cleaner synthesis. *Chemical Society Reviews*, 41(1): 413–447.
- Jampilek, J. & Dohnal, J. 2012. Investigation of carbohydrates and their derivatives as crystallization modifiers. Carbohydrates -comprehensive studies on glycobiology and glycotechnology, Prof. Chuan-Fa Chang (Ed.). In Tech. 10:5772/50626. **http://www.intechopen.com/books/carbohydrates-comprehensive-studies-on-glycobiology-and-glycotechnology/investigation-of-carbohydrates-and-their-derivatives-as-crystallization-modifiers**. [20 June 2015]
- Karki, S., Fábián, L., Friščić, T. & Jones, W. 2007. Powder X-ray diffraction as an emerging method to structurally characterize organic solids. *Organic Letters*, 9(16):3133–3136.
- Kato, F., Otsuka, M. & Matsuda, Y. 2006. Kinetic study of the transformation of mefenamic acid polymorphs in various solvents and under high humidity conditions. *International Journal of Pharmaceutics*, 321(1–2):18–26.
- Khalili, F., Henni, A. & East, A.L.L. 2009. pK_a Values of Some Piperazines at (298, 303, 313, and 323) K. Journal of Chemical & Engineering Data, 54(10): 2914–2917.

- Kovalchuk, M.V. 2011. Crystallography as a methodology for scientific development in the 21st century: a review. *Crystallography Reports*, 56(4):539–552.
- Lazinicek M.& Senius K. E. O. 1986 Protein binding of tolfenamic acid in the plasma from patients with renal and hepatic disease. *European Journal of Clinical Pharmacology*, 30: 591-596.
- Ohlan S., Nanda S. & Pathak D. P. 2013 Synthesis, characterization, in vitro hydrolysis and pharmacodynamic profiles of potential novel mutual prodrugs of N-(2,3-xylyl anthranilic acid). *Medical Chemistry Research*, 22:5120–5128.
- Otwinowski. Z. & Minor. W. 1997*. Processing of X-ray Diffraction Data Collected in Oscillation Mode: Methods in enzymology macromolecular crystallography*, Academic Press, New York. 276: 307-326.
- Peterson, M.L., Stanton, M.K., Kelly, R.C., Staples, R. & Cheng, A. 2011. Preparation, solid state characterization, and single crystal structure analysis of N-(4-(6-(4-(trifluoromethyl) phenyl) pyrimidin-4-yloxy) benzo[d]thiazol-2-yl)acetamide crystal forms. *CrystEngComm*, 13(4):1170–1180.
- PoV-Ray for Windows: Version 3.le.watcom.win32: The persistence of Vision Development Team: © 1991-1999.
- Bruker. 2004. SAINT-Plus Version 7.12. AXS Inc. Madison, Wisconsin, USA.
- SamorÃ, P. & Cacialli, F. 2014. *Functional supramolecular architectures: for organic electronics and nanotechnology,* Weinheim: Wiley-VCH.
- SeethaLekshmi, S. & Guru Row, T.N. 2012. Conformational polymorphism in a non-steroidal anti-inflammatory drug, mefenamic acid. *Crystal Growth & Design*, 12(8): 4283–4289.
- Sheldrick, G.M. & Schneider, T.R. 1997. SHELXL: High resolution refinement. *Macromolecular. Crystallography* , 277: 319-343.
- Sheldrick, G.M. 2002. University of Göttingen, Germany.
- Steed, J.W. 2013. The role of co-crystals in pharmaceutical design. *Trends in Pharmacological Sciences*, 34(3):185–193.
- Stieger, N., Aucamp, M., Zhang, S.-W. & De Villiers, M.M. 2012. Hot-stage optical microscopy as an analytical tool to understand solid-state changes in pharmaceutical materials. American Pharmaceutical Review. http://www.americanpharmaceuticalreview.com/Featured-Articles/39283-Hot-stage-Optical-Microscopy-as-an-Analytical-Tool-to-Understand-Solid-state-Changes-in-Pharmaceutical-Materials. [12 October 2015].

- Suitchmezian, V., J. & Näther, C. 2006. Crystal structures and properties of two new pseudopolymorphic modifications of the glucocorticoide triamcinolone diacetate. *Solid State Sciences*, 8(11):1373–1379.
- Surov, A.O., Simagina, A.A., Manin, N.G., Kuzmina, L.G., Churakov, A.V. & Perlovich, G.L. 2015. Fenamate co-crystals with 4,4′-bipyridine: structural and thermodynamic aspects. *Crystal Growth & Design*, 15(1):228–238.
- Takata, N., Shiraki, K., Takano, R., Hayashi, Y. & Terada, K. 2008. Co-crystal screening of stanolone and mestanolone using slurry crystallization. *Crystal Growth & Design*, 8(8):3032–3037.
- Vangala, V.R., Chow, P.S. & Tan, R.B.H. 2013. The solvates and salt of antibiotic agent, nitrofurantoin: structural, thermochemical and desolvation studies. *CrystEngComm*, 15(5):878–889.
- Vitez, I.M., Newman, A.W., Davidovich, M. & Kiesnowski, C. 1998. The evolution of hot-stage microscopy to aid solid-state characterizations of pharmaceutical solids. *Thermochimica Acta*, 324(1–2):187–196.
- Weast, R.C. 1980. CRC Handbook of Chemistry and Physics. 60th ed. New York. CRC Press.
- Wittering, K.E., Agnew, L.R., Klapwijk, A.R., Robertson, K., Cousen, A.J.P., Cruickshank, D.L. & Wilson, C.C. 2015. Crystallisation and physicochemical property characterisation of conformationally-locked co-crystals of fenamic acid derivatives. *CrystEngComm*, 17(19):3610–3618.
- Wunderlich, B. 1990. *Thermal analysis*. Boston: Academic Press.
- XPREP, Data Preparation and Reciprocal Space Exploration, Version 5.1/NT ©1997, Bruker Analytical X-Ray Sytems.
- Yvon, K., Jeitschko, W. & Parthe, E.J. 1997. LAZY PULVERIX, a computer program, for calculating X-ray and neutron diffraction powder patterns. *Journal of Applied Crystallography,* 10:73-74.
- Zhang, Y., Evans, J., Rowe, W., Dinehart, K., Quinn, B. & Connelly, P. 2012. Dosable solvates of ivacaftor with high boiling point liquids. *CrystEngComm*, 14(7):2422–2427.

CHAPTER 3

THE SOLVATES OF MEFENAMIC AND TOLFENAMIC ACIDS

Solvates are crystalline compounds wherein the starting materials are solids and solvents. Solvatomorphism is the process whereby a specific solvent is included in a crystal lattice of a compound in order to form a solvate. In the study reported on here there was to be no proton transfer. Rather two compounds interacted by means of non-covalent reactions. In this chapter, solvates of mefenamic and tolfenamic acid are reported on and the properties of these new compounds are determined.

3.1 Solvates of mefenamic acid and pyridine derivatives

3.1.1 Introduction

In a vial, 30 mg of mefenamic acid (MA) was introduced together with 10 ml of the respective pyridine derivative. A clear solution was obtained after stirring the mixture at 30 °C and the saturated solution was then left to crystallize by slow evaporation at room temperature (RT=25°C). The crystals formed were characterised by a block-like habit which appeared more pronounced in some samples e.g. the solvate of MA and 3-picoline.

Most of the resulting solvates crystallized in the primitive triclinic space group *P*$\bar{1}$. The ΔpK_a recorded for the different solvates varied between -1.48 to 1.82. These values were less than 2 which fall below the range described by Cruz Cabeza (2012) for the possibility of a formation of a salt. The C-O distances were also measured to confirm that no proton was transferred. Furthermore, the crystal structures also showed the intramolecular interaction N-H•••O. This intramolecular interaction was reported on elsewhere by Fang et al. (2004), Nawaz et al. (2007), Fábián et al. (2011), SeethaLekshmi & Guru Row, (2012) and Surov et al. (2015). Furthermore, the hydrogen bond linking the molecules of MA and the substituted pyridines was the same i.e. (COOH)•••N. This interaction formed a heterotrimer similar to that reported by Surov et al. (2015) in his study conducted with fenamate co-crystals with 4,4'-bipyridine.

It was notable that the recrystallization of the **MA•2PIC** solvate resulted in another form of the solvate. The polymorph belonged to a different primitive space group and demonstrated a much larger number of molecules present in the unit cell when compared with the first form. Tables 3.1, 3.3 and 3.5 provide the crystallographic data information of the different solvates and further details concerning their structural behaviour are discussed below.

3.1.2 Structural analysis of the solvates of mefenamic acid

3.1.2.1 Solvates of mefenamic acid with 2-picoline (MA•2PIC FORMS I & II)

Yellow block crystals were obtained after two weeks of slow evaporation of MA in a 2-picoline (2PIC) and isopropanol mixture at ambient temperature. After single crystal analysis, the crystals were identified as belonging to the triclinic space group *P*$\bar{1}$. One molecule of the

MA and one molecule of 2PIC were found in the asymmetric unit. Subsequent attempts to recrystallize the bulk material resulted in a polymorph which was successfully solved in the monoclinic space group $P2_1/n$. Crystal data and parameters are shown in Table 3.1.

From the structural analysis, it was observed that **MA•2PIC** presented two major interactions illustrated in Figure 3.1. It should be noted that for all the numbering schemes, the hydrogen atoms were omitted except for those involved in the major hydrogen bonding. This was applied throughout the thesis where applicable. These major interactions consisted of an intramolecular hydrogen bond, N-H•••O, formed by nitrogen connecting the two benzene rings of the acid and the carbonyl group. The N1•••O1 distance was 2.667(1) Å and the N1–H7•••O1 angle was 139° in form I. In the case of form II, the N1•••O1 distance was 2.638(2) Å with an N1-H7•••O1 angle of 132°. Furthermore, one strong hydrogen bond, O–H•••N linked the fenamate acids to the 2PIC molecules. The O2•••N2 distance was 2.613(1) Å for form I and 2.629(2) Å was recorded in form II. The different O2–H2•••N2 angles were 178° and 176° for forms I and II respectively.

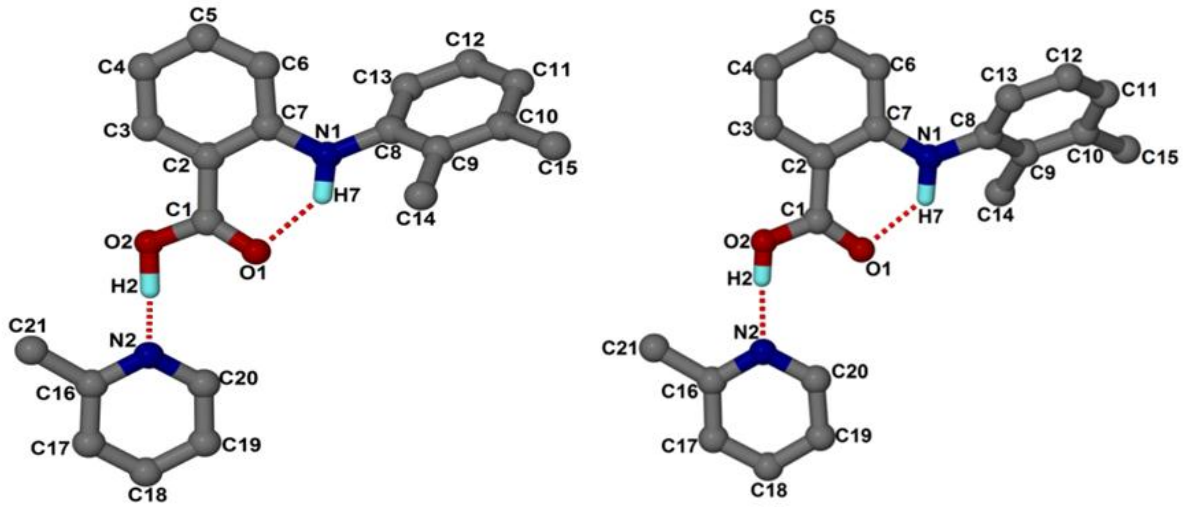

Figure 3-1: Numbering scheme for MA•2PIC (a) Form I and (b) Form II.

Form I had neighbouring molecules of MA linked together by two weak hydrogen bonds (Desiraju et al. 2011). One consisted of C12-H12•••O1 with a C12•••O1 distance of 3.482(2) Å and a C12-H12•••O1 angle of 155°. The neighbouring MA also interacted by C15-H15•••O1: distance 3.326(2) Å and angle 129°. In form II, these acid molecules were linked by C4-H4•••O1: with C4•••O1 distance of 3.434(2) Å and a C4-H4•••O1 angle of 150°.

A weak interaction was observed between the MA and the 2PIC molecules characterized by C21-H21B•••O1 (3.449(3) Å; 138°) (see Figure 3.2). Table 3.2 provides the different hydrogen bond data noted for these two structures.

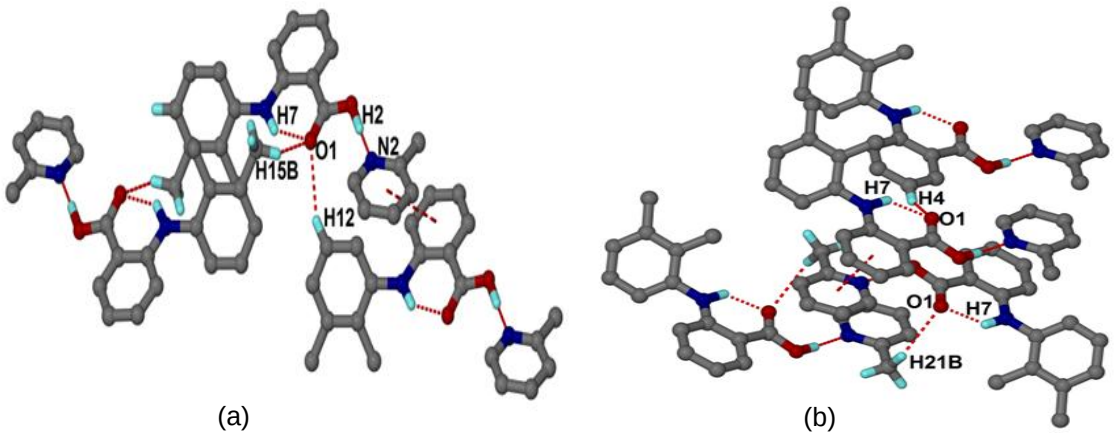

(a) (b)

Figure 3-2: Hydrogen bonding and π•••π interactions in MA•2PIC (a) form I and (b) form II (some hydrogen atoms were omitted).

The different molecules packed in a zigzag 2D layer along [010] in form I where 2-picoline molecules alternated with molecules of mefenamic acid (see Figure 3.3 (a). These alternating molecules formed wave-like sheets in form II (see Figure 3.3). The molecules also packed as columns where the carboxylic acid functional groups are orientated in opposing directions.

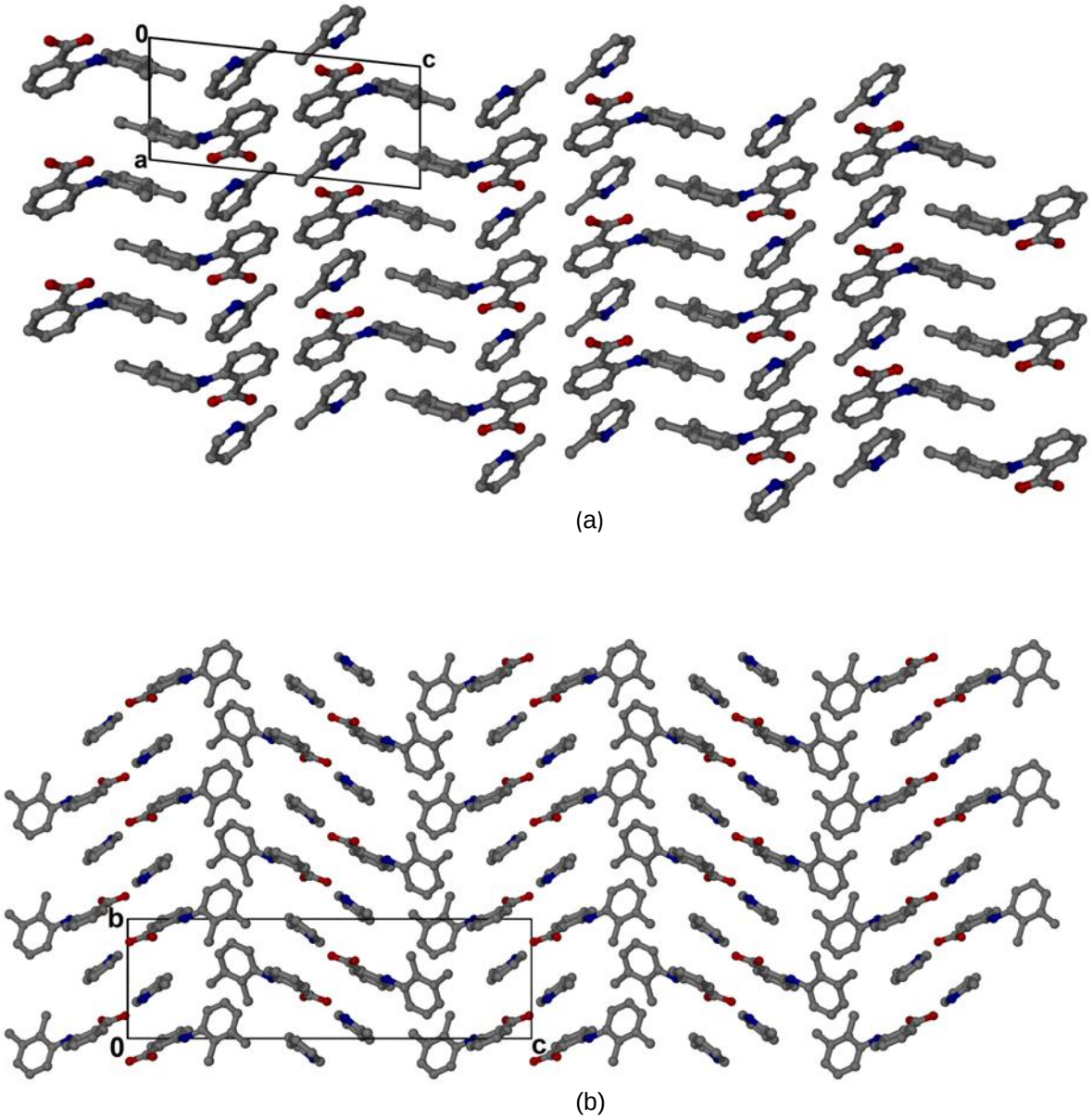

Figure 3-3: Crystal packing of MA•2PIC down [010] form I (a) and down [100] form II (b) (hydrogen atoms were omitted).

The different packing arrangements were stabilized by π•••π interactions with distances of 3.744 Å and 3.858 Å for form I and II respectively. Figure 3.4 presents the different channels along which the solvent molecules were located [100]. The solvent molecules were deleted from the structure in order to show the space occupied by the solvent and this was applied throughout the thesis where applicable.

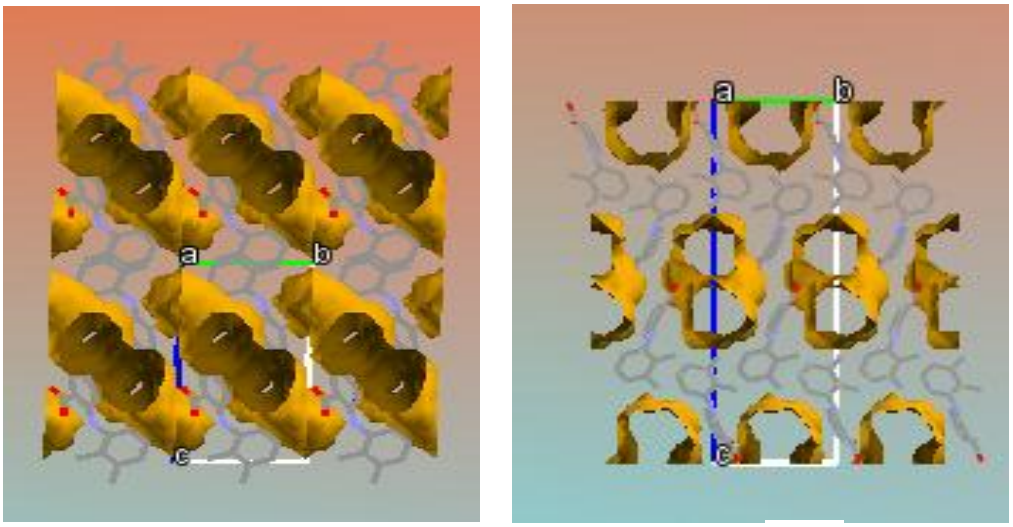

(a) (b)

Figure 3-4: Channels showing the location of 2-picoline molecules down [100] (a) form I and (b) form II respectively.

Table 3-1: Crystal data and data collection parameters for MA•2PIC and its polymorph.

Compound	MA•2PIC FORM I	MA•2PIC FORM II
Host:guest ratio	1:1	1:1
Molecular formula	$C_{21}H_{22}N_2O_2$	$C_{21}H_{22}N_2O_2$
Formula weight [g mol^{-1}]	334.41	334.41
Crystal system	Triclinic	Monoclinic
Space group	*P*$\bar{1}$	$P2_1/n$
Z	2	4
D_{calc} [g cm^{-3}]	1.250	1.256
a [Å]	7.6021(15)	7.7857(16)
b [Å]	8.4538(17)	8.1859(16)
c [Å]	15.375(3)	27.953(6)
α [°]	88.99(3)	90
β [°]	84.05(3)	96.87(3)
γ [°]	64.75(3)	90
V [Å^3]	888.5(3)	1768.8(6)
μ (Mo-Kα) [mm^{-1}]	0.081	0.081
λ (Å)	0.71073	0.71073
T [K]	173(2)	173(2)
$2\theta_{Max}$ [°]	56.9	54.2
No. reflections collected	22483	7473
No. unique reflections	4474	3893
No. reflections with I>2σ(I)	3761	2908
Parameters	231	231
R_1 [I>2σ(I)]	0.0434	0.0560
wR_2	0.1207	0.1616
GOOF	1.025	1.201

Table 3-2: Geometrical data of the hydrogen bonds.

	D-H/Å	H•••A/Å	D•••A/Å	<(DHA)/°	Symmetry operation
MA•2PIC FORM I					
O2-H2•••N2	1.09	1.52	2.613(1)	178	-
N1-H7•••O1	0.94	1.88	2.667(1)	139	-
C12-H12•••O1	0.95	2.60	3.482(2)	155	X, Y-1, Z
C15H15B•••O1	0.98	2.63	3.326(2)	129	2-X, 1-Y, -Z
MA•2PIC FORM II					
O2-H2•••N2	0.87	1.76	2.629(2)	176	-
N1-H7•••O1	0.97	1.89	2.638(2)	132	-
C4-H4•••O1	0.95	2.58	3.434(2)	150	1+X, Y, Z
C21-H21B•••O1	0.98	2.66	3.449(3)	138	1-X, 1-Y, -Z

3.1.2.2 Solvates of mefenamic acid with 3-picoline/3-chloropyridine (MA•3PIC/MA•3ClPYR)

After two weeks at room temperature, **MA•3PIC** formed orange block-like crystals. After three weeks, the 3-chloropyridine (3ClPYR) solvate formed smaller yellow block-like crystals. Both solvates were prepared by slow evaporation of dilute solutions of MA and the respective solvent. The new compounds crystallised in the triclinic space group $P\bar{1}$ with Z = 2. Further analysis showed the same packing arrangements and matching was obtained after overlaying the two structures using Mercury (version 3.5, 2015) (Figure 3.5).

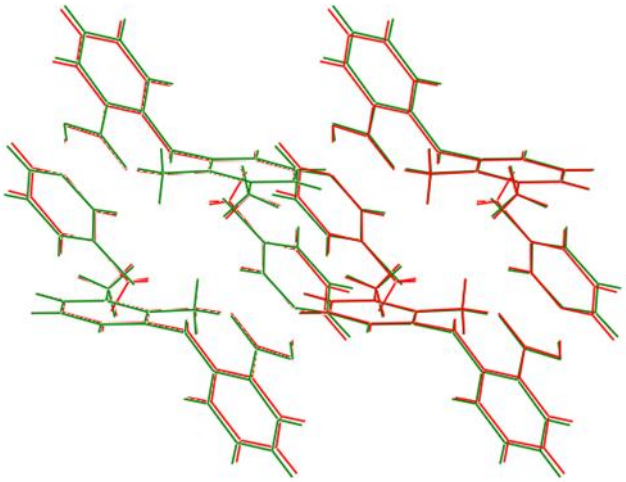

Figure 3-5: Overlay of MA•3PIC (red) and MA•3ClPYR (green) down [001].

The same intramolecular and intermolecular hydrogen bonds as recorded for **MA•2PIC** involving N1–H7•••O1 and O2–H2•••N2 were observed (Figure 3.6). The N1•••O1 distances were 2.650(1) Å for **MA•3PIC** and 2.659(2) Å in the **MA•3ClPYR** solvate with N1–H7•••O1 angles of 138° and 137° respectively. For the intermolecular hydrogen bonding, the O2•••N2 distances were 2.646(2) Å for the **3ClPYR** solvate with an O2–H2•••N2 angle of 171°. In the case of the 3-picoline (3PIC) solvate, the O2•••N2 distance was 2.602(1) Å with an O2–H2•••N2 angle of 179°.

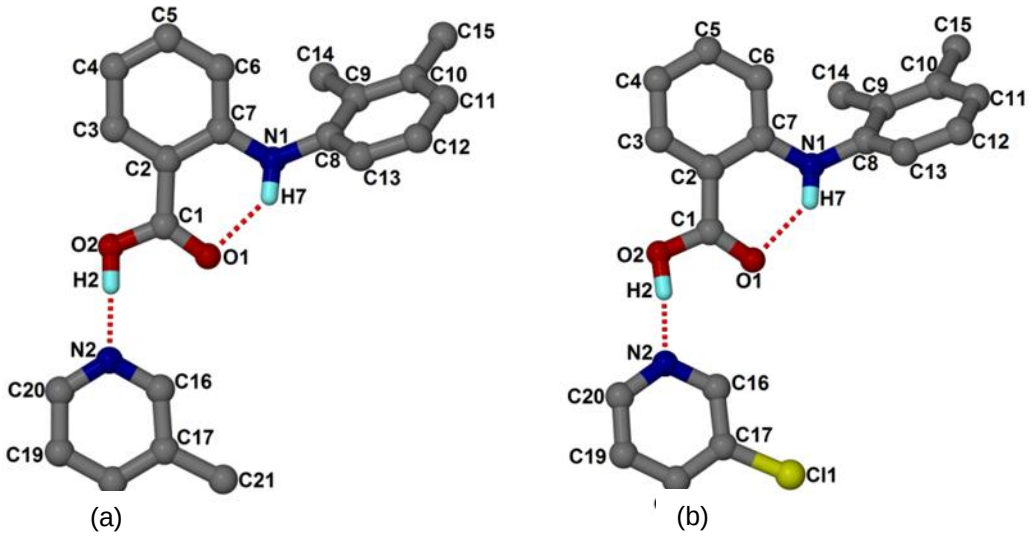

Figure 3-6: Numbering scheme for MA•3PIC (a) and MA•3ClPYR (b).

The packing arrangements along [100] of **MA•3PIC** and **MA•3ClPYR** are illustrated in Figure 3.7. The structure was arranged in columns whereby two columns of solvent molecules were located between two columns of MA molecules. In this case, the carboxylic acid groups were orientated toward each other, while the solvent molecules orientated the chlorine atoms and methyl groups in different directions (upward and downward) to accommodate interaction with the oxygen of the carbonyl group.

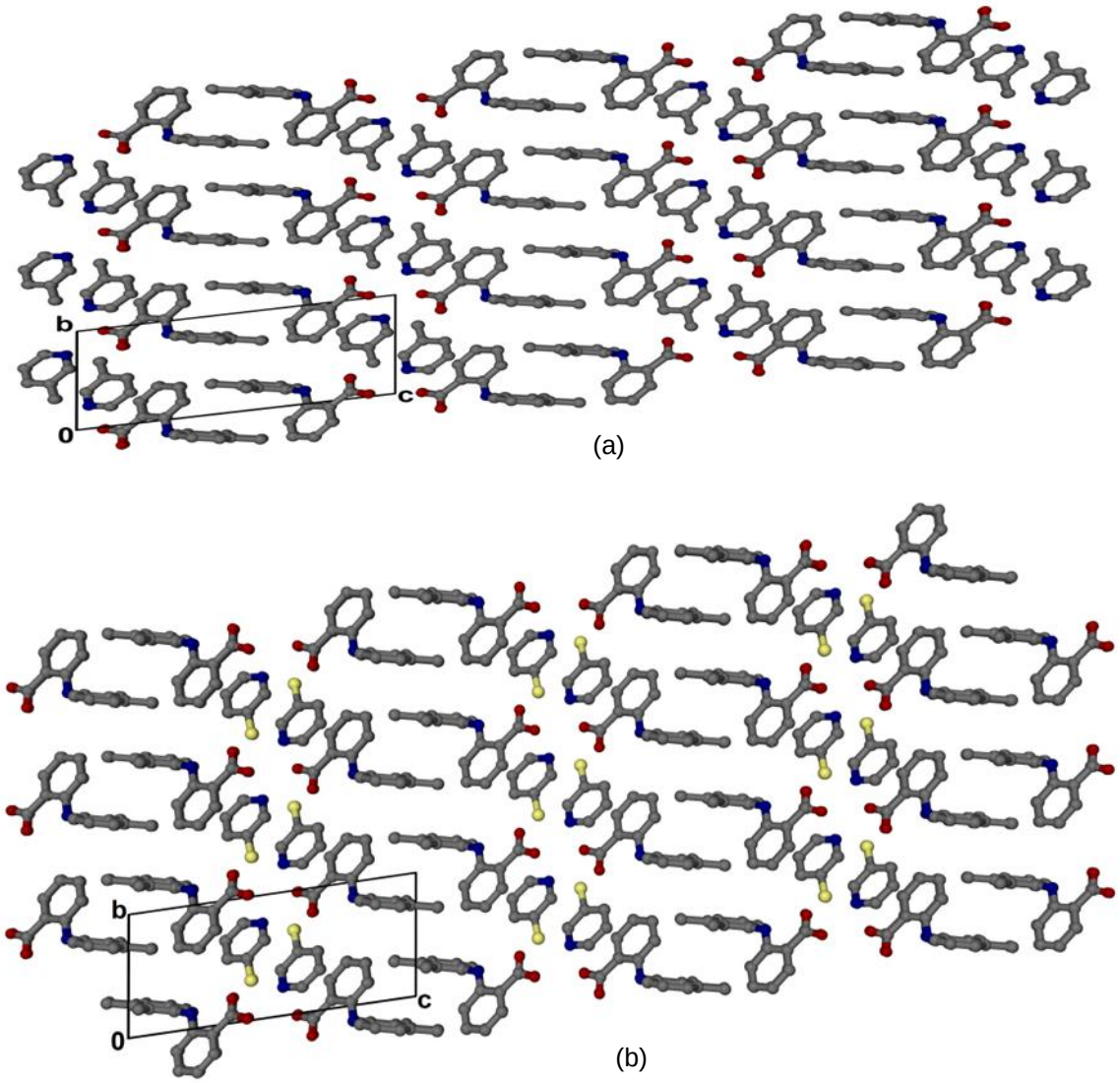

Figure 3-7: Packing diagram of (a) MA•3PIC and (b) MA•3ClPYR view down [010] (hydrogen atoms were omitted).

Additionally, π•••π interactions were found between the pyridine ring and the ring containing the carboxylic acid group of the mefenamic acid. The π•••π distances were 3.62 Å and 3.67 Å for **MA•3ClPYR** and **MA•3PIC** respectively.

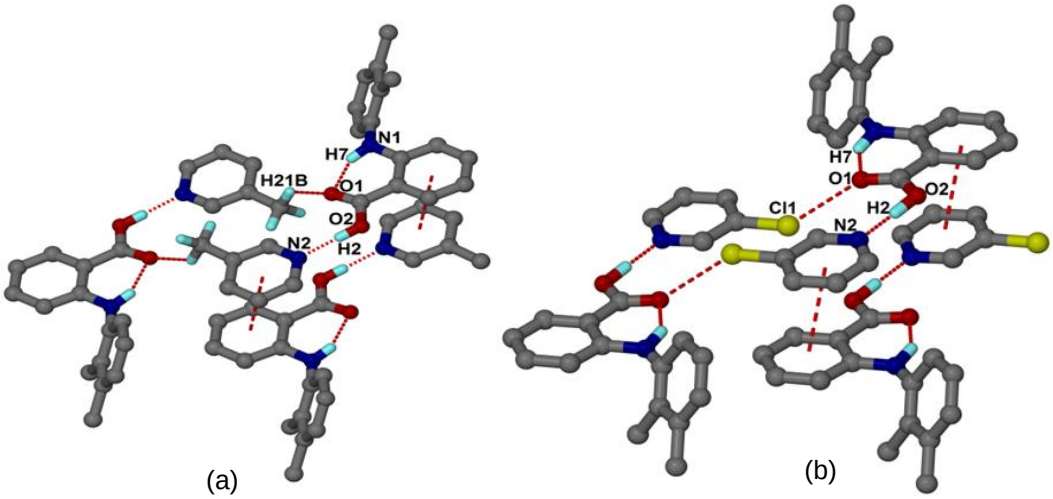

Figure 3-8: Weak hydrogen bonding, halogen interaction and π•••π interactions in (a) MA•3PIC and (b) MA•3ClPYR (some hydrogen atoms were omitted).

The packing of MA molecules only is presented in Figure 3.9 where it was seen to group in columns parallel to [100]. The solvent molecules occupied channels, demonstrated in Figure 3.10.

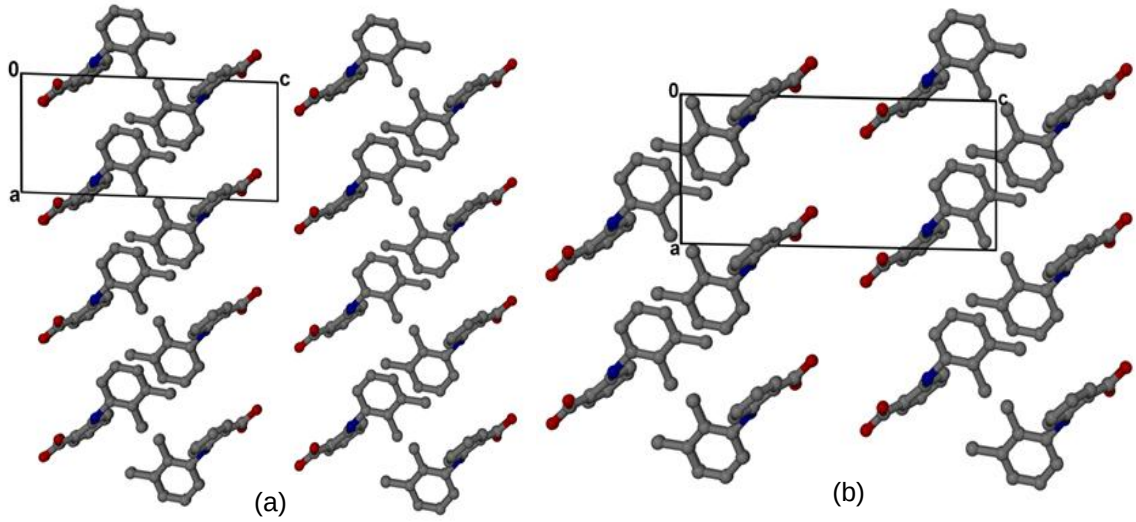

Figure 3-9: Packing arrangement down [010] for (a) MA•3PIC and (b) MA•3ClPYR without the guest (hydrogen atoms were omitted).

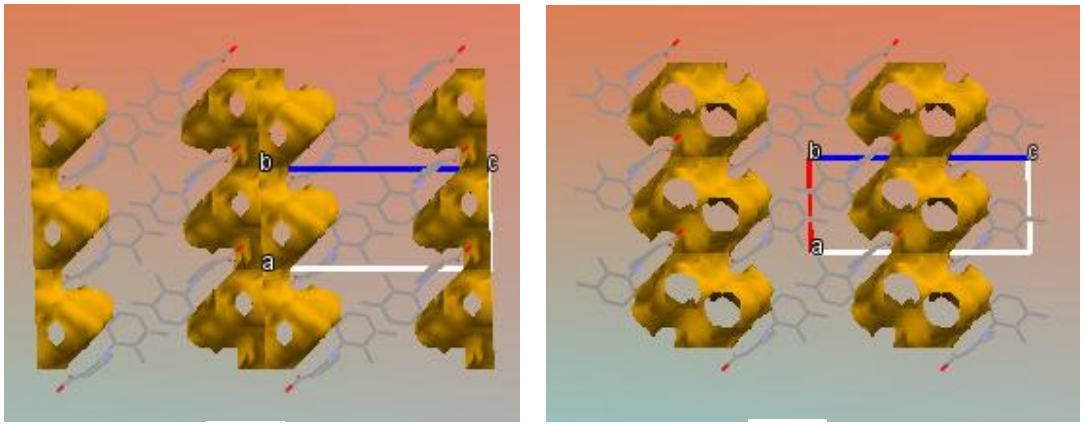

(a) (b)

Figure 3-10: Channels showing the location of 3-picoline (a) and 3Cl-pyridine (b) molecules down [010].

Table 3-3: Crystal data and data collection parameters for MA•3PIC and MA•3ClPYR.

Compound	MA•3PIC	MA•3ClPYR
Host:guest ratio	1:1	1:1
Molecular formula	$C_{21}H_{22}N_2O_2$	$C_{20}H_{19}ClN_2O_2$
Formula weight [g mol^{-1}]	334.41	354.82
Crystal system	Triclinic	Triclinic
Space group	$P\bar{1}$	$P\bar{1}$
Z	2	2
D_{calc} [g cm^{-3}]	1.288	1.379
a [Å]	7.6738(6)	7.6718(15)
b [Å]	7.7598(6)	7.7441(15)
c [Å]	16.2725(12)	16.056(3)
α [°]	78.9570(10)	80.06(3)
β [°]	83.673(2)	84.88(3)
γ [°]	65.0940(10)	65.50(3)
V [Å^3]	862.12(11)	854.8(3)
μ (Mo-Kα) [mm^{-1}]	0.083	0.240
λ [Å]	0.7107	0.7107
T [K]	173(2)	173(2)
$2\theta_{Max}$ [°]	56.9	57.0
No. reflections collected	20017	13863
No. unique reflections	4332	4290
No. reflections with I>2σ(I)	3671	3370
Parameters	231	230
R_1 [I>2σ(I)]	0.0408	0.0402
wR_2	0.1153	0.1131
GOOF	1.036	1.073

Table 3-4: Geometrical data for hydrogen bonds of MA•3PIC and MA•3ClPYR.

	D-H/ Å	H•••A/ Å	D•••A/ Å	<(DHA)/°	Symmetry operation
MA•3PIC					-
O2-H2•••N2	0.90	1.71	2.602(1)	179	-
N1-H7•••O1	0.86	1.96	2.650(1)	137	-
C16-H16•••O1	0.95	2.54	3.225(1)	129	-
C21-H21B•••O1	0.98	2.69	3.478(2)	138	-X, 1-Y, -Z
MA•3ClPYR					
O2-H2•••N2	0.95	1.71	2.646(2)	171	-
N1-H7•••O1	0.87	1.95	2.659(2)	138	-
C16-H16•••O1	0.95	2.52	3.194(2)	128	-

3.1.2.3 Solvate of mefenamic acid with 4-picoline (MA•4PIC)

The MA solvate with 4-picoline (4PIC) crystals formed one month after preparation. The crystal structure was also solved in the triclinic space group $P\bar{1}$ with one molecule of MA and one molecule of 4PIC in the asymmetric unit.

The intramolecular interaction N–H7•••O found in the structures of the previous solvates was also observed in this compound. The measured distance of N1•••O1 was 2.614(2) Å with an N1–H7•••O1 angle of 136°. The hydrogen bond used to link the MA and the 4PIC was characterised by an O2•••N2 distance of 2.678(2) Å and an O2–H2•••N2 angle of 176° (Figure 3.11).

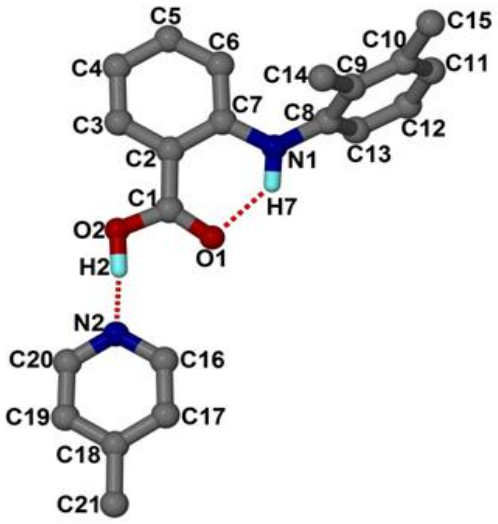

Figure 3-11: Numbering scheme for MA•4PIC.

The packing along [010] was similar to that noted for previous structures (Figure 3.12). This arrangement of molecules led to π•••π interactions with a distance of 3.74 Å between the centroids of the benzoic acid (MA) and the pyridine ring.

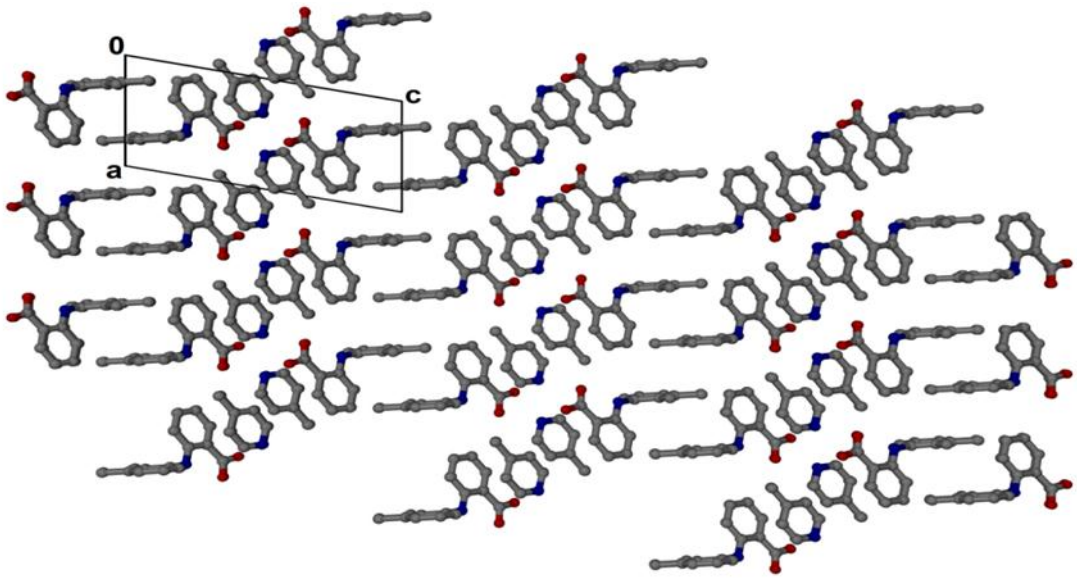

Figure 3-12: Crystal packing of MA•4PIC down [010] (hydrogen atoms were omitted).

When the guest is removed, the host packing is similar to that of the previous two structures (Figure 3.13). The solvent molecules occupy channels as shown in Figure 3.14.

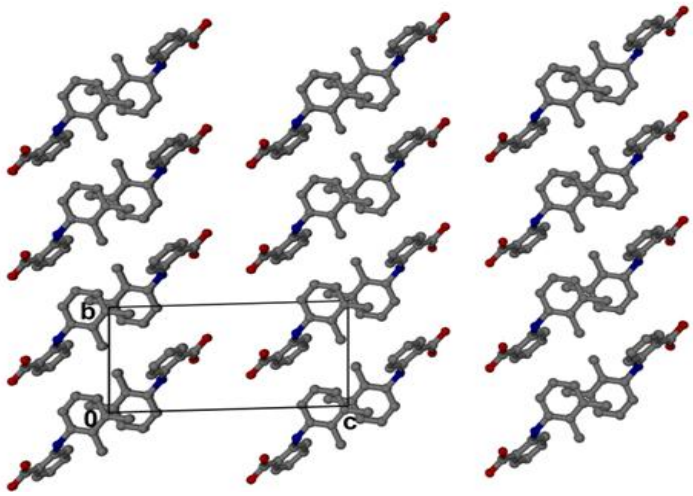

Figure 3-13: Packing diagram down [100] of MA•4PIC without the guest (hydrogen atoms were omitted).

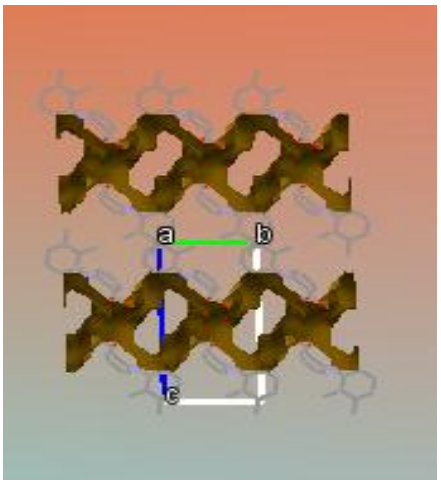

Figure 3-14: Channels showing the location of 4-picoline molecules down [100].

Table 3-5: Crystal data and data collection parameters for MA•4PIC.

Compound	MA•4PIC
Host:guest ratio	1:1
Molecular formula	$C_{21}H_{22}N_2O_2$
Formula weight [g g molmol^{-1}]]	334.41
Crystal system	Triclinic
Space group	$P\bar{1}$
Z	2
D_{calc} [g cm^{-3}]	1.271
a [Å]	7.5271(15)
b [Å]	7.5702(15)
c [Å]	15.664(3)
α [°]	88.11(3)
β [°]	78.41(3)
γ [°]	89.20(3)
V [Å^3]	873.9(3)
μ (Mo-Kα) [mm^{-1}]	0.082
λ [Å]	0.71073
T [K]	173(2)
$2\theta_{Max}$ [°]	55.9
No .reflections collected	8595
No .unique reflections	4147
No. reflections with I>2σ(I)	3128
Parameters	231
R_1 [I>2σ(I)]	0.0460
wR_2	0.1268
GOOF	1.056

Table 3-6: Geometrical data for hydrogen bonds of MA•4PIC.

	D-H/Å	H•••A/Å	D•••A/Å	<(DHA)/°	Symmetry operation
O2-H2 •••N2	1.00	1.62	2.678(2)	176	-
N1-H7 •••O1	0.92	1.94	2.614(2)	136	-

3.1.3 Torsion and dihedral angles of mefenamic acid with pyridines

For this section of the study, work done by SeethaLekshmi & Guru Row (2012) was used as a reference for the analysis of torsion angles. The conformational behaviour of MA was based upon the torsion angles of the twisting of the carboxylic group (O2C1C2C7), rotation of the phenyl ring (C2C7N1C8) and the twisting of the 2,3-dimethylphenyl (C7N1C8C9) (SeethaLekshmi & Guru Row, 2012). It should also be noted that the positive and negative signs used to denote the measured angles were not considered during the analysis.

The torsion angles for the rotation of the phenyl ring (C2C7N1C8) are comparable for all the structures (Table 5) with the highest value observed in **MA•2PIC** form II. The dihedral angle increased as the methyl substituent moved from the ortho position (57°, **MA•2PIC** form I; 50°, **MA•2PIC** form II) to the meta (63°, **MA•3PIC**; 64°, **MA•3ClPYR**) and para positions (75°, **MA•4PIC**) of the pyridine derivative.

However, the twisting of the carboxylic acid group does not depend on the position of the methyl substituent as the different torsion angles were 177° for **MA•2PIC** (forms I & II), **MA•3ClPYR** and **MA•4PIC** (Table 3.7). It was expected that **MA•3PIC** would follow this trend, because it has the same packing arrangement as **MA•3ClPYR,** but a higher value was obtained (179°). One of the most important differences observed was the twisting of the 2,3-dimethylphenyl rings. The torsion angles were similar for the *meta* (**MA•3PIC**: 72°; **MA•3ClPYR**: 71°) and *para* (**MA•4PIC**: 79°) substituted pyridines even though there was a slight increase of the torsion angle for the **MA•4PIC**. Conversely, the MA molecules present in the **MA•2PIC** solvates showed an increased value for the torsion angle of 136° and 135° when taking into account the twisting of 2,3-dimethylphenyl ring.

Table 3-7: Torsion and dihedral angles of MA•2PIC, MA•3ClPYR, MA•3PIC and MA•4PIC.

	MA•2PIC FORM I	MA•2PIC FORM II	MA•3PIC	MA•3ClPYR	MA•4PIC
Torsion angle/°					
O2C1C2C7	-177	177	-179	-177	177
C2C7N1C8	168	-177	-170	-171	172
C7N1C8C9	136	-135	-72	-71	79
Dihedral angle/°	57	50	63	64	75

Figure 3.16 shows the configuration of the **MA•2PIC FORM I** (a), **MA•2PIC FORM II** (b) and **MA•3ClPYR** (c). The carboxylic acid (**MA•2PIC FORM I** & **II)** is in a *cis*-conformation relative to the two methyl substituents which are in a *trans*-conformation in the **MA•3ClPYR**. The torsion angle seems to be twisted thereby justifying the higher of the torsion angle of **MA•2PIC** (**FORM I** & **FORM II**). Similarly, it explains why the packing diagrams of these solvates are slightly different to that recorded for other substituted pyridine solvates (**MA•3PIC/3ClPYR/4PIC**). Conversely, the two polymorphs of **MA•2PIC** differed in the direction of the 2,3-dimethylphenyl ring. In form I, the ring is directed forwards while in form II it is directed backward relative to the plane. Figure 3.16 (d) is an improved illustration of these differences. Form I is indicated in grey and form II magenta.

Most variation was observed in the twisting of 2,3-dimethylphenyl (C7N1C8C9) and research done by Surov et al. (2014) focused on this specific torsion angle. The **MA•2PIC** (FORM I: 136° and FORM II: 135°) showed a similar torsion angle to that noted for the mefenamic acid nicotinamide co-crystal (137°) as reported by Fabian et al (2011). The MA form I (119°) reported by SeethaLekshmi & Guru Row (2012) and by Fang et al. (2002). The **MA•4PIC** (79°) had a torsion angle similar to the 77° observed elsewhere for the co-crystal of mefenamic acid and bipyridine (Surov et al. 2015). The dihedral angles (Figure 3.15) were also in the range of previously published values which varied between 50.4° (MA nicotinamideco-crystal) and 80.3° (MA Form III) (Surov et al. 2015). The dihedral angle in the **MA•DMF** (75.3°) was found to be close in value to that recorded for **MA•4PIC** (75.0°).

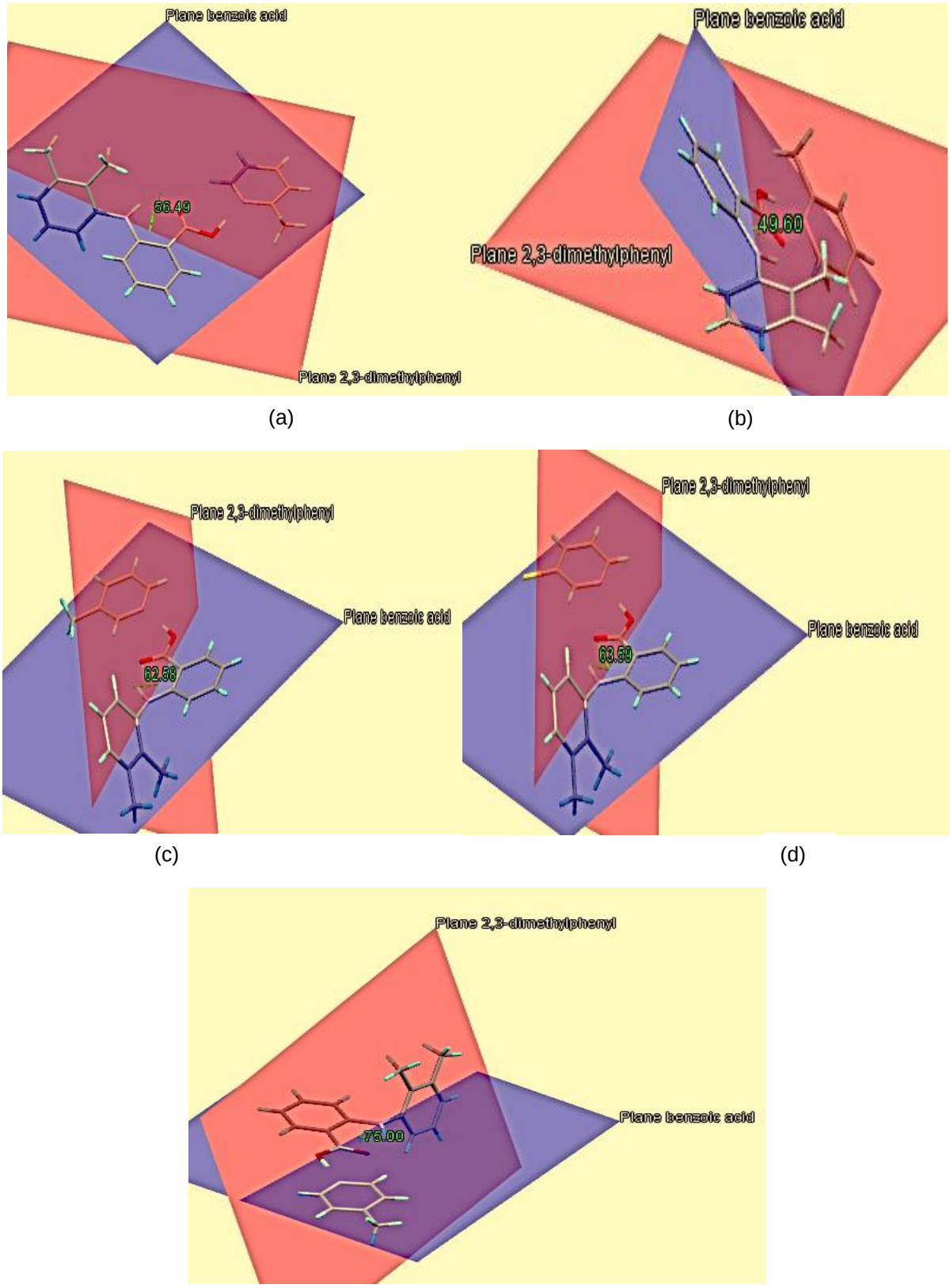

Figure 3-15: Dihedral angles between the planar grouping consisting of the 2,3-dimethylphenyl group (red) and the benzoic acid group (blue) of (a) MA•2PIC FORM I, (b) MA•2PIC FORM II, (c) MA.3PIC, (d) MA•3ClPYR and (e) MA•4PIC.

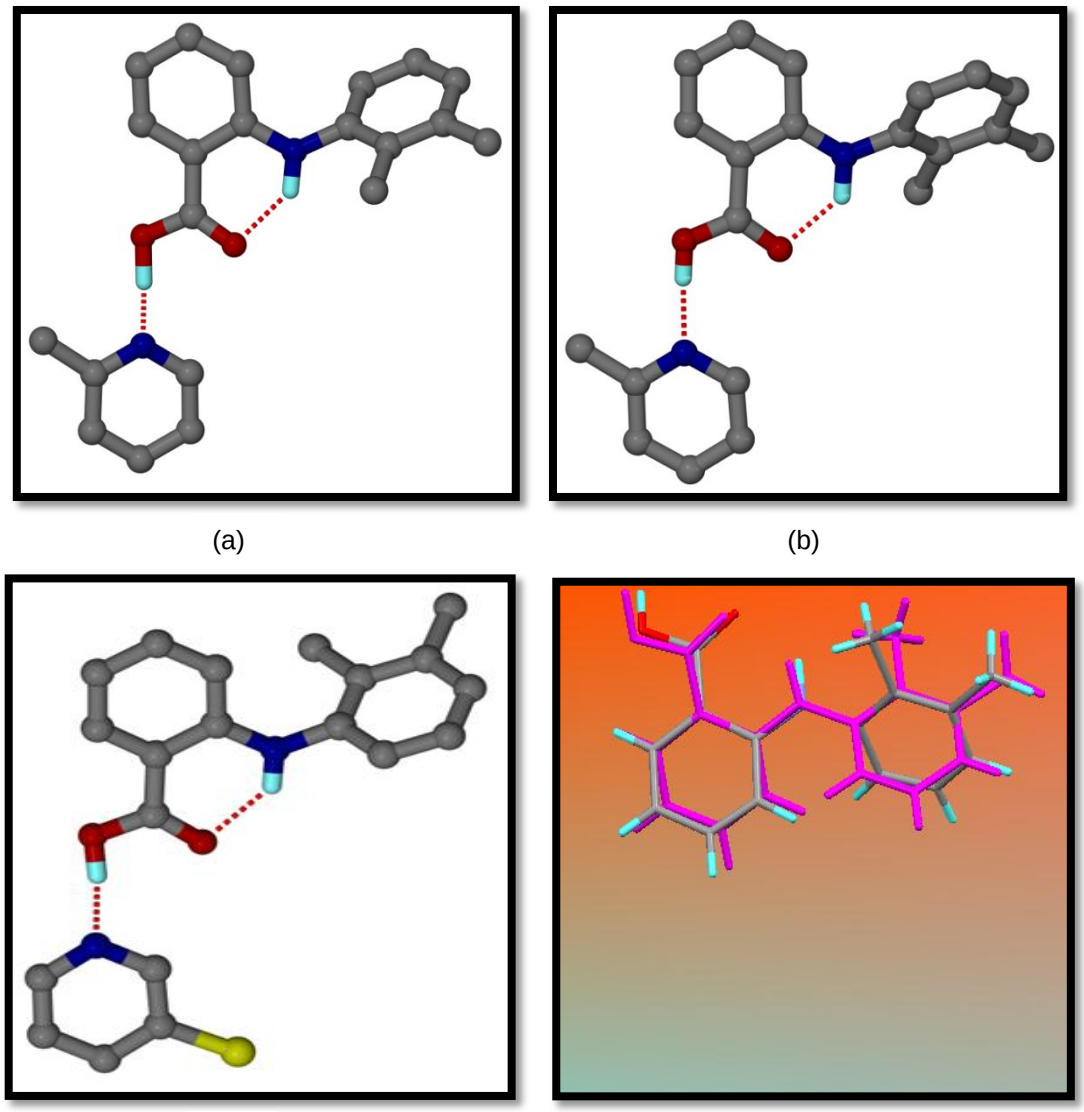

Figure 3-16: Differences noted for the 2,3-dimethylphenyl groups in the MA•2PIC (a) Form I, (b) Form II; (c) MA•3ClPYR (some hydrogen are omitted) and the overlay of MA•2PIC Forms I & II in (d).

3.1.4 Thermal analysis of mefenamic acid with pyridines

The TGA traces of the different solvates showed losses in % mass of 23.2% for **MA•2PIC** (form II), 26.1% for **MA•3PIC**, 30.3% for **MA•3ClPYR** and 25.6% for **MA•4PIC**. The calculated % mass loss for a 1:1 stoichiometry was 27.8% for the picoline solvates and 32.0% for the 3-chloro pyridine solvate. The experimental mass loss for **MA•2PIC** (form II) was much less than the expected value. This is possibly due to the fact that the crystals tend to desolvate rapidly once removed from the mother liquor.

Table 3-8: Thermal analysis data of MA•2PIC, MA•3ClPYR, MA•3PIC and MA•4PIC

SOLVATES	MA•2PIC	MA•3PIC	MA•3ClPYR	MA•4PIC
Host: Guest ratio	1:1	1:1	1:1	1:1
TG theo. % mass loss	27.8	27.8	32.0	27.8
exp. % mass loss	23.2	26.1	30.3	25.6
DSC endotherm for loss of solvent (T_{on}/K)	334	336	336	348
DSC endotherm of mefenamic acid (T_{on}/K)	503	503	503	502
Solvent normal bp (K)	401	417	421	418
T_{on}/T_{bp}	0.8	0.8	0.8	0.8

(Solvents boiling point retrieved from Weast, 1980)

The DSC curves show two endotherms for the solvates; one for the loss of solvent and the other for the melt of the mefenamic acid. The temperature of onset (T_{on}) varied depending on the position of the methyl group ie. *ortho* substituted pyridine (334 K in form I); *meta* (336 K); *para* (348 K). The various solvents were observed to evaporate at temperatures lower than their boiling points (Table 3.8) possibly due to their location in channels. Figure 3.17 shows the TGA and DSC curves for the different solvates tested.

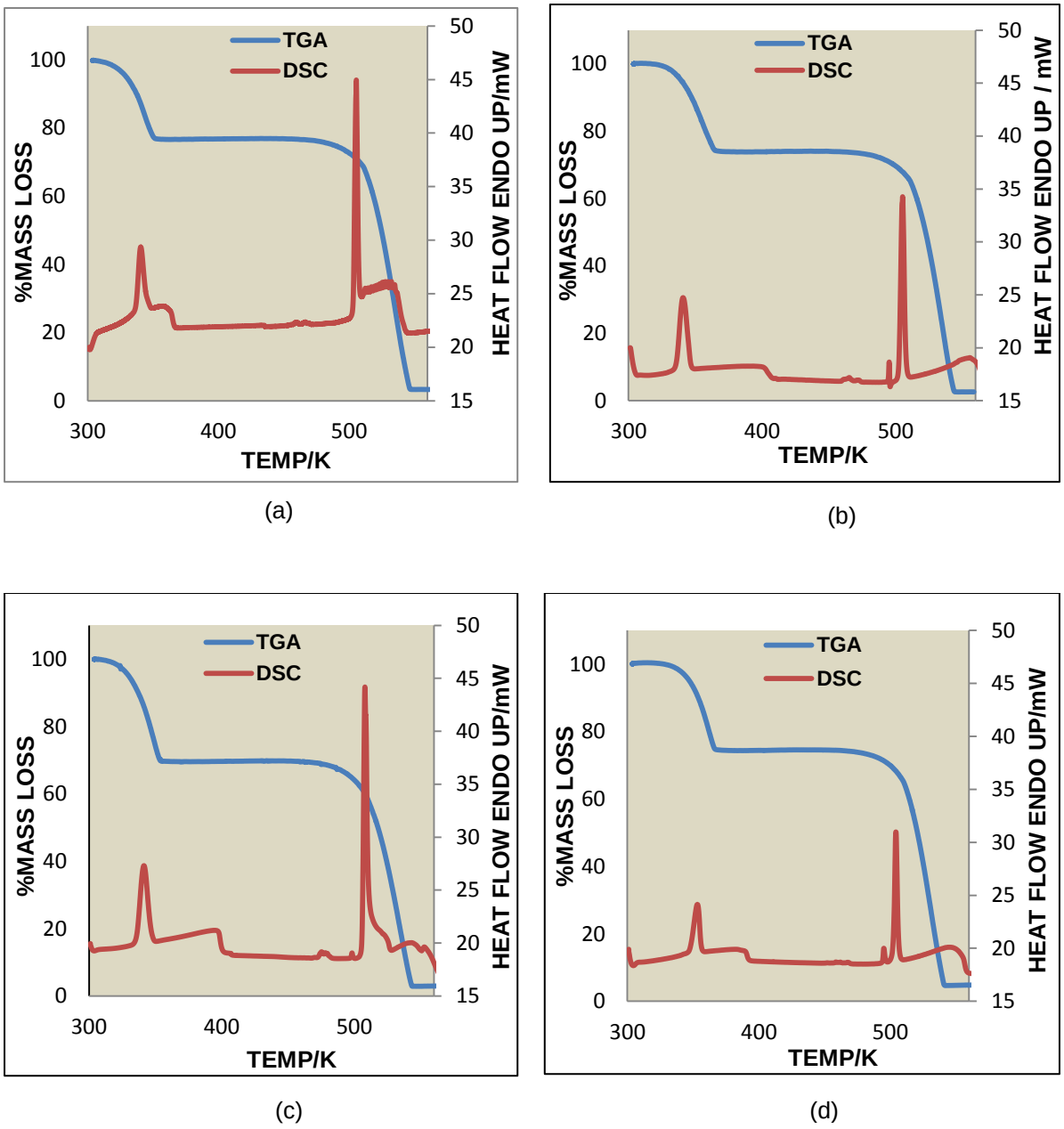

Figure 3-17: TGA and DSC curves of (a) MA•2PIC, (b) MA•3ClPYR, (c) MA•3PIC and (d) MA•4PIC.

The T_{on} representing the melting of MA was found to be similar for all solvates screened and was approximately 502.8 K. The thermal stability of all the solvates as measured by the T_{on}/T_b values was approximately 0.8 and this was related to similarities in the packing and the common intra and inter molecular interactions.

3.1.5 Powder X-Ray diffraction (PXRD) of mefenamic acid with pyridines

Powder X-ray diffraction was used to compare the theoretical patterns of the single crystal with those obtained from the grinding, prepared slurry, bulk sample and the starting material (MA). This was done to determine whether the solvates obtained from crystallisation could be reproduced by using different methods. The presence of a beamstop in the D2 phaser instrument did not allow the collection of data at 2-theta values less than 7°.

Material underwent a mechanical grinding procedure wherein 40 mg of the starting material were mixed with 2-3 drops of solvent (Chapter 2: section 2.4.8.1). After 20 min of grinding, the sample was left to dry until a powder was obtained from the mixture. A slurry was obtained by mixing 60 mg of the acid with an excess of solvent (section 2.4.8.2 in Chapter 2). The mixture was stirred at 30 °C until the acid was completely dissolved. Thereafter, the mixture was stirred at room temperature to form a suspension. The resulting powder was filtered and left to dry at ambient temperature prior to analysis. Finally, the different powders obtained from these processes were individually analysed by using PXRD.

Two different forms of the **MA•2PIC** solvate were identified by PXRD. After analysis of the bulk, grinding and slurry powders it was found that the resulting patterns did not match those obtained from the single crystal of the initial samples. Crystals from the bulk material were analysed using single crystal X-ray diffraction and it was determined that a new form of the solvate had been produced. The calculated pattern obtained from LAZYPULVERIX (Yvon et al*.* 1997) of this polymorph was similar to those associated with the bulk, grinding and slurry samples. Additional unassigned peaks obtained were attributed to unreacted starting material (Figure 3.18).

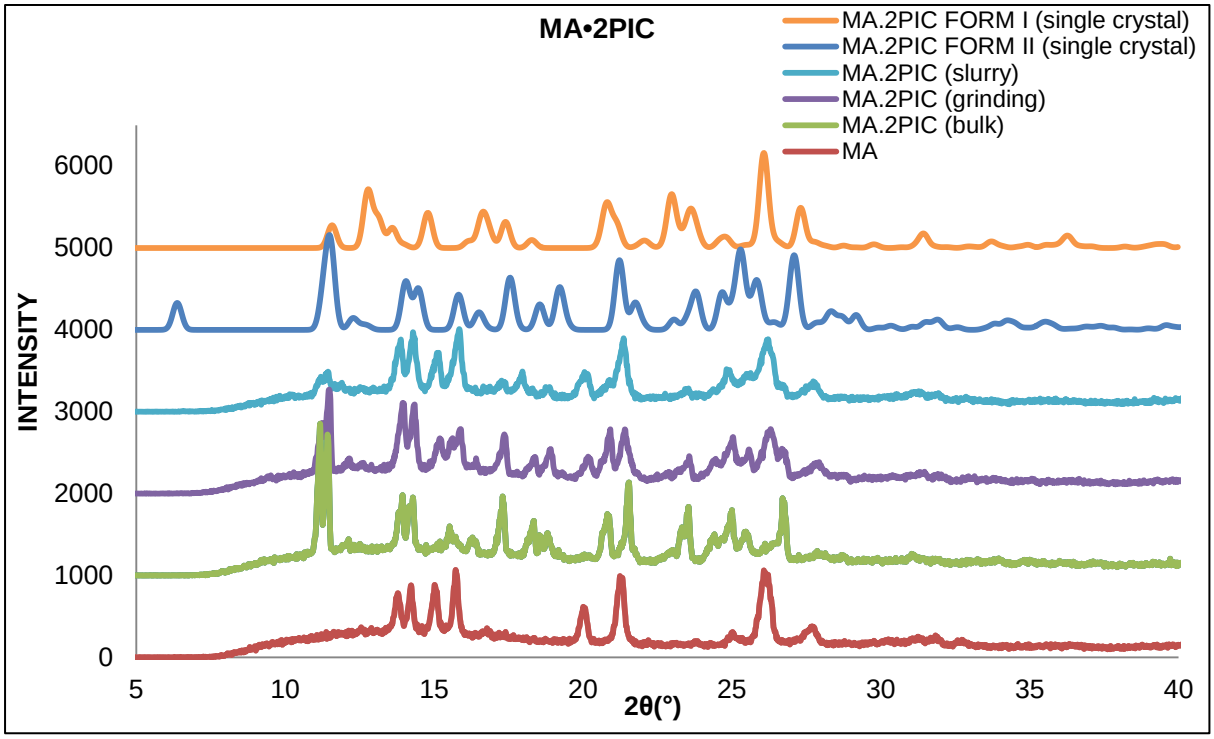

Figure 3-18: PXRD analyses of MA•2PIC calculated pattern obtained from LAZYPULVERIX of Form II (orange) and Form I (blue), and patterns from the slurry experiment (light blue); the grinding experiment (purple), bulk sample (green) and starting material MA (red).

Figure 3.19 shows the PXRD patterns recorded for **MA•3PIC**. The PXRD patterns showed acceptable matches in all the samples when compared with the PXRD patterns recorded for the single crystals.

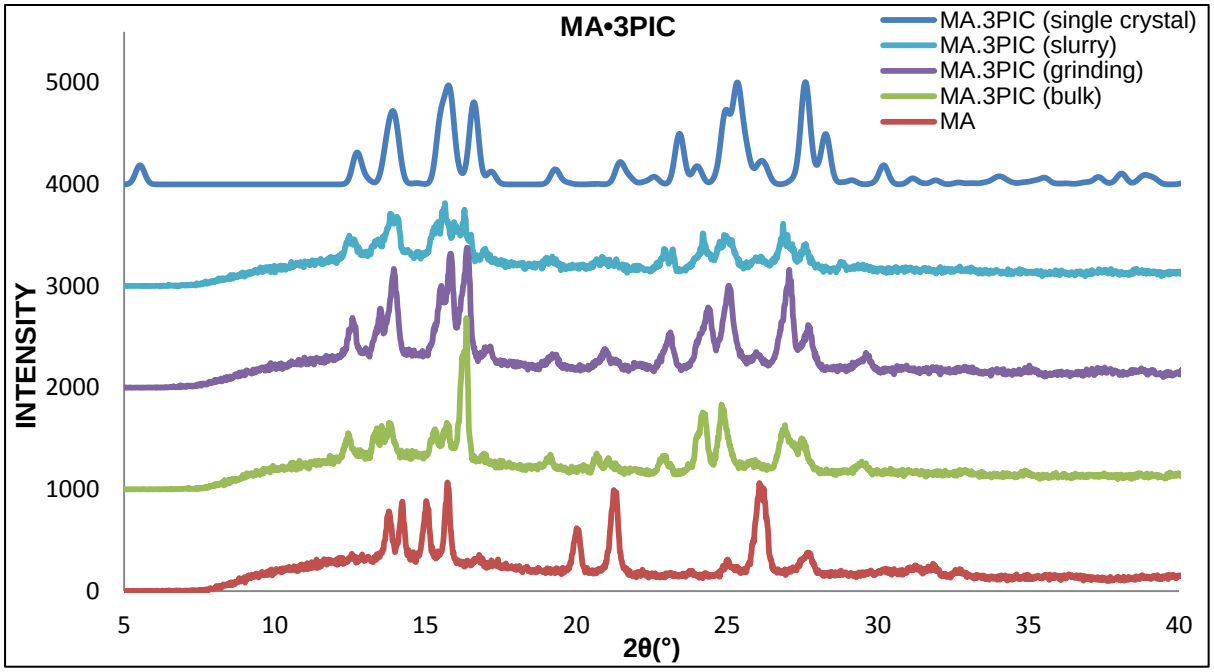

Figure 3-19: PXRD analyses of MA•3PIC: calculated pattern obtained from LAZYPULVERIX (blue), and patterns from the slurry experiment (light blue); the grinding experiment (purple), bulk sample (green) and starting material MA (red).

In the case of the **MA•3ClPYR** analyses the bulk, grinding and slurry samples showed PXRD patterns similar to the calculated pattern (Figure 3.20).

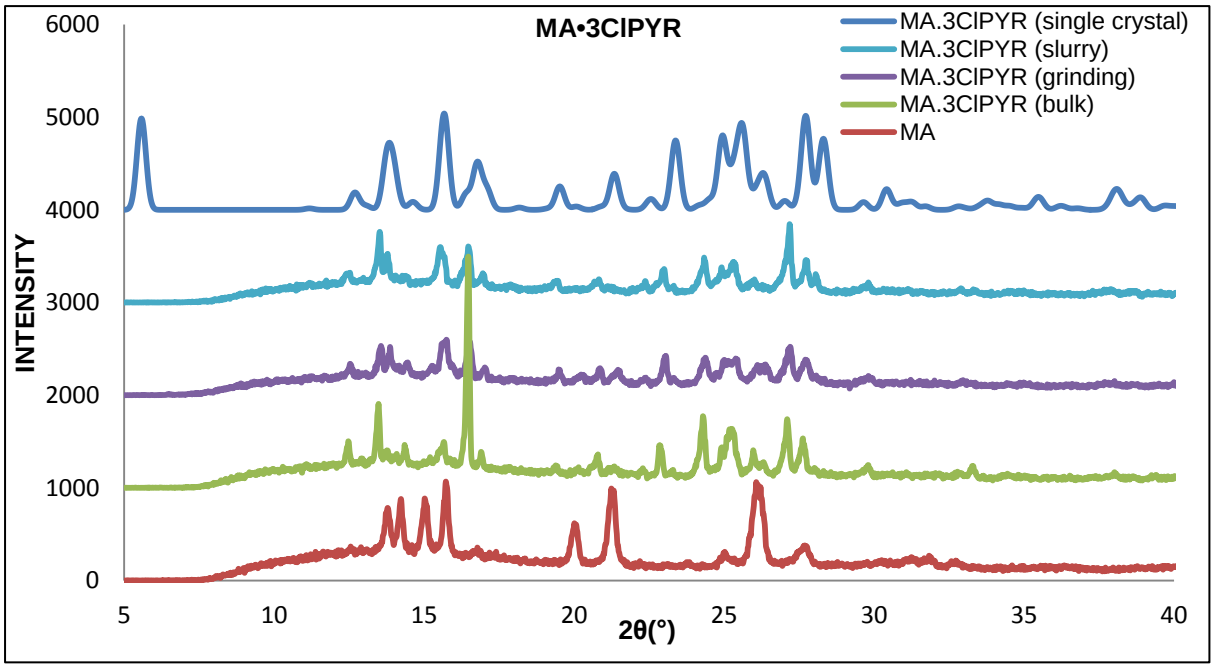

Figure 3-20: PXRD analyses of MA•3ClPYR: calculated pattern obtained from LAZYPULVERIX (blue), and patterns from the slurry experiment (light blue); the grinding experiment (purple), bulk sample (green) and starting material MA (red).

When **MA•4PIC** was subjected to PXRD analyses the various samples had profiles similar to that of the calculated pattern (Figure 3.21).

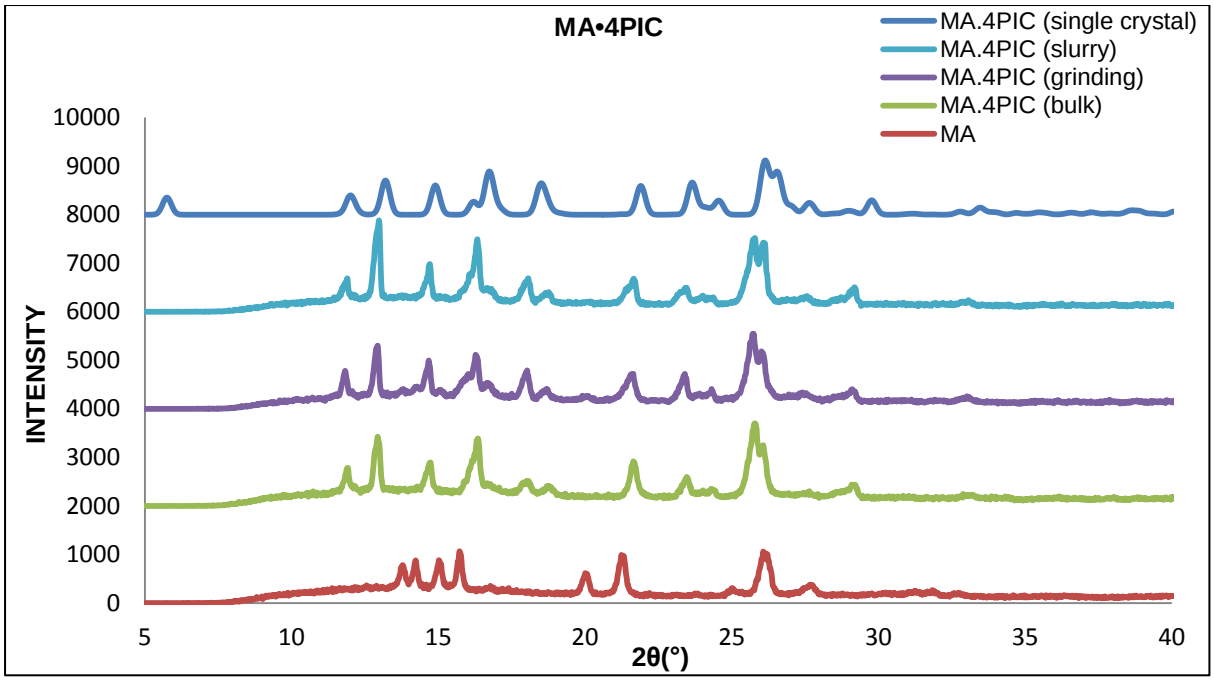

Figure 3-21: PXRD analyses of MA•4PIC calculated pattern obtained from LAZYPULVERIX (blue), and patterns from the slurry experiment (light blue); the grinding experiment (purple), bulk sample (green) and starting material MA (red).

3.1.6 Kinetics of desolvation of mefenamic acid with pyridine

The decomposition of the different solvates was determined by using non-isothermal kinetics. The experiments were carried out by crushing crystals of a specific solvate and then analysing them using TGA operating at different heating rates. The log β vs 1/T graphs which were obtained were used to determine the activation energies (β = heating rate) (Flynn & Wall, 1966). The activation energies were obtained from the following (refer Section 2.4.9, Chapter 2):

Slope= -0.457 $\frac{E_a}{R}$

- **MA•3PIC**

The TGA experiments for this solvate were carried out using heating rates of 2, 8, 16 and 30 K min^{-1}. The resulting graphs can be observed in Figure 3.22. The activation energy varied between 62-97 kJ mol^{-1}.

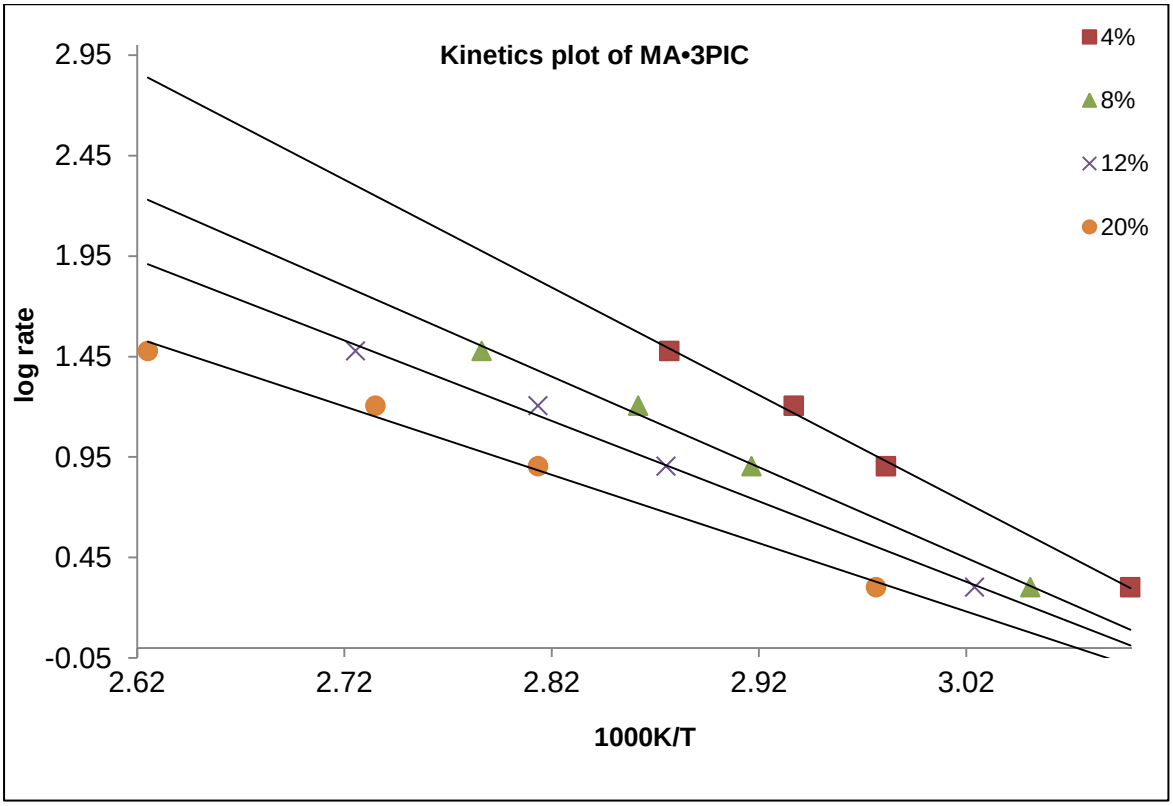

Figure 3-22: Log rate vs. 1/T graphs obtained for MA•3PIC.

For this solvate, experiments were carried out at heating rates of 6, 10, 24 and 30 $Kmin^{-1}$ (Figure 3.23). The activation energy ranged between 96-119 kJ mol^{-1}.

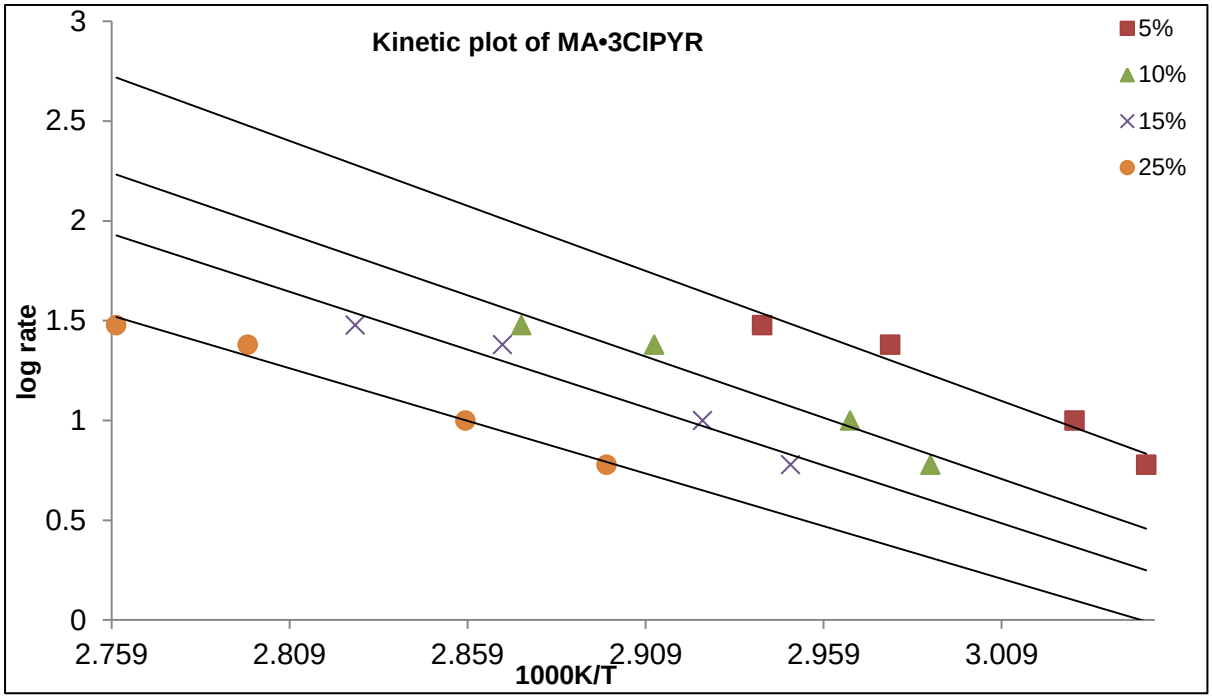

Figure 3-23: Log rate vs. 1/T graphs obtained for MA•3ClPYR.

The **MA•4PIC** solvate showed activation energies ranging between 111-120 kJ mol^{-1} where 2, 4, 6 and 8 K min^{-1} were the rates of heating (Figure 3.24).

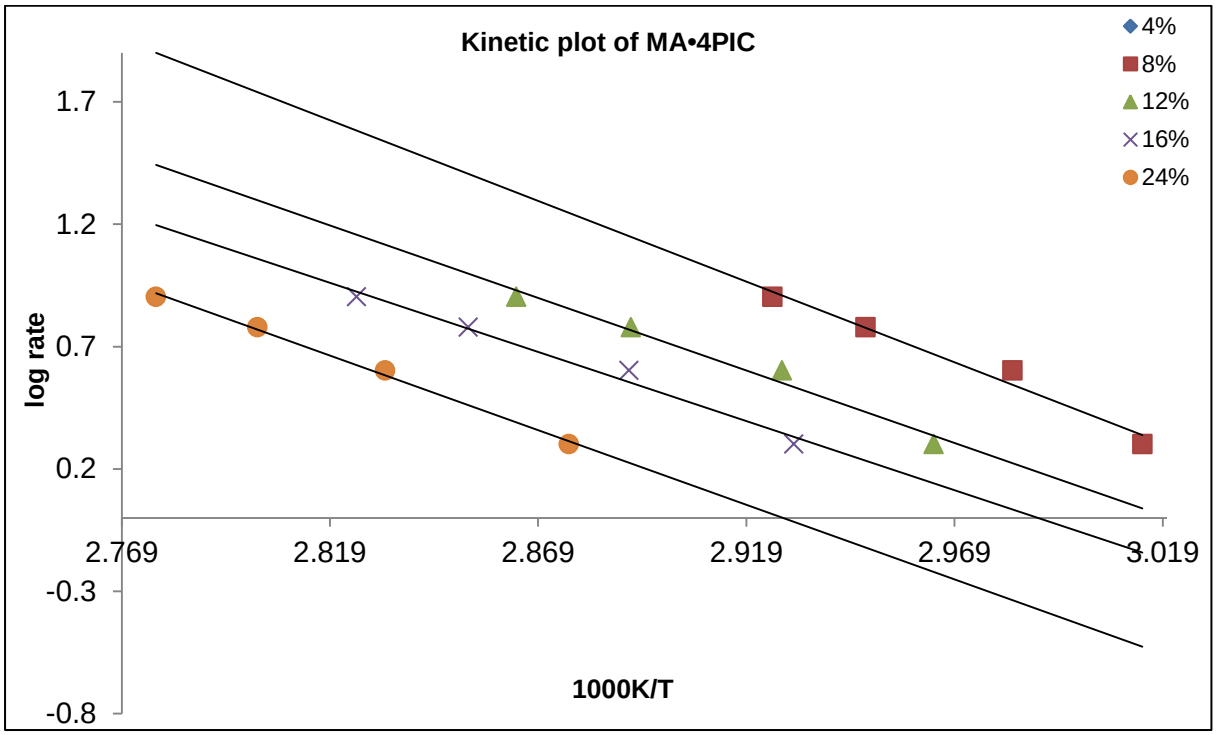

Figure 3-24: Log rate vs. 1/T graphs obtained for MA•4PIC.

3.1.7 Desolvation studies of mefenamic acid with pyridines

The desolvation of the solvates was performed by using two different methods. The first method required the solvent to be evaporated at room temperature (RT) over a period of one month. In the second method, samples were heated at 90°C for 24 h. The samples were then tested using TGA to confirm that no solvent was present in the powders. Thereafter, all samples were analysed using PXRD and compared to PXRD results obtained for the different polymorphs of mefenamic acid (Figure 3.25). A summary of the findings is provided in table 3.9.

The PXRD results obtained for the desolvated powders from both methods corresponded well with the PXRD analyses of form I with code XYANAC (McConnell & Company, 1976) in the Cambridge Structural Database (CSD, version 5.36, Nov 2014). Additionally, the resulting powders were also similar to the starting material (Figures 3.26 & 3.27).

Table 3-9: Desolvation data recorded for MA•2PIC, MA•3ClPYR, MA•3PIC and MA•4PIC.

	Desolvation at 90 °C for 24hr	Desolvation at RT for 1 month
MA•2PIC	Form I	Form I
MA•3PIC	Form I	Form I
MA•3ClPYR	Form I	Form I
MA•4PIC	Form I	Form I

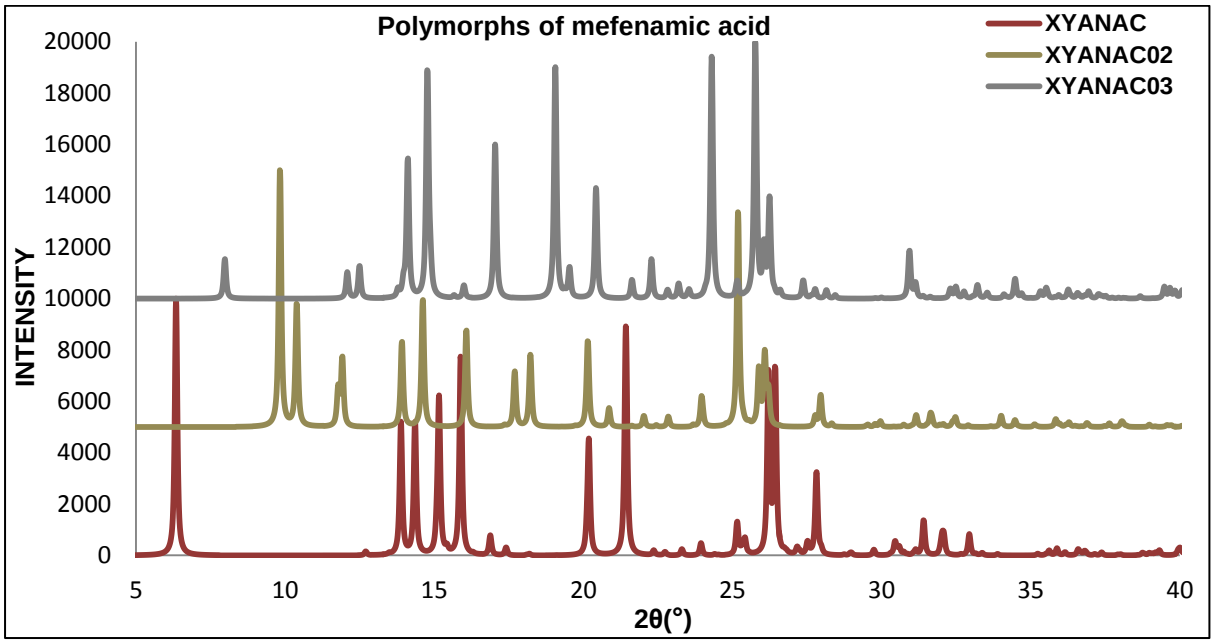

Figure 3-25: Simulated PXRD patterns of mefenamic acid polymorphs.

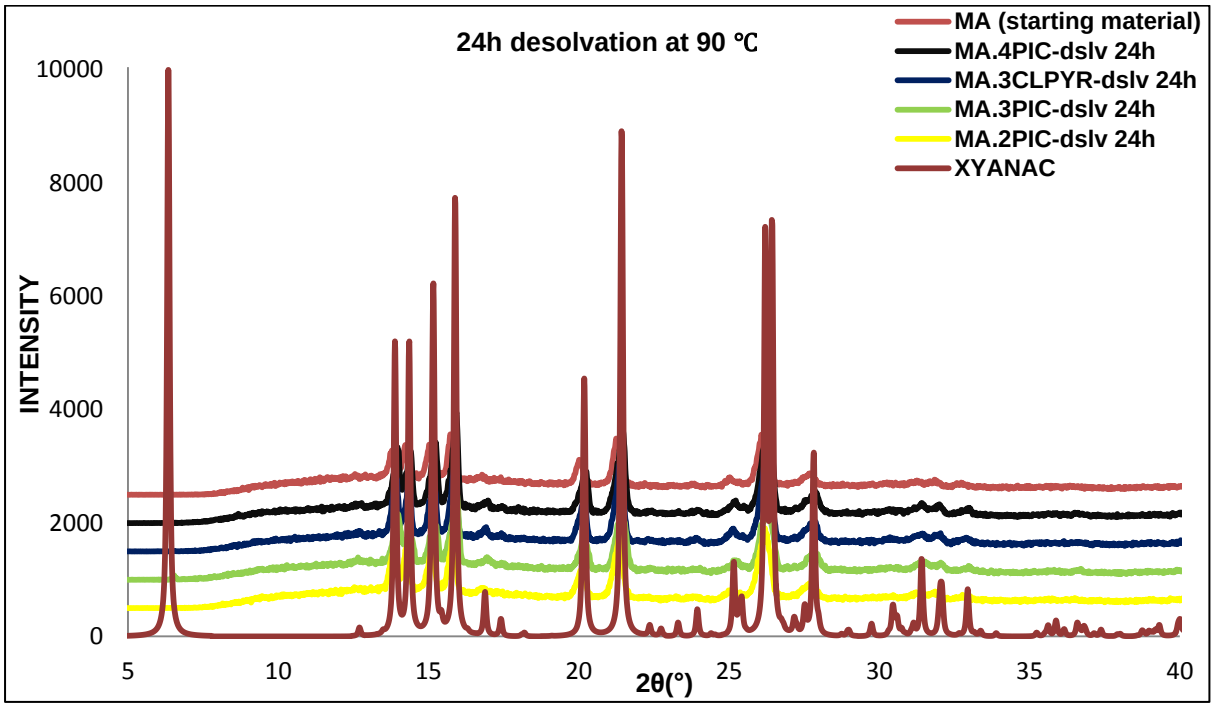

Figure 3-26: Patterns obtained from the PXRD analyses of mefenamic acid solvates subjected to 24 h desolvation at 90 °C.

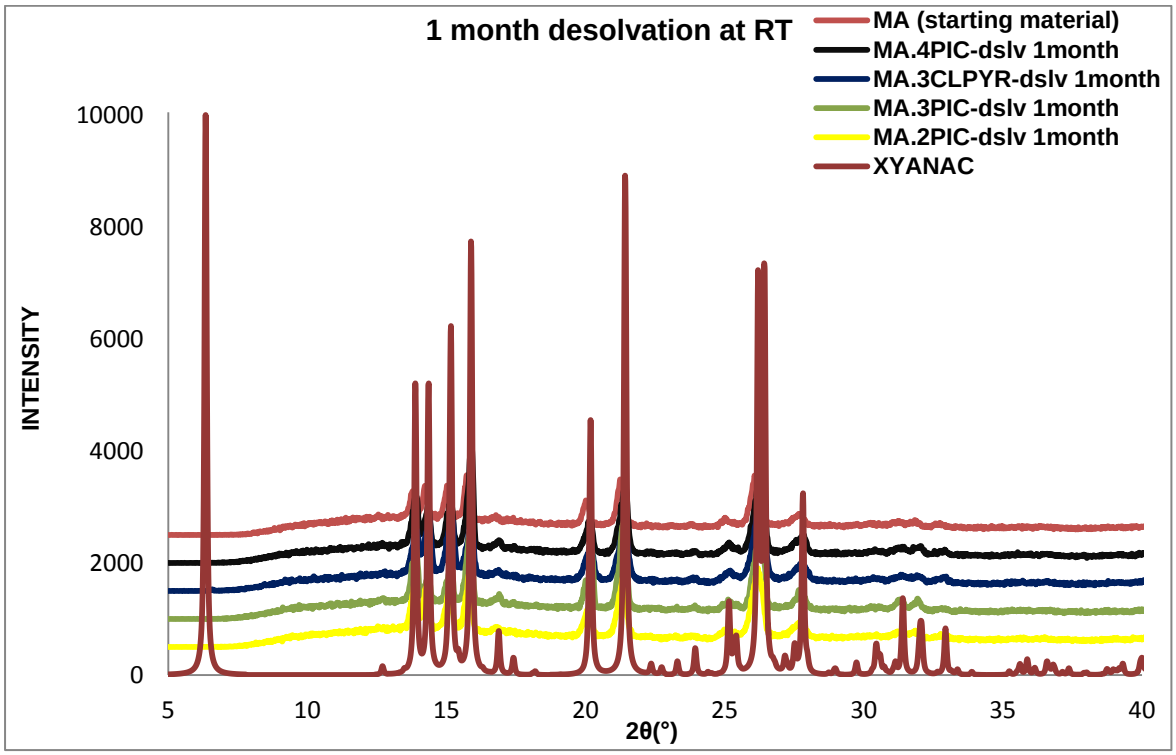

Figure 3-27: Patterns obtained from the PXRD analyses of mefenamic acid solvates after one month of desolvation at room temperature.

3.2 Solvates of tolfenamic acid with pyridine derivatives

3.2.1 Introduction

Tolfenamic acid was selected as a fenamate to form solvates as it has a molecular structure similar to that of MA. The single difference is the substitution of a methyl group by a chlorine. Research by Fabian et al. (2011) showed that co-crystals of MA and TFA with nicotinamide had similar hydrogen bonding and packing arrangements. Therefore in the current study, a trial was done to establish whether TFA would produce structurally similar solvates to MA when pyridine derivatives were used.

After preparation of mixtures of TFA with selected pyridine derivatives, the results indicated that solvates were produced when 2-picoline (2PIC), 3-picoline (3PIC) and 3-bromopyridine (3BrPYR) were used. The most remarkable observation was the difference in packing of tolfenamic acid-3-bromopyridine (**TFA•3BrPYR**) with tolfenamic acid-2-picoline (**TFA•2PIC**) and tolfenamic acid-3-picoline (**TFA•3PIC**). However **TFA•3BrPYR** was found to be isostructural to **MA•3PIC** and **MA•3ClPYR** as the packing arrangement was identical. The following section discusses the characterization of these structures in more detail.

3.2.2 Structural analysis of tolfenamic acid with pyridine derivatives

3.2.2.1 Solvates of tolfenamic with 2-picoline (TFA•2PIC)

Crystallization of TFA from 2PIC resulted in crystals characterized as 1:1 **TFA•2PIC** solvates. They appeared as block-like crystals after two weeks of slow evaporation of the mixed components. These crystals solved and refined in the monoclinic $P2_1/c$ space group with the asymmetric unit consisting of one molecule of the host with one molecule of the guest solvent. The crystallographic data is presented in Table 3.10.

Intramolecular and intermolecular hydrogen bond characteristics of MA solvates with the pyridine derivatives were also observed for TFA solvates (Figures 3.28, 3.31and 3.34). The measured distances and angles of these two interactions are reported in Table 3.11. There were also several weak interactions linking the molecules in the solvates. One weak hydrogen bond was observed between adjacent acids through C4-H4•••O1. It was characterized with a C4-•••O1 distance of 3.416(2) Å and a C4-H4•••O1 angle of 148°. Two

weak interactions were observed between the pyridine and the acid through C19 and C20 with O1. The measured distances between C19•••O1 and C20•••O1 were found to be 3.217(2) Å and 3.405(2) Å respectively. The angles measured were 125° for C19-H19•••O1 and 128° for C20-H20A•••O1.

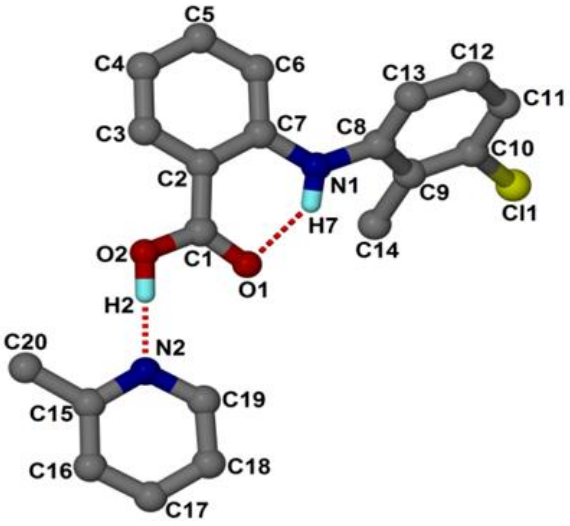

Figure 3-28: Numbering scheme for TFA•2PIC.

Figure 3.29 shows the arrangement of the molecules generating a type of wave-like sheet down [100]. This packing consisted of the alternation of TFA chlorine groups forming a column down [100]. The chlorine atom was orientated towards the carbons of the solvent and the host instead of the oxygen, but no close interactions were observed between chlorine and the carbon atoms. The TFA molecules organized to form columns whereby the -COOH groups were directed towards the nitrogen atom of the solvent. The compound was further stabilised through π•••π interactions between the acidic ring and the pyridine ring with a distance of 3.80 Å between the two centroids. The 2PIC molecules lay in constricted channels (Figure 3.30) parallel to [100].

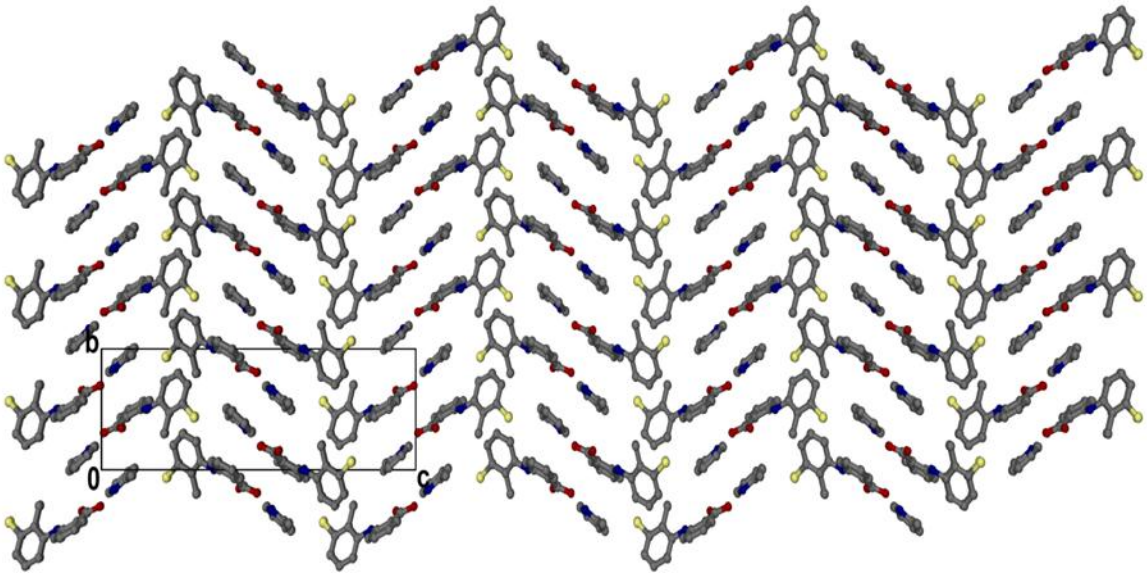

Figure 3-29: Crystal packing structure of TFA•2PIC view down [100] (hydrogen atoms were omitted).

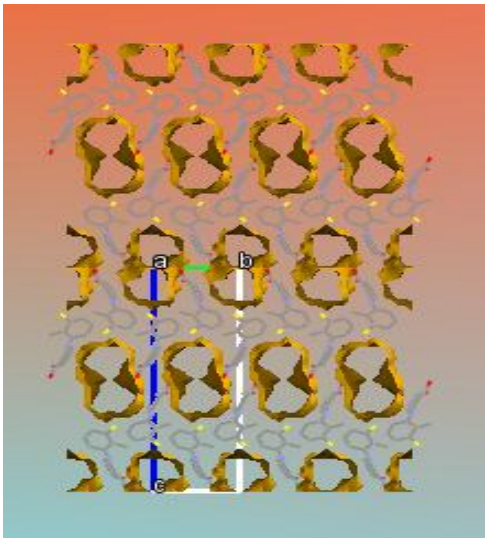

Figure 3-30: Channels showing the location of 2-picoline molecules down [100].

Table 3-10: Crystal data and data collection parameters of TFA•2PIC.

Compound	TFA•2PIC
Host:guest ratio	1: 1
Molecular formula	$C_{20}H_{19}ClN_2O_2$
Formula weight [g mol^{-1}]	354.82
Crystal system	monoclinic
Space group	$P2_1/n$
Z	4
D_{calc} [g cm^{-3}]	1.353
a [Å]	7.7585(16)
b [Å]	8.0699(16)
c [Å]	28.056(6)
α [°]	90
β [°]	97.29(3)
γ [°]	90
V [Å^3]	1742.4(6)
μ (Mo-Kα) [mm^{-1}]	0.235
λ [Å]	0.71073
T [K]	173(2)
$2\theta_{Max}$ [°]	56.8
No. reflections collected	24570
No. unique reflections	4345
No. reflections with I>2σ(I)	3478
Parameters	230
R_1 [I>2σ(I)]	0.0387
wR_2	0.1001
GOOF	1.014

Table 3-11: Geometrical data of hydrogen bonding in TFA•2PIC.

	D-H/Å	H•••A/Å	D•••A/Å	<(DHA)/°	Symmetry operation
O2-H2•••N2	0.91	1.70	2.611(2)	177	-
N1-H7•••O1	0.83	1.96	2.637(2)	139	-
C4-H4•••O1	0.95	2.57	3.416(2)	148	X-1, Y, Z
C19-H19•••O1	0.95	2.57	3.217(2)	125	-
C20-H20A•••O1	0.98	2.72	3.405(2)	128	1-X, 1-Y, 1-Z

3.2.2.2 Solvates of tolfenamic acid with 3-picoline (TFA•3PIC)

TFA•3PIC formed as platelet crystals one week after preparation. The structure was solved and refined in the orthorhombic space group *Pbca*. The unit cell contains four molecules of 3-picoline and four molecules of TFA. The crystal data parameters are given in Table 3.12 and the geometrical data for hydrogen bonding provided in Table 3.13.

A robust hydrogen bond, O–H•••N linked the fenamate to 3-picoline and an O2•••N2 distance of 2.599(2) Å was measured with an O2–H2•••N2 angle of 172° (Figure 3.31). There was a

weak C–H•••O interaction involving two TFA molecules and this was characterised by a C12•••O1 distance of 3.285(2) Å with a C12-H12•••O1 angle of 137°. The 3PIC also interacted with the MA through weak interactions by means of C19 and O2 with a distance of 3.372 Å and a C19-H19•••O2 angle of 151°.

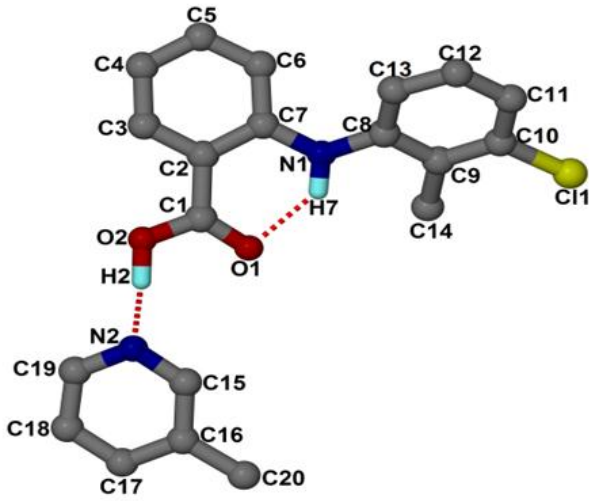

Figure 3-31: Numbering scheme for TFA•3PIC.

The structure of this solvate is similar to the packing arrangement of MA solvates with pyridine. Similarities were observed in the organisation of the paired molecules of the acid and the base. The packing is columnar but TFA is distributed in a helical manner (Figure 3.32). These helices are formed around the chlorine atom directed toward both the methyl substituted group on the picoline and the O2. However, no close interaction was observed. The acidic group (hydrophilic) of the fenamate is directed toward the nitrogen of the picoline. The packing is also stabilised by a C–H•••π interaction between the 3-picoline with the acidic ring of the fenamate characterised by a C17•••π distance of 3.40 Å. The 3PIC is positioned in channels along [100] as seen in Figure 3.33.

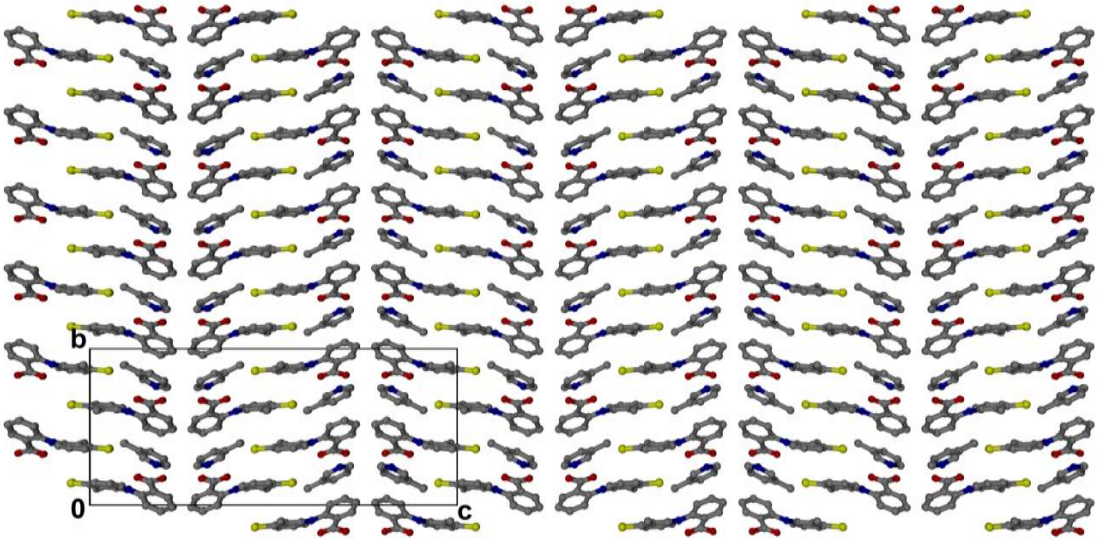

Figure 3-32: Packing diagram of TFA•3PIC down [100] (hydrogen atoms were omitted).

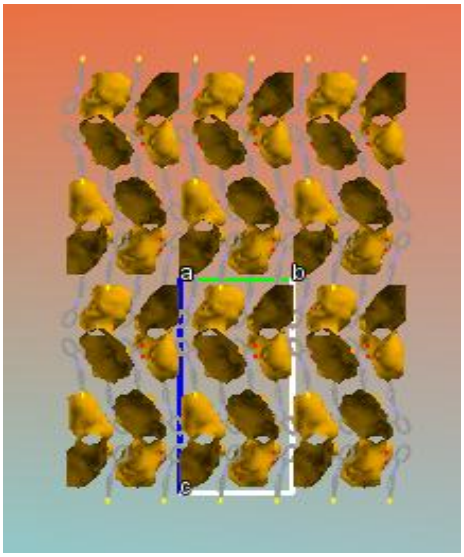

Figure 3-33: Channels showing the location of 3-picoline molecules along [100].

Table 3-12: Crystal data and data collection parameters for TFA•3PIC.

Compound	TFA•3PIC
Host:guest ratio	1:1
Molecular formula	$C_{20}H_{19}ClN_2O_2$
Formula weight [g mol^{-1}]	354.82
Crystal system	orthorhombic
Space group	*Pbca*
Z	8
D_{calc} [g cm^{-3}]	1.341
a [Å]	7.8069(16)
b [Å]	13.987(3)
c [Å]	32.185(6)
α [°]	90
β [°]	90
γ [°]	90
V [Å^3]	3514.5(12)
μ (Mo-Kα) [mm-1]	0.233
λ [Å]	0.71073
T [K]	173(2)
2θ Max [°]	56.8
No. reflections collected	51960
No. unique reflections	4397
No. reflections with I>2σ(I)	3281
Parameters	230
R_1 [I>2σ(I)]	0.0397
wR_2	0.0935
GOOF	1.026

Table 3-13: Geometrical data for the hydrogen bonds of TFA•3PIC.

	D-H/Å	H•••A/Å	D•••A/Å	<(DHA)/°	Symmetry operation
O2-H2•••N2	0.97	1.63	2.599(2)	172	-
N1-H7•••O1	0.88	1.95	2.671(2)	138	-
C12-H12•••O1	0.95	2.53	3.285(2)	137	1+X, Y, Z
C19-H19•••O2	0.95	2.51	3.372(2)	151	X- $^1/_2$, Y, $^3/_2$- Z

3.2.2.3 Solvates of tolfenamic acid with 3-bromopyridine (TFA•3BrPYR)

Crystallisation of TFA with 3BrPYR resulted in colourless block-like crystals obtained after 3 months. Single crystal analysis determined that the crystals belonged to the triclinic crystal system with space group *P*$\bar{1}$. The distance and angles of the intramolecular (N1•••O1, 2.657(3) Å; N1H7•••O1, 137°) and intermolecular (O2•••N2, 2.672(3) Å; O2H2•••N2, 173°) interaction are shown in Table 3.15. The most common interactions are illustrated in Figure 3.34.

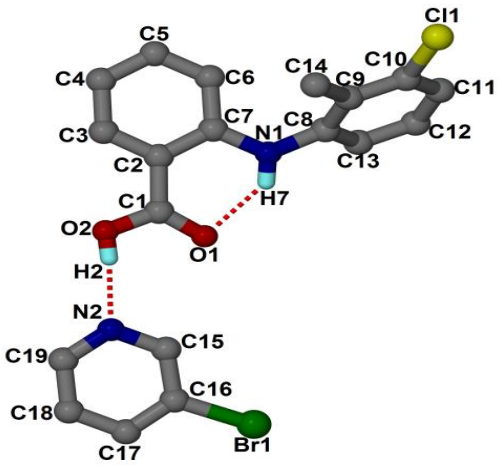

Figure 3-34: Numbering scheme for TFA•3BrPYR.

The bromine atom is directed towards O2 with the distance between the two atoms of 3.14 Å. It was also observed that the chlorine atom interacts with C6-H6, and the C6•••Cl1 distance is 3.695 Å with a C-H•••Cl angle of 140° (Figure 3.35). No notable interaction was observed between the two halogens of the solvent and the acid.

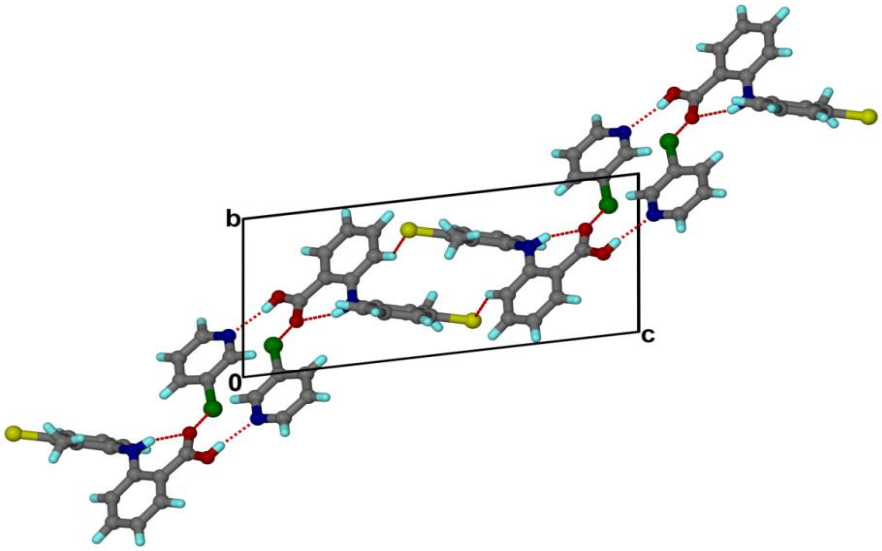

Figure 3-35: Hydrogen bonding and halogen interactions of TFA•3BrPYR down [100].

This particular solvate showed the same molecular packing as observed in the **MA•3PIC**/**MA•3ClPYR** (Figure 3.36). A columnar arrangement was found whereby two solvent molecules are positioned between the two acid molecules.

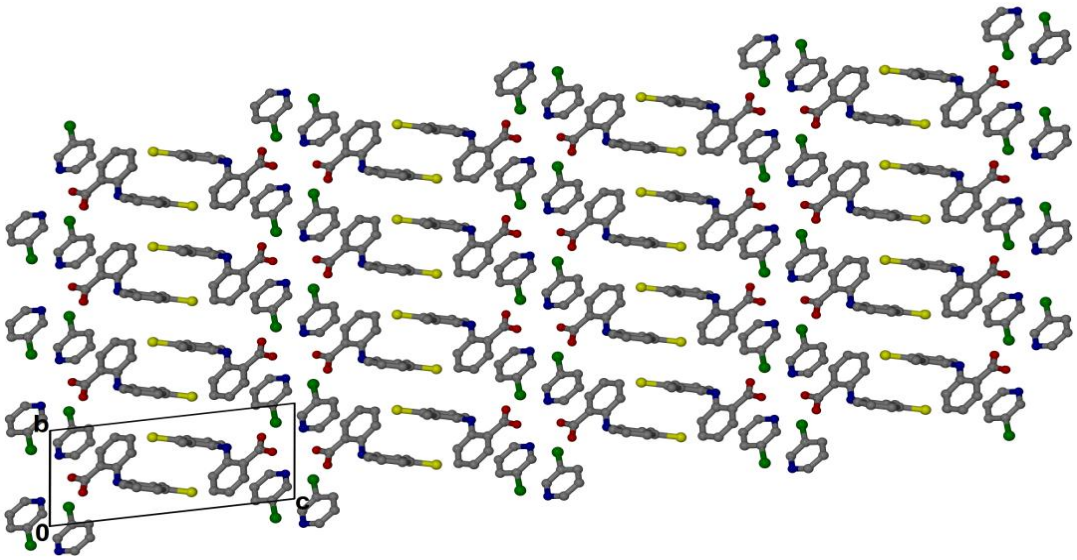

Figure 3-36: Crystal packing diagram of TFA•3BrPYR viewed down [100] (hydrogen atoms were omitted).

The compounds are stabilised by several C-H•••π and π•••π interactions. The C-H•••π interaction occurs between the carbon of the acidic phenyl group and the halogenated phenyl ring of the neighbouring TFA molecule with a C5•••π distance of 3.69 Å recorded. One of the observed π•••π interactions is situated between two substituted pyridine rings and the distance between the ring centroids is 3.69 Å. Another interaction originated from the 3BrPYR interaction with the acidic ring of the TFA where the distance is 3.68 Å between the ring centroids. Figure 3.37 shows the packing of the TFA molecules with the 3BrPYR solvent removed from the crystal lattice of **TFA•3BrPYR**. This packing was similar to that of the **MA•3PIC** solvate. Tables 3.14 and 3.15 provide the crystal data parameters of the solvate and the hydrogen bonds respectively.

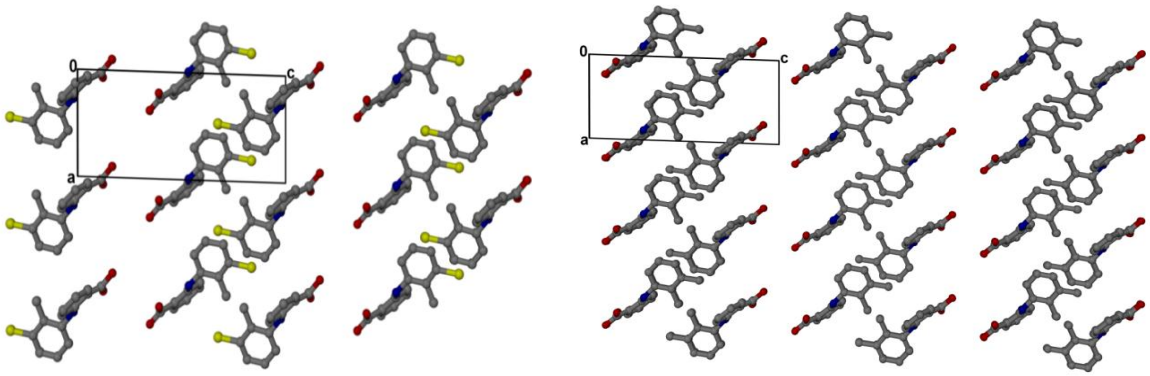

(a) (b)

Figure 3-37: Packing of TFA•3BrPYR (a) and MA•3PIC (b) along [010] with the guest removed (hydrogen atoms were omitted).

Table 3-14: Crystal data and data collection parameters of TFA•3BrPYR.

Compound	TFA•3BrPYR
Host:guest ratio	1:1
Molecular formula	$C_{19}H_{16}BrClN_2O_2$
Formula weight [g mol^{-1}]]	419.70
Crystal system	triclinic
Space group	$P\bar{1}$
Z	2
D_{calc} [g cm^{-3}]	1.603
a [Å]	7.7483
b [Å]	7.8164
c [Å]	16.096
α [°]	81.21
β [°] [^{0}]	84.77
γ [°]	64.53
V [Å^3]	869.4
μ (Mo-Kα) [mm^{-1}]	2.533
λ [Å]	0.71073
T [K]	173
$2\theta_{Max}$ [°]	56.0
No. reflections collected	20346
No. unique reflections	7533
No. reflections with I>2σ(I)	5844
Parameters	464
R_1 [I>2σ(I)]	0.0367
wR_2	0.0705
GOOF	1.048

Table 3-15: Geometrical data for hydrogen bonds of TFA•3BrPYR.

	D-H/Å	H•••A/Å	D•••A/Å	<(DHA)/°	Symmetry operation
O2-H2•••N2	0.73(4)	1.94(4)	2.672(3)	173(4)	-
N1-H7•••O1	0.80(3)	2.01(3)	2.657(3)	137(3)	-

3.2.3 Torsion and dihedral angles of tolfenamic acid with pyridines

The study of the torsion angles and the dihedral angles (Figure 3.37) was done using the methods as utilised for MA. Thus the angles used were identical: O2C1C2C7 (twisting of the carboxylic acid); C2C7N1C8 (rotation of the phenyl ring); C7N1C8C9 (twisting of the 3-chloro/2-methylphenyl) (Table 3.16) (SeethaLekshmi & Guru Row, 2012).

Table 3-16: Torsion and dihedral angles of TFA•2PIC, TFA•3PIC and TFA•3BrPYR

	TFA•2PIC	TFA•3PIC	TFA•3BrPYR
Torsion angle/°			
O2C1C2C7	177	173	175
C2C7N1C8	-177	-159	175
C7N1C8C9	-136	-157	68
Dihedral angle/°	49	44	65

The torsion angles measured which showed twisting of the carboxylic acid (O2C1C2C7) decreased when the methyl group from the *ortho* position (**TFA•2PIC**: 177°) was displaced to the *meta* position (**TFA•3PIC**: 173°) on the pyridine ring. However, when the methyl group was replaced by the bromine atom in the *meta* position, the decrease of the angle was less (**TFA•3BrPYR**: 175°). Likewise, the same trend was observed with the rotation of the phenyl ring. The torsion angle, C2C7N1C8, decreased from **TFA•2PIC** (177°) to **TFA•3PIC** (159°). However, a smaller decrease was observed for **TFA•3BrPYR** (175°).

In addition, the dihedral angle decreased when 2PIC was replaced by 3PIC; **TFA•2PIC:** 49° and **TFA•3PIC:** 44°. The largest dihedral angle was measured in **TFA•3BrPYR** at 65°. Thus the trend observed for MA with the substituted pyridines was not maintained as the MA dihedral angle increased as follows **MA•2PIC** < **MA•3PIC** < **MA•4PIC**.

Regarding the twisting of the 2,3-dimethylphenyl ring (torsion angle C7N1C8C9) as observed for the MA solvates, a different trend was also observed for TFA solvates. The twisting of the 3-chloro-2-methylphenyl ring exhibited the lowest value reported for the **TFA•3BrPYR** viz. 68° while the highest value was measured for the solvates **TFA•3PIC** (157°) and **TFA•2PIC** (136°). When observing the structural conformation of the **3BrPYR** solvate and comparing this to the **TFA•3PIC** illustrated in Figure 3.39, it was noted that the chlorine atom was orientated in a *trans*-conformation relative to the carboxylic acid of the TFA. This is similar to the MA in the **MA•2PIC** solvate. The bromine atom behaved like the methyl group in 3PIC and directed the substituted chlorine into a *trans* conformation relative to the COOH group (Figure 2.39 a).

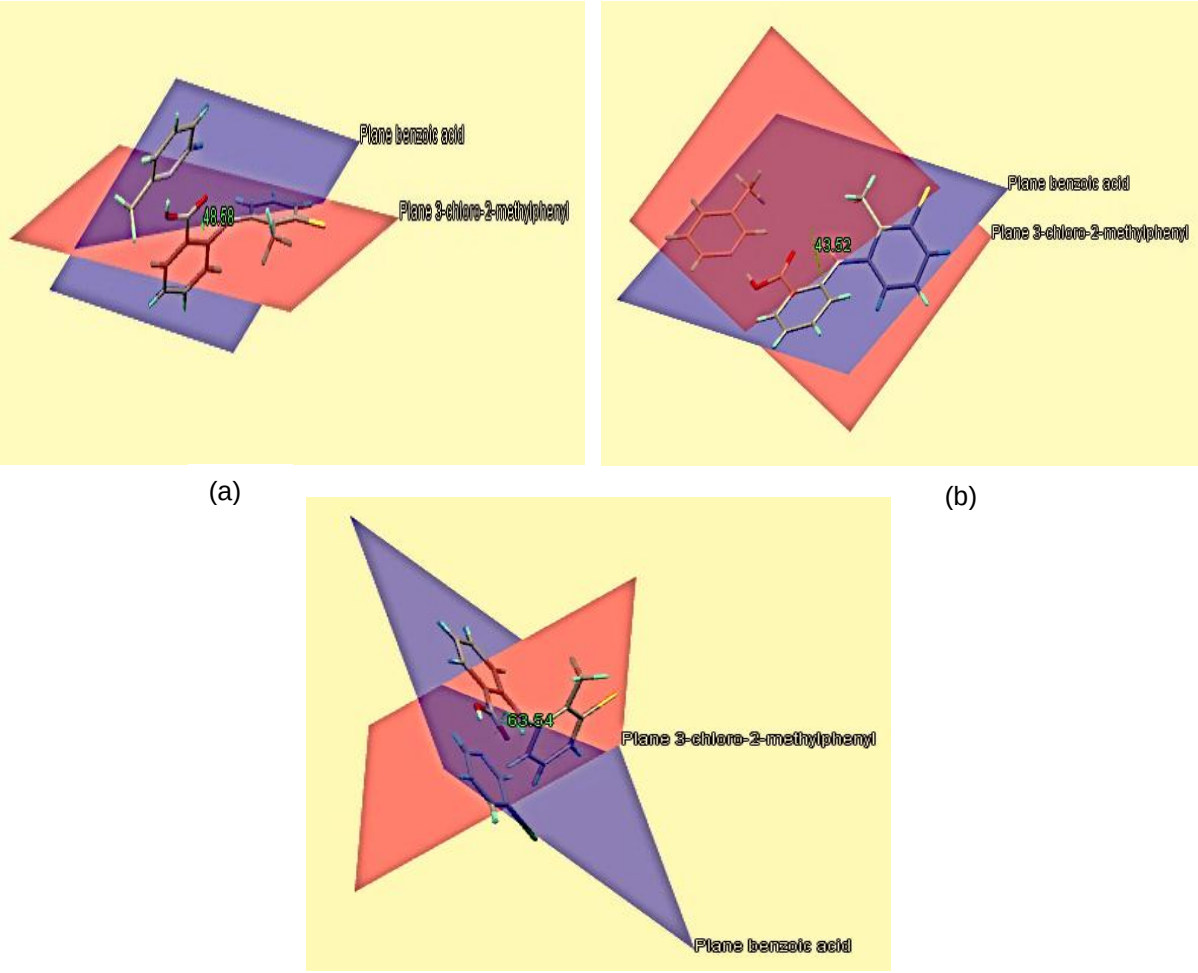

Figure 3-38: Dihedral angles between the planar grouping consisting of the 3-chloro-2-methylphenyl group (red) and the benzoic acid group (blue) of (a) TFA•2PIC, (b) TFA•3PIC and (c) TFA•3BrPYR.

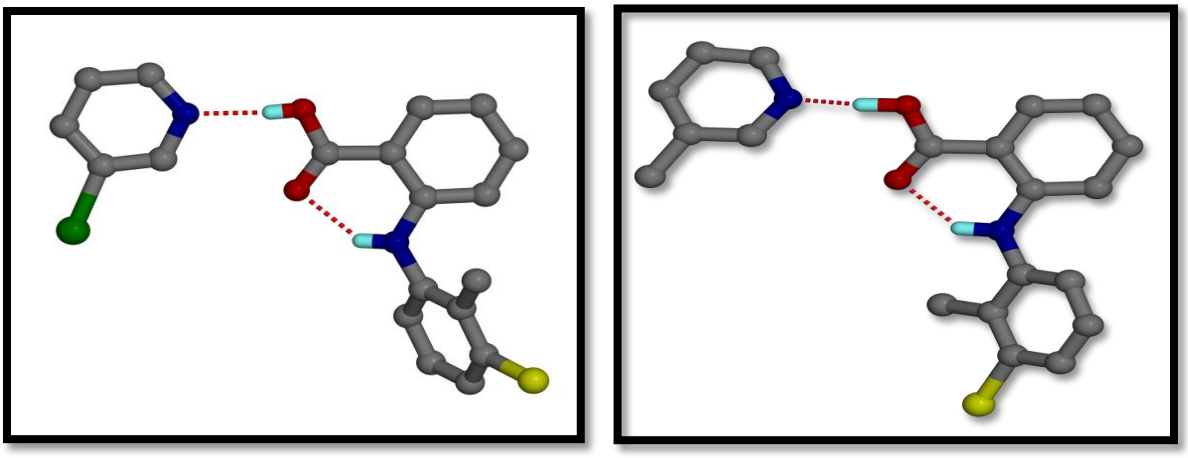

Figure 3-39: Difference between 2,3-dimethylphenyl groups in the (a) TFA•3BrPYR and (b) TFA•3PIC.

The **TFA•3PIC** dihedral angle (43°) was not in the ranges observed for the structures reported in the Cambridge structural database (CSD; version 5.36, Nov 2014) (polymorphs as well as co-crystals). However, it is similar to that found in the TFA form III (44.5°). Additionally, the torsion angles recorded for C7N1C8C9 for TFA solvates did not fall within the reported range which varied from a minimum of 75° to a maximum of 138°.

3.2.4 Thermal analysis of tolfenamic acid with pyridines

The thermal analysis results (Table 3.17) for the solvates of TFA were different from those obtained for the solvates of MA. Figure 3.40 shows the different TGA and DSC graphs recorded for the TFA solvates. The TGA curves in Figure 3.40 showed a single step which indicated the loss of each pyridine derivative. Furthermore, the theoretical and experimental losses in %mass recorded for **TFA•2PIC**, **TFA•3PIC** and **TFA•3BrPYR** concurred and are shown in Table 3.17.

DSC graphs exhibit two endotherms for the release of the solvents and the melting of the TFA respectively (Figure 3.40). In this case, the determined thermal stability trend was **TFA•2PIC** > **TFA•3PIC** > **TFA•3BrPYR**. Finally, the actual boiling point of each solvent (solvent normal bp/ K: table 3.17) was greater than the temperature at which the solvent was released (endotherm of loss of solvent in table 3.17) from the crystal.

Table 3-17: Thermal analysis data of TFA•2PIC, TFA•3PIC and TFA•3BrPYR.

SOLVATES	TFA•2PIC	TFA•3PIC	TFA•3BrPYR
Host: Guest ratio	1:1	1:1	1:1
TGA calc % mass loss	26.2	26.2	37.7
exp % mass loss	25.0	25.7	36.2
DSC endotherm for loss of solvent (T_{on}/K)	359.0	347.5	333.6
DSC endotherm of tolfenamic acid (T_{on}/K)	486	489	484
Solvent normal bp/ K	401	417	445
T_{on}/T_{bp}	0.90	0.84	0.75

(Solvents boiling point retrieved from Weast, 1980)

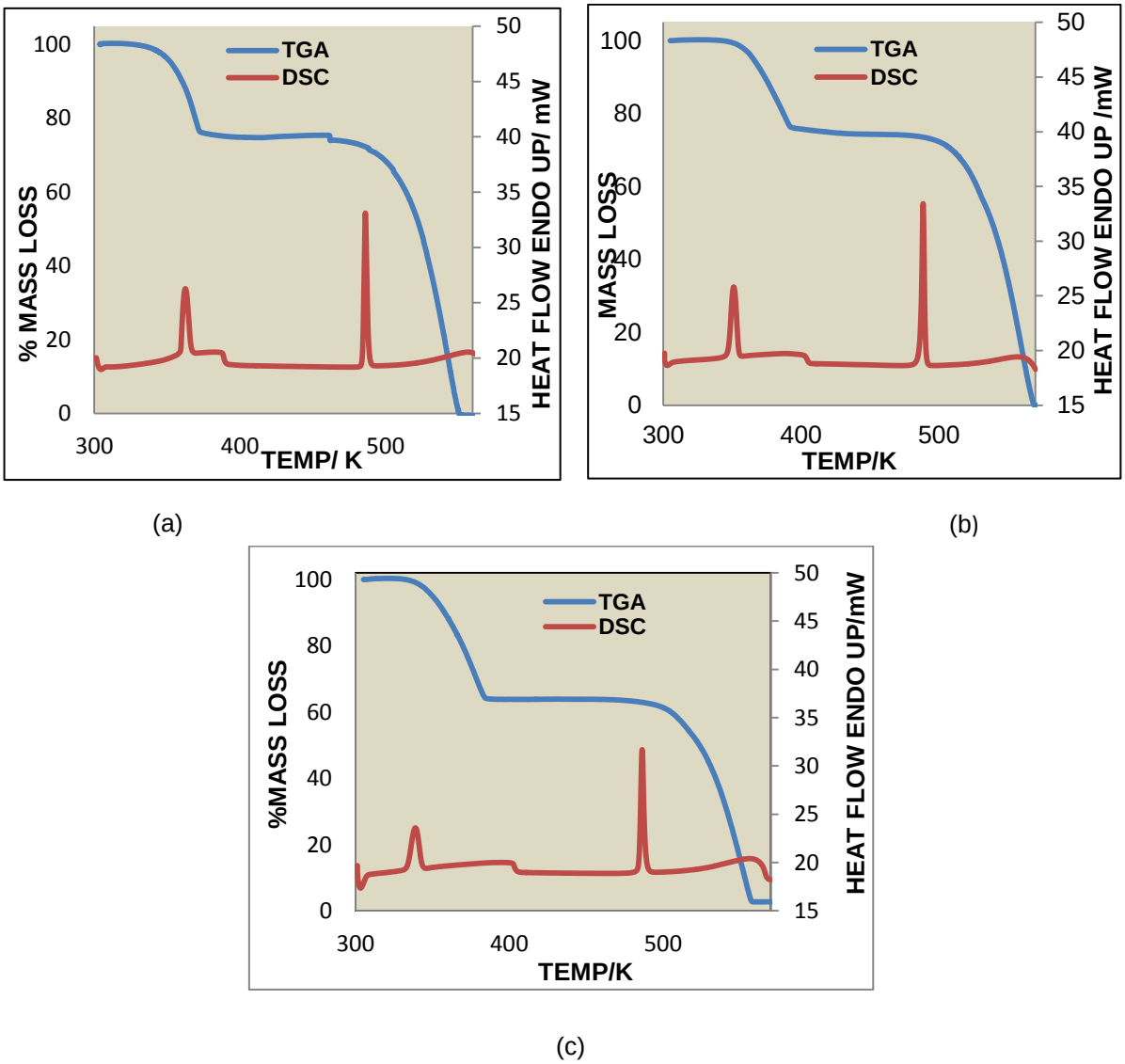

Figure 3-40: DSC and TGA curves obtained for (a) TFA•2PIC, (b) TFA•3PIC and (c) TFA•3BrPYR.

3.2.5 Powder X-ray diffraction (PXRD) of tolfenamic acid with pyridines

Ground and slurry samples of the solvates of TFA were obtained through processes similar to those for the solvates of MA (Section 3.1.5). The powders obtained from the grinding and slurry experiments were analysed with PXRD. The resulting patterns were compared to the theoretical patterns from the single crystal analysis, bulk sample and the starting material.

Figure 3.41 shows the PXRD graphs recorded for **TFA•2PIC**. The PXRD patterns showed acceptable matches in all the samples and also to the theoretical pattern observed for the

single crystal. When **TFA•3PIC** was analysed, the different methods also had a PXRD pattern similar to the theoretical pattern.

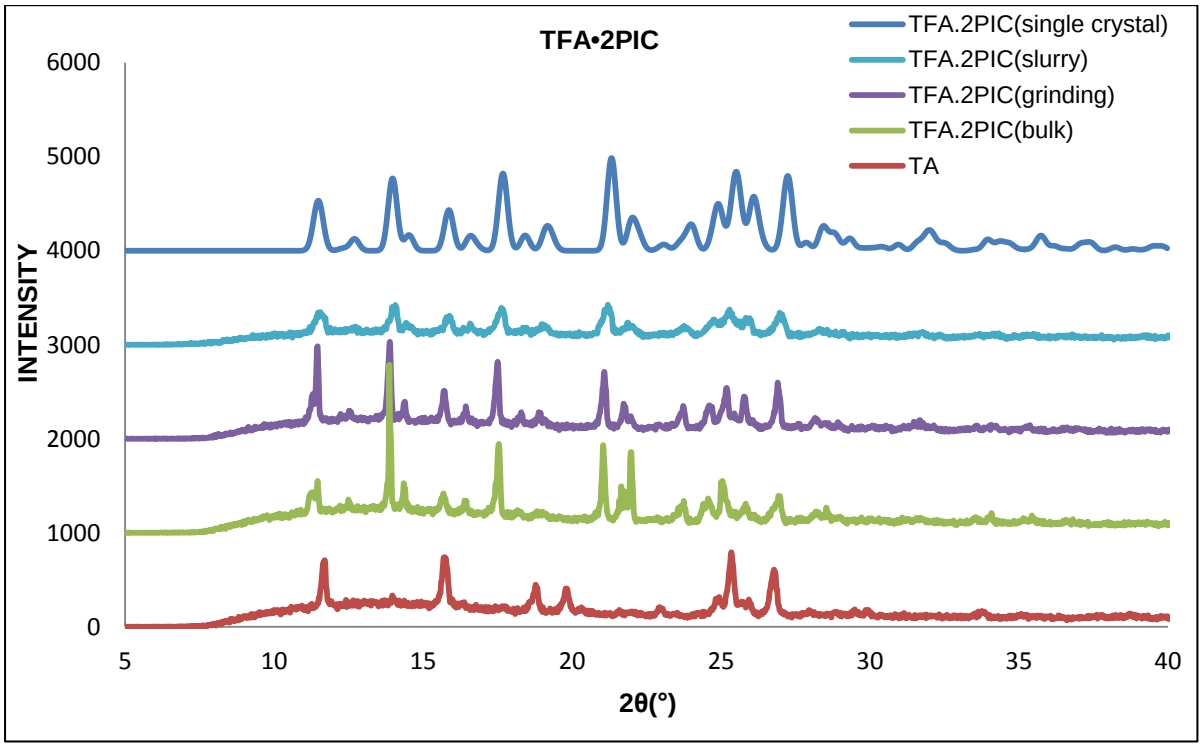

Figure 3-41: PXRD analyses of TFA•2PIC: calculated pattern obtained from LAZYPULVERIX (blue), and patterns from the slurry experiment (light blue);the grinding experiment (purple), bulk sample (green) and starting material TFA (red).

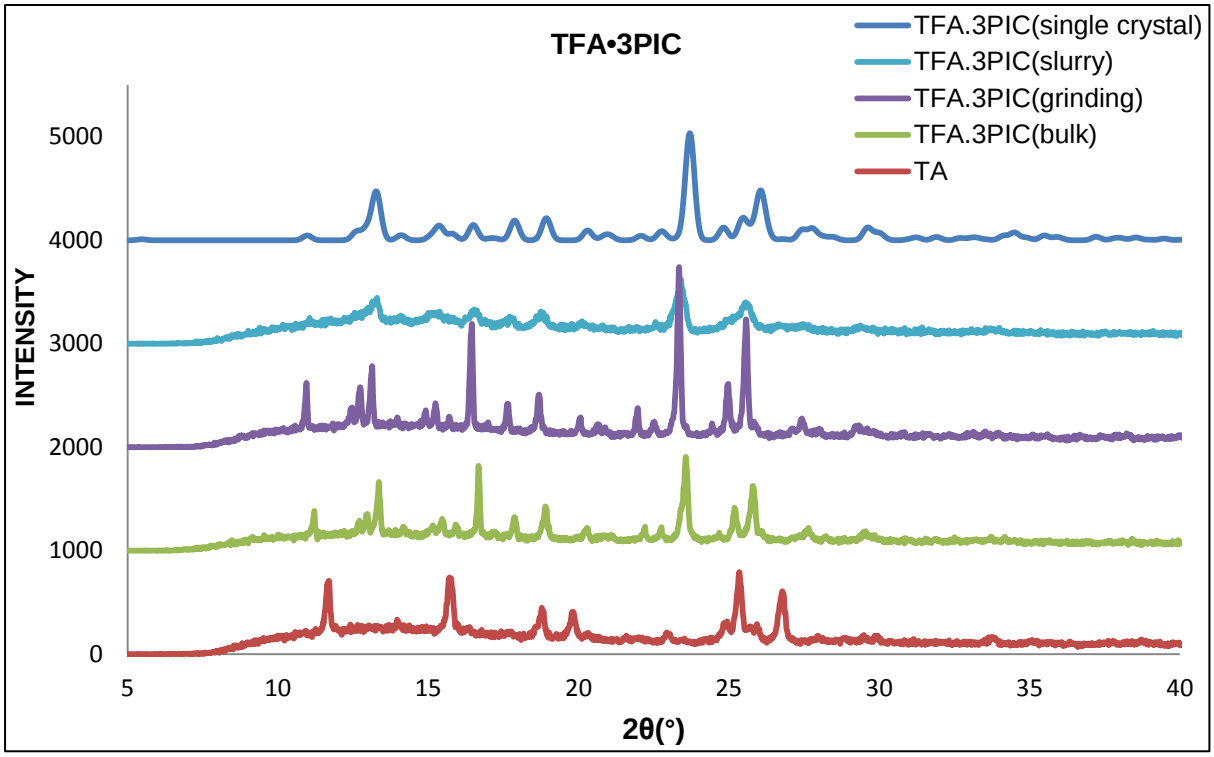

Figure 3-42: PXRD analyses of TFA•3PIC: calculated pattern obtained from a LAZYPULVERIX (blue),and patterns from the slurry experiment (light blue); the grinding experiment (purple), bulk sample (green) and starting material TFA (red).

Ground, slurry and bulk samples PXRD patterns of **TFA•3BrPYR** (Figure 3.43) showed similarities to the peaks recorded for the theoretical pattern. There was an absence of the sharp peak at 2 thetas = 5.5° in the experimental PXRD patterns because of the problem encountered with the D2 phaser instrument in detecting peaks for 2 thetas <7°. Furthermore, at approximately 2 thetas = 11.6°, a peak was observed to occur in the ground and slurry samples, and was also present in the starting material. Hence this unassigned peak was attributed to the presence of unreacted TFA in the samples.

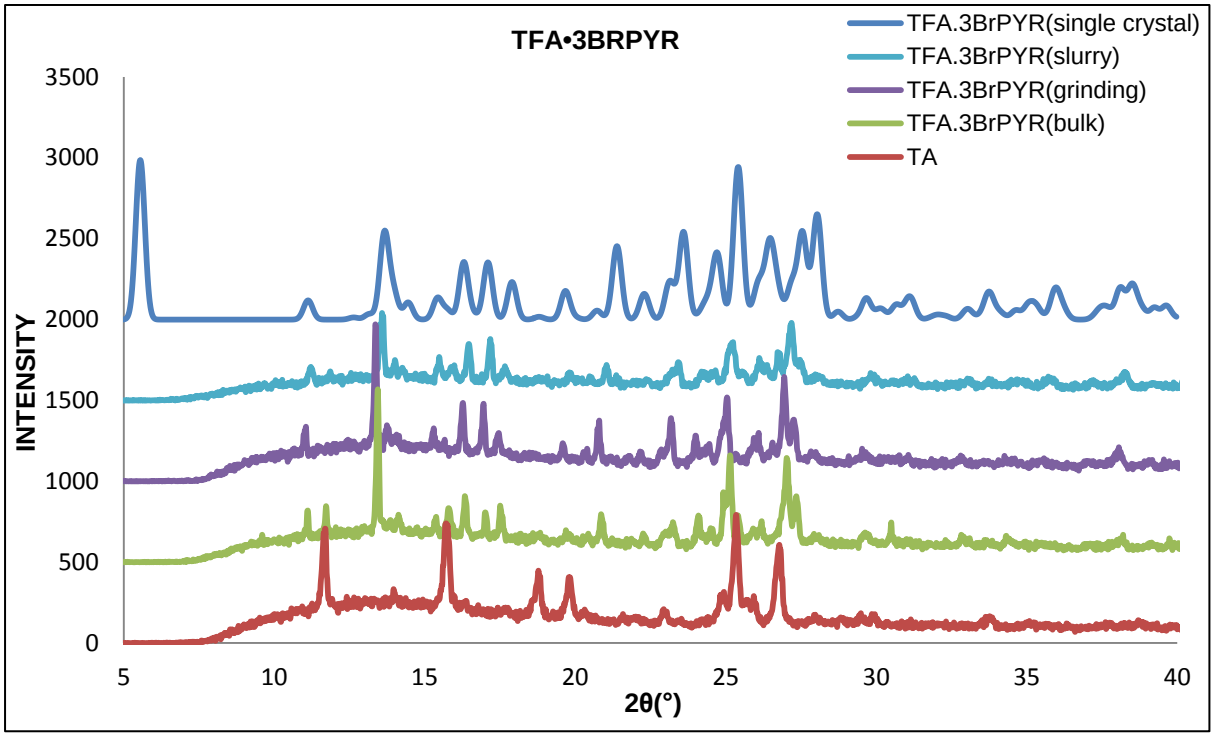

Figure 3-43: PXRD analyses of TFA•3BrPYR: calculated pattern obtained from LAZYPULVERIX (blue), and patterns from the slurry experiment (light blue); the grinding experiment (purple), bulk sample (green) and starting material TFA (red).

3.2.6 Kinetics of desolvation of tolfenamic acid with pyridines

Kinetics studies required the analysis of a sample at different heating rates using TGA. The resulting TGA graphs were converted into log β vs 1/T, where β represented the heating rate. Activation energies were subsequently determined using each slope, calculated by using the following formula:

$$\text{Slope} = -0.457\,\frac{E_a}{R}$$

The **TFA•2PIC** kinetics data shown in Figure 3.44 was obtained by using 2, 6, 10 and 24 K min^{-1} as heating rates. The activation energies were determined from the slopes of the graph shown in Figure 3.44. These varied between 79.4 and 85.6 kJ mol^{-1}. The kinetics of desolvation of **TFA•3PIC** had activation energies varying between 68.5 and 105.7 kJ mol^{-1} (Figure 3.45). In the case of **TFA•3BrPYR,** the activation energies varied between 62.1 and 76.3 kJ mol^{-1}.

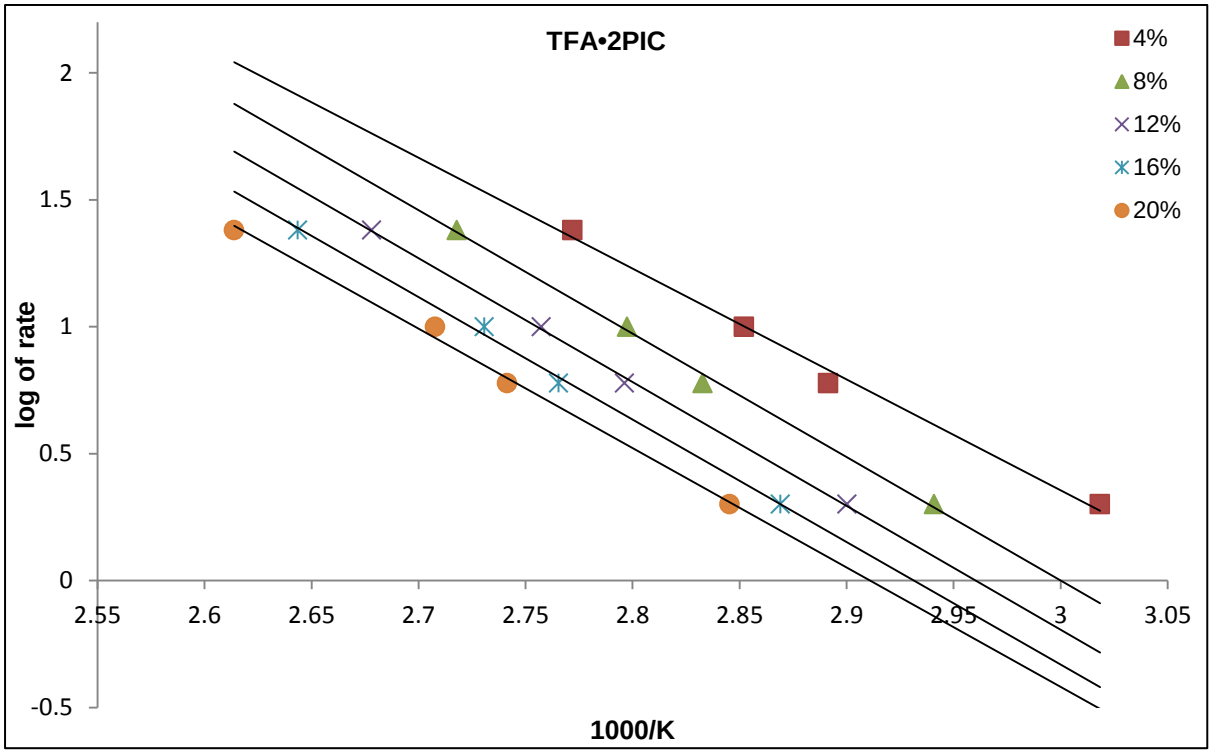

Figure 3-44: Log rate vs. 1/T graphs obtained for TFA•2PIC.

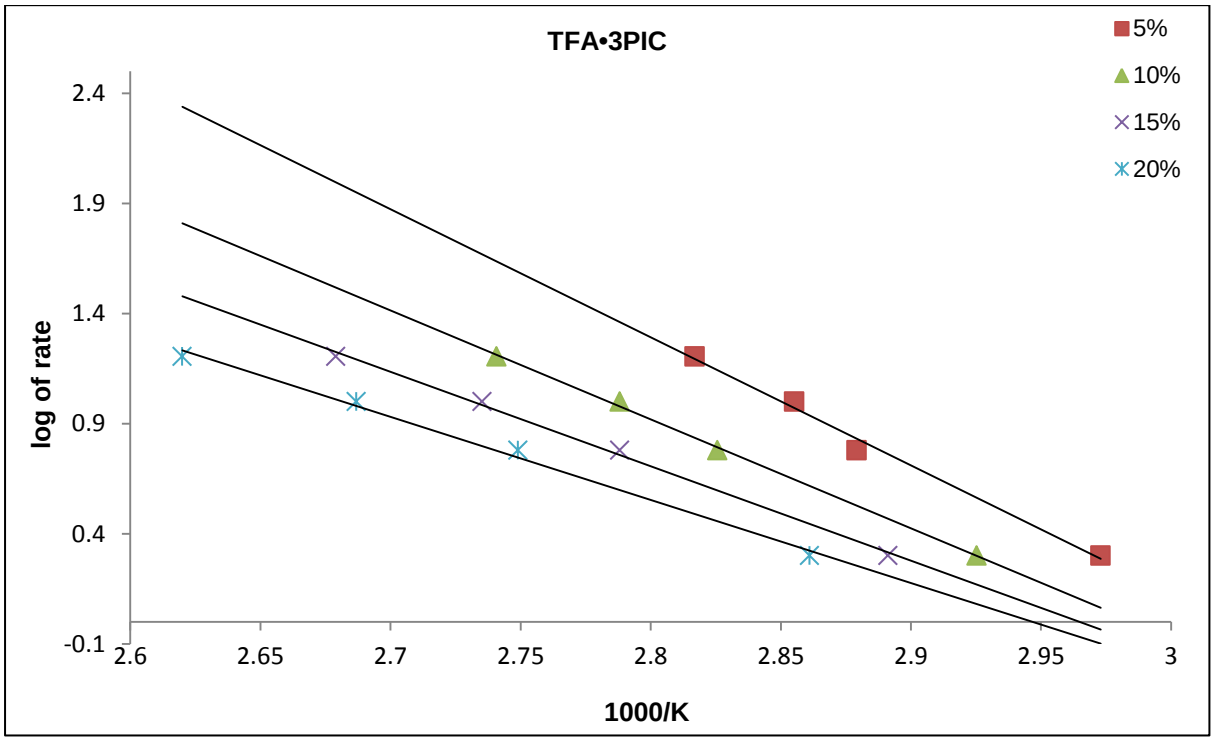

Figure 3-45: Log rate vs. 1/T graphs obtained for TFA•3PIC.

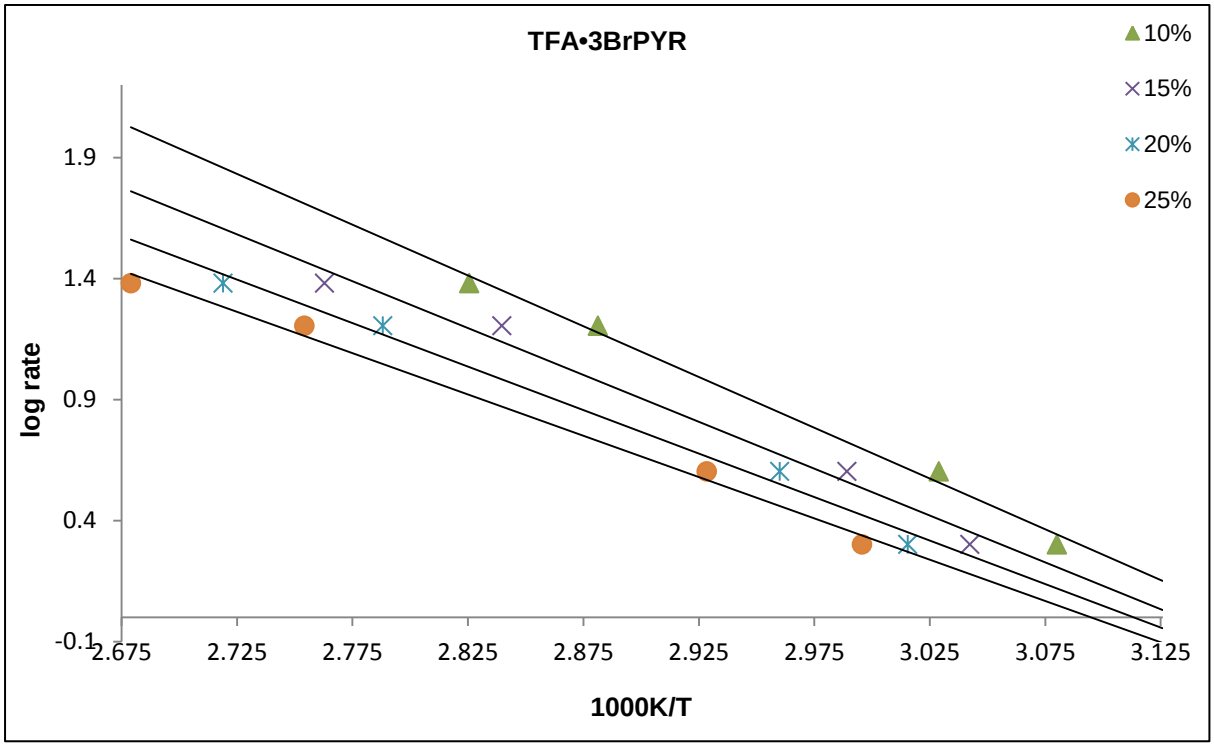

Figure 3-46: Log rate vs. 1/T graphs obtained for TFA•3BrPYR.

3.2.7 Desolvation studies of tolfenamic acid with pyridines

Tolfenamic acid is renowned for its ability to form a number of polymorphs. Currently, five forms of TFA are known and the PXRD patterns, obtained from (CSD, version 5.36, Nov 2014), are shown in Figure 3.47. According to Du et al. (2015) forms I and II are the most commonly encountered polymorphs of TFA. In the current study, desolvation of the different solvates was carried out by using methods employed for the solvates of MA (Section 3.1.7). Firstly, the crystals were placed in open glassware at ambient temperature for one month. Secondly, an additional sample of the solvate was left to dry in an oven set at 90℃ for 24 h. The resultant powders were analysed for confirmation of the desolvated form of the crystal by implementing TGA followed by the generation of PXRD patterns. The patterns showed **TFA•2PIC**, **TFA•3PIC** and **TFA•3BrPYR** desolvated to form II with CSD (version 5.36, Nov 2014) code KAXXAI01 (Andersen et al. 1989).

Overall the PXRD patterns showed a better match to KAXXAI01 (Figures 3.48 and 3.49; Table 3.18) although differences in intensity were noted. These differences could be attributed to the different experimental conditions used to obtain the two samples.

Table 3-18: Desolvation data recorded for TFA•2PIC, TFA•3PIC and TFA•3BrPYR.

Solvate	Desolvation at 90 °C for 24h	Desolvation at RT for 1 month
TFA•2PIC	Form I (starting material)	Form I (starting material)
TFA•3PIC	Form I (starting material)	Form I (starting material)
TFA•3BrPYR	Form I (starting material)	Form I (starting material)

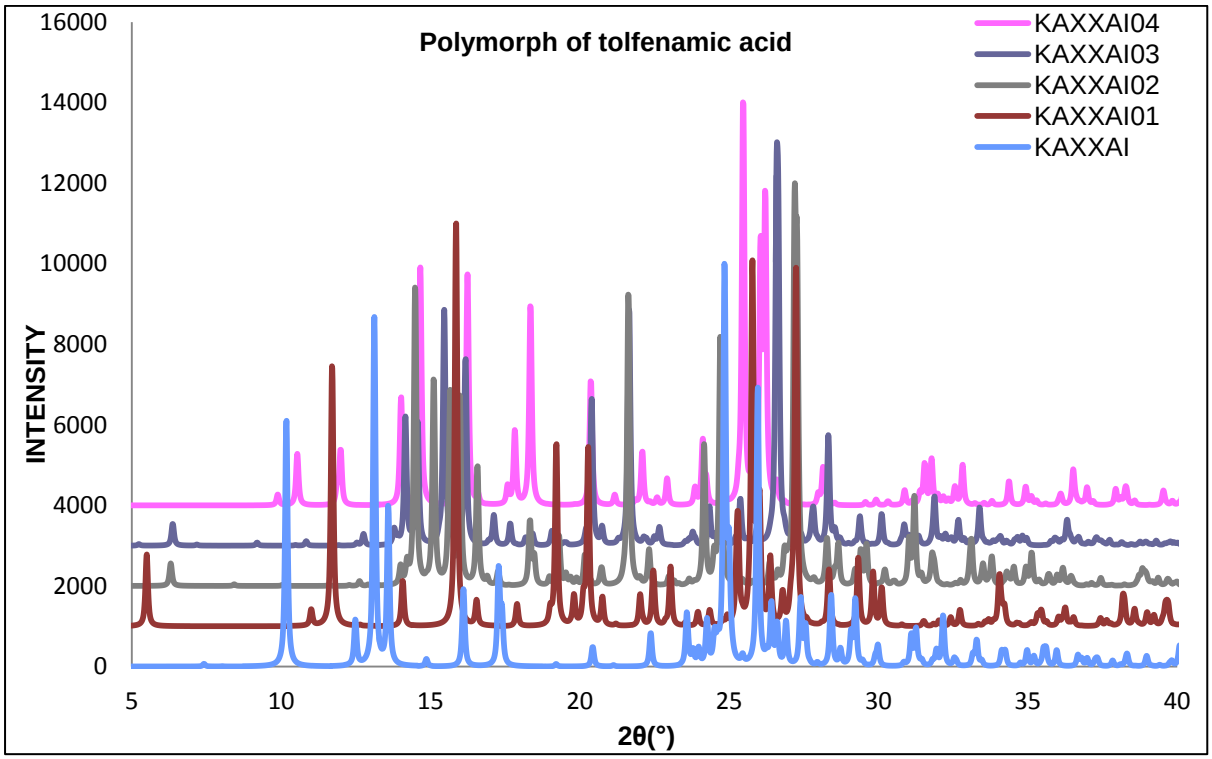

Figure 3-47: Simulated PXRD patterns of tolfenamic acid polymorphs.

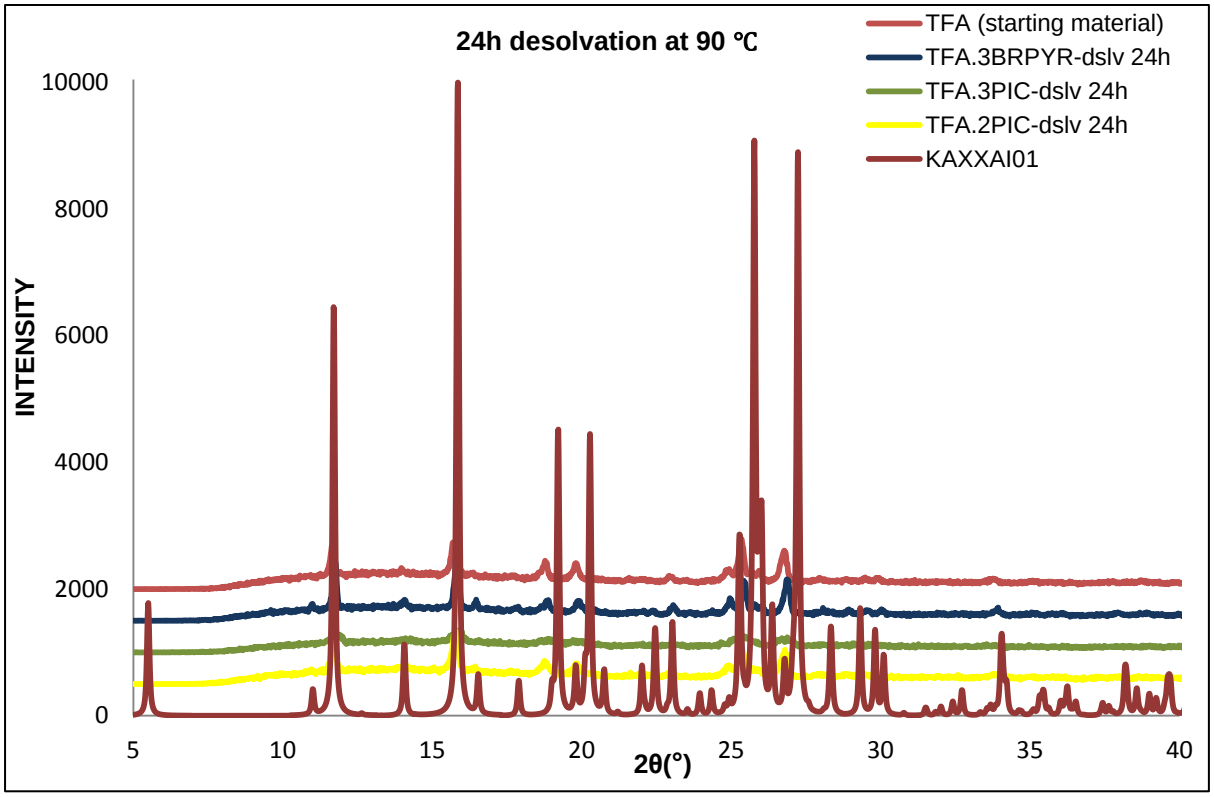

Figure 3-48: Patterns obtained from the PXRD analyses of tolfenamic acid solvates after 24h desolvation at 90 °C.

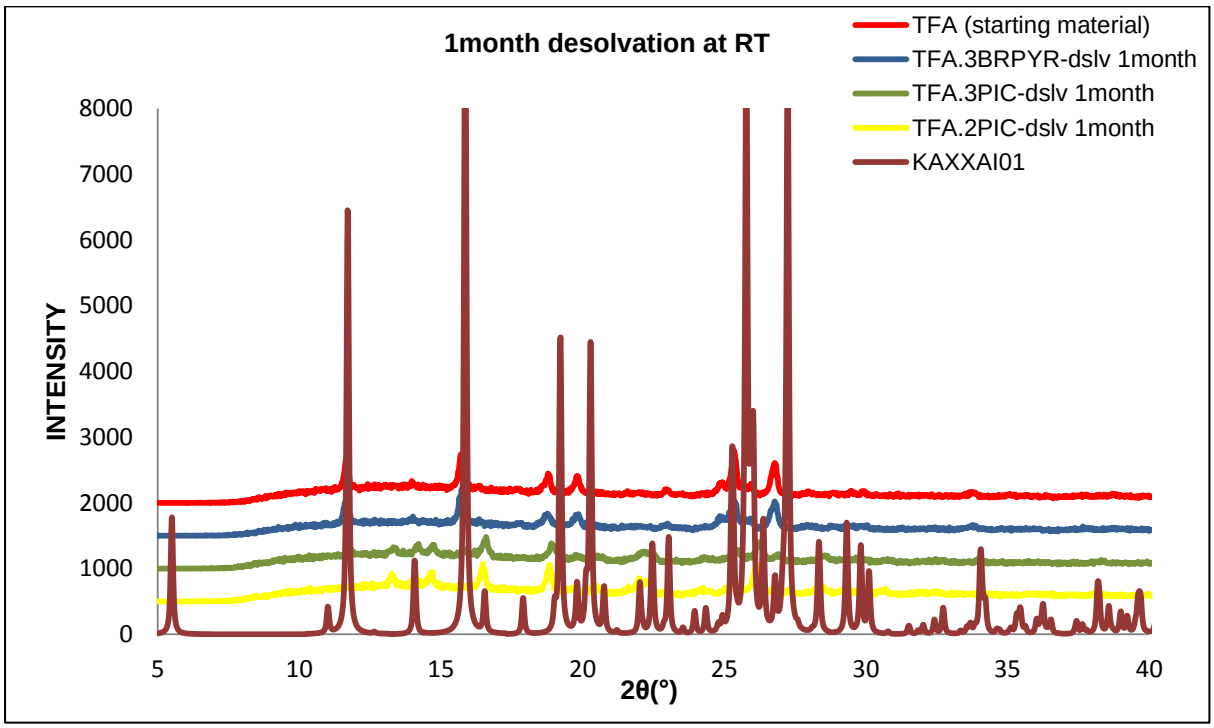

Figure 3-49: Patterns obtained from the PXRD analyses of tolfenamic acid solvates with pyridines after one month of desolvation at RT.

3.3 Differences between mefenamic and tolfenamic acid solvates

The various structures obtained from the two compounds showed similarities in their arrangement. The solvate structures had a tendency to form separate hydrophobic and hydrophilic regions grouped as columns. These observations were also made by Fábián et al. (2011) in their analysis of co-crystals of mefenamic, tolfenamic , flufenamic and niflumic acid. Furthermore, Surov et al. (2015) also reported a similar columnal arrangement of the different co-crystal structures in selected fenamates (MA and TFA included). It can be concluded that a columnal arrangement of the fenamates is usually preferred and it does not depend on the substituents present on the fenamate acid.

The conformations of TFA and MA were different with regard to the phenyl rings. In the case of TFA, the 3-chloro-2-methyl phenyl was in a *trans*-position to the carboxylic acid in the fenamate acid backbone in both **TFA•2PIC** and **TFA•3PIC**. However, in MA the substituted phenyl ring was in a *cis* position relative to the acidic part of the fenamate acid for most solvates (**MA•3PIC/3ClPYR/4PIC**) (Figure 3.50). Different conformations were observed in **MA•2PIC** and **TFA•3BrPYR** solvates.

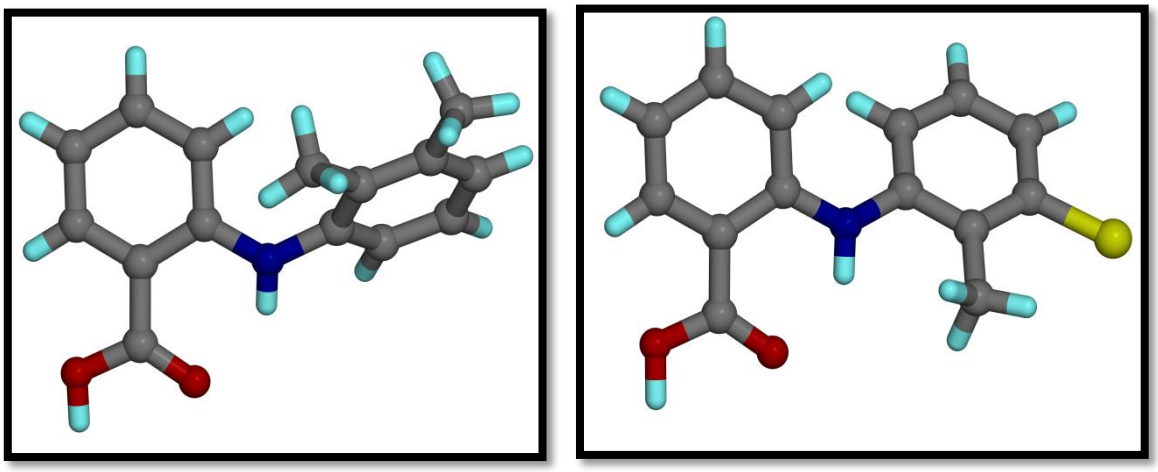

(a) (b)

Figure 3-50: Difference between the 2,3-dimethyl and 3-chloro-2-methyl phenyl groups (a) MA conformation (in MA•3PIC) and (b) TFA conformation (in TFA•3PIC).

Both MA and TFA were able to adjust to accommodate the interaction of the carboxylic acid in the acid and the nitrogen of the pyridine derivative. Thus conformational variation was

observed in both of the two fenamic acids studied. The MA conformation was altered by the solvent included .ie. the position of the methyl group on the pyridine ring affected the conformation of the MA. Figure 3.51 shows the difference in the MA conformation in **MA•4PIC** and **MA•3PIC.**

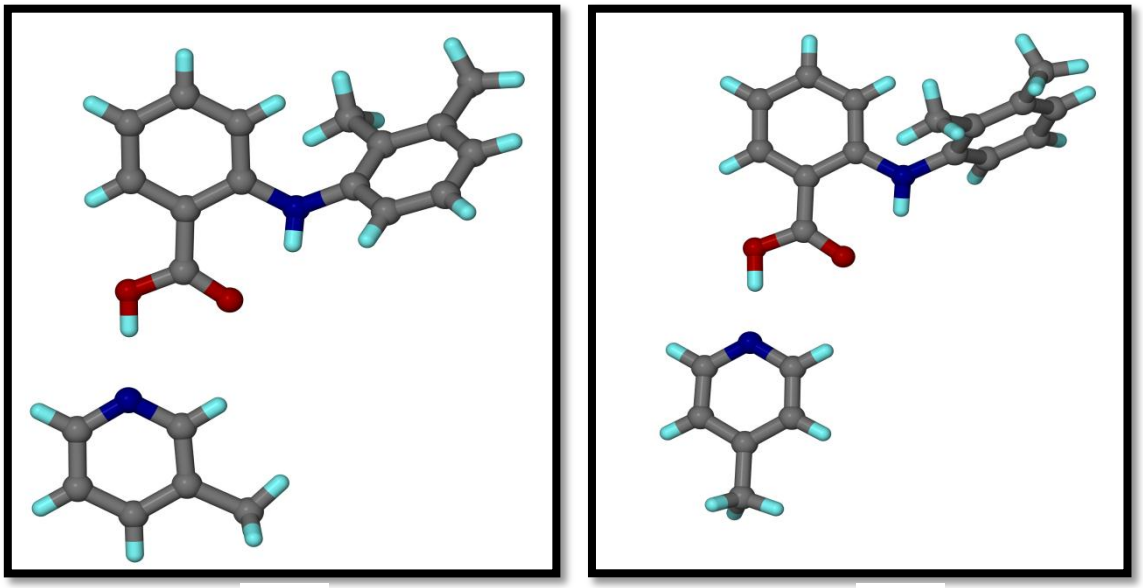

(a) (b)

Figure 3-51: Difference between 2,3-dimethylphenyl group in (a) MA•3PIC and (b) MA•4PIC (note the direction of the 2,3-dimethylphenyl to the plane of the acid).

Similar changes in the TFA torsion angle occurred in **TFA•2PIC** and **TFA•3PIC**, but only the presence of the halogen atom in 3-bromopyridine completely altered the conformation of TFA. The 3-chloro-2-methylphenyl was transformed from a *cis*-conformation to the carboxylic acid in the **TFA•2PIC** to a *trans*-conformation in the **TFA•3BrPYR**.

3.4 Conclusion:

Comparison of the structures of MA and TFA showed that replacement of a methyl group by a halogen affected both the packing arrangement of the particular compounds and the conformation of the acid.

The thermal stability trend as determined by the T_{on}/T_b values for the solvates of TFA was **TFA•2PIC** > **TFA•3PIC** > **TFA•3BrPYR** while for the solvates of MA there was no variation in the T_{on}/T_b values. Desolvation analysis of the solvates led to the same polymorphic form of the acid as the respective starting material. The reproduction of these compounds was successfully done through slurry, grinding and crystallisation methods.

Bibliography

- Allen F. H. 2002. *Acta Crystallographica*, B58, 380-388.
- Andersen, K.V., Larsen, S., Alhede, B, Gelting, N. & Buchardt, O. 1989. Characterization of two polymorphic forms of tolfenamic acid, *N*-(2-methyl-3-chlorophenyl)anthranilic acid: their crystal structures and relative stabilities. *Journal of the Chemical Society, Perkin Transactions 2*, 10: 1443-1447.
- Cruz-Cabeza, A.J. 2012. Acid–base crystalline complexes and the pKa rule. *CrystEngComm*, 14(20):6362–6365.
- Desiraju, G.R., Vittal, J.J. & Ramanan, A. 2011. *Crystal engineering: a textbook*. Hackensack: World Scientific: IISc Press.
- Du, W., J. Cruz-Cabeza, A., Woutersen, S., J. Davey, R. & Yin, Q. 2015. Can the study of self-assembly in solution lead to a good model for the nucleation pathway? The case of tolfenamic acid. *Chemical Science*, 6(6):3515–3524.
- Fábián, L., Hamill, N., Eccles, K.S., Moynihan, H.A., Maguire, A.R., McCausland, L. & Lawrence, S.E. 2011. Co-crystals of fenamic acids with nicotinamide. Crystal Growth & Design, 11(8) 3522–3528.
- Fang, L., Numajiri, S., Kobayashi, D., Ueda, H., Nakayama, K., Miyamae, H. & Morimoto, Y. 2004. Physicochemical and crystallographic characterization of mefenamic acid complexes with alkanolamines. *Journal of Pharmaceutical Sciences*, 93(1):144–154.
- Flynn. J. H.: Wall. L. A. *J. Polym. Sci; Part B: Polym. Lett*. 1966,4323.
- Nawaz, H., Khawar Rauf, M., Ebihara, M. & Badshah, A. 2007. Methyl 2-(2,3-dimethyl-anilino)benzoate. *Acta Crystallographica Section E: Structure. Reports Online*, 63(4):1658–1659.
- SeethaLekshmi, S. & Guru Row, TN. 2012. Conformational polymorphism in a non-steroidal anti-inflammatory drug, mefenamic acid. *Crystal Growth & Design*, 12(8):4283–4289.
- Surov, A.O., Simagina, A.A., Manin, N.G., Kuzmina, L.G., Churakov, A.V. & Perlovich, G.L. 2015. Fenamate co-crystals with 4,4′-bipyridine: structural and thermodynamic aspects. *Crystal Growth & Design*, 15(1):228–238.
- Weast, R.C. 1980. CRC Handbook of Chemistry and Physics. 60th ed. New York. CRC Press.
- Yvon, K., Jeitschko, W. & Parthe, E.J 1997. LAZY PULVERIX, a computer program, for calculating X-ray and neutron diffraction powder patterns. *Journal of Applied Crystallography*, 10:73-74.

CHAPTER 4

THE SALTS OF MEFENAMIC AND TOLFENAMIC ACIDS

When a proton is transferred from one entity to another the resulting compound is called a salt. Compared to the solvates, starting materials used for the formation of salts may be a solid and a solvent or two different solids. The difference in pK_a values of the two starting compounds usually determines whether or not a proton is transferred. This chapter presents the study of salts prepared from the two selected fenamates.

4.1 Mefenamic acid salts

4.1.1 Introduction

Mefenamic acid (MA) formed salts in the presence of ethylenediamine (EDM), triethylamine (TA) or 1-methypiperazine (MP). On a hot plate set at 60 °C, 2 ml of the solvent was mixed with approximately 30 mg of the acid and left open to the atmosphere to crystallise at room temperature.

In the salt structures studied, a proton was transferred from the acid to the nitrogen of the solvent. The ΔpK_a recorded for these different compounds were found to be 4.94, 6.51 and 6.81 for **$(MA^-)(MP^+)$**; **$(MA^-)(EDM^+)$** and **$(MA^-)(TA^+)$** respectively. These values validate the ΔpK_a rule described by Stahl & Wermuth (2008) since a proton transfer is expected to occur for ΔpKa greater than 2-3. The C-O distances of the acid were also analysed to confirm the formation of the salts. Furthermore, the intramolecular N-H•••O interaction of MA observed in the solvates was present in these compounds.

4.1.2 Structural analysis of mefenamic acid salts

4.1.2.1 Salt of mefenamic acid with ethylenediamine $(MA^-)(EDM^+)$

The (**$MA^-)(EDM^+$**) formed needle-like crystals three months after the crystallisation experiment commenced (Section 2.41, Chapter 2). The structure was solved in $P\bar{1}$. It was found that a single ion of the mefenamate and half of the ethylenediammonium ion were located in the asymmetric unit of (**$MA^-)(EDM^+$**). Figure 4.1 shows the numbering scheme used for this asymmetric unit.

All of the N-H bonds of the (**EDM^+**) were found to form hydrogen bonds with the carboxylate of (**MA^-**). Each (**EDM^+**) ion was attached to four (**MA^-**) ions by means of hydrogen bonds (Figure 4.2). The N–H•••O hydrogen bonds were characterized by N2•••O2 distances of 2.769(2) Å, 2.705(2) Å and 2.953(2) Å. Further details are given in Table 4.2.

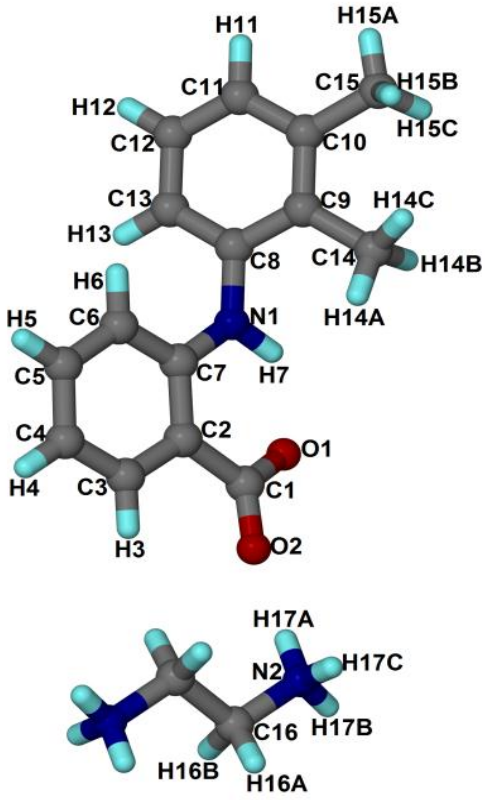

Figure 4-1: The numbering scheme used for (MA-)(EDM+).

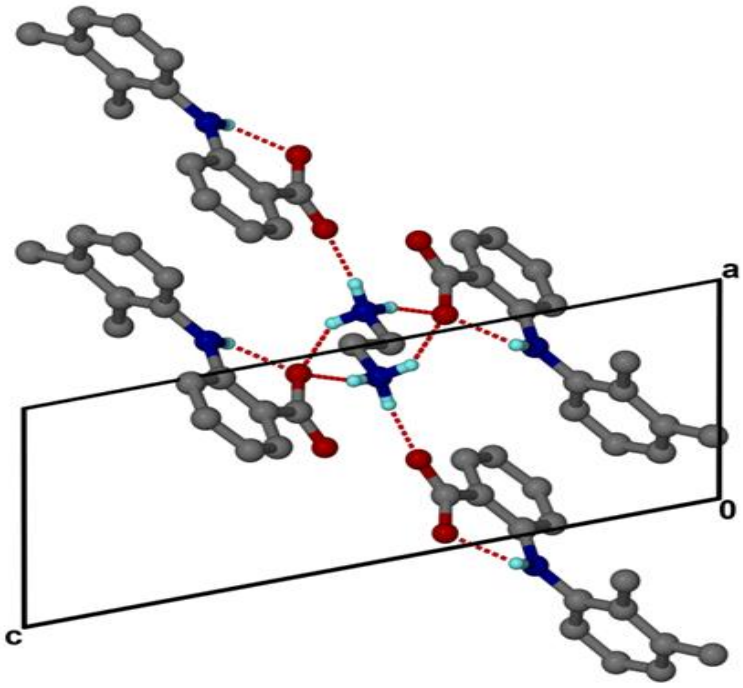

Figure 4-2: Scheme showing the hydrogen bonding in (MA-)(EDM+) (some hydrogen atoms were omitted).

The different interactions are described by the graph sets observed in Figure 4.3. The largest hydrogen bonded ring (Figure 4.3 (c)) can be described as $R_4^4(18)$ and was characterised by an interaction between b- N2-H17C•••O1 and c allocated to N2-H17A•••O2. The $R_4^4(12)$ ring (Figure 4.3 (b)) was formed by the sequential interaction of c-N2-H17A•••O2 and b- N2-H17B•••O1. Finally, the smallest ring can be described as $R_4^2(8)$ and involved O1, with the (**EDM$^+$**) cation interacting through d-N2-H17B•••O1 and b- N2-H17C•••O1. There were also several chains with the longest being $C_4^4(18)$. It consists of a successive interaction of an **(EDM$^+$)** to (**MA$^-$**) to another **(EDM$^+$)** (see figure 4.3 d).

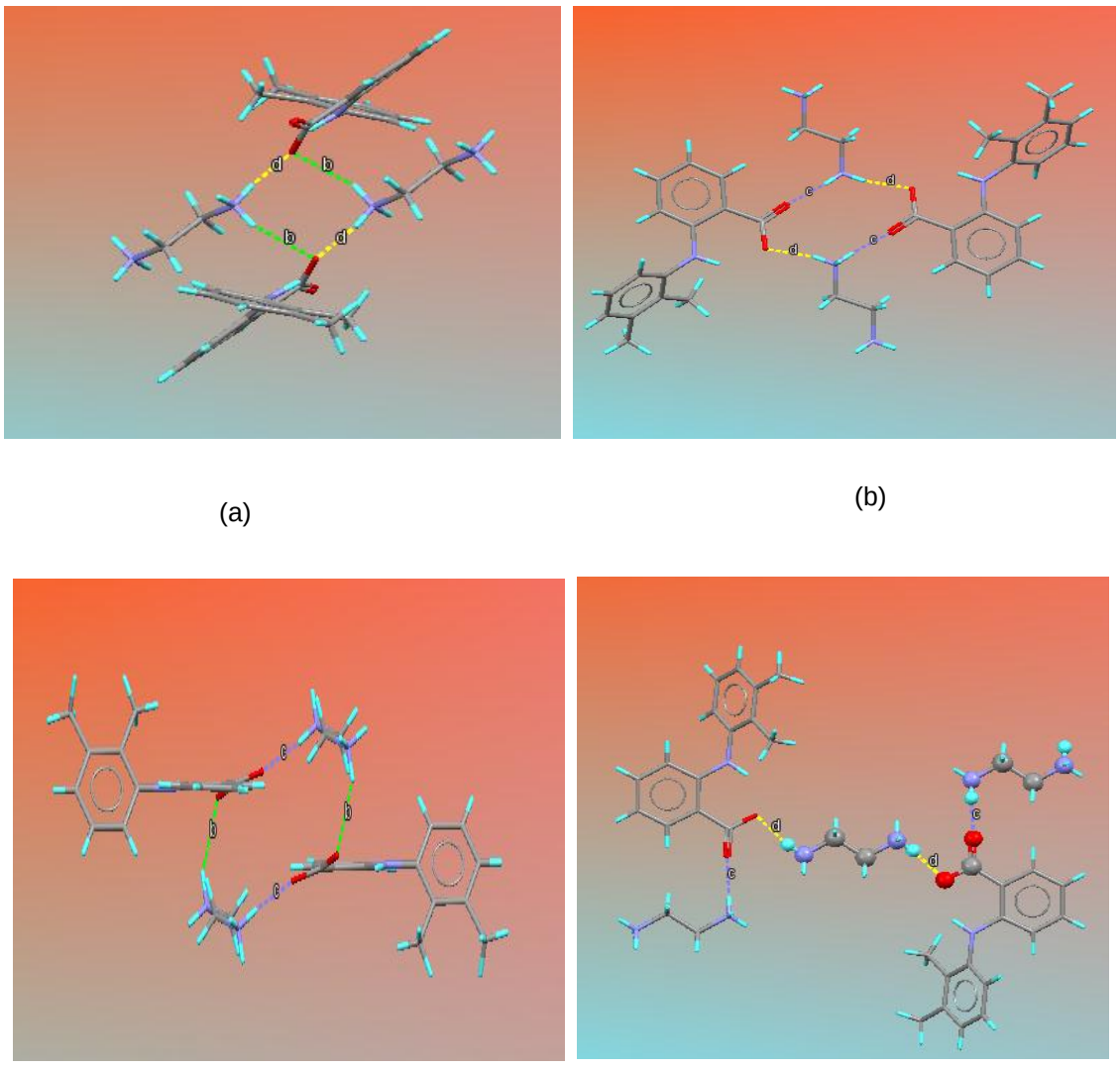

(a) (b)

(c) (d)

Figure 4-3: Hydrogen bonding motifs recorded for (MA$^-$)(EDM$^+$).

A columnar arrangement of the ions was observed in this salt (Figure 4.4). The carboxylate groups of **MA**$^-$ are directed towards the middle of the column to accommodate bonding with the **EDM**$^+$. Fang et al. (2004) designated this type of arrangement as segregated hydrophobic and hydrophilic regions in the crystals. The structure is stabilized by several C-H•••π interactions. One of them resulted from an aromatic ring of **MA**$^-$interacting with **EDM**$^+$ with a distance of 3.44 Å between the two centroids. The (**MA**$^-$)(**EDM**$^+$) crystal data collection and the hydrogen bond parameters are provided in Tables 4.1 and 4.2 respectively. Figure 4.5 shows the individual cavities occupied by the **(EDM**$^+$) ions in the crystal lattice of the (**MA**$^-$)(**EDM**$^+$) salt.

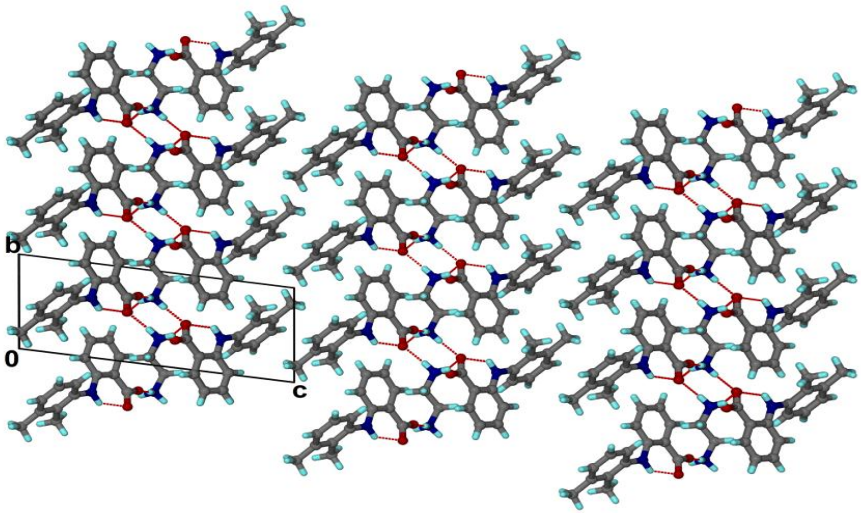

Figure 4-4: Crystal packing of (MA$^-$)(EDM$^+$) parallel to [100].

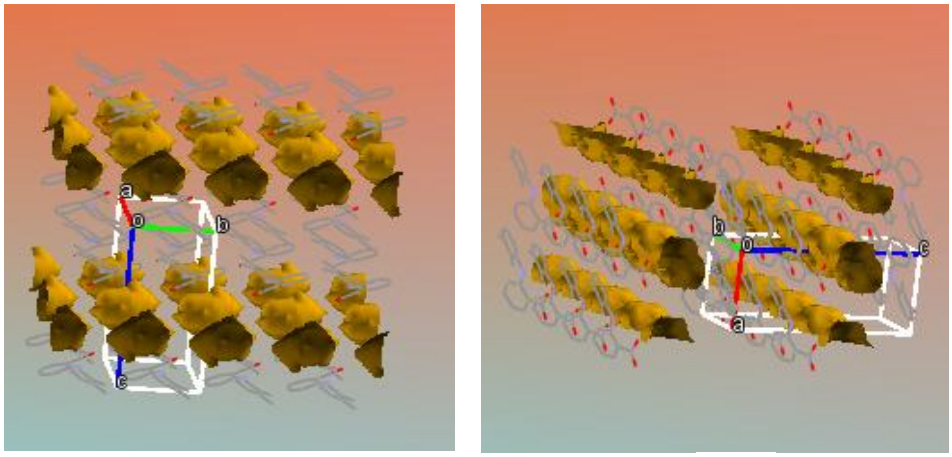

(a) (b)

Figure 4-5: Cavities showing the location of EDM$^+$ ions along (a) [100] and (b) [010] (hydrogen atoms are omitted).

Table 4-1: Crystal data collection parameters of (MA^-)(EDM^+).

Compound	(MA^+)(EDM^-)
Host:guest ratio	$1:\frac{1}{2}$
Molecular formula	$C_{16}H_{18}N_2O_2$
Formula weight [g mol^{-1}]	271.33
Crystal system	triclinic
Space group	$P\bar{1}$
Z	2
D_{calc} [g cm^{-3}]	1.296
a [Å]	6.7950(14)
b [Å]	7.1075(14)
c [Å]	16.056(3)
α [°]	93.56(3)
β [°]	100.86(3)
γ [°]	112.63(3)
V [Å^3]	695.1(2)
μ (Mo-Kα) [mm^{-1}]	0.086
λ (Å)	0.71073
T [K]	173(2)
$2\theta_{Max}$ [°]	56.0
No. reflections collected	10876
No. unique reflections	3341
No. reflections with I>2σ(I)	2785
Parameters	187
R_1 [I>2σ(I)]	0.0420
wR_2	0.1182
GOOF	1.057

Table 4-2: Geometrical data of the hydrogen bonds of (MA^-)(EDM^+).

	D-H/Å	H•••A/Å	D•••A/Å	<(DHA)/°	Symmetry operation
N2-H17A•••O2	0.88	1.89	2.769(2)	172.8	-
N1-H7•••O1	0.93	1.93	2.673(2)	135.0	-
N2-H17B•••O1	0.85	1.87	2.705(2)	166.2	1-X, 1-Y,1-Z
N2-H17C•••O1	0.88	2.19	2.953(2)	145.2	1+X, Y, Z

4.1.2.2 Salt of mefenamic acid formed with triethylamine (MA^-)(TA^+)

Mefenamic acid (30 mg) and 2 ml of trimethylamine with a few drops of methanol were stirred while heating at 30 °C. The solution was left to crystallise at room temperature. Block-like crystals were observed to form after three days. The crystal structure was solved in

Pbca with single ions of (**MA**$^-$) and **(TA**$^+$**)** observed in the asymmetric unit. Figure 4.6 shows the robust intermolecular interactions as well as the intramolecular interaction present in the salt.

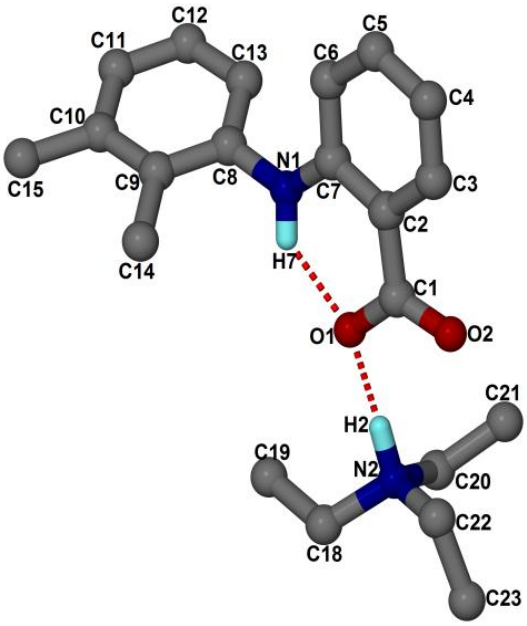

Figure 4-6: Numbering scheme used for (MA$^-$)(TA$^+$).

The salt structure has strong N-H•••O hydrogen bonds and there are several weak interactions occurring as C-H•••O (Table 4.4). The N-H•••O interaction is characterized by N2•••O1 with a measured distance of 2.709(2) Å and an N2-H2•••O1 angle of 173°. The weak interactions between the acidic and the basic ions involved two oxygen atoms, O1 and O2. There are two weak interactions linking O2 and the (**TA**$^+$): C21-H21A•••O2 (3.418(3) Å; 134°) and C22-H22B•••O2 (3.163(3); 118°). In addition to the strong hydrogen bond with the nitrogen atom, O1 interacts weakly with **TA**$^+$ by means of C19-H19B•••O1 with a measured C19•••O1 distance of 3.298(3) Å and a C19-H19B•••O1 angle of 131°. The weak interactions noted between the acidic ions are listed in Table 4.4.

These interactions lead to a columnar arrangement of the (**MA**$^-$) ions with the (**TA**$^+$) ions along [010] (Figure 4.7). The packing arrangement shows that (**TA**$^+$) and (**MA**$^-$) ions alternate along [001] (Figure 4.8).

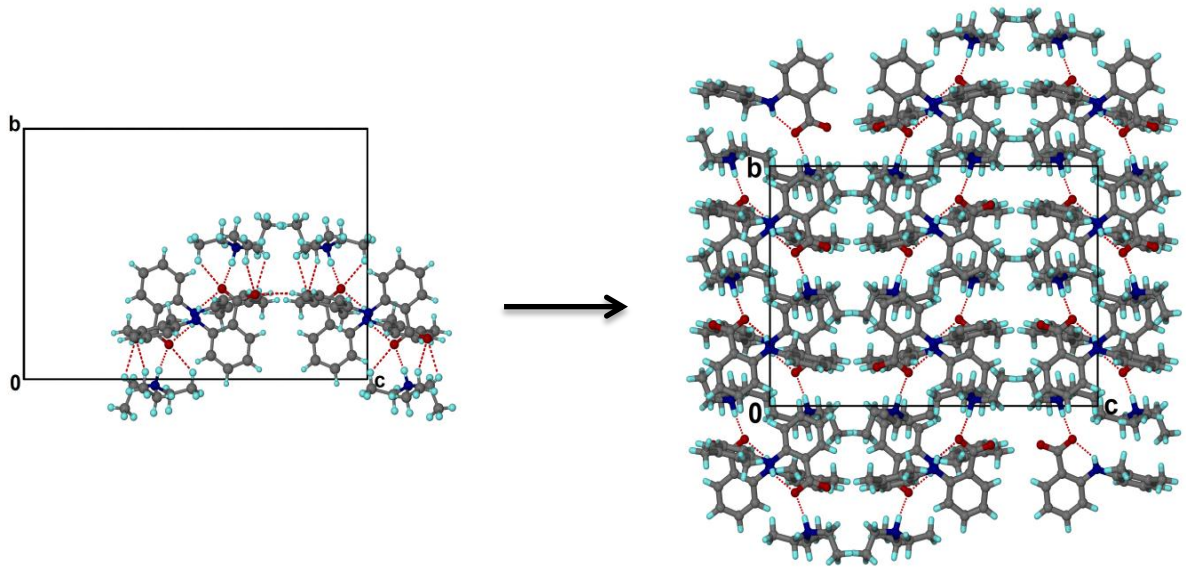

Figure 4-7: Packing of (MA^-)(TA^+) down [100] showing different interactions

The crystal structure is further stabilised through C–H•••π interactions between the 2,3-dimethylphenyl ring and the acidic rings of the (**MA**$^-$) with a calculated C5•••π distance of 3.620 Å. Figure 4.9 shows the channels down [100] and [001] which are occupied by the (**TA**$^+$) ions.

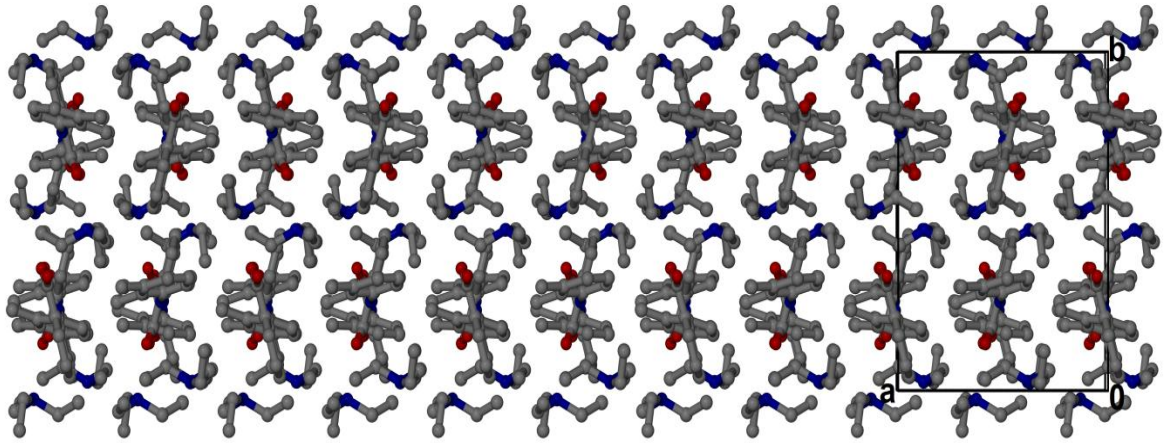

Figure 4-8: Packing arrangement of (MA^-)(TA^+) along [001] (hydrogen atoms were omitted).

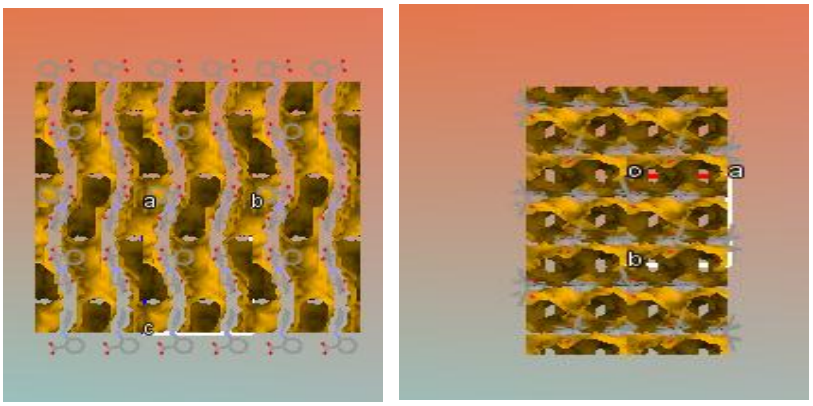

Figure 4-9: Channels showing the location of TA^+ ions along (a) [100] and (b) [001] (hydrogen atoms are omitted).

Table 4-3: Crystal data and data collection parameters for $(MA^-)(TA^+)$.

Compound	$(MA^-)(TA^+)$
Host:guest ratio	1:1
Molecular formula	$C_{21}H_{30}N_2O_2$
Formula weight [g mol^{-1}]	342.47
Crystal system	orthorhombic
Space group	*Pbca*
Z	8
D_{calc} [g cm^{-3}]	1.188
a [Å]	11.201(2)
b [Å]	15.206(3)
c [Å]	22.491(5)
α [°]	90
β [°]	90
γ [°]	90
V [Å^3]	3830.8(13)
μ (Mo-Kα) [mm^{-1}]	0.076
λ[Å]	0.71073
T [K]	173(2)
$2\theta_{Max}$ [°]	56.7
No. reflections collected	28710
No. unique reflections	4785
No. reflections with I>2σ(I)	3284
Parameters	233
R_1 [I>2σ(I)]	0.0564
wR_2	0.1497
GOOF	1.030

Table 4-4: Geometrical data for hydrogen bonds of (MA^-)(TA^+).

	D-H/Å	H•••A/Å	D•••A/Å	<(DHA)/°	Symmetry operation
N1-H7•••O1	0.83	1.96	2.647(2)	140	-
N2-H2•••O1	0.97	1.75	2.709(2)	173	-
C11-H11•••O2	0.95	2.60	3.459(2)	145	X, $^1/_2$ -Y, $^1/_2$ +Z
C15-H15B•••O2	0.98	2.43	3.386(3)	165	X, $^1/_2$ -Y, $^1/_2$ +Z
C19-H19B•••O1	0.98	2.57	3.298(3)	131	-
C21-H21A•••O2	0.98	2.67	3.418(3)	134	-
C22-H22B•••O2	0.99	2.57	3.163(3)	118	-

4.1.2.3 Salt of mefenamic acid formed with 1-methylpiperazine (MA^-)(MP^+)

The (**MA^-**)(**MP^+**) was obtained by mixing 30 mg of MA with 2 ml of 1-methylpiperazine and small volumes of nitromethane. The latter was used as a co-solvent. This was done as when nitromethane was mixed with the acid there was no polymorph, salt or solvate formation. The solution was left to crystallise at room temperature until thick block-like crystals appeared approximately one month after preparation. The structure was solved in $P2_1/c$ with two ions of mefenamate and one 1-methylpiperazinium cation in the unit cell. The crystal data for (**MA^-)(MP^+**) are shown in Table 4.5. Figure 4.10 indicates the numbering scheme of the salt.

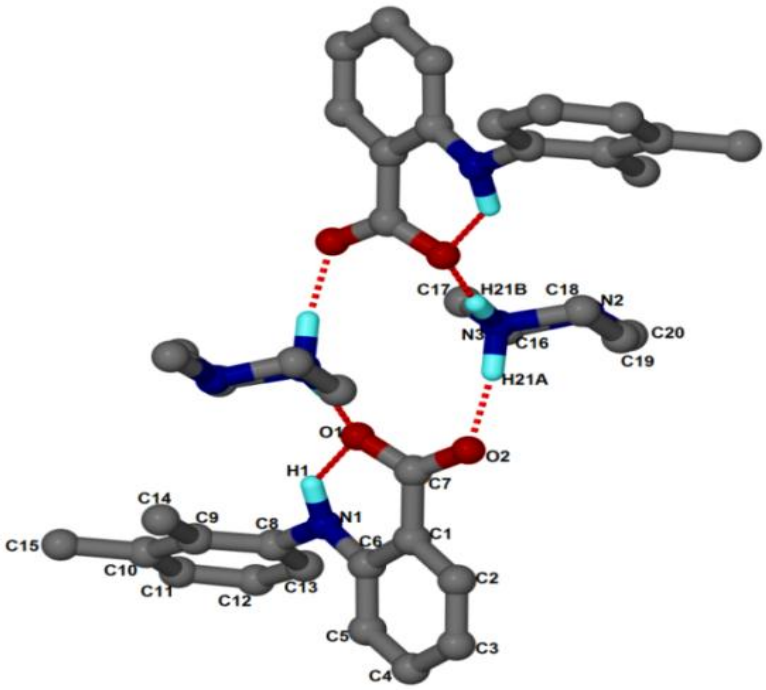

Figure 4-10: Numbering scheme for (MA^-)(MP^+); the hydrogen bonding motif $R_4^4(12)$ is also observed (some hydrogens atoms were omitted).

The four ions are linked together by N–H•••O hydrogen bonds forming a ring $R_4^4(12)$ around Wyckoff position *d*. The robust N–H•••O hydrogen bonds have O1•••N3 and O2•••N3 distances of 2.731(2) Å and 2.728(2) Å respectively. The N3–H21B•••O1 and N3–H21A•••O2 angles both measured 171°. Weak hydrogen bonds were observed which connect the dimethylphenyl of the acid to the acidic group of a neighbouring (**MA^-**) by means of C-H•••O interactions. The two acids interact at C11-H11•••O2 and C15-H15B•••O2 (Table 4.6). The $R_4^4(12)$ of (**MA^-)(MP^+**) observed in Figure 4.10 was maintained by hydrogen bonds stacked as columns parallel to [010] (Figure 4.11).

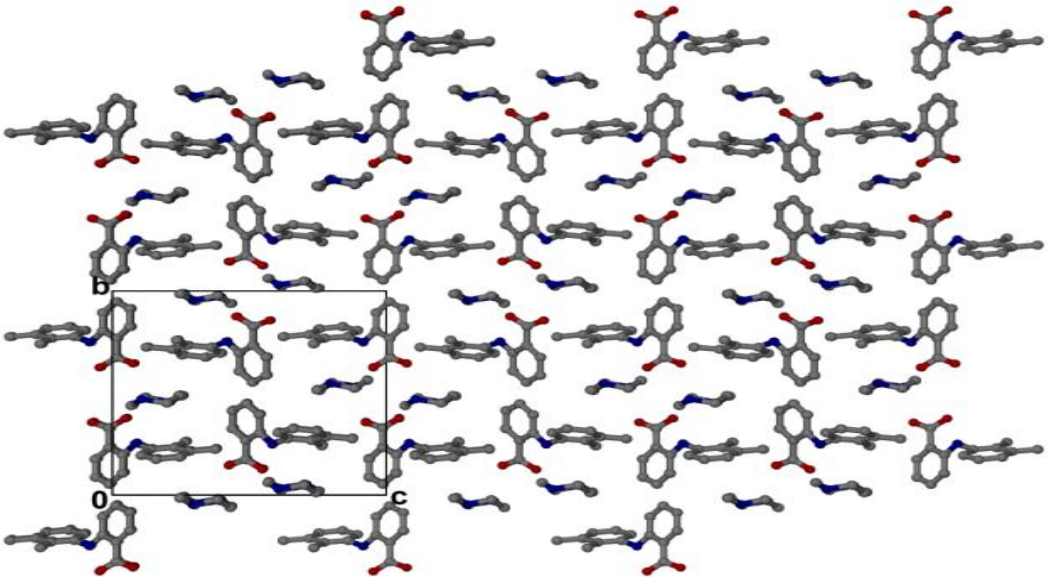

Figure 4-11: Crystal packing arrangement of (MA^-)(MP^+) down [100] (hydrogen atoms were omitted).

Figure 4.12 shows the packing down [001] where parallel layers of (**MA^-**) ions (in blue) were interleaved between layers of (**MP^+**) ions (in red). This arrangement of the solvent and the 2,3-dimethylphenyl group of the acid resulted in a CH•••π interaction viz. C20•••π = 3.851 Å. Figure 4.13: shows the channels wherein the MP^+ ions are located along [100].

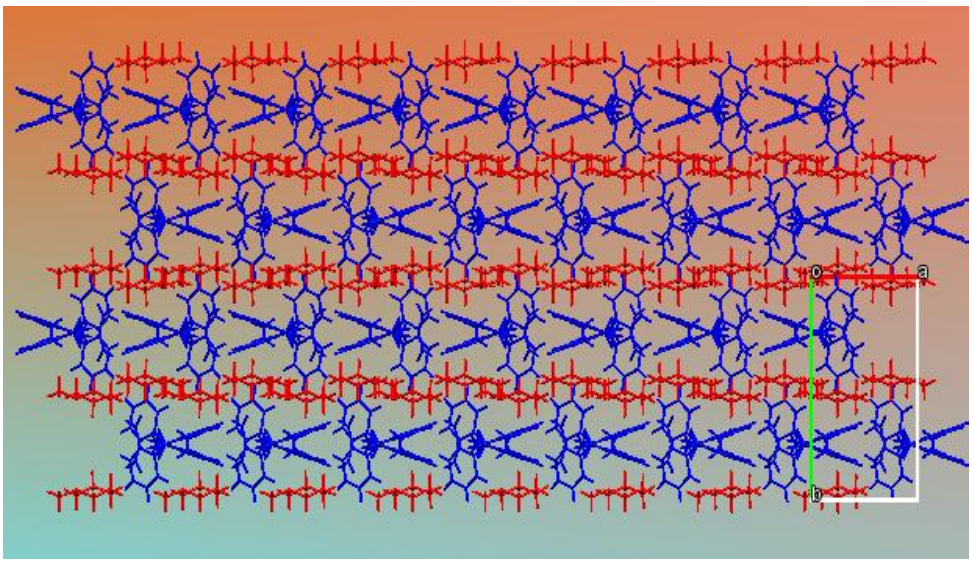

Figure 4-12: Crystal packing arrangement of (MA^-)(MP^+) down [001].

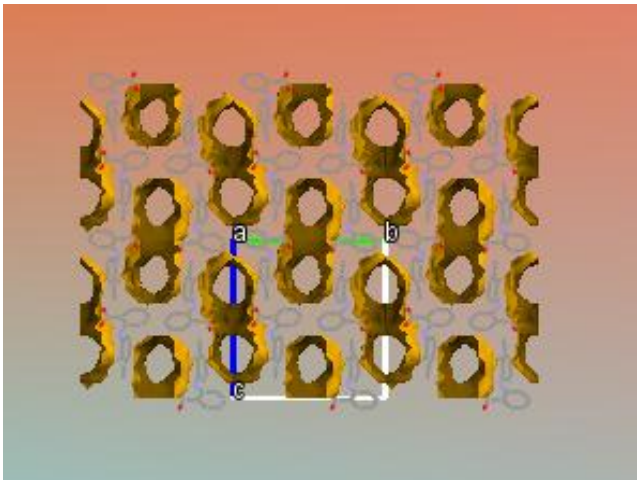

Figure 4-13: Channels showing the location of (MP^+) ions along [100] (hydrogen atoms are omitted).

Table 4-5: Crystal data and data collection parameters of (MA^-)(MP^+).

Compound	(MA^-)(MP^+)
Host:guest ratio	1:1
Molecular formula	$C_{20}H_{27}N_3O_2$
Formula weight [g mol^{-1}]	341.45
Crystal system	monoclinic
Space group	$P2_1/c$
Z	4
D_{calc} [g cm^{-3}]	1.229
a [Å]	7.5963(15)
b [Å]	15.389(3)
c [Å]	15.791(3)
α [°]	90
β [°]	91.96(3)
γ [°]	90
V [Å^3]	1844.9(6)
μ (Mo-Kα) [mm^{-1}]	0.080
λ (Å)	0.71073
T [K]	173(2)
$2\theta_{Max}$ [°]	54.9
No .reflections collected	8245
No. unique reflections	4202
No. reflections with I>2σ(I)	2864
Parameters	232
R_1 [I>2σ(I)]	0.0505
wR_2	0.1169
GOOF	1.043

Table 4-6: Geometrical data obtained for the hydrogen bonds of (MA^-)(MP^+).

	D-H/Å	H•••A/Å	D•••A/Å	<(DHA)/°	Symmetry operation
N1-H7•••O1	0.98	1.91	2.677(2)	133	-
N3-H21B•••O1	0.99	1.75	2.731(2)	171	1-X, -Y, 1-Z
N3-H21A•••O2	1.01	1.72	2.728(2)	171	-
C11-H11•••O2	0.95	2.55	3.430(2)	154	X-1, $^1/_2$ -Y, $^1/_2$ +Z
C15-H15B•••O2	0.98	2.56	3.495(2)	160	X-1, $^1/_2$ -Y, $^1/_2$ +Z

4.1.3 Torsion angles and dihedral angle analysis of mefenamic acid salts

Torsion angles were analysed through the use of O2C1C2C7, C2C7N1C8 and C7N1C8C9 as described in Chapter 3 (Section 3.1.3/3.2.3). The MA salt structures showed differences in the torsion angles. This was dependent on the type of solvent used. The twisting of the carboxylic acid (O2C1C2C7) of MA decreased from (**MA^-)(TA^+**) (172.1°) to (**MA^-)(MP^+**) (161.7°) (Table 4.7). Having the smallest number of atoms thus lowest molecular mass, EDM (60.1g mol^{-1}: Section 2.3.2 Chapter 2) was the smallest of these compounds but did not induce a structure with the smallest O2C1C2C7 torsion angle. This infers that there is no correlation between the molecular mass (size of the solvent) and the twisting of the carboxylic acid. The dihedral angles of (**MA^-**)(**EDM^+**) (53.26°) and (**MA^-**)(**TA^+**) (64.15°) increased as the solvent molecular weight was increased from EDM (60.1 g mol^{-1}: Section 2.3.2, Chapter 2) to TA (101.2 g mol^{-1}: Section 2.3.2, Chapter 2) (Figure 4.17; Table 4.7). However, **(MA^-)(MP^+)** had a much greatly increased dihedral angle (69.75°) when compared with the (**MA^-**)(**EDM^+**) and (**MA^-**)(**TA^+**) salts. This suggests that the cyclical form of MP could be responsible for the increase of the dihedral angle in (**MA^-**).

Table 4-7: Torsion and dihedral angles data recorded for mefenamic acid salts.

	(MA^-)(EDM^+)	(MA^-)(TA^+)	(MA^-)(MP^+)
Torsion angle/°			
O2C1C2C7	165.1	172.1	161.7
C2C7N1C8	-178.0	177.1	176.6
C7N1C8C9	124.8	-115.8	-109.0
Dihedral angle/°	53.26	64.15	69.75

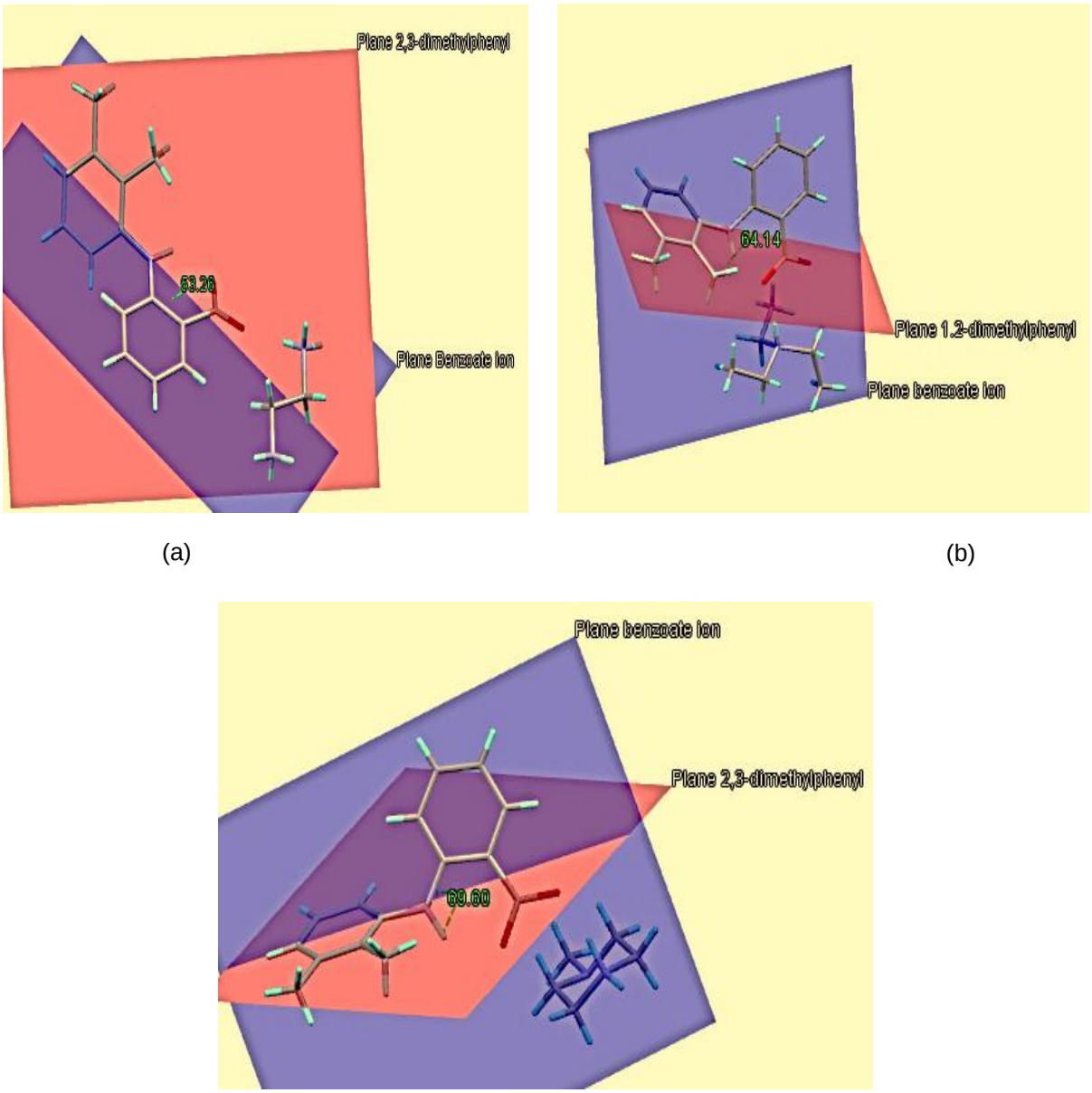

Figure 4-14: Dihedral angles between the planar grouping consisting of the 2,3-dimethyl group (red) and the benzoic acid group (blue) of (a) (MA^-)(EDM^+), (b) (MA^-)(TA^+), (c) (MA^-)(MP^+).

The twisting of the 2,3-dimethylphenyl (C7N1C8C9) torsion angle values obtained were in the ranges previously reported elsewhere. These angles varied in value between 68.2° and 137.1° (Surov et al. 2015; Fábián et al. 2011; Fang et al. 2004). The dihedral angles measured were in the range expected i.e. between 50.4° and 80.3°. However, the (**MA^-)(TA^+**) showed values which were similar to those recorded from MA Form I reported by SeethaLekshmi & Guru Row (2012).

4.1.4 Thermal analysis of mefenamic acid salts

The thermal analysis results are shown in Table 4.8. The solvent loss has to be preceded by proton transfer back to the particular acid. The DSC analysis showed two endotherms attributable to the loss of the solvent and the melting of MA. There was a similarity between the experimental and theoretically calculated mass losses for (**MA)(MP$^+$**) and (**MA$^-$)(TA$^+$**). In the case of the (**MA$^-$)(EDM$^+$**) salt, the loss in mass for the experimental sample (5.51%) did not coincide with the theoretical value calculated (for 1:0.5 ratio a mass loss of 11.09% was expected). It is suggested that a quarter of the EDM was released before the remainder which evaporated during the melt of MA.

The DSC analysis revealed a single broad peak where T_{on} = 364 K which coincided with the release of the solvent for (**MA$^-$)(TA$^+$**). An additional exothermic peak was observed with T_{on} = 439 K; it was attributed to the polymorphic transition which was further confirmed by the desolvation studies. A sharp peak was also observed indicating the melt of the fenamate (T_{on} = 500 K) (Figure 4.15). However, the DSC results obtained for (**MA$^-$)(MP$^+$**) showed the melting of fenamate to be characterised by a broad peak (Figure 4.15 c) of which the endotherm was 509 K, and the solvent was released at T_{on} = 413 K.

Table 4-8: Thermal analysis data recorded for mefenamic acid salt.

SALTS	(MA$^-$)(MP$^+$)	(MA$^-$)(TA$^+$)	(MA$^-$)(EDM$^+$)
Host:Guest ratio	1:1	1:1	1:½
TGA calc % mass loss	29.36	29.57	11.09
exp % mass loss	30.07	29.51	5.51
DSC endotherm for loss of solvent (T_{on}/K)	413	364	352
DSC endotherm of mefenamic acid (T_{on}/K)	509	500	462/included release of remaining EDM
DSC exotherm of mefenamic acid (T_{on}/K)	-	439	-
Solvent normal bp	411*	363*	390*
T_{on}/T_{bp}	1.01	1.00	0.90; 1.18

(Solvents boiling point retrieved from Weast, 1980)

The most interesting changes were observed in the (**MA$^-$**)(**EDM$^+$**) salt where the assigned (**MA$^-$**) T_{on} was different from all other compounds tested (salts or solvates). The T_{on} for the second endotherm was 462 K whereas for the other compounds it varied from 500 K to 509 K. The arrangement of the MA and the solvent is unique as the (**EDM$^+$**) ions occupy

cavities whilst the other two solvents in (**MA**$^-$)(**MP**$^+$) and (**MA**$^-$)(**TA**$^+$) occupied channels. Additionally, there were three strong N2–H•••O hydrogen bonds in the (**MA**$^-$)(**EDM**$^+$) whilst there were three recorded in **(MA**$^-$**)(MP**$^+$**)** and one in **(MA**$^-$**)(TA**$^+$**)**.

The thermal stability (T_{on}/T_{bp}) of (**MA**$^-$)(**EDM**$^+$) was calculated from the first endotherm (352) and the second endotherm (462) observed in the DSC graphs. While the thermal stability of the (**MA**$^-$**)(MP**$^+$) and (**MA**$^-$**)(TA**$^+$) was 1, the (**MA**$^-$**)(EDM**$^+$) thermal stability varied between 0.90 and 1.18.

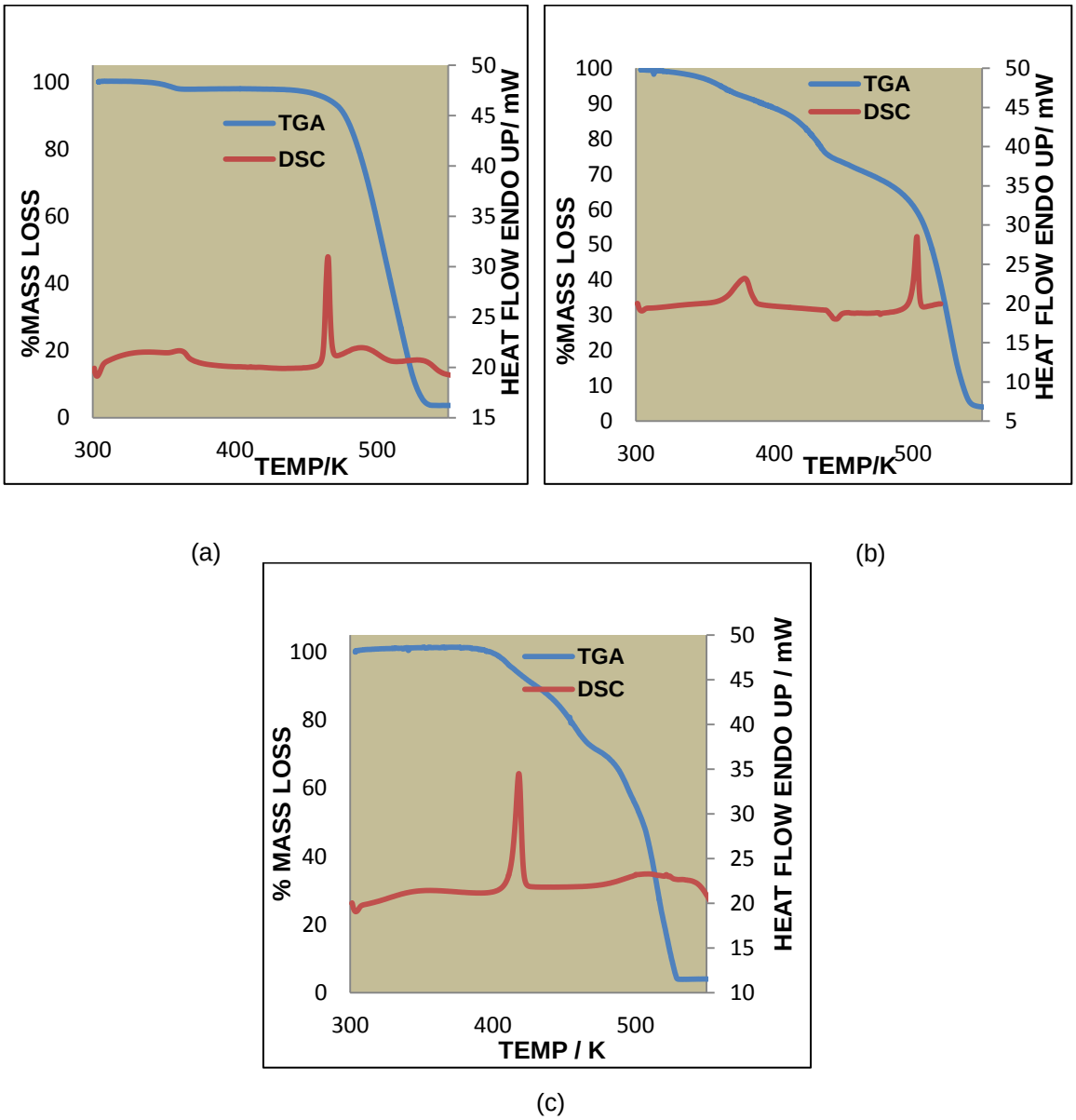

Figure 4-15: The DSC and TGA curves obtained for (a) (MA$^-$)(EDM$^+$), (b) (MA$^-$)(TA$^+$) and (c)(MA$^-$)(MP$^+$).

4.1.5 Hot stage microscopy of mefenamic acid salts

During the hot stage microscopy (HSM) analyses, selected crystals of specific salts were placed between two glass microscope cover slips and a drop of silicone was released onto the crystal (chapter 2: section 2.4.7). These were then analysed to observe the changes that occurred when the temperature was increased from 298 to 573 K.

Figure 4.16 shows changes that occurred when the (**MA$^-$)(EDM$^+$**) salt was subjected to heat. An isolated needle-like crystal from the sample held at room temperature was removed from the mother liquor and analysed (Figure 4.16 a). At 430 K bubbles appeared due to the release of the solvent (Figure 4.16 b). The crystal commenced melting at 542 K (Figure 4.16 c).

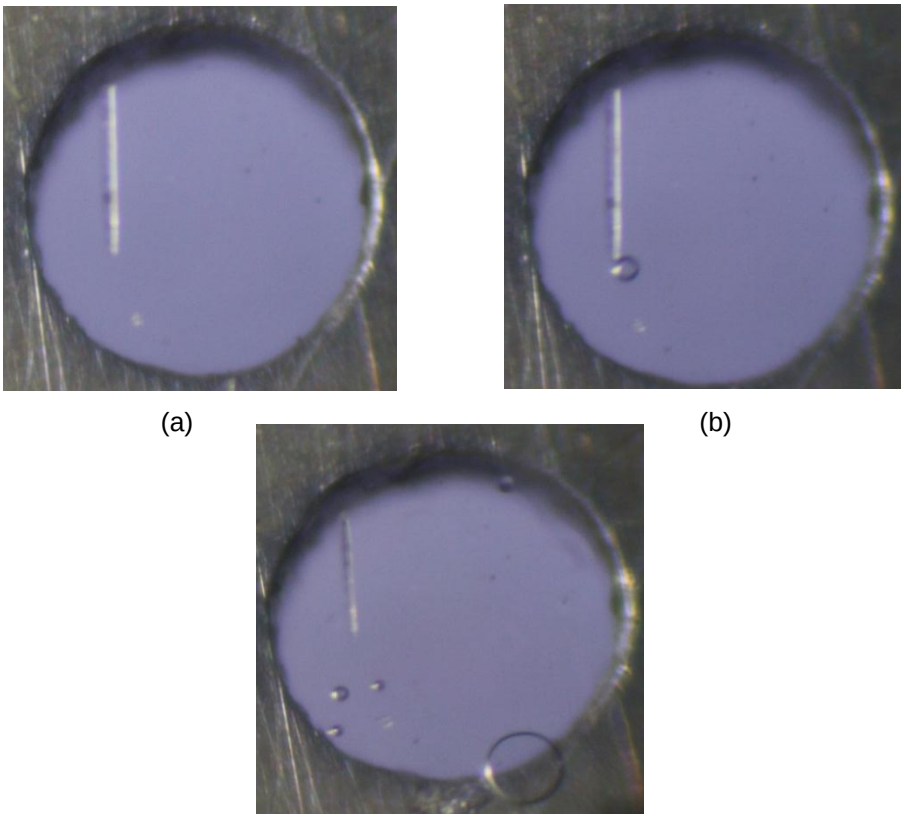

Figure 4-16: The HSM photography of (MA$^-$)(EDM$^+$) a) crystal at 298 K, (b) crystal at 430 K (c) crystal at 542 K.

The (MA^-)(TA^+) crystal which had been held at room temperature (Figure 4.17 a) was observed to change from colourless to white at approximately 408 K. At 435 K the crystal became thinner and solvent vapour was released from the crystal. At approximately 455 K the crystal melted Figure 4.17 (d).

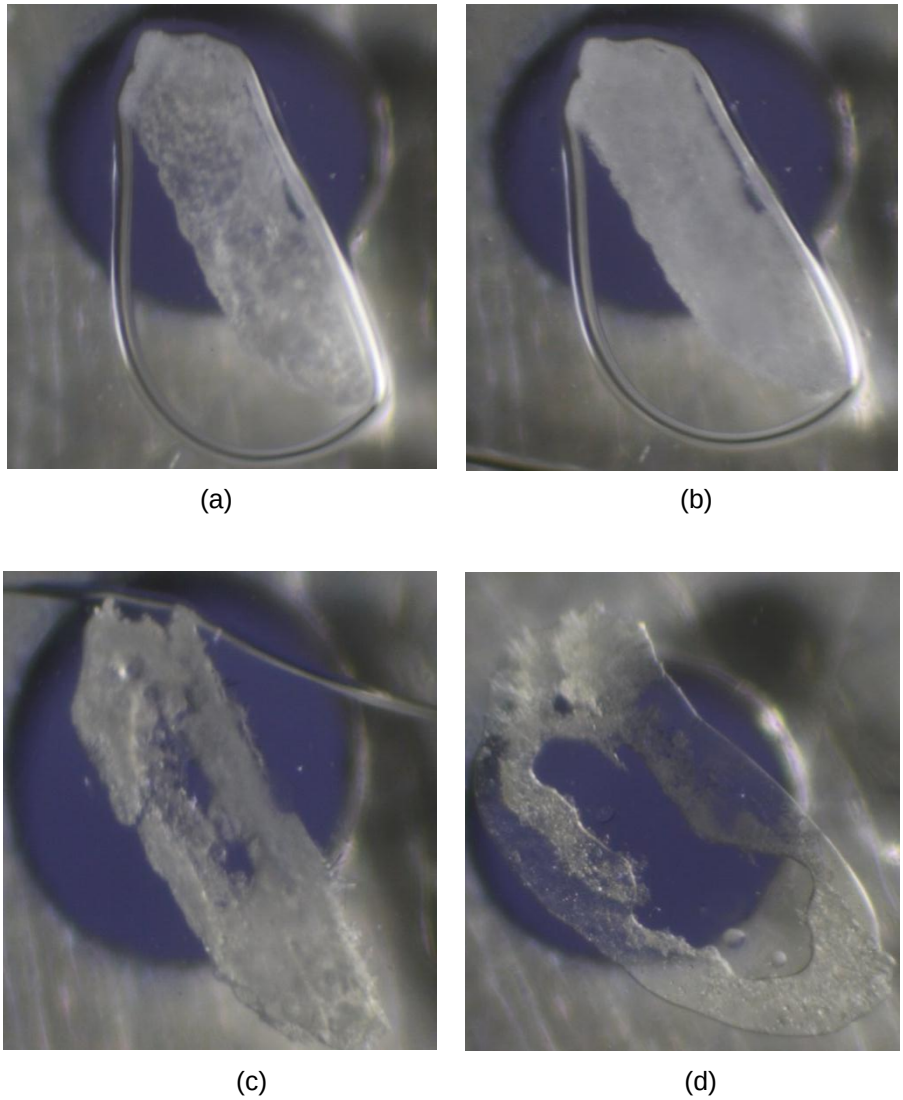

(a) (b)

(c) (d)

Figure 4-17: HSM analyses of (MA^-)(TA^+) (a) crystal at 298 K, (b) crystal at 408 K (c) crystal at 435 K (d) crystal at 455 K.

In the **(MA^-)(MP^+)** sample, small bubbles appeared when the temperature reached approximately 455 K. This was followed by the evolution of further bubbles at 466 K. The crystal was observed to melt at 483 K.

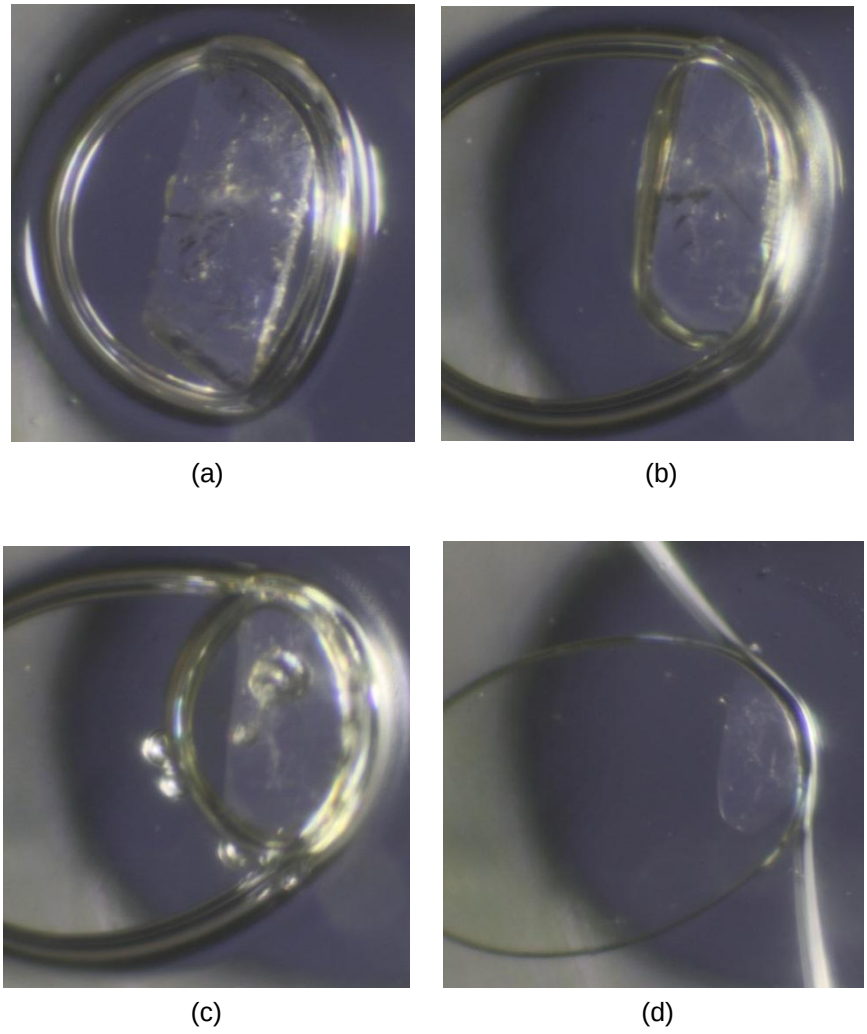

Figure 4-18: The HSM analyses of (MA^-)(MP^+) a) crystal at 298 K, (b) crystal at 455K (c) crystal at 466 K (d) crystal at 483 K.

4.1.6 Powder X-ray diffraction (PXRD) study of mefenamic acid salts

Grinding and slurry experiments were employed to study the reproduction of the salts of MA using methods other than the use of slow evaporation to form crystals. Therefore, as described in Section 3.2.5 of Chapter 3, the ground and slurry samples were prepared with the use of the acid and the respective solvent. The powders obtained underwent PXRD analysis to confirm that the salts could be reproduced by the slurry and grinding methods.

The most interesting characteristics of the salts were observed in the (**MA^-)(EDM^+**) salt (Figure 4.19). The bulk (green) and single crystal (violet) pattern of (**MA^-)(EDM^+**) showed similar peaks. However, when compared to the peaks of the graph obtained from the grinding and slurry experiments, there were no similarities. Instead, additional peaks were

seen in the PXRD analysis of the grinding experiment with one peak being at 2θ =12.8°. Similarly, the slurry material (blue) also showed extra peaks with one being at 2θ= 23.1°. These peaks were not present in the starting material (MA). Therefore, the powders produced from the slurry and grinding experiments were new compounds with different structural characteristics.

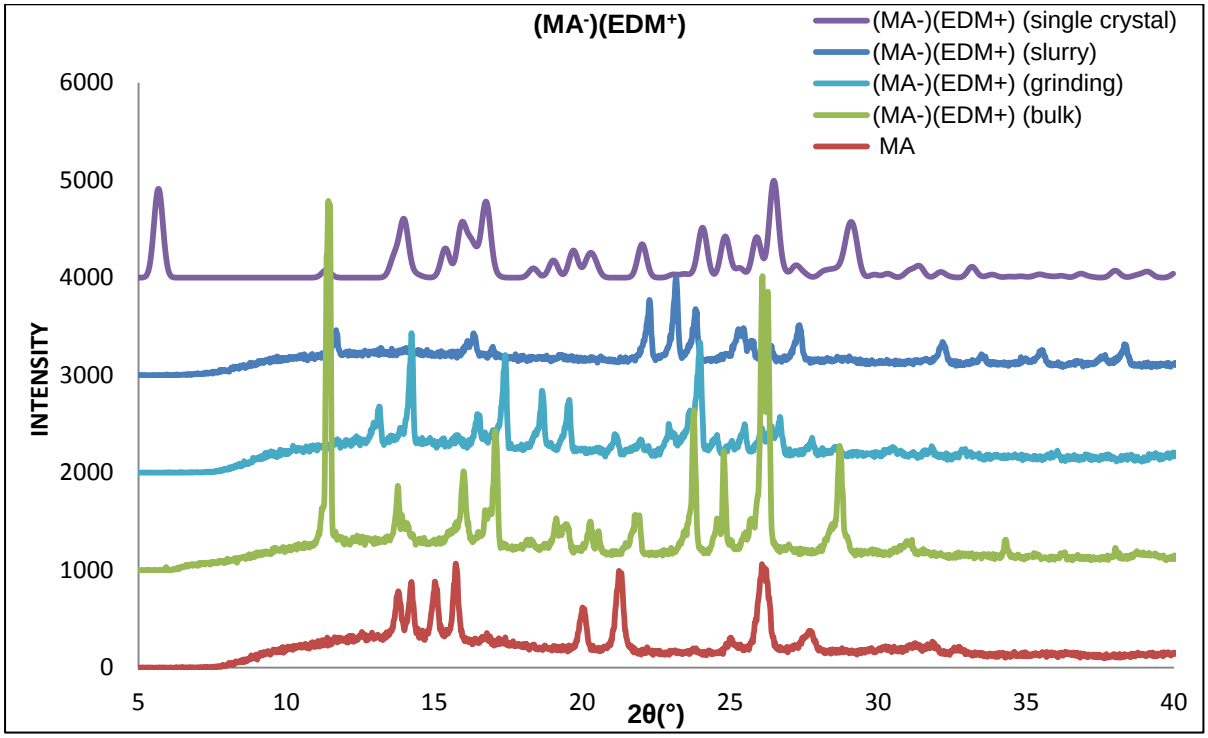

Figure 4-19: PXRD analyses of (MA^-)(EDM^+), calculated patterns obtained from LAZYPULVERIX (blue), and from the slurry experiment (light blue); grinding experiment (purple), bulk sample (green) and starting material MA (red).

Figures 4.20 and 4.21 show the PXRD data obtained from the (**MA^-)(MP^+**) and **(MA^-)(TA^+)** samples respectively. All the PXRD results obtained, regardless of the method used to prepare the samples (ground, slurry and bulk material) showed an excellent match to the theoretical values as determined by using LAZYPULVERIX (Yvon et al. 1977). These values were different from those of the starting material.

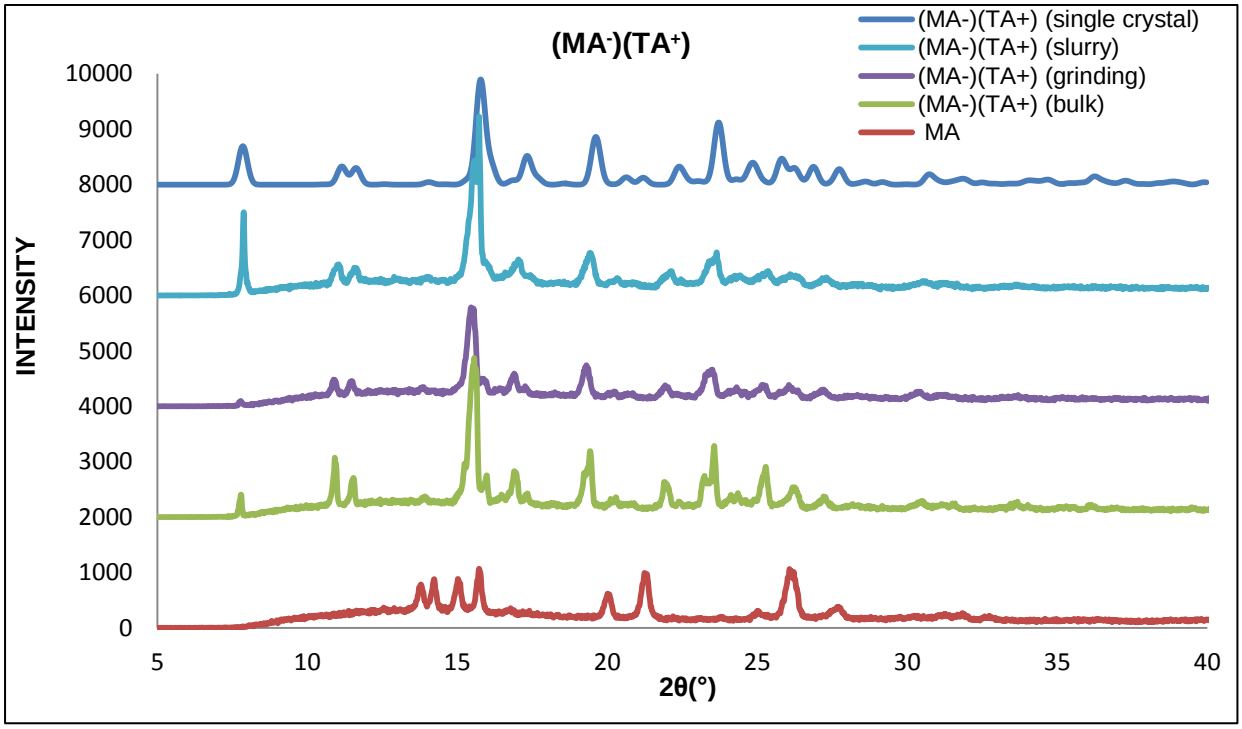

Figure 4-20: PXRD analyses (MA^{-})(TA^{+}), calculated pattern obtained from LAZYPULVERIX (blue), and from the slurry experiment (light blue); the grinding experiment (purple), bulk sample (green) and starting material MA (red).

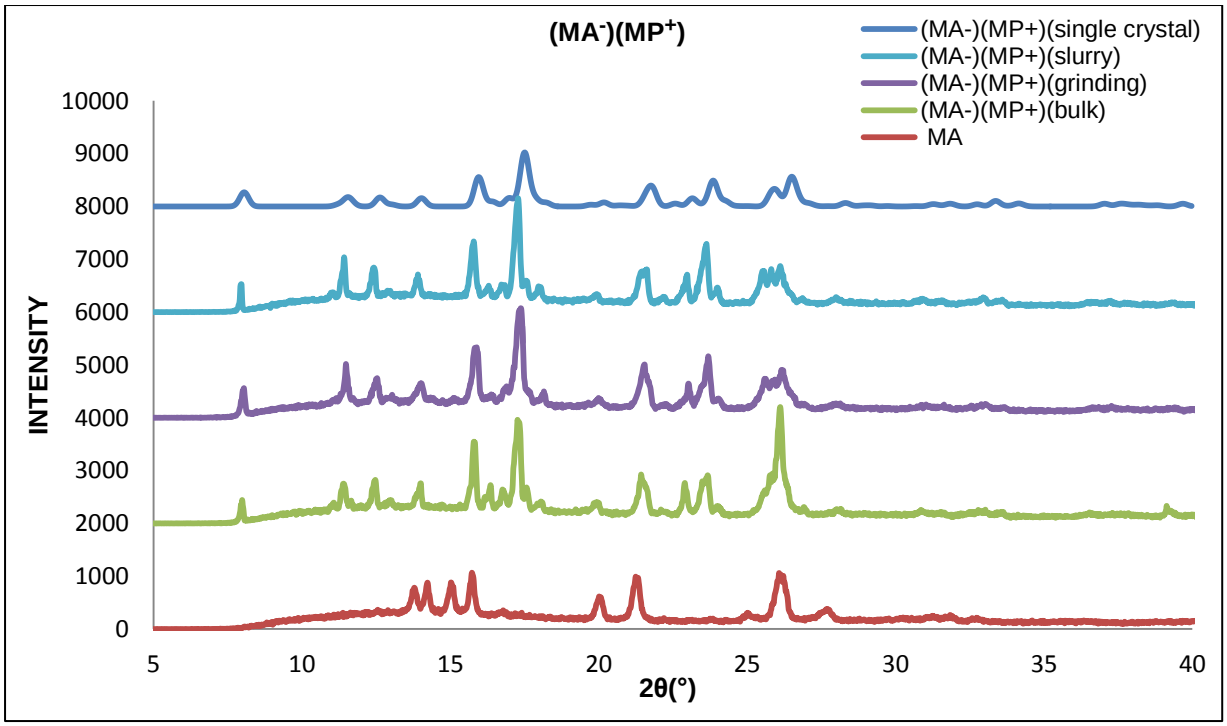

Figure 4-21: PXRD analyses for (MA^{-})(MP^{+}): calculated patterns obtained from LAZYPULVERIX (blue), and from slurry experiment (light blue); the grinding experiment (purple), bulk sample (green) and the starting material MA (red).

4.1.7 Desolvation studies of mefenamic acid salts

Desolvation studies were performed on salts obtained from MA with trimethylamine/1-methylpiperazine/ethylenediamine. Samples were left to desolvate at either room temperature for a month or in an oven for 24 h at 120 °C. No desolvation was observed in the samples left exposed to the atmosphere over a period of one month. Thus the salts of MA were stable at room temperature.

In the desolvation experiments carried out at 120 °C for 24 h the **(MA^-)(EDM^+)** crystals liquified. Hence no results were obtained. The PXRD pattern obtained for the (**(MA^-)(MP^+)**) desolvated sample was similar to that of form I (XYANAC) (Figure 4.22). Conversely the desolvated sample of **(MA^-)(TA^+)** coincided predominantly with that of form II with the CSD code XYANAC02 (Lee et al. 2006). Additional peaks at 2θ= 15.2° and 21.5° matched those of form I. Hence it was deduced that the resulting powder from **(MA^-)(TA^+)**, represented a mixture of XYANAC and XYANAC02 (Figure 4.23).

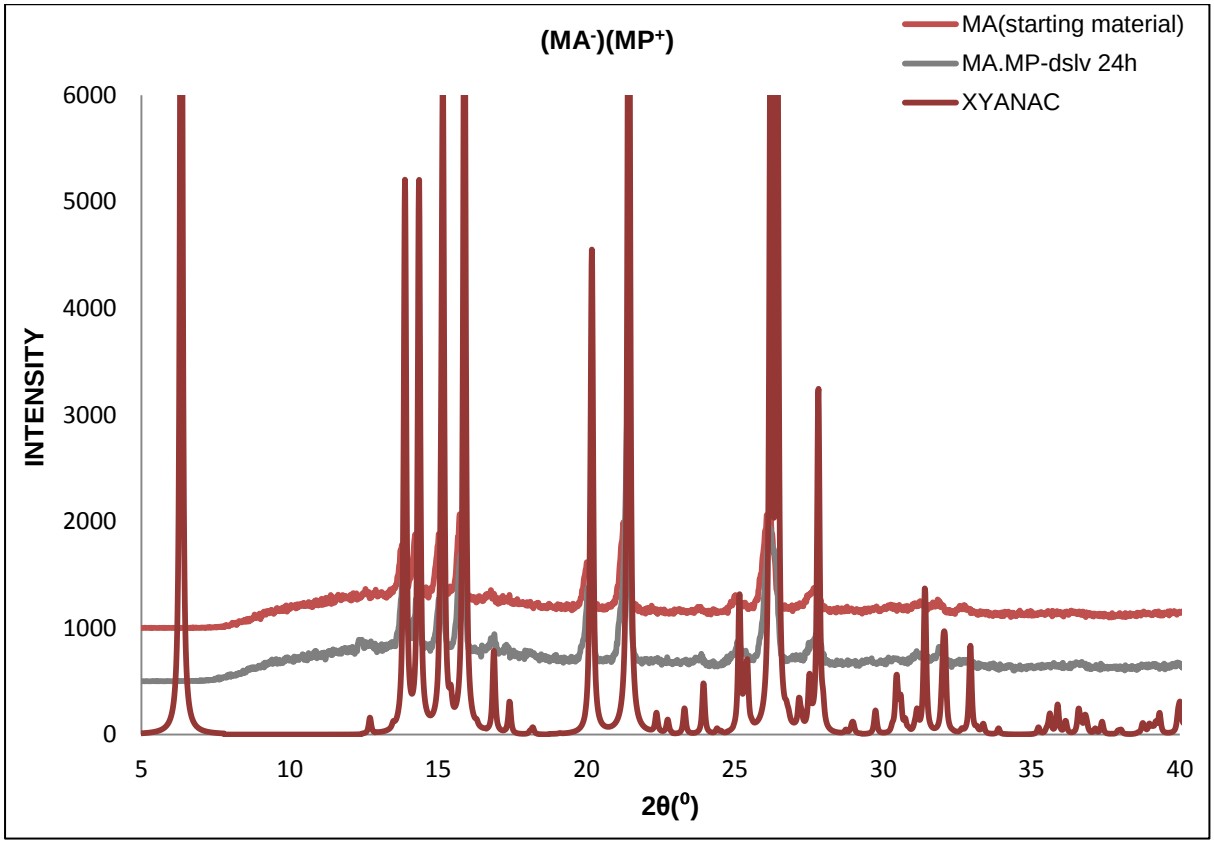

Figure 4-22: Comparison of patterns of (MA^-)(MP^+) after 24 h desolvation at 120 °C with XYANAC and starting material.

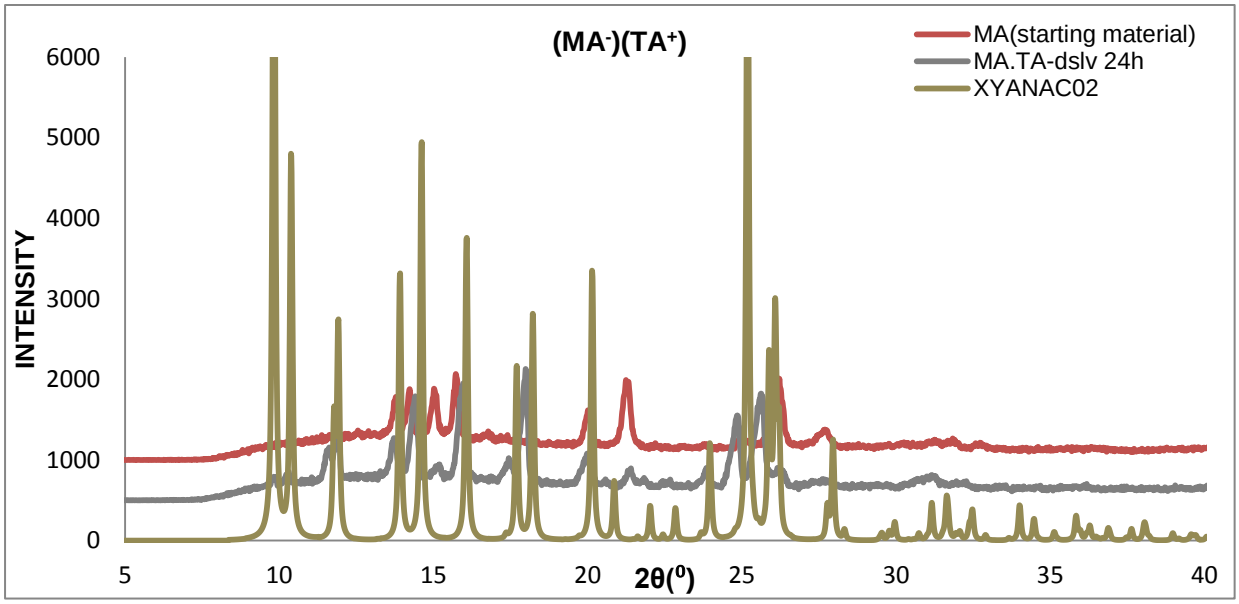

Figure 4-23: Comparison of patterns of $(MA^-)(TA^+)$ after 24 h desolvation at 120 °C with XYANAC02 and the starting material.

4.2 Tolfenamic acid salts

4.2.1 Introduction

Salts of TFA were obtained with morpholine (MOP) and diethanolamine (DOHA). The crystals showed identical crystal systems but the packing arrangement was dissimilar. In this case, the recorded ΔpK_a were 5.18 and 4.63 **$(TFA^-)(DOHA^+)$** and **$(TFA^-)(MOP^+)$** respectively which also agreed with the ΔpK_a rule. Furthermore, the API showed a conformation that was different from that reported by Fábián et al. (2011) and Surov et al. (2015).

4.2.2 Structural analysis of tolfenamic acid salts

4.2.2.1 Salt of tolfenamic acid formed with diethanolamine $(TFA^-)(DOHA^+)$

$(TFA^-)(DOHA^+)$ was prepared by mixing TFA with diethanolamine at 30 °C until the acid dissolved. The solution was left to crystallise at room temperature and block-like crystals were observed after two weeks. **$(TFA^-)(DOHA^+)$** crystallised in the monoclinic space group

*P*2$_1$/*c* with one ion each of **TFA$^-$** and **DOHA$^+$** in the asymmetric unit (Table4.9). Figure 4.24 shows the numbering scheme used for **(TFA$^-$)(DOHA$^+$)**.

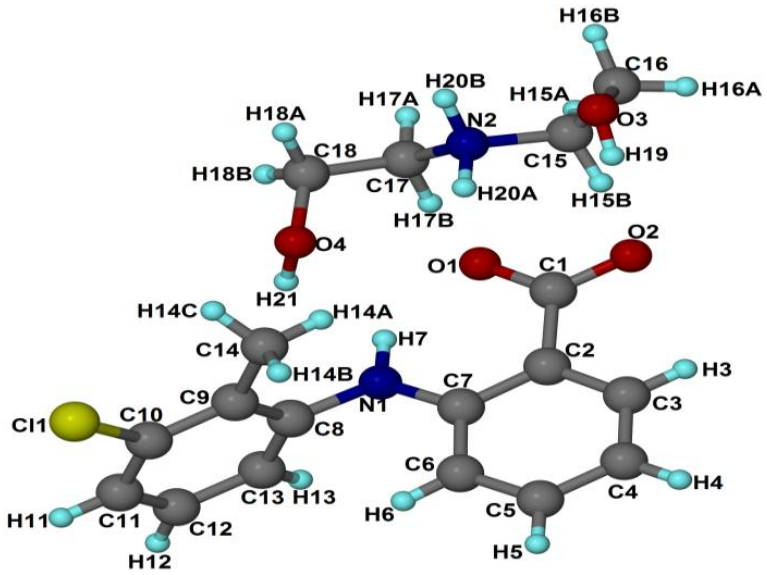

Figure 4-24: Numbering system for (TFA$^-$)(DOHA$^+$).

Robust hydrogen bonds were attributable to the amino, hydroxyl and carbonyl groups in the structure. These are characterised by N2–H20A•••O1 with a distance of 2.719(3) Å and an angle of 168°. In addition, N2–H20B•••O2 was characterised with an N2•••O2 distance 2.758(3) Å and an N2–H20B•••O2 angle of 173°. Additionally, the O3–H19•••O2 interaction had an O3•••O2 distance 2.661(3) Å and an angle of 174°. The O4–H21•••O3 interaction was characterised with an O4•••O3 distance of 2.792(3) Å and an angle of 170°. Weak interactions occurred between C13–H13•••O2 with a measured distance of 3.502(4) Å and an of angle 142°; C15–H15B•••O3 with a distance of 3.568(4) Å and an angle of 164°; C16–H16A•••O1 with a distance of 3.594(4) Å and an angle of 150° and C17–H17B•••O4 with a distance of 3.491(4) Å and an angle of 155° (Table 4.10).

Even though numerous graph sets occurred in the structure, only one ring could be observed and was identified as $R_2^2(9)$ (Figure 4.25). This was due to the successive interaction of N2–H20A•••O1 and O3–H19•••O2. These various interactions were responsible for the columnar packing of the crystal structure observed in Figure 4.26.

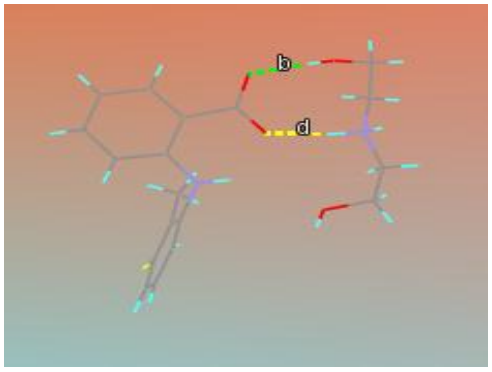

Figure 4-25: Hydrogen bonding motif in (TFA^+)($DOHA^-$) with graph set $R_2^2(9)$.

The packing down [010] whereby two **TFA^-** anions surrounded the **$DOHA^+$** cation is shown in Figure 4.26. The carboxyl group was directed toward the solvent molecules to accommodate the acid interaction with the solvent. The **(TFA^-)($DOHA^+$)** formed segregated hydrophobic and hydrophilic layers as described by Fang et al. (2004). A similar packing arrangement was observed in the mefenamate diethanolammonium salt (Fang et al. 2004). No close interaction was observed between the chlorine and oxygen atoms as they were orientated away from one another. Figure 4.27 shows the constricted channels in the [100] direction in **(TFA^-)($DOHA^+$).** These were occupied by the solvent**.**

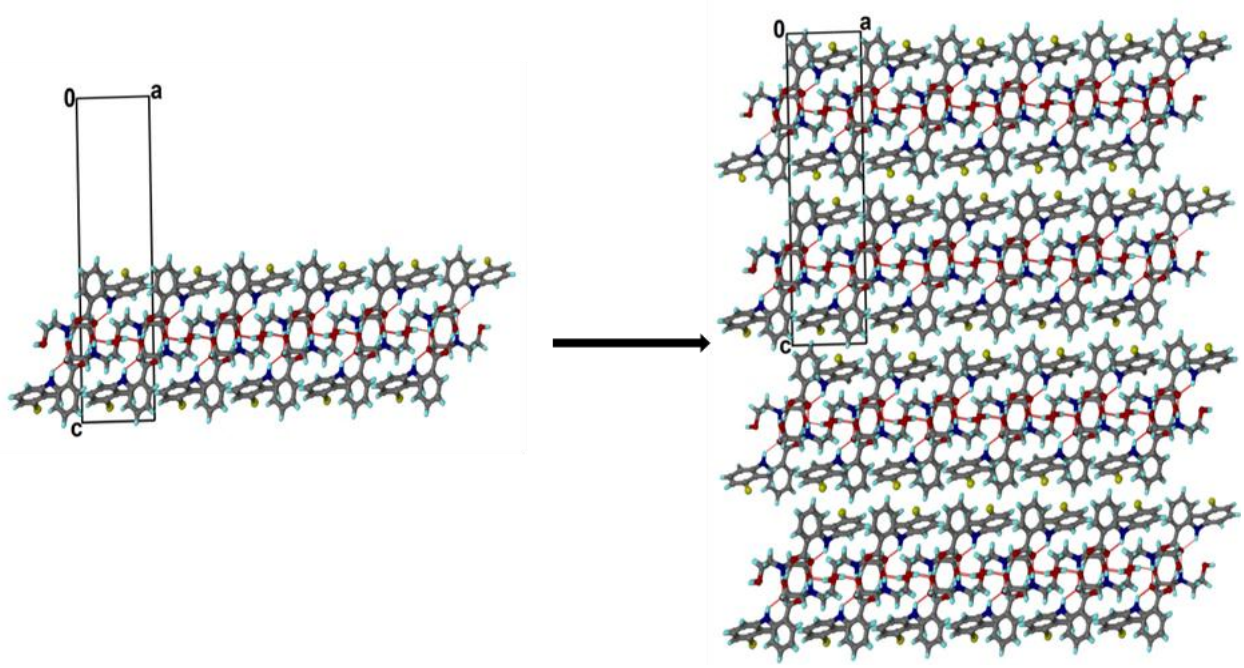

Figure 4-26: Crystal packing arrangement of (TFA^+)($DOHA^-$) down [010].

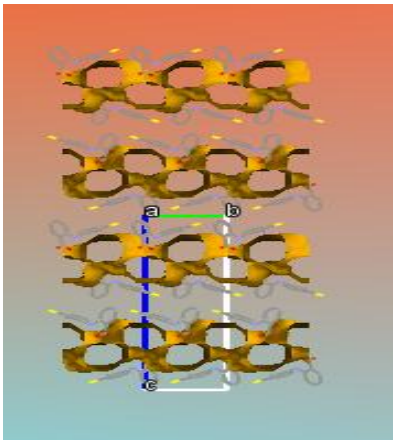

Figure 4-27: Channels showing the location of ($DOHA^+$) ions view down [010] (hydrogen atoms are omitted for clarity).

Table 4-9: Crystal data and data collection parameters obtained for (TFA^-)($DOHA^+$).

Compound	(TFA^-)($DOHA^+$)
Host:guest ratio	1:1
Molecular formula	$C_{18}H_{23}ClN_2O_4$
Formula weight [g mol^{-1}]	366.83
Crystal system	monoclinic
Space group	$P2_1/c$
Z	4
D_{calc} [g cm^{-3}]	1.377
a [Å]	7.5644(15)
b [Å]	8.1191(16)
c [Å]	28.813(6)
α [°]	90.00
β [°]	90.32(3)
γ [°]	90.00
V [$Å^3$]	1769.6(6)
μ (Mo-Kα) [mm^{-1}]	0.242
λ (Å)	0.71073
T [K]	173(2)
$2\theta_{Max}$ [°]	54.9
No. reflections collected	40479
No. unique reflections	4059
No. reflections with I>2σ(I)	2659
Parameters	232
R_1 [I>2σ(I)]	0.0664
wR_2	0.1511
GOOF	1.111

Table 4-10: Geometrical data obtained for hydrogen bonds of (TFA^+)($DOHA^-$).

	D-H/Å	H•••A/Å	D•••A/Å	<(DHA)/°	Symmetry operation
O3-H19•••O2	0.84	1.82	2.661(3)	174	-
O4-H21•••O3	1.01	1.79	2.792(3)	170	X-1, Y, Z
N1-H7•••O1	0.93	1.92	2.620(3)	130	-
N2-H20A•••O1	1.05	1.69	2.719(3)	168	-
N2-H20B•••O2	0.96	1.80	2.758(3)	173	2-X, $^1/_2$ +Y, $^1/_2$ -Z
C13-H13•••O2	0.95	2.70	3.502(4)	142	X-1, Y, Z
C15-H15B•••O3	0.99	2.61	3.568(4)	164	2-X, Y- $^1/_2$, $^1/_2$ -Z
C16-H16A•••O1	0.99	2.70	3.594(4)	150	2-X, Y- $^1/_2$, $^1/_2$ -Z
C17-H17B•••O4	0.99	2.57	3.491(4)	155	1-X, Y- $^1/_2$, $^1/_2$ -Z

4.2.2.2 Salt of tolfenamic acid formed with morpholine (TFA^-)(MOP^+)

This salt was obtained after three weeks of slow evaporation at RT from a saturated solution of TFA and morpholine with nitromethane used as a co-solvent. Plate-like crystals of **(TFA^-)(MOP^+)** were observed and the crystal structure was solved in the space group $P2_1/n$. Unlike the observation for **(MA)(MOP)** (Chapter 5)**,** in **(TFA^-)(MOP^+)** a proton was transferred to the nitrogen atom of MOP to form MOP^+. Crystal data and data collection parameters of this salt are provided in Table 4.11. Figure 4.28 illustrates the numbering scheme used for (**(TFA^-)(MOP^+)**), as well as a ring with graph set $R_4^4(12)$.

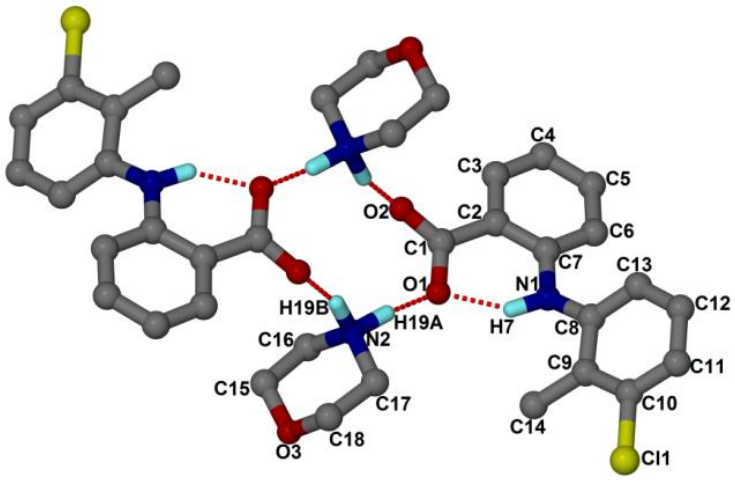

Figure 4-28: Numbering scheme used for (TFA^-)(MOP^+) with graph set $R_4^4(12)$.

The **(TFA^-)** and **(MOP^+)** ions formed individual columns of solvent and acid which alternated parallel to [010] as shown in Figure 4.29.

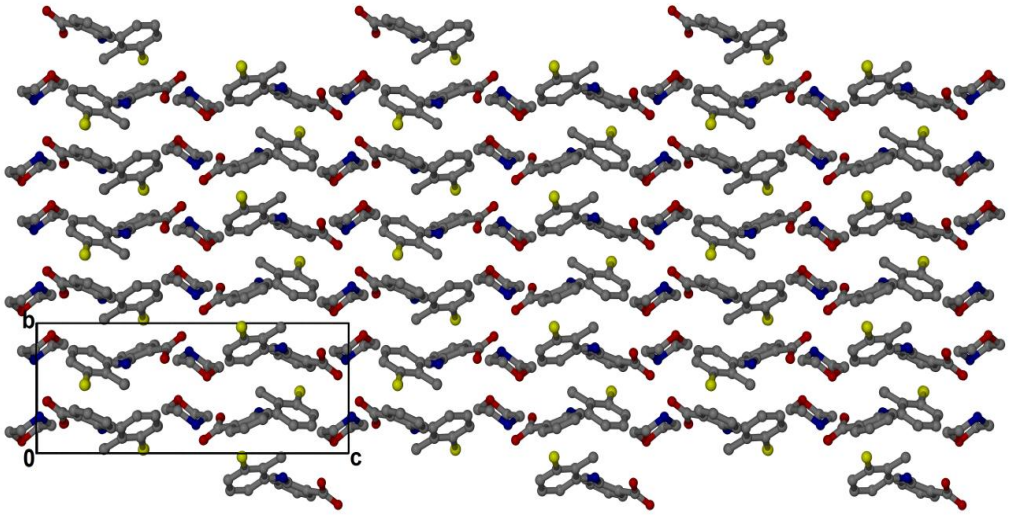

Figure 4-29: Crystal packing arrangement of (TFA^-)(MOP^+) down [100] (hydrogen atoms were omitted for clarity).

The packing arrangement formed infinite wave-like sheets parallel to [100] (Figure 4.30). The C–H•••π interactions occurred between the acidic phenyl ring which interacted with a neighbouring acidic phenyl ring (C6–H6•••π) and also between two neighbouring chloro-methylphenyl rings (C14–H14•••π). Figure 4.31 shows the cavities occupied by **(MOP^+)** cations.

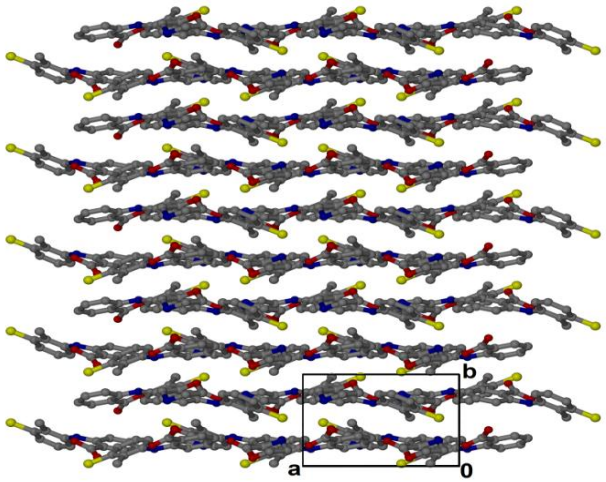

Figure 4-30: Crystal packing arrangement of (TFA^+)(MOP^-) down [001] (hydrogen atoms were omitted).

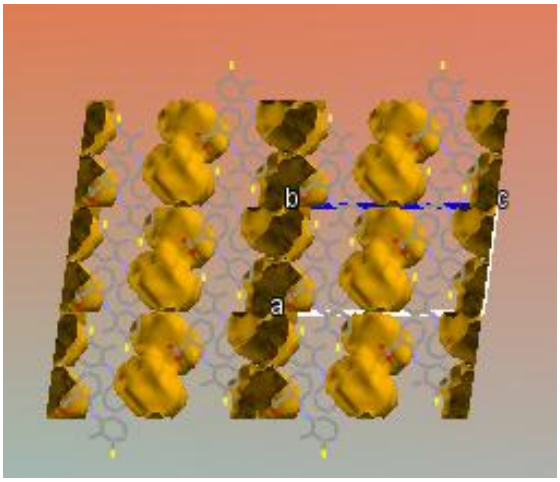

Figure 4-31: Cavities showing the location of (MOP+) cations along [010] (hydrogen atoms were omitted).

Table 4-11: Crystal data and data collection parameters obtained for (TFA^-)(MOP^+).

Compound	(TFA^-)(MOP^+)
Host:guest ratio	1:1
Molecular formula	$C_{18}H_{19}ClN_2O_3$
Formula weight [g mol^{-1}]	346.80
Crystal system	monoclinic
Space group	$P2_1/n$
Z	4
D_{calc} [g cm^{-3}]	1.343
a [Å]	10.689(2)
b [Å]	7.6553(15)
c [Å]	21.143(4)
α [°]	90.00
β [°]	97.48(3)
γ [°	90.00
V [Å^3]	1715.3(6)
μ (Mo-Kα) [mm^{-1}]	0.241
λ (Å)	0.71073
T [K]	173(2)
$2\theta_{Max}$ [°]	55.9
No. reflections collected	22003
No. unique reflections	4109
No. reflections with I>2σ(I)	3059
Parameters	221
R_1 [I>2σ(I)]	0.0413
wR_2	0.0945
GOOF	1.020

Table 4-12: Geometrical data for hydrogen bonds of (TFA^-)(MOP^+).

	D-H/Å	H•••A/Å	D•••A/Å	<(DHA)/ °	Symmetry operation
N1-H7•••O1	0.94	1.82	2.645(2)	144	-
N2-H19A•••O1	1.03	1.66	2.674(2)	166	-
N2-H19B•••O2	1.05	1.67	2.697(2)	164	1-X, 2-Y, 1-Z
C11-H11•••O2	0.95	2.47	3.360(2)	155	X- $^1/_2$, $^3/_2$ -Y, Z- $^1/_2$
C12-H12•••O3	0.95	2.61	3.345(2)	134	$^1/_2$ +X, $^3/_2$ -Y, Z- $^1/_2$
C16-H16B•••O1	0.99	2.45	3.246(2)	138	1-X, 1-Y, 1-Z

4.2.3 Torsion angles and dihedral angle analysis of tolfenamic acid salts

Torsion angles were investigated relative to the twisting of the carboxylic acid (O2C1C2C7), rotation of the phenyl ring (C2C7N1C8) and the twisting of the 3-chloro-2-methylphenyl (C7N1C8C9) (SeethaLekshmi & Guru Row, 2012). The dihedral angle measured between the two phenyl rings is shown in Table 4.13.

The angles measured from C2C7N1C8 and O2C1C2C7 in the two salts showed little variation. In addition, in **(TFA^-)(MOP^+)** the twisting of the 3-chloro-2-methylphenyl (C7N1C8C9 = 168°) is comparable to other torsion angles observed (C2C7N1C8 = 164^0; O2C1C2C7 = 150°).

Table 4-13: Torsion and dihedral angles obtained for (TFA^-)(MOP^+) and (TFA^-)($DOHA^{+\cdot}$)

	(TFA^-)($DOHA^+$)	(TFA^-)(MOP^+)
Torsion angle/°		
O2C1C2C7	175	-164
C2C7N1C8	-173	150
C7N1C8C9	82	168
Dihedral angle/°	86.32	40.94

It was observed that C2C7N1C8 was reduced to approximately half the value recorded for **(TFA^-)($DOHA^+$)** and had a torsion angle of 82°. This is to be expected as **(TFA^-)($DOHA^+$)** had more hydrogen bond interactions than did **(TFA^-)(MOP^+)**. Therefore, the **TFA^-** anion had to be flexible in order to facilitate interactions with **($DOHA^+$)**. The **(TFA^-)($DOHA^+$)** C2C7N1C8 and C7N1C8C9 angles were similar to those measured in **(MA^-)($DOHA^+$)** as reported by Fang et al. 2004 viz. 173° and 80.6° respectively. Therefore, the replacement of the methyl

group by the chlorine atom does not alter the conformation of the acid anion in salt structures where DOHA was used.

Dihedral angles reported for TFA polymorphs and co-crystals varied between 44.5° and 76.9° (Surov et al. 2015). The values for **(TFA$^-$)(MOP$^+$)** and **(TFA$^-$)(DOHA$^+$)** recorded during the current study were 40.94° and 86.32° respectively which was not within the expected range (Figure 4.32). Twisting of the 3-chloro-2-methylphenyl angles reported elsewhere varied between 75° and 143° (Surov et al. 2015). In the current study, although the torsion angle for **(TFA$^-$)(DOHA$^+$)** was 81.9° and occurred within this range, **(TFA$^-$)(MOP$^+$)** had an increased value of 168°.

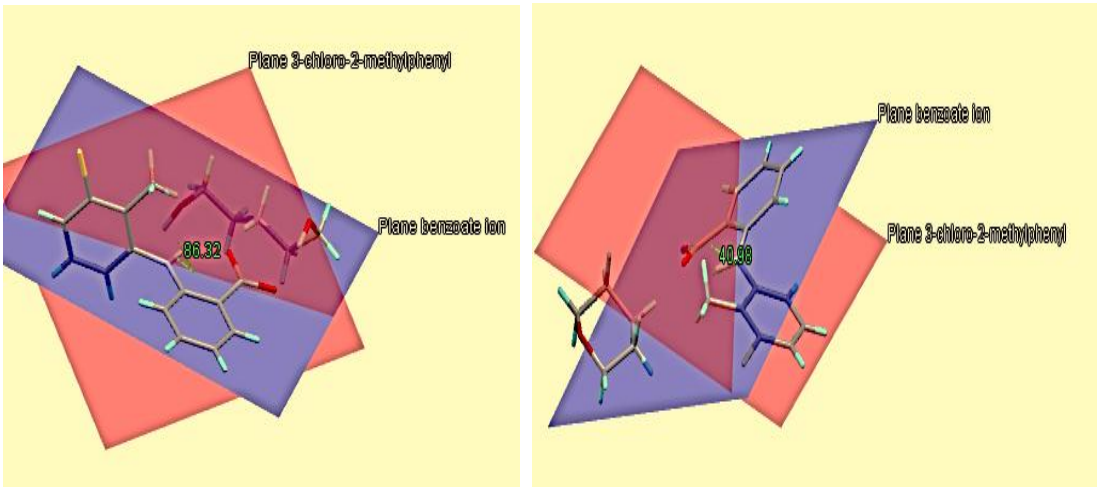

(a) (b)

Figure 4-32: Dihedral angles recorded for (a) (TFA$^-$)(DOHA$^+$) and (b) (TFA$^-$)(MOP$^+$).

4.2.4 Thermal analysis of tolfenamic acid salts

The DSC and TGA curves of (**TFA**$^-$)(**MOP**$^+$) and (**TFA**$^-$)(**DOHA**$^+$) are shown in Figure 4.33. Results of the TGA analysis agreed with the calculated theoretical mass losses of **(TFA$^-$)(MOP$^+$)** and **(TFA$^-$)(DOHA$^+$)** (Table 4.14). The TGA curves were characterised by a single mass loss which represented the release of the solvent. The DSC graphs show a broad endothermic peak for (**TFA$^-$)(MOP$^+$**) and two different endotherms for (**TFA$^-$)(DOHA$^+$**).

Table 4-14: Thermal analysis data obtained for tolfenamic acid salts.

SALTS	$(TFA^-)(DOHA^+)$	$(TFA^-)(MOP^+)$
Host:Guest ratio	1:1	1:1
TGA calc % mass loss	28.71	24.96
Exp% mass loss	29.58	25.86
DSC endotherm 1 (T_{on}/K)	418	434
DSC endotherm 2 (T_{on}/K)	511	
Solvent normal bp/K	544	402
T_{on}/T_{bp}	0.77	0.93

(Solvents boiling point retrieved from Weast, 1980)

The broad endothermic peak observed in the DSC graph recorded for (**TFA^-)(MOP^+**) was characterised with a T_{on} of 434 K. This peak represented the release of morpholine and the melting of the TFA. Alternatively, (**TFA^-)($DOHA^+$**) showed two distinct peaks corresponding to the release of the solvent with the fenamate. In the latter case, TFA melted at T_{on} = 511 K while the solvent was released at T_{on} = 418 K. This value is lower than the boiling point of 544 K of DOHA. The previously reported values for the **TFA•2PIC**, **TFA•3PIC** and **TFA•3BrPYR** solvates (section 3.2.4, Chapter 3) showed that the melt of TFA varied between 484 K and 489 K. Surov et al. (2015) reported a melting point of TFA form I of 485 K. This indicated that the formation of the salt with diethanolamine increased the melting point of TFA. The thermal stability of the salts measured by the T_{on}/T_b values reported in Table 4.14 were 0.93 for (**TFA^-)(MOP^+**) and 0.77 (**TFA^-**)(**$DOHA^+$**). The latter values do accord with the different packing arrangements noted since MOP molecules are located in cavities while the DOHA molecules are located in channels.

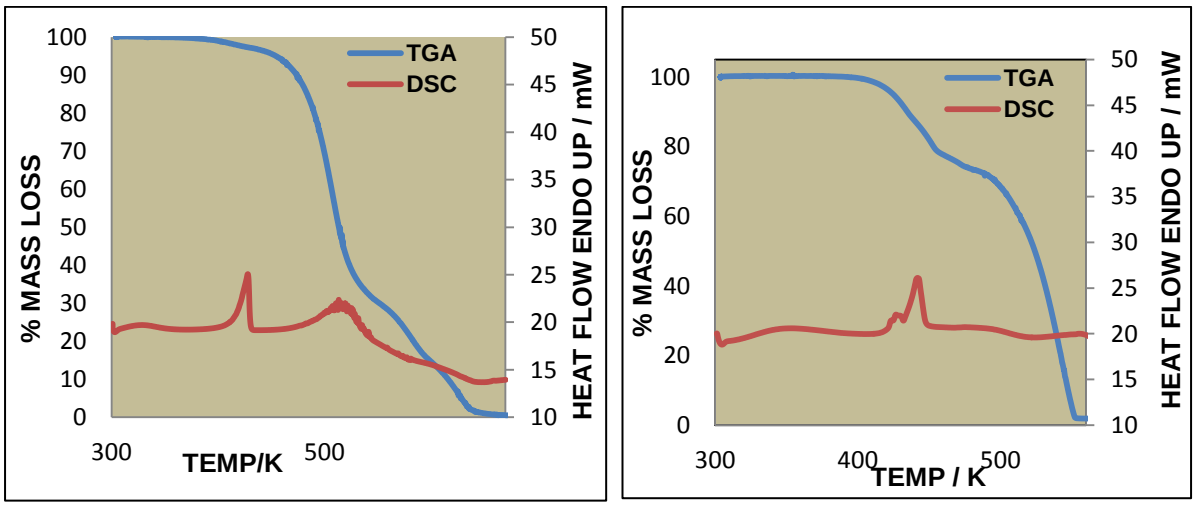

Figure 4-33: TG and DSC curves of (a) $(TFA^-)(DOHA^+)$ and (b) $(TFA^-)(MOP^+)$.

4.2.5 Powder X-ray diffraction (PXRD) of tolfenamic acid salts

Experiments where samples were pulverized or from which slurries were prepared (Section 2.4.8 Chapter 2.) were done and the resulting materials were analysed to obtain PXRD patterns.

From the grinding, and slurry of (**TFA**)(**DOHA**) PXRD patterns, an overall acceptable similarity to the theoretical calculated PXRD was observed (Figure 4.34). Additionally, these materials matched the bulk sample and were different from the starting material.

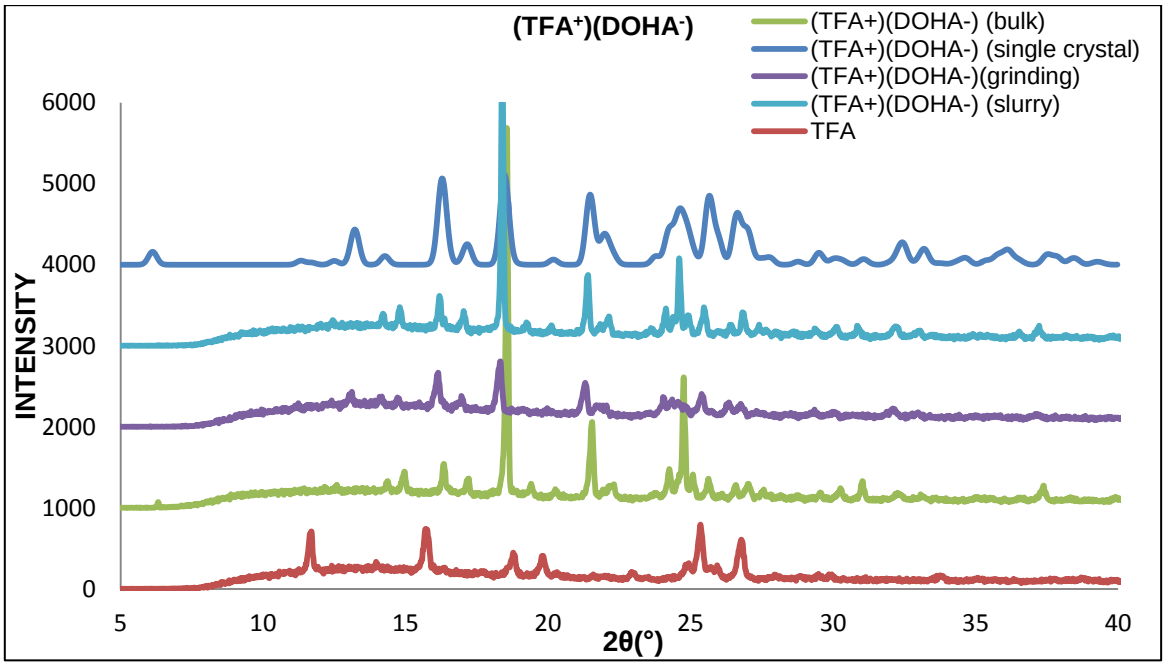

Figure 4-34: PXRD analyses of (TFA^-)($DOHA^+$), calculated patterns obtained from LAZYPULVERIX (blue), and from the slurry experiment (light blue); the grinding experiment (purple), bulk sample (green) and starting material TFA (red).

The (**TFA^-)(MOP^+**) PXRD results shown in Figure 4.35 indicated that samples which were either pulverised or prepared as slurries agreed with values predicted by the theoretical pattern. Most of the observed peaks were also similarly recorded from the PXRD data obtained from the bulk material.

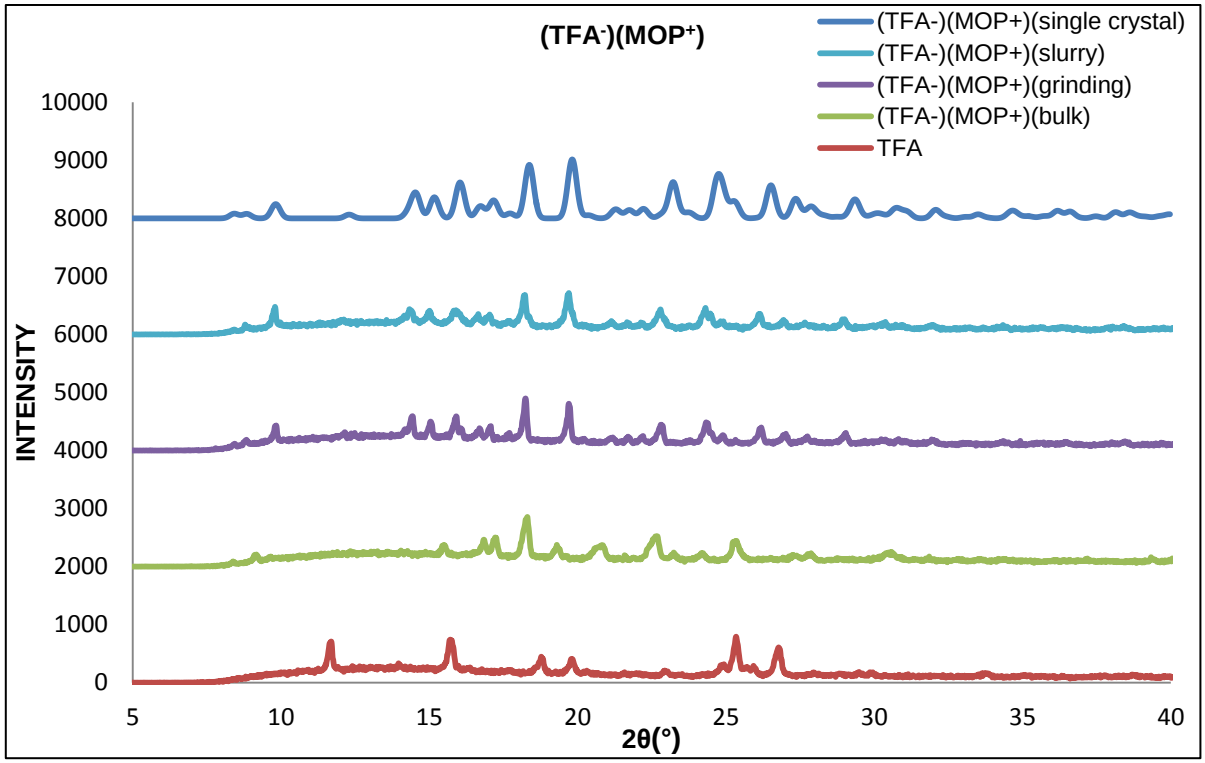

Figure 4-35: PXRD analyses of (TFA$^-$)(MOP$^+$), calculated patterns obtained from LAZYPULVERIX (blue), and from the slurry experiment (light blue); the grinding experiment (purple), bulk sample (green) and starting material MA (red).

4.2.6 Kinetics of desolvation obtained from tolfenamic acid salts

A non-isothermal kinetics study was conducted on (**TFA$^-$)(MOP$^+$**) as the TGA data derived from this compound revealed a distinct loss of the solvent which was followed by the melt of the acid. Crystals were removed from the mother liquor and analysed by using TGA operating at heating rates of 2, 6, 10 and 18 K min^{-1}. The results were converted to semilogarithms as illustrated in Figure 4.36. The activation energy was calculated and varied between 102 and 130 kJ mol^{-1}.

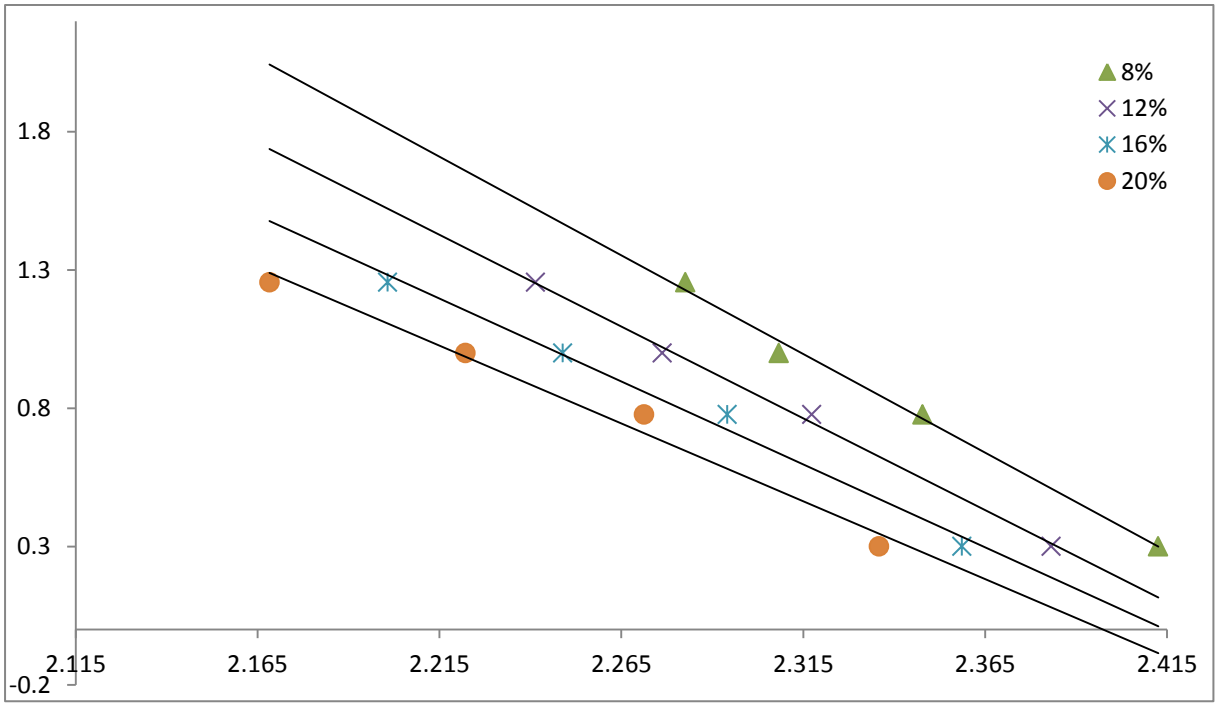

Figure 4-36: Log rate *vs.* 1/T graphs for (TFA^-)(MOP^+).

4.2.7 Desolvation studes of tolfenamic acid salts

It was not possible to carry out a (**TFA^-)($DOHA^+$**) desolvation study as the boiling point of the solvent (544 K) was higher than the melting point of the TFA (481 K). No desolvation was observed in the (**TFA^-)(MOP^+**) salt when the crystals were exposed to the atmosphere for a time period of one month. However, a desolvated form was obtained from the mixture when subjected to heating in an oven at 170 °C. This was confirmed by TGA. The PXRD results obtained for the desolvated powder agreed with those obtained from the starting material. Therefore, no alteration was observed as the TFA retained the identical form after desolvation (Figure 4.37).

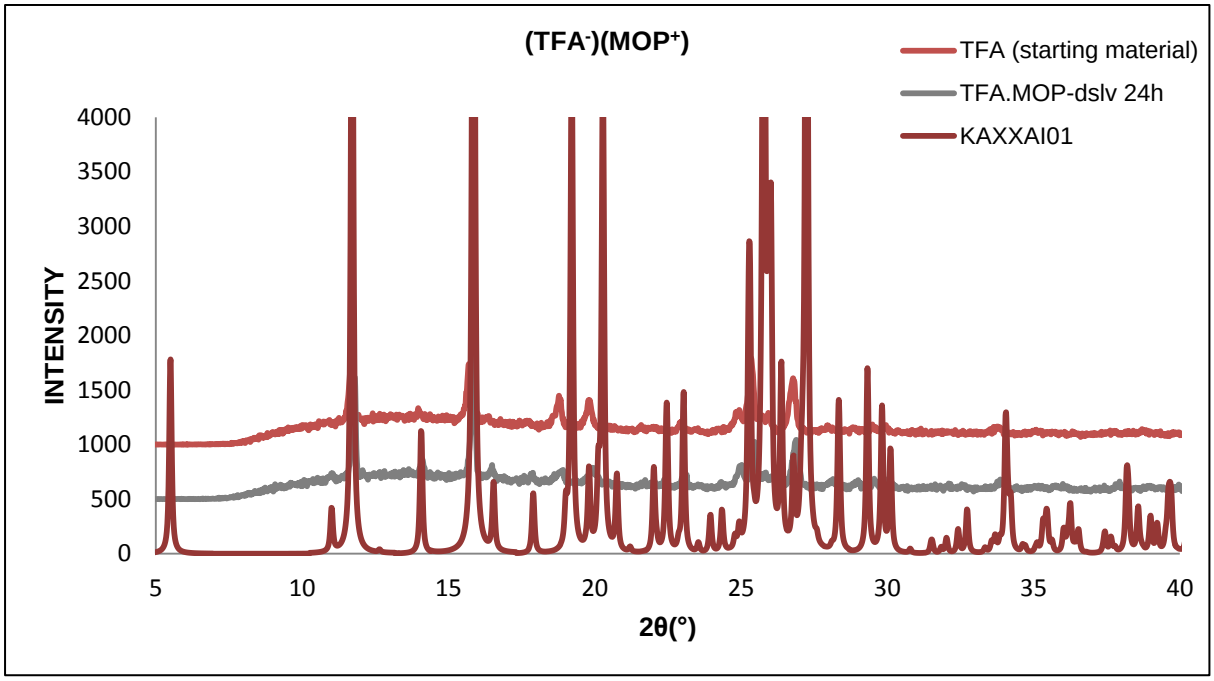

Figure 4-37: Comparison of resulting patterns of (TFA^-)(MOP^+) from 24 h desolvation at 170 °C with KAXXAI01 and the starting material (TFA).

4.3 Conclusion

In the form of salts, both MA and TFA presented similar characteristics. The packing arrangement of these compounds remained in the form of columns but the arrangement of the latter varied depending on the type of solvent used. For example, the DOHA and EDM salts displayed a crystal packing arrangement wherein both hydrophobic and hydrophilic regions were segregated. This was unlike the arrangements observed for the MOP, TA and MP salts. Therefore, the replacement of a methyl group by a chlorine atom did not greatly impact on the conformation and packing of the salts.

The 2-3-dimethylphenyl and 3-chloro-2-methylphenyl rings had different conformations relative to the carboxylic acid (COOH group) in the salts and solvates structures of MA and TFA. The salts only showed a *cis* conformation while the solvates of MA and TFA showed both *cis* and *trans* conformations. Additionally, the thermal stability of the salts of MA and TFA were similar. Generally, the desolvation studies showed a crystalline form which was similar to that of the starting materials. An exception was **(MA^-)(TA^+)** where a mixture of form I and form II was observed. Apart from the **(MA^-)(EDM^+)** sample, all salts studied in the current investigation were reproduced after both pulverising and slurry preparation procedures.

Bibliography

- Fábián, L., Hamill, N., Eccles, K.S., Moynihan, H.A., Maguire, A.R., McCausland, L. & Lawrence, S.E. 2011. Co-crystals of fenamic acids with nicotinamide. *Crystal Growth & Design,* 11(8): 3522–3528.
- Fang, L., Numajiri, S., Kobayashi, D., Ueda, H., Nakayama, K., Miyamae, H. & Morimoto, Y. 2004. Physicochemical and crystallographic characterization of mefenamic acid complexes with alkanolamines. *Journal of Pharmaceutical Sciences*, 93(1):144–154.
- Lee, E.H., Byrn, S.R. & Carvajal, M.T. 2006. Additive-induced metastable single crystal of mefenamic acid, *Pharmaceutical Research,* 23(10): 2375-2380
- McConnell, J.F. & Company, F.Z. 1976. *N*-(2,3-xylyl) anthranilic acid, C15H15NO2 mefenamic acid, *Crystal Structure Communications.* 5: 861-864.
- SeethaLekshmi, S. & Guru Row, T.N. 2012. Conformational polymorphism in a non-steroidal anti-inflammatory drug, mefenamic acid. *Crystal Growth & Design*, 12(8):4283–4289.
- Stahl, P.H. & Wermuth, C.G. 2008. Handbook of pharmaceutical salts. Properties, selection, and use. Weinheim: John Wiley & Sons.
- Surov, A.O., Simagina, A.A., Manin, N.G., Kuzmina, L.G., Churakov, A.V. & Perlovich, G.L. 2015. Fenamate co-crystals with 4,4′-bipyridine: structural and thermodynamic aspects. *Crystal Growth & Design*, 15(1):228–238.
- Weast, R.C. 1980. CRC Handbook of Chemistry and Physics. 60th ed. New York. CRC Press.

CHAPTER 5

ZWITTERIONIC FORM OF MEFENAMIC ACID

A PARTICULAR CASE OF SOLVATE

A zwitterion is a type of compound containing formal negative and positive charges on different atoms (Cleaves II, 2011; McMurry, 2010). Since the hydrogen is transferred within the molecule, zwitterions are usually referred to as an inner salt. Mefenamic acid contains an acidic and amine group and in the presence of morpholine, a proton was transferred from the carboxylic acid to the amine group. This formed a zwitterion **MA•MOP** which is characterised in this chapter. Since the proton was not transferred to the solvent, this particular compound was treated as a solvate.

5.1 Structural analysis

The mefenamic acid (MA) was dissolved in a mixture of morpholine and nitromethane (Section 2.4.1, Chapter 2). After slow evaporation at room temperature, the crystals appeared three weeks after preparation. The crystals were observed to be block-like. In this structure, the proton was not transferred to the solvent molecule but instead to the nitrogen atom located on the MA. Both N-H hydrogen atoms of the MA were found in the difference electron density map. However, for the final refinement these atoms were placed in geometrically calculated positions. Furthermore, the morpholine was disordered and had final site occupancy factors of 0.41 and 0.59. The crystal data parameters are presented in Table 5.1. Figure 5.1 shows the numbering scheme of the **MA•MOP** and Figure 5.2 shows the packing arrangement of the compound down [100].

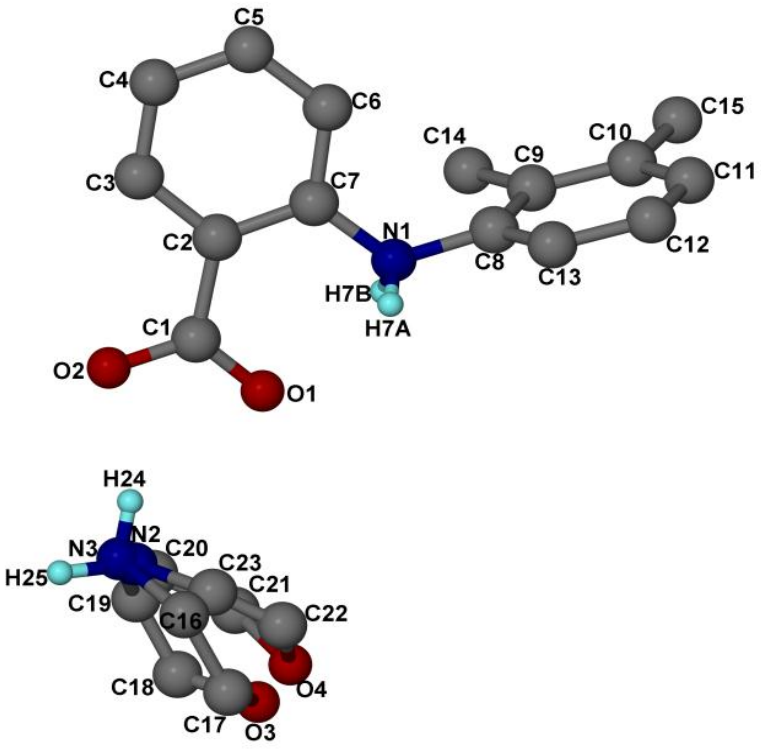

Figure 5-1: Numbering scheme for MA•MOP (some hydrogen atoms were omitted for clarity).

The MA interacts with morpholine (MOP) *via* the N-H hydrogen atoms of the MOP and the deprotonated oxygen atom (O2) of MA. The N2H24•••O2 interaction is characterised by an N2•••O2 distance of 2.740(2) Å and an N2H24•••O2 angle of 160°. The N2H25•••O2

interaction had an N2•••O2 measured distance of 2.860(3) Å and an N2H25•••O2 angle of 166°. These strong interactions created a ring structure displaying the graph set $R_4^2(8)$. Morpholine molecules interact with one another by means of weak hydrogen bonds. These interactions include C18H18A•••O3 (2.883(1) Å, 125.5°) and C18H18B•••O4 (3.453(1) Å; 137.8°). The hydrogen bonds are summarised in Table 5.2. Figure 5.3 shows the cavities occupied by morpholine along [100] and [010].

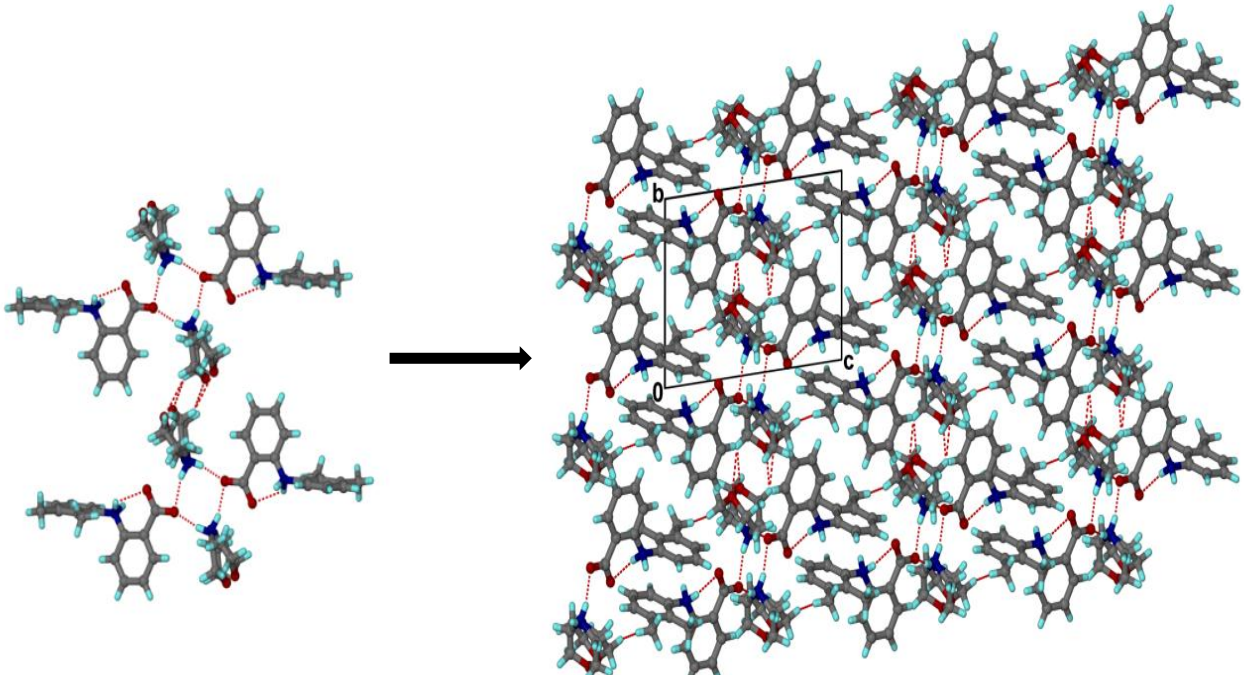

Figure 5-2: Crystal packing of MA•MOP along [100] showing the different hydrogen bond interactions.

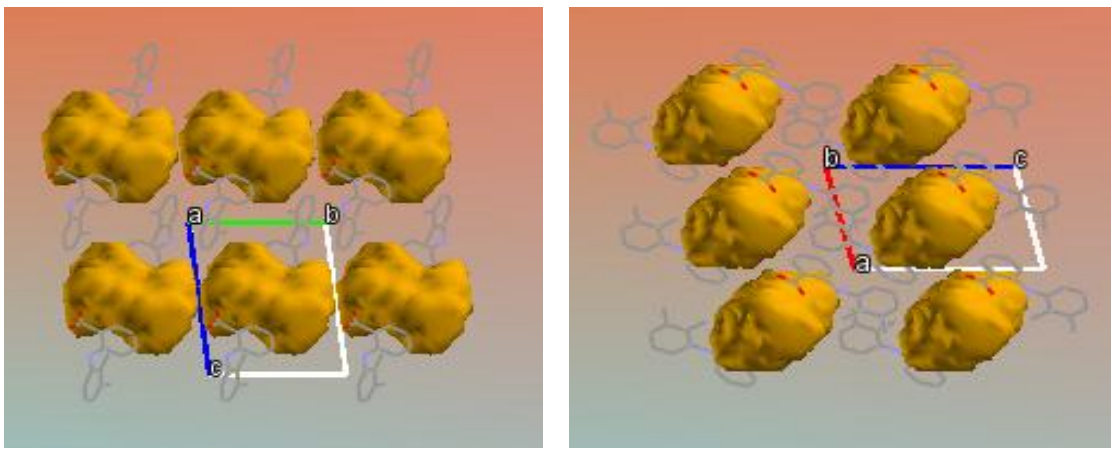

(a) (b)

Figure 5-3: Cavities showing the location of MOP along (a) [100] and (b) [010].

Table 5-1: Crystal data and data collection parameters obtained for MA•MOP.

Compound	MA•MOP
Host:guest ratio	1:1
Molecular formula	$C_{19}H_{24}N_2O_3$
Formula weight [g mol^{-1}]	328.40
Crystal system	triclinic
Space group	$P\bar{1}$
Z	2
D_{calc} [g cm^{-3}]	1.252
a [Å]	7.8250(16)
b [Å]	9.889(2)
c [Å]	12.291(3)
α [°]	79.10(3)
β [°]	73.65(3)
γ [°]	74.14(3)
V [Å^3]	871.4 (3)
μ (Mo-Kα) [mm^{-1}]	0.085
λ[Å]	0.17073
T [K]	173.2
$2\theta_{Max}$ [°]	57.2
No. reflections collected	8494
No. unique reflections	4363
No. reflections with I>2σ(I)	2692
Parameters	282
R_1 [I>2σ(I)]	0.0705
wR_2	0.2110
GOOF	1.046

Table 5-2: Geometrical data recorded for the hydrogen bonds of MA•MOP.

	D-H/Å	H•••A/Å	D•••A/Å	<(DHA)/°	Symmetry operation
N1-H7B•••O1	0.92	2.19	2.641(2)	109	-
N2-H24•••O2	0.84(4)	1.93(4)	2.740(2)	160(4)	-
N3-H25•••O2	1.07(6)	1.81(4)	2.860(3)	166(3)	-X, -Y, -Z
C18-H18A•••O3	0.99	2.19	2.883(1)	125.5	1-X, -Y-1,1-Z
C18-H18A•••O4	0.99	2.66	3.453(1)	137.8	1-X, -Y-1,1-Z

5.2 Torsion angles and dihedral angle analyses of MA•MOP

The MA solvate with morpholine showed a conformational variation similar to that observed in the solvates of MA and pyridine derivatives.

The O2C1C2C7 torsion angle of the twisting of the carboxylic group was 170° (Table 5.3). This angle was less than the value recorded for the angle observed in the MA and pyridine derivatives which varied between 177-179°. However, the O2C1C2C7 torsion angle (170°) was close in value to the torsion angle of **$(MA^-)(TA^+)$** salt (172°). The C2C7N1C8 torsion

angle (177°) was equal in size to the angle observed in **MA•2PIC Form II** (177°). The 2,3-dimethylphenyl ring (C7N1C8C9) in **MA•MOP** (78°) resembled that of the angles which occurred in the solvates. In fact, this latter angle was similar in value to **MA•4PIC** (79°). In addition, the dihedral angle of **MA•MOP** (80.5°) and C7N1C8C9 (-77.5°) torsion angle were almost equal to the values recorded for the MA co-crystal with bipyridine (dihedral angle= 79.3^0; C7N1C8C9 = 77.2^0) (Surov et al. 2015).

Table 5-3: Torsion and dihedral angles of MA•MOP.

	MA•MOP
Torsion angle/°	
O2C1C2C7	170
C2C7N1C8	177
C7N1C8C9	-78
Dihedral angle/°	80.50

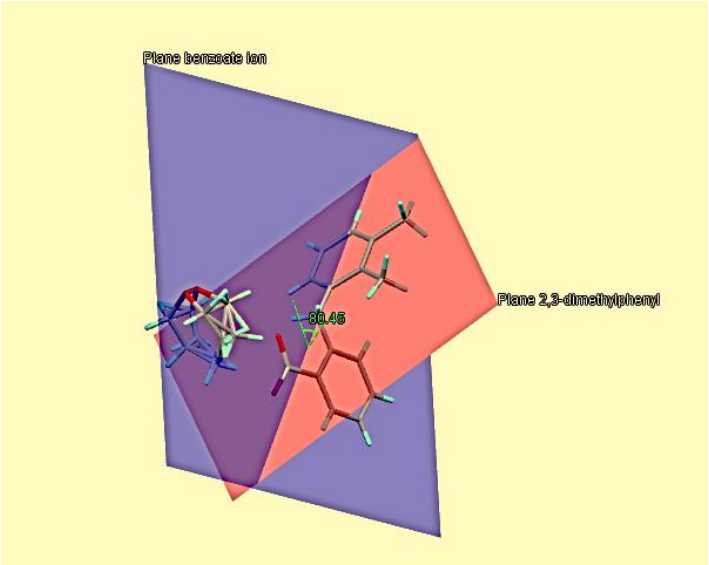

Figure 5-4: Dihedral angle recorded for MA•MOP.

5.3 Thermal analysis of MA•MOP

The thermal analysis data obtained for this solvate are shown in Table 5.4. Figure 5.5 represents the DSC and TGA graphs recorded for the compound. The theoretical and experimental %mass losses correlated well. The DSC graph showed an endotherm at 434 K

which coincided with release of the solvent. A second endotherm was observed when the temperature reached 503 K which represents the melt of MA. It was noted that the solvent was released from the crystal lattice at a temperature (434 K) higher than the known boiling point (402 K) of morpholine. This is explained by the number of interactions observed between the MA and the disordered morpholine. However, this temperature difference could also be due to the observation that the solvent was situated in cavities (Figure 5.3) in the crystal structure. Furthermore, the thermal stability as measured by the T_{on}/T_b values was approximately 1.08 (Table 5.4).

Table 5-4: Thermal analysis data obtained for MA•MOP (* bp retrieved from Budavari, 1989).

	MA•MOP
Host:guest ratio	1:1
TGA calculated % mass loss	26.55
Actual experimental % mass loss	25.92
DSC endotherm representing the loss of solvent (T_{on}/K)	434
DSC endotherm for mefenamic acid (T_{on}/K)	503
Solvent normal boiling point (bp) (K)	402*
T_{on}/T_{bp}	1.08

(Solvent boiling point retrieved from Weast, 1980)

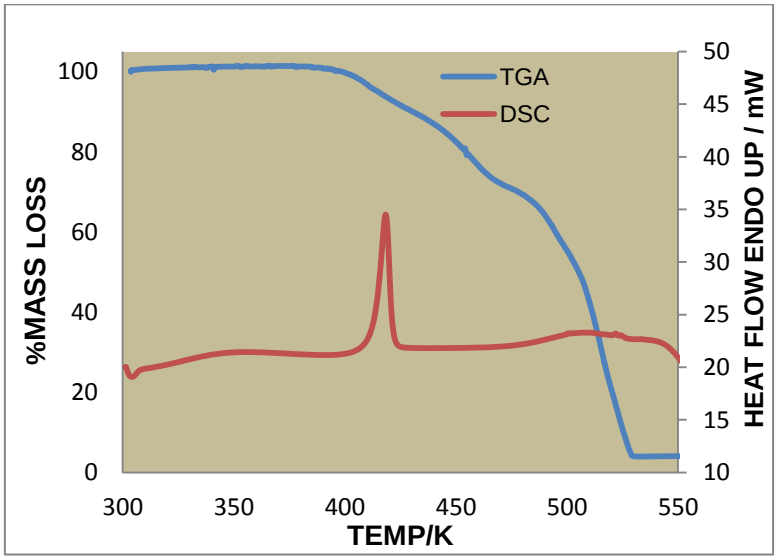

Figure 5-5: DSC and TGA curves of MA•MOP.

5.4 Hot stage microscopy (HSM) studies of MA•MOP

Hot stage microscopy (Section 2.4.7, Chapter 2) was done on a single crystal selected from the bulk sample of **MA•MOP** (Figure 5.6).

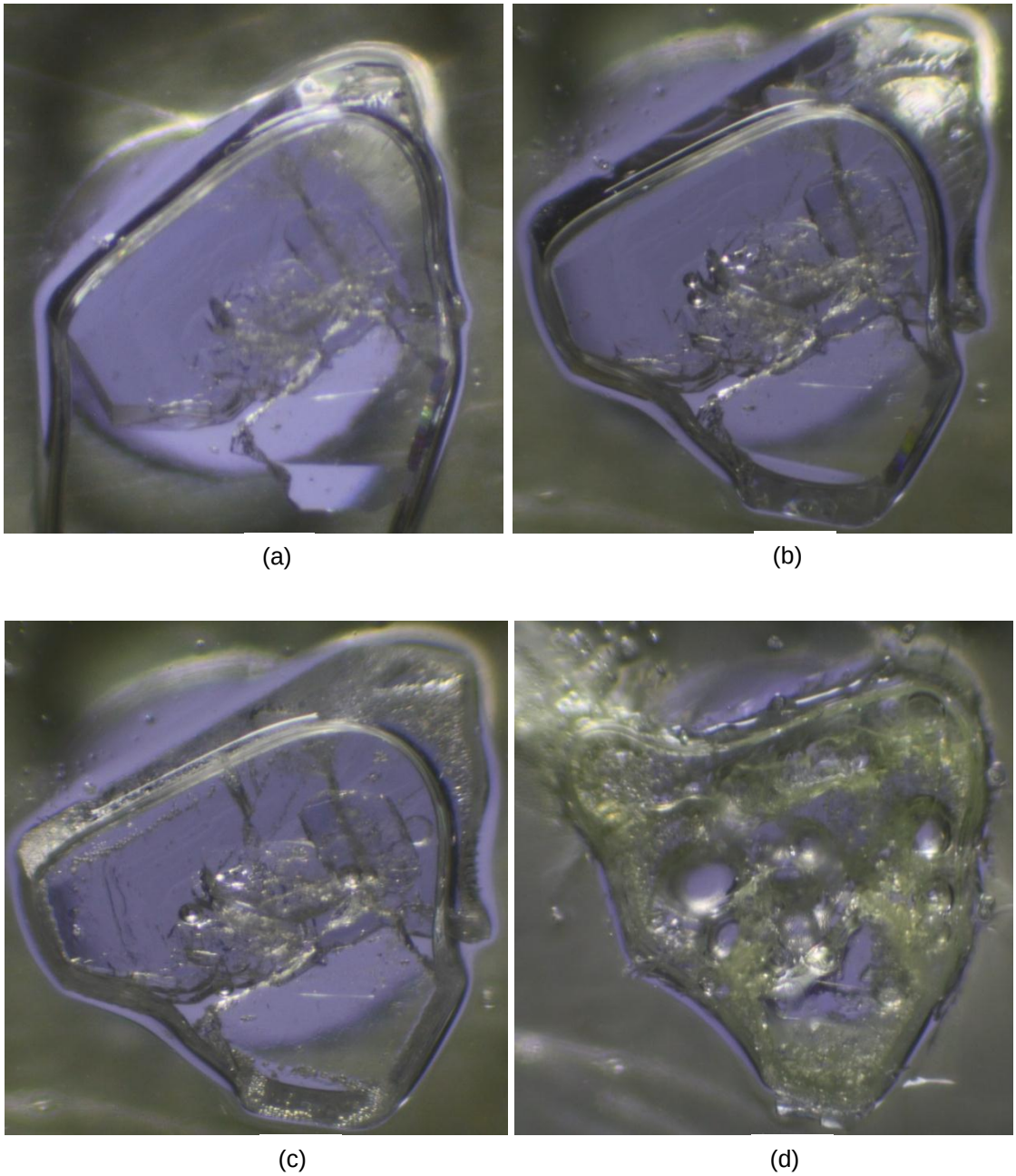

(a) (b)

(c) (d)

Figure 5-6: HSM photography of MA•MOP a) crystal at 298 K, (b) crystal at 382 K (c) crystal at 437 K (d) crystal at 521 K.

The initial state of the crystal at 298 K is shown in Figure 5.6 (a). At 382 K (Figure 5.6 b), bubbles started to appear and this coincided with the commencement of solvent release. As time progressed the temperature reached approximately 437 K and more bubbles appeared (Figure 5.6 c). The crystal was observed to melt at 521 K (Figure 5.6 d). Upon melting, the crystal became yellow in colour. The evolution of bubbles also continued at that temperature.

5.5 Powder X-ray diffraction (PXRD) analyses of MA•MOP

All the PXRD patterns (ground, slurry and bulk material: chapter-2 section 2.4.8) showed a perfect match to the single crystal pattern obtained from LAZYPULVERIX (Yvon et al.1997). They were different from that of the starting material and can be observed in Figure 5.7.

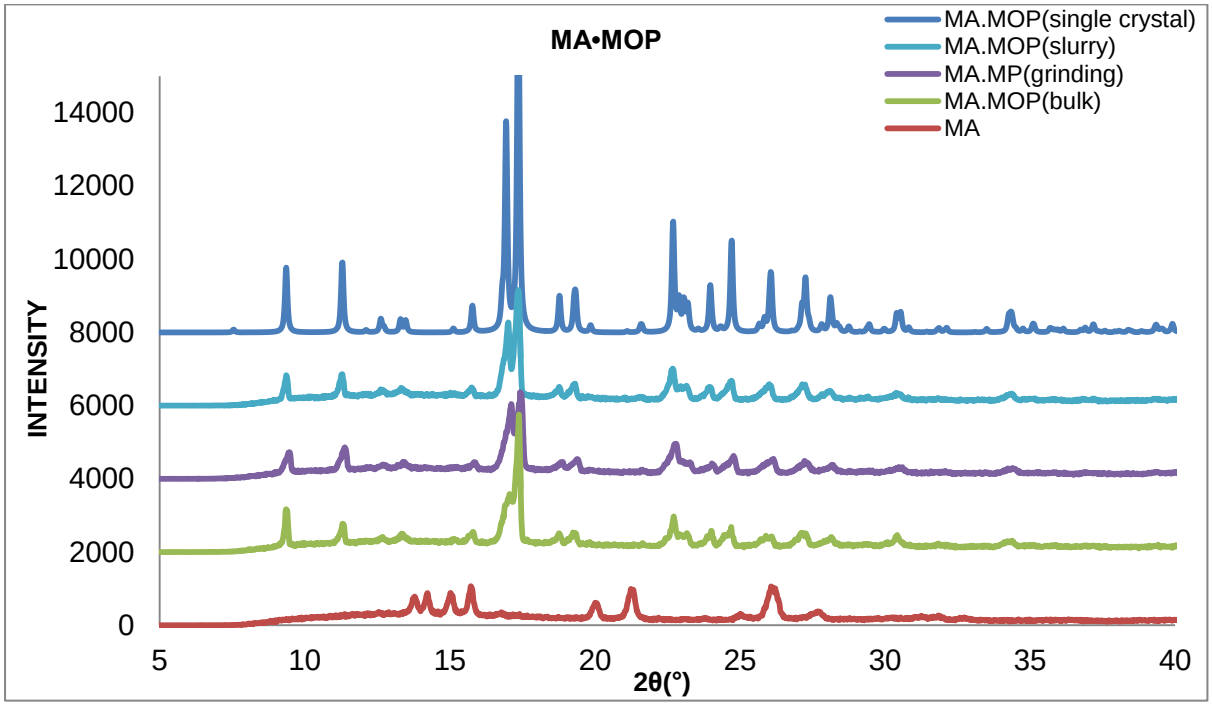

Figure 5-7: PXRD analyses of MA•MOP, calculated patterns obtained from LAZYPULVERIX (blue), and from the slurry experiment (light blue);the grinding experiment (purple), bulk sample (green) and starting material MA (red)

5.6 Kinetics of desolvation of MA•MOP

Non-isothermal kinetics of desolvation were performed on **MA•MOP** by using TGA operated at varying rates of heating (Section 2.4.9, Chapter 2). The graph representing log rate vs 1/T is shown in Figure 5.8. The activation energy showed a restricted range of 98-100 kJ mol^{-1}.

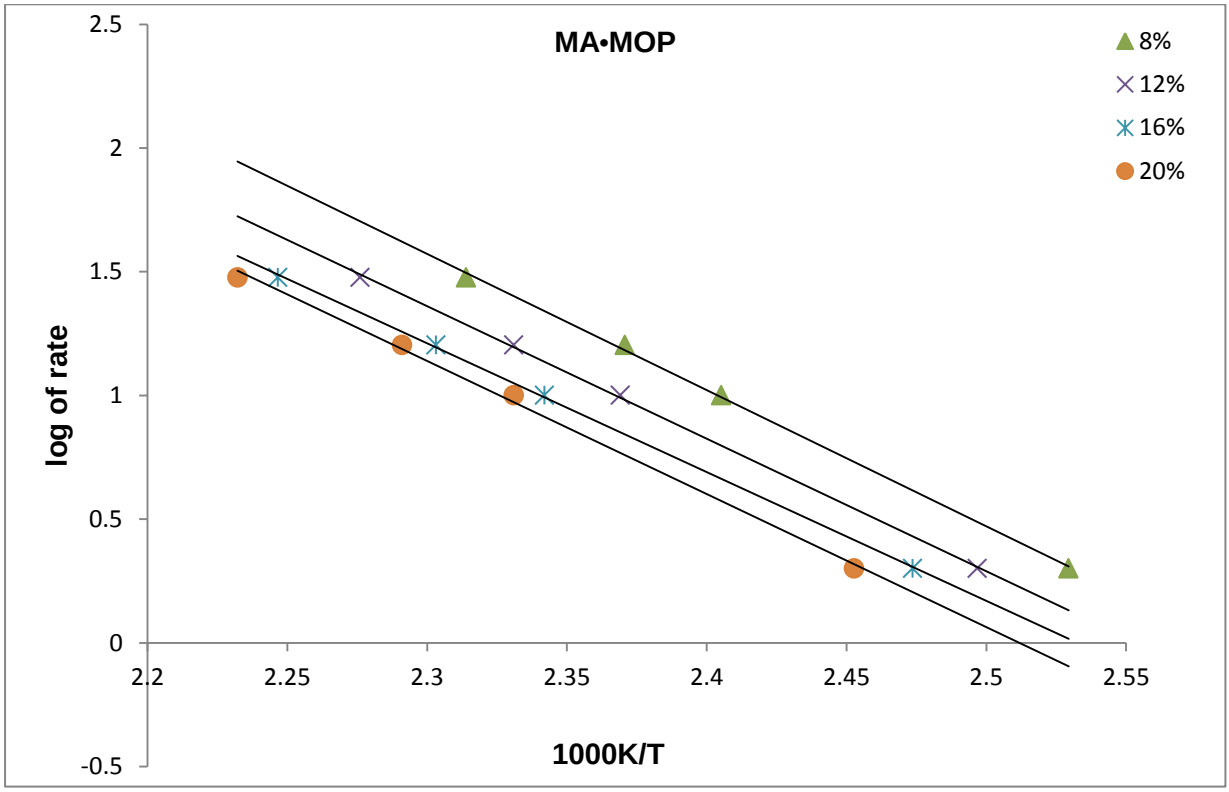

Figure 5-8: Log rate vs. 1/T graphs obtained for MA•MOP.

5.7 Desolvation studies of MA•MOP

Crystals of **MA•MOP** were left in an open vessel for one month but no solvent loss was observed with TGA. The sample showed no change in morphology, thus indicating that **MA•MOP** was as stable as (**MA^-**)(**EDM^+**), (**MA^-**)(**TA^+**) and **(MA^-)(MP^+)**. In a second experiment, crystals were placed in an oven at a temperature of 125 °C for 24 h. Even under these conditions, no solvent loss was detected by the TGA. Only when crystals were subjected to a temperature of 463 K for 24 h, was a desolvated powder recorded by TGA. When analysed by PXRD, the results obtained did not correspond to those of the starting material. Rather, the data showed a similarity to another form of MA sample XYANACO2 Cambridge Structural Database (CSD, version 5.36, Nov 2014) (Figure 5.9).

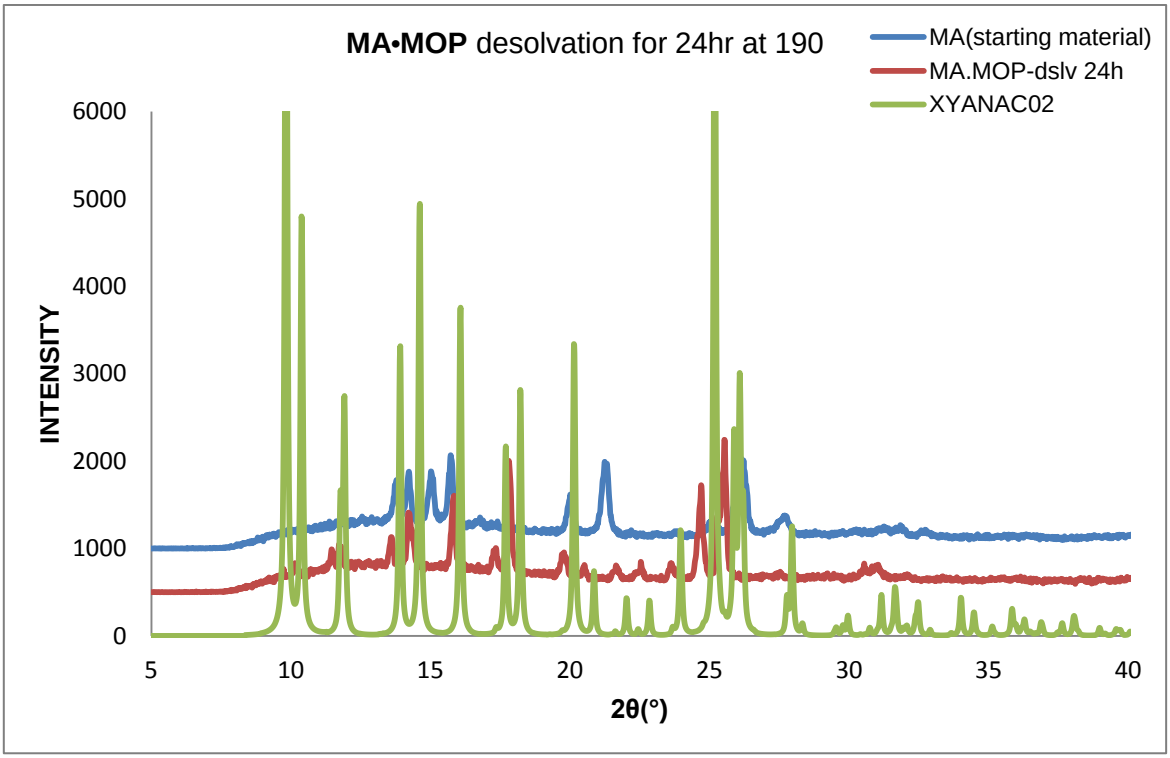

Figure 5-9: Comparison of patterns of MA•MOP after 24 h desolvation at 120°C with XYANAC02 and the starting material

5.8 Conclusion:

MA•MOP showed properties typical of both a salt and a solvate of MA. One of the characteristics of this compound was that during thermal analysis studies solvent was released only when the temperature was in excess of the known boiling point. This observation was in contrast with the release of solvent noted for the solvates obtained with MA and pyridine derivatives, where the solvent was always released at temperatures below the boiling point. Experiments done wherein samples were prepared as slurries or pulverised powders showed that recrystallization could be achieved by using different methods. Furthermore, the kinetics of desolvation of the solvate showed an activation energy range of 98-100 kJ mol^{-1}.

Bibliography

- Cleaves, D.H.J. 2011. Zwitterion. Gargaud, M. Amils, P. R. J. Quintanilla, C. Cleaves II, D. H. J. Irvine, W. M. Pinti, P. D. L. & Viso, M. *Encyclopedia of astrobiology.* Springer Berlin Heidelberg: 1796–1796. **http://link.springer.com/referenceworkentry/10.1007/978-3-642-11274-4_1708** [22 October 2015].
- McMurry, J. 2010. *Organic chemistry*. 8th ed. Singapore Brooks/Cole Cengage Learning.
- Surov, A.O., Simagina, A.A., Manin, N.G., Kuzmina, L.G., Churakov, A.V. & Perlovich, G.L. 2015. Fenamate co-crystals with 4, 4′-bipyridine: structural and thermodynamic aspects. *Crystal Growth & Design*, 15(1):228–238.
- Yvon, K., Jeitschko, W. & Parthe, E.J 1997. LAZY PULVERIX, a computer program, for calculating X-ray and neutron diffraction powder patterns. *Journal of Applied Crystallography*, 10:73-74.
- Weast, R.C. 1980. CRC Handbook of Chemistry and Physics. 60th ed. New York. CRC Press.

CHAPTER 6

CONCLUSION AND RECOMMENDATIONS

Fenamates are known to exist as several different polymorphs. Desolvation of solvates/salts can produce a polymorph of the starting material. Although the fenamic acids may be used to treat a number of inflammatory illnesses in humans, they can cause a multitude of undesirable side effects. However, in the form of a salt, these side-effects may be minimised. Hence the conversion of fenamic acids to salts would be favourable to the pharmaceutical industry.

The principal aim of this research was to produce solvates and salts of mefenamic (MA) and tolfenamic acids (TFA). Previous studies done elsewhere showed that these two compounds had similar characteristics in their molecular packing arrangement. This is despite the fact that there are differences in the molecular structure between the two acids. In particular, this is due to the presence of a methyl group in MA which is replaced by a chlorine atom in TFA. During the current research, the two fenamates were investigated and were crystallised with nitrogen-containing solvents. In order to ascertain the impact of the replacement of a methyl group by a chlorine atom, the structures of both the solvates and salts were critically compared. The effect that the different solvents had on the conformation of the fenamic acids was also investigated.

The solvates of MA with pyridine derivatives had similar characteristics and structural packing arrangements. Conversely, the solvates of TFA with the pyridines showed different packing arrangements. Furthermore, all solvates of TFA solved in differing space groups. However, in the case of the salts tested, the packing arrangement did not show much variation between MA and TFA. The compounds obtained when morpholine was used showed variable characteristics. In MA, no proton transfer occurred between the MA and the morpholine. Rather, the proton was transferred within the MA to form a zwitterion. In contrast, TFA underwent deprotonation and the morpholine was protonated to form a salt.

The conformation of the backbone of the two acids varied depending on the solvent included. In the solvates, the MA most commonly showed a *trans*-conformation of the methyl substituents to the acidic moiety whereas TFA revealed a *cis*-conformation in the fenamic rings. The exceptions were **MA•2PIC** and **TFA•3BrPYR**. These latter salts had a conformation matching that of the MA and TFA where a similar orientation of the dimethyl and chloro-methyl substituted rings was observed.

Different methods (grinding, slurry preparation) used to prepare the solvates and salts of TFA were successful. In contrast, not all of these methods could be used to prepare the solvates and salts of MA. It was not possible to produce (**MA**$^-$)(**EDM**$^+$) by either grinding or slurry preparation. However, (**MA**$^-$)(**EDM**$^+$) was produced by recrystallization at room

temperature. One of the most interesting observations was that the recrystallisation of **MA•2PIC** produced a different form. Desolvation studies of the solvates (except in the case of the zwitterion) created a crystalline form identical to that of the starting material. Additionally, the salts of the MA and TFA produced the same crystalline form as occurred in the starting material in most salts. However, this was not observed in the MA and triethylamine preparation where a mixture of two polymorphs of MA (forms I and II) was observed. Remarkably, desolvation of the zwitterionic form of the MA (with morpholine) produced form II of the acid.

Generally, the replacement of a methyl group (MA) by a chlorine atom (TFA) had an effect on the structural arrangement of the final compounds. Even though the two fenamic acids have similar arrangements in their salt forms, MA and TFA compounds had different characteristics. Future studies should investigate the solubility of the salts/solvates which could benefit the pharmaceutical industry. Additionally, marked differences in the conformation of the MA and TFA structures were found and these could be further investigated. Supplementary investigations may provide further knowledge regarding the improvement of solvate formation in the field of crystallography.